POLYOXAZINONES FROM ROMP

by

Joshua Michael Fishman

A dissertation submitted in partial fulfillment of

the requirements for the degree of

Doctor of Philosophy

(Chemistry)

at the

UNIVERSITY OF WISCONSIN – MADISON

2015

Date of final oral examination: 6/11/2015

The dissertation is approved by the following members of the Final Oral Committee:
Laura L. Kiessling, Professor, Chemistry & Biochemistry
Ronald T. Raines, Professor, Chemistry & Biochemistry
Kristyn S. Masters, Associate Professor, Biomedical Engineering
Sandro Mecozzi, Associate Professor, Chemistry & Pharmacy
Eric R. Streiter, Assistant Professor, Chemistry

POLYOXAZINONES FROM ROMP

Joshua M. Fishman

Under the supervision of Professor Laura L. Kiessling

At the University of Wisconsin – Madison

The ring-opening metathesis polymerization (ROMP) is a powerful methodology to generate synthetic macromolecules whose structures and functions are diverse. Control over the polymer architecture is enabled through the use of well-defined metal alkylidene catalysts, which are able to polymerize a cadre of cyclic olefin monomers in a living manner. Furthermore, specific catalysts possess exquisite chemoselectivity for olefin metathesis in the presence of polar functionality. This functional group tolerance enables ROMP scaffolds to be decorated with various chemical elements that engender the resultant polymers with properties consummate for materials, electronic, and biological applications.

Although widely applicable, extant polymers from ROMP, like the majority of synthetic polymers, are non-degradable. They therefore lead to refuse accumulation. A functional and degradable polymer would allow the synthetically useful traits of ROMP to be combined with the growing need for new degradable polymer scaffolds. To address this demand, my thesis identifies bicyclic oxazinones as able substrates for ROMP. The polymerization of bicyclic oxazinones leads to a novel degradable material: polyoxazinones. Through polymerization optimization, polyoxazinones were generated with good control over molecular weight and polydispersity. In addition, synthetic routes were designed to functionalize polyoxazinones to tailor their properties for various applications.

Polymers that are both modular and degradable are needed as scaffolds for drug delivery and next-generation vaccine development. To explore the applicability of polyoxazinones for this purpose, the biocompatibility and biodegradability of these ROMP polymers was tested. I show that polyoxazinones are bioinert macromolecules, yet can be functionalized with bioactive ligands to activate immune cells through interactions with specific cell-surface receptors. In addition, I developed an assay based on Förester Resonance Energy Transfer (FRET) to be used to gauge whether polyoxazinoes can degrade inside living cells.

Finally, by characterizing the physical properties of polyoxazionones, I found that these polymers possess unusually high thermal stabilities for degradable materials. Therefore, it is envisioned that polyoxazinones can be used to supplement existing non-degradable polymers where high thermal stability is needed. Additionally, I explored methods to generate ROMP-derived copolymers using bicyclic oxazinones and 1,5-cyclooctadiene (COD). Synthetic access to both random and block copolymers was achieved.

“Make big plans…remembering that a noble,
logical diagram once recorded will not die…”

- Daniel H. Burnham (Architect)

Acknowledgements

Graduate school is, concurrently, both an intensely solitary and a highly collaborative endeavor. While the individual must carry out the requisite experiments, he is not alone in the planning and discussion of the projects or the dissemination of the results. For all the people who have been a part of my journey, thank you.

First and foremost, I owe a debt of gratitude to Professor Laura L. Kiessling. Laura has been a constant source of encouragement over the last five years as I have played around with my own research ideas and grown into the scientist I am today. In addition, I have been fortunate to receive a number of awards during my time in graduate school and Laura's words of support were indispensable in my receipt of these honors. I will be proud to say that I am a Kiessling Group alumnus.

I would also like to thank my committee members Professors Ronald Raines, Kristyn Masters, Sandro Mecozzi, and Eric Streiter. The University of Wisconsin - Madison is blessed to have many amazing faculty members and I am honored that you have agreed to sit on my committee; I look forward to a stimulating discussion. Additionally, Professor Mahesh Mahanthappa has been indispensable in giving me advice during my time in graduate school. It saddens me that Mahesh was unavailable on the day of my defense, but I have appreciated his conversations throughout my graduate career.

The Kiessling lab houses a diverse group of scientists with broad research interests and personalities. This mosaic of labmates makes coming to work enjoyable and facilitates a unique culture where many research problems can be tackled and questions can be answered in house. I would like to particularly acknowledge the specific lab mates whom I have worked on projects directly: Lynne Prost, Daniel Zwick, and Murshid Alam. Daniel Zwick deserves additional praise for assisting me in the design of the cell-based assays presented in this text. During this time, Danny would give me his undivided attention to help me run an experiment or think about a new assay perform.

In addition, I have engaged in countless conversations with other members of the lab, both formally and informally, that have led to interesting new ideas and results. For your comradery and insights I would like to thank Nitasha Bennett, Joe Grim, Cassie Jarvis, Rob Brown, Darryl Wesener, Heather Hodges, Rachael Sheridan, and Paul Wrighton. Lastly, I am indebted to Matthew Kraft. Matt served as a mentor and a friend while he was a post-doc in the group during my first three years of graduate school. He was instrumental in getting my first successful project off the ground and remains one of the best scientists that I know.

Finally, the University of Wisconsin has great core facilities with excellent dedicated staff. Specifically, I would like to thank Anna Kiyanova (SML), Charlie Fry (NMR), Julie Last (AFM), the BIF, and the UWCCC Flow Cytometry Core. Your diligence in the maintenance of the instruments, training, and assistance were instrumental when obtaining data throughout my time in graduate school.

To all others who I have forgot to mention, thank you!

Abstract i

Acknowledgements iv

Table of Contents vi

List of Figures xi

List of Schemes xvii

List of Tables xx

List of Equations xxi

List of Abbreviations xxii

Chapter 1: Biologically Active Polymers from ROMP 1

1.1 Introduction 2

1.2 Benefits of ROMP for Bioactive Polymer Synthesis 5

1.2.1 Functional group tolerance 5

1.2.2 Control over polymer length 6

1.2.3 Control over backbone structure 6

1.2.4 End modification 8

1.3 Synthesis of Biologically Active Polymeric Displays 10

1.3.1 Catalyst design 11

1.3.2 Design of ROMP monomers for bioactive polymer synthesis 14

1.3.3 Troubleshooting the polymerization of bioactive ROMP monomers 17

1.3.4 Routes to functionalized ROMP polymers 19

1.4 ROMP Polymers as Imaging Agents 24

1.5 ROMP Polymers as Probes of Biological Processes 26

1.5.1 ROMP polymers as inhibitors 28

1.5.2 ROMP polymers as effectors 28

1.5.3 Cell penetrating ROMP polymers 30

1.5.3.1 ROMP polymers as artificial translocation domains 31

1.5.3.2 Targeted delivery: B-cell internalization 32

1.5.4 Assembling multi-protein complexes 33

1.6 Outlook 35

Chapter 2: Synthesis of a Functionalizable and Degradable Polymer by ROMP 36

2.1 Identification of Bicyclic Oxazinones as Substrates for ROMP 37

2.2 Polymerization of Bicyclic Oxazinones 39

2.3 Covalent Modification of Polyoxazinones 45

2.3.1 Functionalization of polyoxazinones through monomer synthesis 45

2.3.2 Functionalization of polyoxazinones through post-polymerization modification 48

2.3.3 Reduction of polyoxazinone-oxime conjugates 57

2.3.4 PPM Summary and Outlook 58

2.4 Degradation of Polyoxazinones 59

2.5 Conclusions 62

2.6 Materials and Methods 62

2.6.1 General methods 62

2.6.2 Synthesis of small molecules 64

2.6.3 Synthesis of polymers 83

2.6.4 Monitoring the degradation of polymers 88

Chapter 3: Assessing the Bioactivity and Biocompatibility of Polyoxazinones 90

3.1 Impetus for a Degradable and Bioactive ROMP Polymer 91

3.2 Generation of Multivalent Polyoxazinone Antigens 93

3.2.1 Introduction 93

3.2.2 Interactions with the B-cell Receptor 94

3.2.3 Interactions with DC-SIGN 97

3.2.4 Non-specific uptake of polyoxazinone conjugates 102

3.2.5 Conclusions 105

3.3 Design of a Fluorescent Polyoxazinones Probe to Detect Degradation Inside Cells 105

3.3.1 Methods to detect polymer decomposition 105

3.3.2 Synthesis of fluorescent polyoxazinone probes to detect degradation in cells 107

3.4 Future Directions: Assessing the Degradation of Polyoxazinones in Living Cells 113

3.5 Materials and Methods 117

3.5.1 General methods 117

3.5.2 Synthetic procedures 119

3.5.3 Cell Culture 131

3.5.4 Procedures for the selective internalization of polymer probe ***3.08*** *and* ***ManBSA*** *by DC-SIGN expressing Raji Cells* 132

3.5.5 Procedures for the internalization of polymer probes ***3.01****,* ***3.02****, and* ***3.12*** *by A20 and A20HL cells* 132

3.5.6 In vitro degradation of ***3.21*** 133

3.5.7 Procedures for monitoring the degradation of polymers by FRET in live cells 133

Chapter 4: Examination of the Thermal Properties of Polyoxazinones and the Synthesis of Oxazinone-Cyclooctadiene Copolymers 134

4.1 Thermal characterization of polyoxazinones 135

4.2 Synthesis of Oxazinone-Cyclooctadiene Copolymers 140

4.2.1 Introduction to copolymers 140

4.2.2 Synthesis of poly(oxazinone-b-cyclooctadiene) copolymers 142

4.2.3 Synthesis of poly(oxazinone-r-cyclooctadiene) copolymers 153

4.2.4 Conclusions 157

4.3 Future Directions 157

4.4 Materials and Methods 158

4.4.1 General methods 158

4.4.2 Synthetic Procedures 160

4.4.3 Monitoring the polymerization of monomer ***4.04*** 165

4.4.4 Degradation of polymer ***4.07*** 165

Appendix A: Synthesis of Synthetic Antigens with Tunable Stiffness 166

A.1 Mechanosensing in the Immune System 167

A.2 Synthesis and Functionalization of Hydrogel Nanoparticles 170

A.3 Characterization of the Stiffness of Polyacrylamide Hydrogel Nanoparticles 174

A.4 Future Directions 176

A.5 Materials and Methods 177

A.5.1 General methods 177

A.5.2 Synthesis of ligand ***A.01*** 178

A.5.3 Synthesis of hydrogel nanoparticles 179

A.5.4 Functionalization of hydrogel particles 180

A.5.5 Hexose Assay 180

A.5.6 Preparation of hydrogel substrates for AFM 181

A.5.6.1 Attachment of hydrogel particles 181

A.5.6.2 Synthesis of hydrogel surfaces 181

A.5.6 Procedures for AFM 182

Appendix B: NMR Spectra 184

Compiled References 251

List of Figures

Figure 1.1. Biologically active polymers from ROMP can be used in diverse applications. 3

Figure 1.2. Schematic view of the diversity of polymer modifications accessible through ROMP. 4

Figure 1.3. Decoration of ROMP polymers via post-polymerization modification. 5

Figure 1.4. ROMP affords control over polynorbornene microstructure. 7

Figure 1.5. Control over the spacing between ligands conjugated to ROMP polymers is achievable using homo- and co-polymers composed of cyclobutene, cyclohexene, and/or cyclooctene monomers. 8

Figure 1.6. Strategies to end-label ROMP polymers. 10

Figure 1.7. Ruthenium carbene catalysts used to generate biologically active polymers. 12

Figure 1.8. Scope of degradable ROMP polymers. 16

Figure 1.9. Additives can be introduced to facilitate the polymerization of monomers that aggregate in solution or chelate to ruthenium carbene intermediates. 17

Figure 1.10. Steric congestion around the olefin functionality hinders ROMP. 18

Figure 1.11. Strategies to combine AAC and ROMP. 22

Figure 1.12. Polynorbornene *in vivo* imaging agents. 25

Figure 1.13. Multivalent ligands can engage a target receptor through different binding modes. 27

Figure 1.14. ROMP polymers can serve as synthetic antigens to study immune cell signaling. 30

Figure 1.15. ROMP polymers decorated with a polyguanidinium block mimic protein transduction domains and promote polymer internalization into mammalian cells. 31

Figure 1.16. A caged fluorophore was used to monitor internalization of ROMP polymers by B cells. When exposed to intracellular esterases, the fluorophore is revealed. 33

Figure 2.1. Strategies to synthesize functionalizable and degradable ROMP polymers. 37

Figure 2.2. ROMP catalysts screened during the optimization of the polymerization of bicyclic oxazinone monomers. 41

Figure 2.3. Polymerization of monomer **2.01a** under optimal conditions. 43

Figure 2.4. Optical properties of pyrene conjugates. 46

Figure 2.5. Strategies to diversify polyoxazinones: grafting-through and PPM. 48

Figure 2.6. Quantitative conversion of acetophenone-functionalized polymer **2.22** to oxime conjugate **2.24** and subsequent reduction to polymer **2.28** was followed by ^{1}H-NMR. 54

Figure 2.7. GPC analysis of polymers **2.22**, **2.24**, and **2.28**. 54

Figure 2.8. Absorbance and emission spectra for pyrene conjugates **2.25** and **2.26** and ligand **2.08e**. 56

Figure 2.9. Degradation profile of polymer **2.03b** under acidic and basic conditions. 60

Figure 2.10. Degradation of **2.03e** was monitored by comparing the ratio of polymeric pyrene excimer emission (λ_{max} = 480 nm) to monomer emission (λ_{max} = 377 nm). 61

Figure 3.1. Structures of polyoxazinones used in cellular internalization assays. 94

Figure 3.2. Upon binding DNP-conjugate **3.01**, the surface exposed BCRs of A20HL cells are internalized and routed to early endosomes. 95

Figure 3.3. Confocal imaging of A20HL B cells exposed to DNP conjugate **3.01**, triethylene glycol conjugate **3.02**, and mannose conjugate **3.03** at 4 ^{o}C and 37 ^{o}C and co-localization analysis of polymers **3.01**, **3.02**, and **3.03** with the BCR and the early endosomal marker transferrin. 97

Figure 3.4. Mannosylated polymeric antigen is internalized by Raji B cells that express the cell surface receptor DC-SIGN. 99

Figure 3.5. Selective internalization of polymer **3.08** and **ManBSA** by the surface receptor DC-SIGN. 101

Figure 3.6. Structures of the fluorophores conjugated to PTD mimics **3.10**, **3.11**, and **3.12**. 103

Figure 3.7. Internalization of polymers **3.01** and **3.12** by A20 and A20HL cells. 104

Figure 3.8. Proteolysis can be monitored *in cellulo* through the construction of a fusion protein composed of a protease sensitive peptide flanked by two fluorescent proteins that are FRET partners. 106

Figure 3.9. Both pyrene homopolymer **3.13** and copolymer **3.14** lead to excimer formation while the sulfopyrene conjugate **3.18** did not. 109

Figure 3.10. Polymer **3.19**, conjugated to the dye SR and the contact quencher DNP, does not undergo significant fluorescence turn-on upon oxazinone degradation at pH = 1.25. 110

Figure 3.11. Emission spectra for polymer **3.20** and fluorophores AF350 and AF488 in water. 112

Figure 3.12. Exposure of polymer **3.21** to pH = 2.0 buffer results in a loss of FRET as the polymer degrades. 112

Figure 3.13. Assay for detecting polyoxazinone degradation inside live cells by FRET. 114

Figure 3.14. The degradation of polyoxazinones in cells was followed by flow cytometry over time. 116

Figure 3.15. Proposed modifications to the synthesis of bicyclic oxazinone monomers to alter the rate of degradation of polyoxazinones. 117

Figure 4.1. Structures of polyoxazinones with aromatic or alkyl functionality. Polyoxazinones have structural elements that resemble polystyrene and cyclic olefin copolymers. 136

Figure 4.2. The glass transition temperature for polymer **4.01** as a function of molecular weight. At each molecular weight tested, the glass transition temperature of the polyoxazinone sample was greater than that of the corresponding polystyrene sample. 137

Figure 4.3. Effect of the side chain structure on the glass transition temperature of polyoxazinones. 138

Figure 4.4. Thermal stability of polyoxazinones as determined by TGA. 139

Figure 4.5. GPC analysis of the block copolymers generated from **4.04** and *cis*-cyclooctene. 144

Figure 4.6. Reaction conversion of monomer **4.04** during ROMP. 145

Figure 4.7. GPC analysis of block copolymers generated from **4.04** and 1,5-cyclooctadiene. 148

Figure 4.8. Exposure of **4.08** to a pH = 0.25 MeOH/THF solution leads to degradation of the polyoxazinone repeats. 148

Figure 4.9. Photodimerization of polymer **4.18** with 350 nm light. 152

Figure 4.10. ^{1}H-NMR confirmed the successful photodimerization of polymer **4.18** through loss of the coumarin olefin signals but retention of the aromatic protons. 153

Figure 4.11. GPC analysis of the photodimerization of polymer **4.18** revealed a shift of elution time but retention of a monomodal molecular weight distribution, indicating complete dimerization. 153

Figure 4.12. DSC analysis of poly(oxazinone-r-cyclooctadiene) at various mol% poly(**4.04**). The glass transition temperatures obtained by DSC are well described by the Fox equation. 156

Figure A.1. The difference in stiffness between mammalian cells and pathogens spans nine orders of magnitude. The elasticity of hydrogel nanoparticles can be tuned to match that of mammalian cells or bacterial pathogens by varying the crosslink densities. 167

Figure A.2. The extent of DNP conjugated to carboxylic acid containing hydrogels was assessed using UV-Vis. 172

Figure A.3. The hexose assay was performed on mannose ligand **A.02** to generate a calibration curve used to assess the mannose content on the hydrogel nanoparticles. 174

Figure A.4. AFM images of 4% and 15% cross-linked particles immobilized on a glass coverslip. 175

List of Schemes

Scheme 2.1. Synthesis of a library of bicyclic oxazinone monomers that undergo ROMP to afford degradable polyoxazinones. 39

Scheme 2.2. Backbiting during the polymerization of bicyclic oxazinones led to the formation of cyclic dimers. 40

Scheme 2.3. Synthesis of a mannosylated polyoxazinone using CuAAC. 47

Scheme 2.4. Performing CuAAC on azido-polyoxazinone **2.03g** led to undesired gelation. 49

Scheme 2.5. Polynorbonene ROMP polymers that display reactive NHS esters are amenable to PPM using amine containing ligands. A synthetic route to a bicyclic oxazinone decorated with an NHS ester. 50

Scheme 2.6. Synthesis of reactive polymer **2.22**, a mimic of poly(*p*-acetyl phenylalanine). 52

Scheme 2.7. Reactive polymer **2.22** can be elaborated via PPM with hydroxylamine ligands. The resulting oxime conjugate, **2.24**, can be further reduced to stabilize the labile oxime linkage. 54

Scheme 2.8. Synthesis of pyrene-oxime conjugates: polymer **2.25** and 1-mer **2.26**. 56

Scheme 2.9. Proposed route to amine and thiol reactive polyoxazinones. 58

Scheme 2.10. Ring-opening cross metathesis of monomer **2.01b** and subsequent hydrolysis of 3-alkoxy-1,3-oxazin-4-one **2.30** under acidic conditions. 60

Scheme 2.11. Degradation of pyrene conjugate **2.03e**. 61

Scheme 3.1. Installation of an amine reactive end group at the chain-end of polyoxazinone **3.07** was achieved through modification of the metathesis catalyst's alkylidene ligand. 100

Scheme 3.2. Structures of polyoxazinones conjugated to fluorophores with concentration dependent spectral properties. 108

Scheme 4.1. Synthesis of block copolymers from **4.04** and *cis*-cyclooctene by ROMP. 143

Scheme 4.2. Synthesis of block copolymers from **4.04** and 1,5-cyclooctadiene by ROMP. 146

Scheme 4.3. Screen of end-capping efficiency for various vinyl ethers. 149

Scheme 4.4. Polymer **4.15** was unable to be conjugated to dihydroxylamine crosslinkers due to solubility incompatibilities. 150

Scheme 4.5. Polymer **4.16** was elaborated with a coumarin moiety at the pCOD terminus. Coumarin functionalization allowed photodimerization of polymer **4.18** with 350 nm light. 152

Scheme 4.6. Bicyclic oxazinone **4.04** and 1,5-cyclooctadiene could be copolymerized by ROMP to afford random copolymers. 154

Scheme A.1. Synthesis of carboxylic acid containing polyacrylamide hydrogel nanoparticles. 169

Scheme A.2. Functionalization of carboxylic acid containing polyacrylamide hydrogel nanoparticles. 171

Scheme A.3. The hexose assay can be used to quantify the amount of surface exposed carbohydrates on bacteria or hydrogels. 173

Scheme A.4. Functionalization of glass coverslips with hydrogel particles for AFM analysis. 175

List of Tables

Table 1.1 Monomers for the synthesis of biologically active ROMP polymers. 15

Table 2.1. Evidence for backbiting during the polymerization of bicyclic oxazinone monomers. 40

Table 2.2. Polymerization of bicyclic oxazinones by ROMP. 42

Table 2.3. Polymerization of benzyl substituted monomer **2.01b**. 43

Table 2.4. Effect of BCy_2Cl on the polymerization of monomer **2.01b**. 45

Table 2.5. Polymerization of monomer **2.21** by ROMP. 53

Table 2.6. Unequal halogenation of the residues of polymer **2.29** occurs during bromination using $PhN(CH_3)_3Br_3$. 58

Table 4.1. Transitions in polymer mass loss from TGA. 140

Table 4.2. Effect of additives on the block copolymerization of **4.04** and COD by ROMP. 147

Table 4.3. Random copolymerization results for bicyclic oxazinone monomer **4.04** and 1,5-cyclooctadiene. 155

Table A.1. Recipes used to generate DEA/VAA hydrogel nanoparticles with different stiffness. 170

Table A.2. DNP conjugation was used to quantify the –COOH content of the hydrogel particles. 172

Table A.3. Mannose content of polyacrylamide hydrogels determined by the hexose assay. 174

Table A.4. Particle aspect ratios as determined by AFM 176

Table A.5. Recipes used to prepare hydrogel surfaces. 181

List of Equations

Equation 4.1. The Fox copolymer equation. 141

Equation A.1. The Hertz model provides a relationship between the loading force and the indentation. 182

Equation A.2. Model for the indentation of an AFM tip into a surface. 182

Equations A.3. Equation for the elasticity of a surface using AFM. 183

List of Abbreviations

^{1}H-NMR	proton nuclear magnetic resonance imaging
^{13}C-NMR	carbon nuclear magnetic resonance imaging
AAC	azide-alkyne [3+2] cycloaddition
AF350	AlexaFluor 350
AF488	AlexaFluor 488
AFM	atomic force microscopy
APS	ammonium persulfate
APTES	aminopropyl triethyl silane
ATD	artificial transduction domain
ATRP	atom transfer radical polymerization
BCR	B-cell antigen receptor
BCy_2Cl	chloro dicyclohexylborane
BIBB	α-bromoisobutyryl bromide
Boc	*O*-^{t}butyl carbonate
CD22	sialic acid binding surface receptor found on B cells
CD22L	carbohydrate ligand for CD22
CFP	cyan fluorescent protein
COC	cyclic olefin copolymer
COD	1,5-cyclooctadiene
COE	*cis*-cyclooctene
ConA	concanavaline A
CS-E	chondroitin sulfate E

CuAAC	copper-catalyzed azide-alkyne [3+2] cycloaddition
DBU	1,8-diazabicyclo[5.4.0]undec-7-ene
DC	dendritic cell
DC-SIGN	dendritic cell-specific ICAM-3-grabbing non-integrin
DEA	diethyl acrylamide
DIEA	diisopropyl ethyl amine
DLS	dynamic light scattering
DMAP	dimethylamino pyridine
DMF	dimethyl formamide
DMSO	dimethyl sulfoxide
DNA	deoxyribonucleic acid
DNP	dinitrophenyl hapten
DP	degree of polymerization
DSC	differential scanning calorimetry
DTG	derivative thermogravimetry
EDCI	1-ethyl, 3-(3-dimethylaminopropyl) carbodiimide
ELVIS	extravasation through leaky vasculature and the subsequent inflammatory cell-mediated sequestration effect
Em	emission wavelength
EPR	enhanced permeability and retention effect
Et_2O	diethyl ether
EtOAc	ethyl acetate
Ex	excitation wavelength

FBS	fetal bovine serum
FRET	Förester Resonance Energy Transfer
GAG	glycosaminoglycan
GPC	gel permeation chromatography
HIV-TAT	human immunodeficiency virus protein trans-activator of transcription
HOAc	acetic acid
HRESI-MS	high resolution electrospray ionization mass spectra
ICG	indocyanine green
M:I	initial monomer to catalyst ratio
ManBSA	mannosylated Bovine Serum Albumin
MBA	methylene bisacrylamide
MeOH	methanol
M_n	number averaged molecular weight
MRI	magnetic resonance imaging
M_w	weight averaged molecular weight
MWCO	molecular weight cutoff
NHS	*N*-hydroxy succinimide
PAMP	pathogen-associated molecular pattern
PBS	phosphate buffered saline solution
pCOD	poly(1,5-cyclooctadiene)
pCOE	poly(*cis*-cyclooctene)
PDI	polydispersity index
PEG	polyethylene glycol

PEMA	polyethylene maleic anhydride
PET	positron emission tomography
PMMA	poly(methyl methacrylate)
PPM	post-polymerization modification
PS	polystyrene
PTD	protein transduction domain
RNA	ribonucleic acid
ROMP	ring-opening metathesis polymerization
ROP	ring-opening polymerization
RPMI	Roswell Park Memorial Institute
SBS	styrene-butadiene-styrene rubber
SDS	sodium dodecyl sulfate
SR	sulforhodamine
$T_{5\%}$	temperature at which a polymer will decompose 5% w/w
TBAF	tetrabutyl ammonium fluoride
T_{change}	change in decomposition rate during TGA
TEMED	*N*,*N*,*N’*,*N’*-tetramethylenediamine
TFA	trifluoroacetic acid
T_g	glass transition temperature
TGA	thermogravimetric analysis
THF	tetrahydrofuran
TLC	thin layer chromatography
TMS	trimethyl silyl group

UV	ultraviolet light
VAA	vinyl acetic acid
YFP	yellow fluorescent protein

Chapter 1: Biologically Active Polymers from ROMP

Portions of this work have been published in:

Kiessling, L.L.; Fishman, J.M. (2005) “Biologically Active Polymers” in Handbook of Metathesis, Set (eds. R.H. Grubbs, A.G. Wenzel, D.J. O’Leary and E. Khosravi), Wiley-VCH Verlag GmbH & Co. KGaA, Weinheim, Germany.

1.1. Introduction

Intregral to biological processes is the formation of macromolecular assemblies, and aberrant assemblies can lead to disease. Elucidating the molecular basis for these interactions and devising strategies to manipulate them are challenges at the forefronts of biology and chemistry. The unique properties of polymers render them valuable in meeting these challenges. With the ability to tailor their bulk physical properties, polymers are ideally suited for purposes that include targeted delivery of drugs or nucleic acids, tumor imaging, and tissue engineering and regenerative medicine.[1] Additionally, polymers have unique recognition properties that allow them to function through mechanisms inaccessible to small molecules.[2,3] Especially valuable is their ability to engage in multivalent interactions, that is, they can form complexes in which multiple recognition elements on the polymer can interact with multiple target receptors.[2-4] Polymers displaying multiple recognition elements can bind avidly to oligomeric proteins or even cell surfaces and thereby act as potent *inhibitors* (Figure 1.1).[2,5] Alternatively, polymers can function as *effectors* through their ability to cluster proteins on or within a cell to activate signal transduction (Figure 1.1).[3,6] All of these applications are advanced by the ability to control and vary polymer structure.

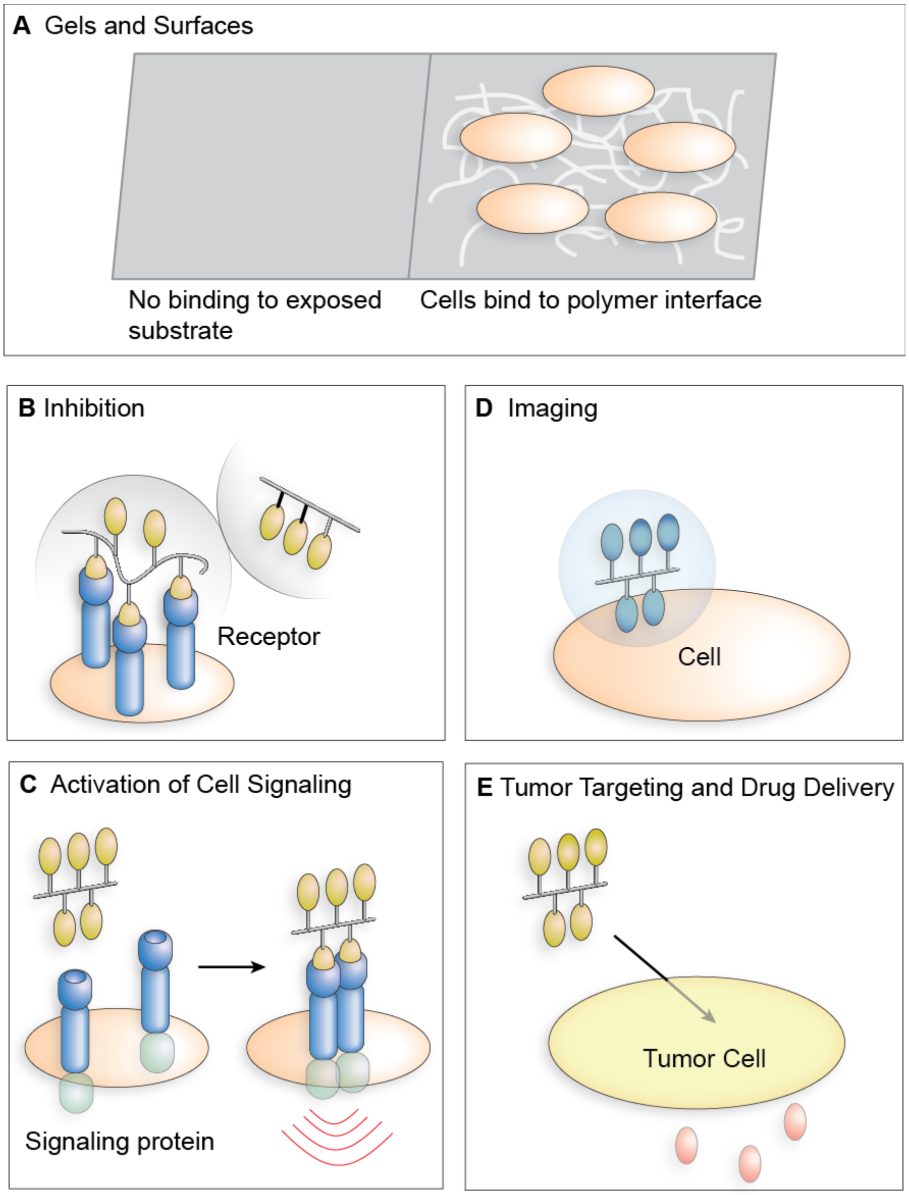
A Gels and Surfaces
No binding to exposed substrate
Cells bind to polymer interface
B Inhibition
Receptor
D Imaging
Cell
C Activation of Cell Signaling
Signaling protein
E Tumor Targeting and Drug Delivery
Tumor Cell

Figure 1.1. Biologically active polymers from ROMP can be used in diverse applications. (a) Polymer coatings on medical devices or implants can enhance biointegration with host cells (shown) or prevent binding to pathogens. (b) By occupying multiple proteins on or within a cell or virus, polymers can function as potent inhibitors of biological processes. (c) Polymers can cluster proteins on or within a cell thereby activating signaling. (d) Polymers carrying many copies of a reporter molecule (e.g., dye, radiotracer, MRI imaging agent) offer enhanced imaging sensitivity. (e) Polymer size can result in their accumulation in the tumor vasculature by enhanced permeation and retention. The display of multiple groups also can faciltate selective cell binding and uptake.

Its attributes render the ring-opening metathesis polymerization (ROMP) a powerful means of generating biologically active polymers (Figure 1.2). For chemical biology applications, ROMP can yield polymers that mimic natural biopolymers or even cell surfaces. Indeed, the first synthesis of a ROMP-generated polymer that was capable of binding a protein revealed that the polymers not only could bind their protein target but also block its ability to mediate cell–cell interactions.[7] As researchers have recognized and exploited ROMP, its limits have been tested. The results are the development of advances in polymerization technology and innovative synthetic strategies that afford a wide range of polymers that function as biomaterials and biopolymer surrogates.

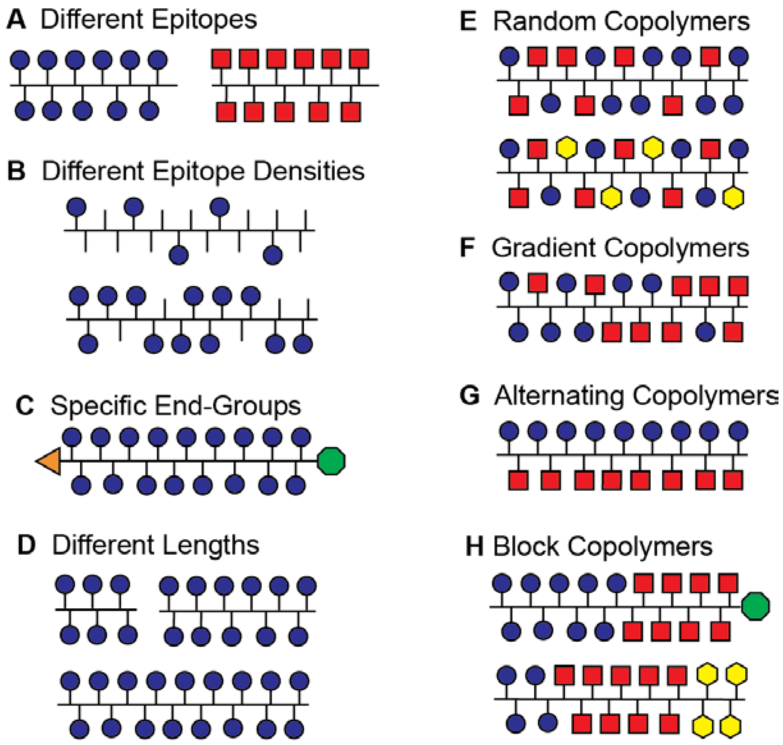
A Different Epitopes
B Different Epitope Densities
C Specific End-Groups
D Different Lengths
E Random Copolymers
F Gradient Copolymers
G Alternating Copolymers
H Block Copolymers

Figure 1.2. Schematic view of the diversity of polymer modifications accessible through ROMP.

1.2. Benefits of ROMP for Bioactive Polymer Synthesis

Exploitation of the reactivity of ROMP initiators and their kinetics affords polymers with tailored properties. An overview of the polymer attributes that can be varied is provided in this section (Figure 1.2). More detailed information with specific examples is found in Section 1.3.

1.2.1. Functional Group Tolerance

Two general strategies have been employed for producing bioactive polymers by ROMP (Figure 1.3). The first is polymerization of a monomer containing the binding group of interest and the second relies on generating a reactive polymer that can be transformed in a post-polymerization modification reaction. Each of these strategies benefit from a metathesis catalysts with outstanding chemoselectivity capable of preferentially reacting with alkenes over many other functional groups. Ruthenium carbene and molybdenum alkylidene complexes have been used as initiators for ROMP. The molybdenum alkylidenes offer excellent control over the

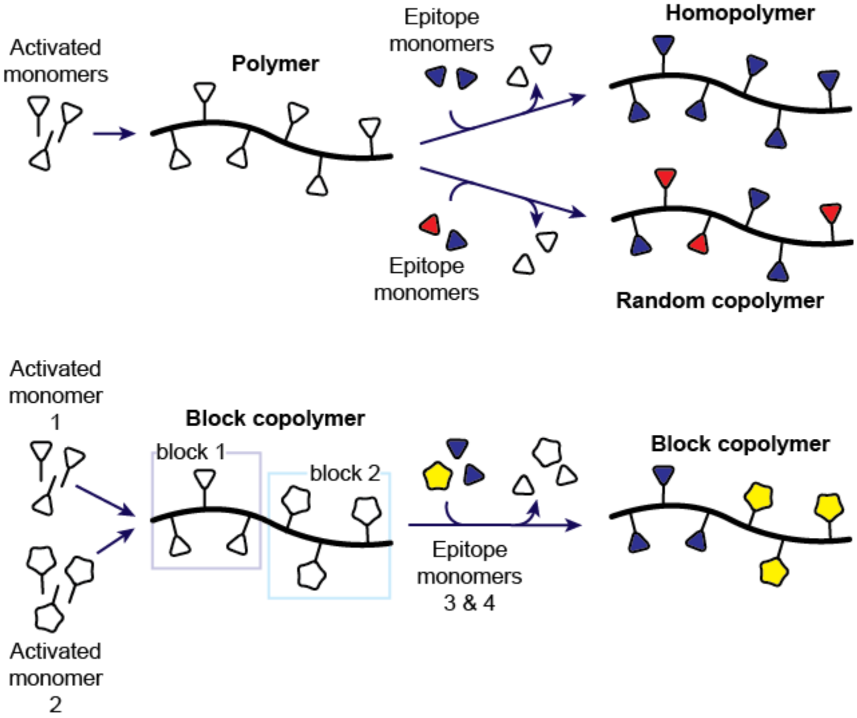
Activated monomers
Polymer
Epitope monomers
Homopolymer
Epitope monomers
Random copolymer
Activated monomer 1
Block copolymer
block 1
block 2
Epitope monomers 3 & 4
Block copolymer
Activated monomer 2

Figure 1.3. Decoration of ROMP polymers via post-polymerization modification. Adapted from ref. 132.

stereochemistry and tacticity of the polymer backbone.[8,9] However, it is the remarkable functional group tolerance of the ruthenium carbene catalysts and their ease of use that has led to their widespread application in bioactive polymer synthesis.[10-12] They promote alkene metathesis even in the presence of functionality such as hydroxyl groups, amides, and sulfate groups.[13-16] The high selectivity of the ruthenium carbene catalysis for strained alkenes also has been exploited to generate reactive polymers, which can be modified further after polymerization to install complex functionality.[17-24]

1.2.2. Control over polymer length

ROMP can give rise to polymers of predictable length and narrow polydispersity (PDI). These reaction attributes are assets for many biological applications, as polymer length can be optimized to elicit a desired function. Polymers of different lengths also can address complex questions about biological recognition[25,26] or elucidate the requirements for signaling[27-31]. Control over polymer length arises when two criteria are met: first, the ROMP reaction is living, such that terminating side reactions cannot compete with elongation; second, the rate of initiation exceeds that of propagation.[32] These conditions can lead to polymers with PDIs approaching unity, and whose length can be varied systematically by altering the monomer to initiator (M:I) ratio. The level of control over polymer length and PDI depends upon the specific catalyst employed (e.g., its stability and the relative rates of initiation versus propagation) and the monomer employed (vide infra).

1.2.3. Control Over Backbone Structure

The microstructure of a polymer’s backbone may influence its biological properties; therefore, the search for methods to control the stereochemistry and tacticity of ROMP polymers has become an area of active research. Molybdenum and tungsten metathesis catalysts have been especially effective for regulating these parameters.[8,33] For example, these catalysts allow the *cis*/*trans* ratio of the polymer's olefin backbone to be adjusted. In addition, isotactic, syndiotactic, and atactic polynorbornenes have been obtained (Figure 1.4). Still, these catalysts have limited tolerance towards polar functionality and are sensitive to moisture, making them challenging to work with when generating bioactive materials. The recent discovery of Z-selective ruthenium olefin metathesis catalysts portends advances that afford ruthenium initiators that exert similarly high levels of control over polymer microstructure.[34-37] In addition to catalyst control, clever monomer design can be exploited to control the spacing of pendant ligands. Polymerization of 1-substituted cyclobutenes[38,39] and 3-substituted cyclooctenes[40-42] proceed in a head-to-tail fashion (Figure 1.5). Hydrogenation of the resultant polymers affords materials with regioregularity.[40,42] Copolymers have also been produced by polymerization of matched monomer pairs, such as cyclobutene/cyclohexene and cyclooctene/cyclobutene (Figure 1.5).[43-45] While studies addressing the consequences of varying polymer backbone on biological activity are still rare,[46,47] control over the microstructure of ROMP polymers can be used to explore these structure-function relationships in the future.

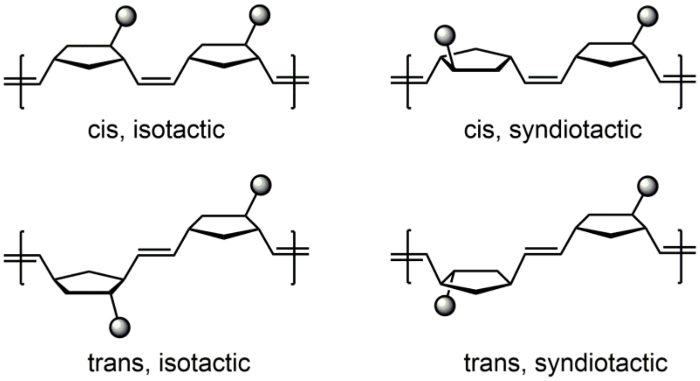

Figure 1.4. ROMP affords control over polynorbornene microstructure.

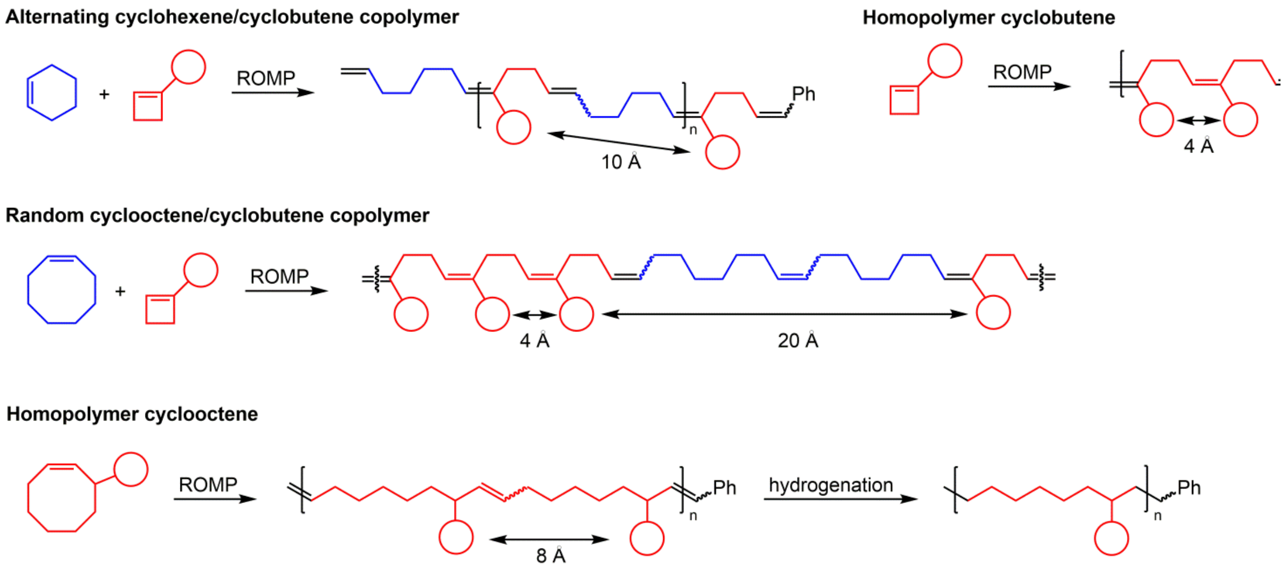

Alternating cyclohexene/cyclobutene copolymer

Homopolymer cyclobutene

Random cyclooctene/cyclobutene copolymer

Homopolymer cyclooctene

Figure 1.5. Control over the spacing between ligands conjugated to ROMP polymers is achievable using homo- and co-polymers composed of cyclobutene, cyclohexene, and/or cyclooctene monomers.

1.2.4. End modification

The features of ROMP can be exploited to install specific end-groups into polymers. For bioactive polymers, the benefit of a unique end-cap is that a functional element, such as a fluorophore or affinity tag, can be appended with control over copy number and regiochemistry. The first example in chemical biology where end modification was utilized was to add a fluorophore to the terminus of a ROMP polymer to visualize interactions between the polymer and cell surface carbohydrate-binding proteins (e.g., the selectins).[48] Since that time, alternative strategies for endgroup modification have been devised to facilitate polymer immobilization, targeting, delivery, or detection.[49-57]

There are three general strategies to end-label ROMP polymers that have been described that exploit reactivity in initiation, propagation, or termination steps. First, metal carbenes with a relevant functional group can be employed as initiators.[49,50,57-59] This strategy necessitates the use of a catalyst that contains a functionalized alkylidene ligand (Figure 1.6A). A benefit of this strategy is excess reagent is not needed (other termination strategies all use super-stoichiometric quantities of reagent) and the conjugation efficiency is quantitative. The barrier to employing this approach is that the functionalized catalyst must be generated.

Second, the addition of a chain transfer agent can be used to intercept polymerization intermediates to terminate elongation (Figure 1.6B).[49] The slow rates of reaction of typical chain transfer agents is a drawback. In addition, the ruthenium catalyst remains active after cross metathesis, which can erode the polydispersity of the polymers. A more recent strategy takes advantage of the living nature of ROMP to add a "sacrifical block" to a polymer.[60,61] The block can be designed such that its degradation can be triggered to afford a polymer with a unique end group (Figure 1.6C). To date, only a handful of chemical biology applications have exploited the polymerization phase to install specific end-groups.[55,62]

The majority of examples in which polymer end groups have been functionalized rely on termination reagents that append an end group while converting the metal carbene into a less reactive entity (Figure 1.6D). The type of termination reagent employed depends on the reactivity of the intermediate carbene. Because the molybdenum alkylidenes are oxophilic, polymerization reactions carried out using these initiators can be selectively terminated with aldehydes.[63,64] The popularity of the ruthenium carbenes, however, stems from their selectivity for alkenes, and it is this reactivity that is most commonly exploited to install unique functional groups at the polymer terminus.[23,48,65,66]. Specifically, the addition of a substituted electron-rich alkene results in the production of a less reactive Fischer carbene. This approach has been employed to immobilize polymers for protein binding assays,[62] to add fluorescent labels to polymers to monitor cell binding,[67] and to visualize the localization of polymer ligands in cells.[28,56] A variation on this approach employs a vinyl carbonate or vinyl lactone, which ultimately yields a polymer with a terminal aldehyde or acid.[68] Although this method has not yet been exploited to generate bioactive polymers, the utility of aldehyde-terminated polymers as cell labeling agents has been established.[48]

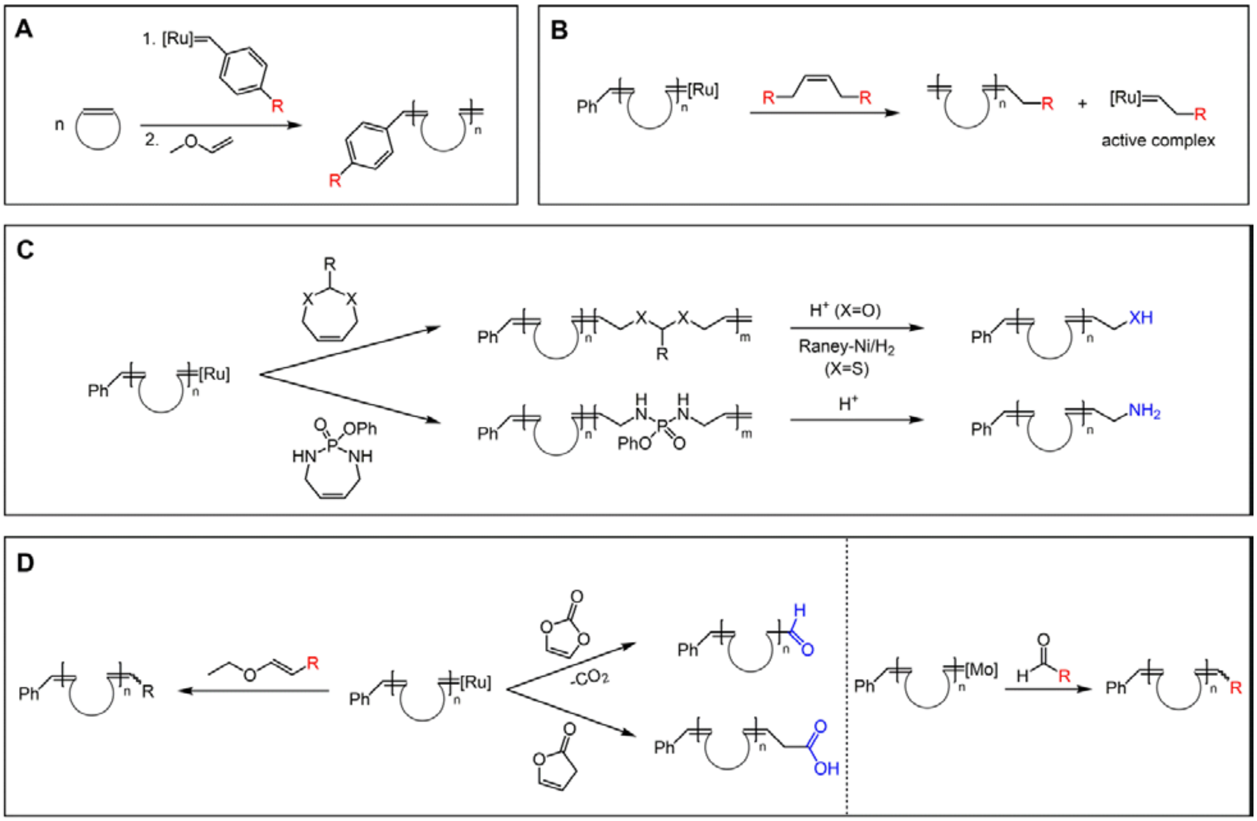
A
1. [Ru]=
R
n
2.
R
n
B
Ph
[Ru]
n
R
R
n
R
+
[Ru]=
R
active complex
C
R
X
X
Ph
[Ru]
n
Ph
n
X
X
R
m
H⁺ (X=O)
Raney-Ni/H₂
(X=S)
Ph
n
XH
O
OPh
P
HN
NH
Ph
n
H
N
P
N
H
PhO
O
m
H⁺
Ph
n
NH₂
D
Ph
n
R
O
R
Ph
[Ru]
n
O
O
O
-CO₂
Ph
n
H
O
O
O
Ph
n
O
OH
Ph
[Mo]
n
O
H
R
Ph
n
R

Figure 1.6. Strategies to end-label ROMP polymers. (A) Application of an initiator with a modified alkylidene. (B) Termination via chain transfer metathesis. (C) Addition of a “sacrifical block” that exposes specific functionality upon degradation. (D) Termination through exposure to reagents which deactivate ruthenium or molybdenum.

1.3. Synthesis of Biologically Active Polymeric Displays

Despite the advantages of ROMP outlined above, the synthesis of biologically active polymers can be challenging. The feasibility of using ROMP to prepare polymers that interact with proteins was first demonstrated in the polymerization of sugar-substituted *oxa*-norbornene monomers with $RuCl_3$.[69] Carbohydrate-substituted polymers were generated efficiently. Although control of the product structure was limited using this undefined catalyst, these studies provided impetus to use defined metathesis catalysts for the synthesis of carbohydrate-substituted polymers.[25,64,70] The water-solubility of the resulting polymers and the high density of functionality within the monomer precursors posed challenges to these early catalysts. One practical solution is to use monomers in which polar functional groups are protected,[64,70] but this approach requires protecting group removal after polymerization. Other approaches, such as emulsion polymerization, also had drawbacks, especially for polymer isolation and purification.[25,70] These initial studies highlighted the challenges inherent in generating materials with a high density of diverse functional groups and a solubility distinct from that of typical organic polymers. Overcoming these barriers has led to innovation in catalyst structure, monomer design, and synthetic strategies.

1.3.1. Catalyst Design

As stated previously, most applications of ROMP to bioactive polymer synthesis have relied on ruthenium catalysts. The early ruthenium carbene metathesis catalysts, namely $(PCy_3)_2Cl_2Ru{=}Ph$ (**1.01**)[71-73] and $(IH_2Mes)(PCy_3)Cl_2Ru{=}Ph$ (**1.02**),[74,75] could be used to prepare diverse types of biologically active polymers (Figure 1.7). For example, catalyst **1.01** can yield polymers decorated with the kind of polar functional groups found on biological ligands, including alcohols, amides, carboxylates, and sulfate groups.[5,13-15,76-81] However, initiator **1.01** can only promote the living polymerization of monomers with high ring-strain, such as norbornene.[11] Carbene **1.01** also suffers from slow initiation and propagation rates. More stable catalysts like **1.02**, which possesses a donating *N*-heterocyclic carbene (NHC) ligand, gave rise to more rapid propagation.[75] Still, some monomers had modest initiation rates and the polymerizations were subject to secondary metathesis reactions that lead to polydisperse polymer products. The problem of side reactions is often exacerbated when the monomers bear functional groups that can chelate to polymerization intermediates.[17,25] A high polydispersity is undesirable if chain length needs to be strictly controlled, as it does in the case of some bioactive polymers.[23,82] Fortunately, new catalysts have been introduced that are highly chemoselective for alkenes, offer greater control over the polymerization reaction, and are tolerant of a wide range of functional groups.

One innovation that is facilitating the synthesis of biologically active polymers is the development of water soluble catalysts.[16,83-87] Catalyst water solubility has been instilled by using a phosphine ligand bearing a quaternary ammonium group (Figure 1.7, **1.03**).[83,84] Catalyst **1.03** retains high activity, undergoes living polymerization reactions to afford polymers with PDI values below 1.25, and is effective in generating block copolymers. Replacing the cationic phosphine ligand with a neutral NHC possessing a PEG substituent led to catalyst **1.04**, which reacts more rapidly. Additionally, its solubility in both aqueous and organic media increases its utility. Water soluble ruthenium complexes are useful when polymerizing highly polar monomers; however, they have not been used widely to generate biologically active polymers. It

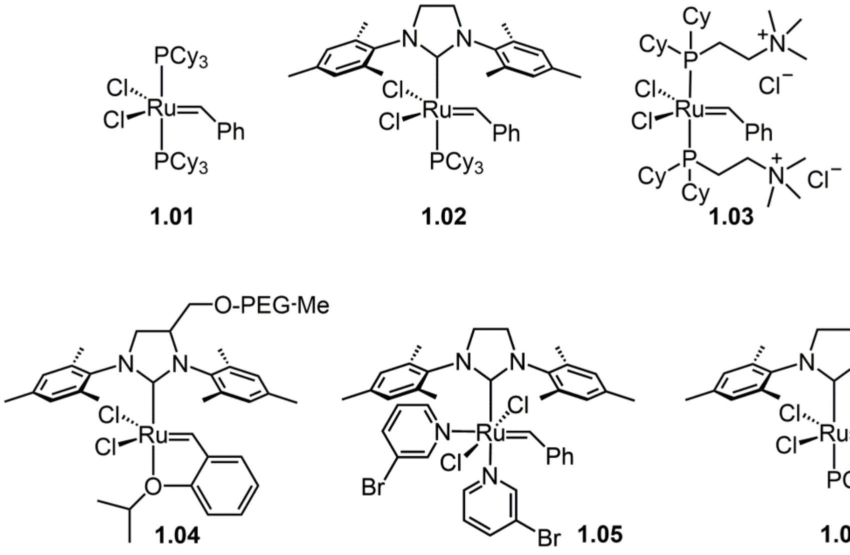

Figure 1.7. Ruthenium carbene catalysts used to generate biologically active polymers.

is possible that the high levels of control and stability of the commercially available catalysts have led many to opt for a post-polymerization modification strategy.[17,22]

A major advancement for the synthesis of biologically active polymers using ROMP was the development of catalyst **1.05** (Figure 1.7). Replacing the phosphine ligand of **1.02** with a pyridine derivative led to enhancements in the rates of both initiation and propagation.[88,89] Another major advantage of catalyst **1.05** is its ability to polymerize moderate and low ring-strain monomers, such as cyclooctene, with good control over chain length and polydispersity (Table 1.1). The advent of this catalyst has significantly expanded the scope of polymers that are attainable through ROMP by affording control over length, backbone flexibility, and ligand spacing.[23,28,29,47,62,82,90]

Most biological applications of ROMP have focused on linear polymers, but for some applications, such as transdermal drug delivery, cyclic polymers may have desirable properties.[91,92] Producing cyclic polymers on the scales relevant for biological applications is often difficult. Innovative methods for cyclizing linear polymers with chemoselective end-caps have been developed[93,94], but these reactions must be conducted at low dilution to prevent oligomerization. The generation of catalyst **1.06** provides an alternative solution.[95,96] The alkylidene-linked NHC ligand of **1.06** ensures that both polymer chain ends remain in close proximity during polymerization. When the monomer pool is exhausted, the system is poised to undergo a ring-closing metathesis reaction between the chain-ends; therefore, regardless of polymer concentration, cyclic polymers are generated. Tethered ruthenium carbene **1.06** is not yet commercially available, which has perhaps curbed the applications of cyclic ROMP polymers; therefore, their ability to generate novel biomaterials is relatively unexplored. However, cyclic ROMP polymers can now be accessed for specific applications.[97]

1.3.2. Design of ROMP Monomers for Bioactive Polymer Synthesis

Selection of an appropriate monomer is critical for producing bioactive polymers with targeted functions. The attributes of the monomer building block govern all aspects of bioactivity: control over polymer length, polydispersity, conformational flexibility, ligand presentation, and degradability. Therefore, the identification of new substrates for ROMP has become an area of active research.

Most biologically active polymers from ROMP are derived from the polymerization of functionalized *oxa*-norbornenes or norbornenes (Table 1.1, entries 1-2). The early ruthenium carbene initiators afforded the greatest control over polymer properties (length, PDI) with norbornene derivatives of this type.[11] Despite their utility, several characteristics complicate their use in some applications: the resulting polymers have heterogeneous backbones (alkene stereoisomers and tacticity is not controlled) and are non-degradable.

One strategy to generate polymers with stereoregular backbones is to use the features of the monomer to favor particular polymerization intermediates.[38,43,44,47,98] The Sampson Group provided an elegant demonstration of this strategy. When they exposed substituted cyclobutenes to initiator **1.05**, head-to-tail polymerization reactions occurred with control over alkene geometry (Table 1.1, entry 4).[15] Functionalized cyclobutenes also can be copolymerized with cyclohexene and cyclooctene monomers to generate alternating or random copolymers (Figure 1.5).[43,44,47] In this way, the spacing between recognition elements can be altered (from 4-20 Å) by varying the number of carbons in the larger cycloalkene monomer. The resultant polymers resemble functionalized polyethylene, a polymer whose backbone has been postulated to be more flexible than that of polynorbornene derivatives. Whatever their flexibility, the two types of backbones undoubtedly have different conformational preferences. The spacing between groups and the backbone conformational preference are factors that were exploited to optimize the antimicrobial properties of ROMP polymers.[47]

A significant barrier to employing ROMP to generate polymers for physiological applications is that the reaction generally affords polymers that are not degradable. Non-degradable polymers are unlikely to be excreted renally or effectively metabolized. One stop-gap approach to this problem is to append a small molecule cargo to the backbone through a cleavable linker (Figure 1.8A). When stimulated by a change in pH[99-102] or exposure to light,[103,104] the small molecule is released and can to interact with its biological target. Still, because it is non-degradable, the backbone remains.

Table 1.1. Monomers for the synthesis of biologically active polymers. R=ligand or other bioactive group.

Entry	**Monomer**	**Polymer**	**Attributes**
1	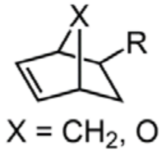	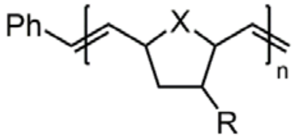	• Living polymerization with all catalysts • Fast polymerization rate
2	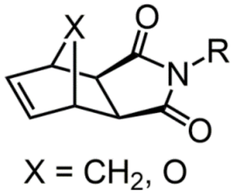	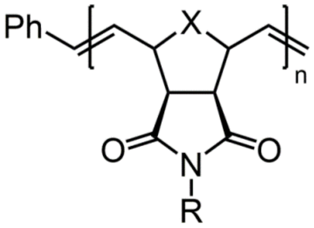	• Living polymerization with all catalysts • Fast polymerization rate
3	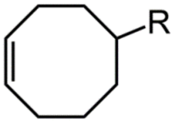	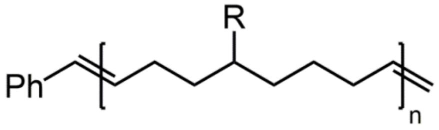	• Living polymerization with catalyst **1.05** • Flexible backbone
4	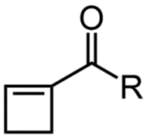	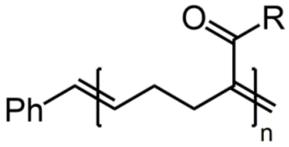	• Stereoregular backbone • Controlled regiochemistry • Living polymerization with catalyst **1.05**
5	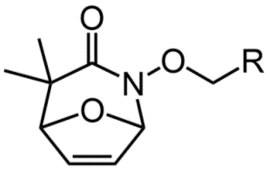	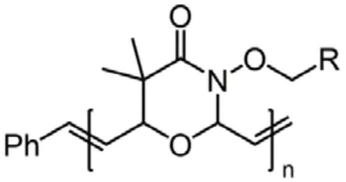	• Living polymerization with catalyst **1.05** • Degradable in acidic or basic media

A solution to the problem of ROMP polymer backbone degradability was reported recently.[57] The key was to identify 8-*oxo*-2-*aza*-bicyclo[3.2.1]oct-6-en-3-ones[105] as monomers with three important attributes (Figure 1.8C). First, these molecules are strained cycloolefins rendering them candidates for polymerization. Second, their polymerization leads to the presence of an oxazinone linkage incorporated along the polymer backbone. This heterocycle is stable at neutral pH but can be hydrolyzed in either acidic or basic media. Third, the polymers can be readily functionalized at a site distal to the bicyclic core. Thus, the properties and cargo of these polymers can be tailored without destabilizing or deleteriously affecting the reactivity of the monomer. Polyoxazinones are the first example, therefore, of a degradable and functionalizable ROMP polymer (Table 1.1, entry 5).[105] Whether or not these scaffolds are biodegradable is explored in this work.

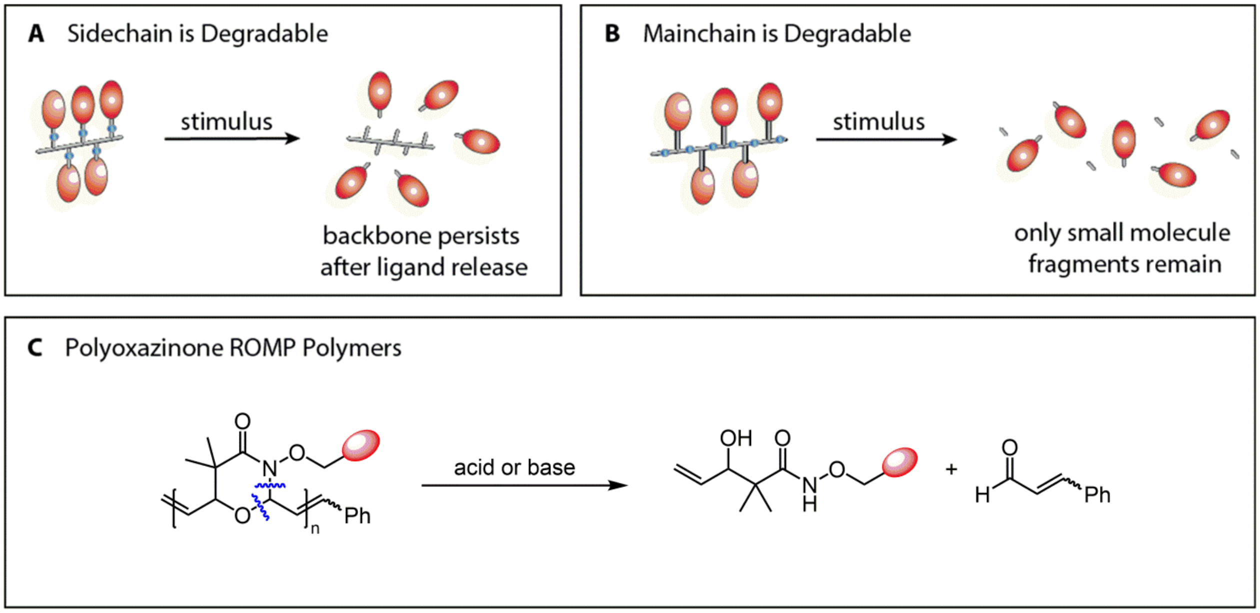
A Sidechain is Degradable
stimulus
backbone persists after ligand release
B Mainchain is Degradable
stimulus
only small molecule fragments remain
C Polyoxazinone ROMP Polymers
O
N
O
O
n
Ph
acid or base
OH
O
N
H
O
+
O
H
Ph

Figure 1.8. A) Therapeutic polymers containing cleavable linkers between the polymer backbone and its cargo. After cargo release, the non-degradable backbone persists. B) Main-chain degradable polymers break down into small molecule fragments, which can be excreted renally. C) Polyoxazinone polymers represent the first main-chain degradable and functionalizable ROMP polymers.

1.3.3. Troubleshooting the Polymerization of Bioactive ROMP Monomers

Despite the functional group tolerance of ruthenium carbenes, the kind of densely functionalized monomers typically used for synthesizing biologically active polymers often pose challenges. The source of the problem is not always obvious. Some explanations include the solubility of the growing polymer, the aggregation state of the polymer or monomer, or deactivation of the ruthenium carbene by either the polymer or monomer. A strategy that side-steps these issues is to use post-polymerization modification (PPM), where a reactive polymer is generated to which ligands or other functional groups of interest can be conjugated (see Section 1.3.4).[17] There are cases, however, in which it is advantageous to devise methods to polymerize directly monomers bearing biologically active moieties. Accordingly, some chemical “tricks” have been developed to promote these types of reactions.

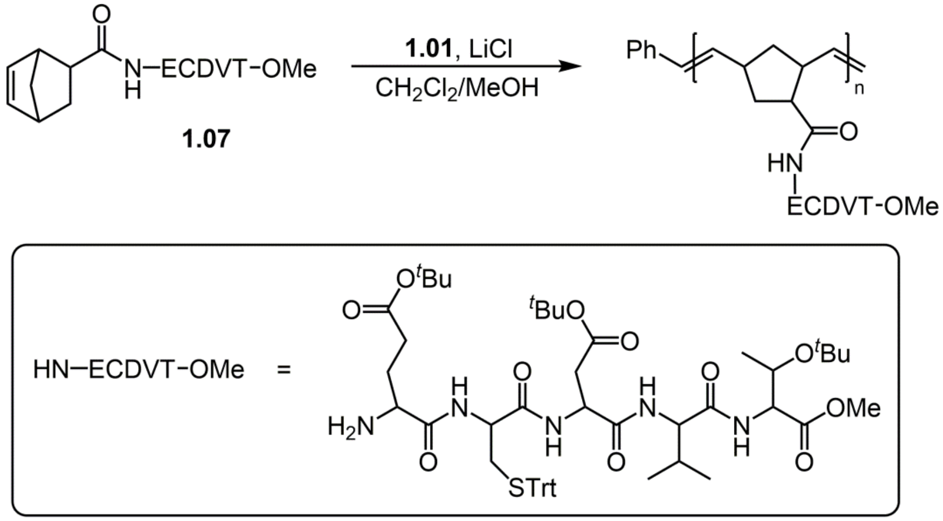

Figure 1.9. Additives, such as LiCl, can be introduced to facilitate the polymerization of monomers that aggregate in solution or chelate to ruthenium carbene intermediates.

An example in which aggregation posed a problem surfaced in the polymerization of monomers bearing the acid-rich oligopeptide sequence Glu-Cys-Asp-Val-Thr. Interest in generating polymers bearing this sequence was driven by its presence in fertilin*β*, a sperm protein that binds to the egg membrane.[106-108] Attempts to polymerize the peptide-substituted monomer led only to short oligomers (DP ~10), presumably because of monomer aggregation (Figure 1.9, **1.07**).[107] The authors found that adding lithium chloride, which is known to disrupt peptide aggregation, led to higher degrees of polymerization.

Another complication that often arises when polymerizing monomers bearing polar functional groups is chelation to the catalyst. Ruthenium carbene interaction with either the monomer or the growing polymer can interfere with elongation or completely prevent it. Primary and secondary amines and free thiols generally must be protected in ROMP. As a result, many polymers have been generated using protected monomers. For instance, the acid side chains of the aforementioned monomer bearing the Glu-Cys-Asp-Val-Thr sequence were protected as t-butyl esters and the thiol as a tritylthioether.

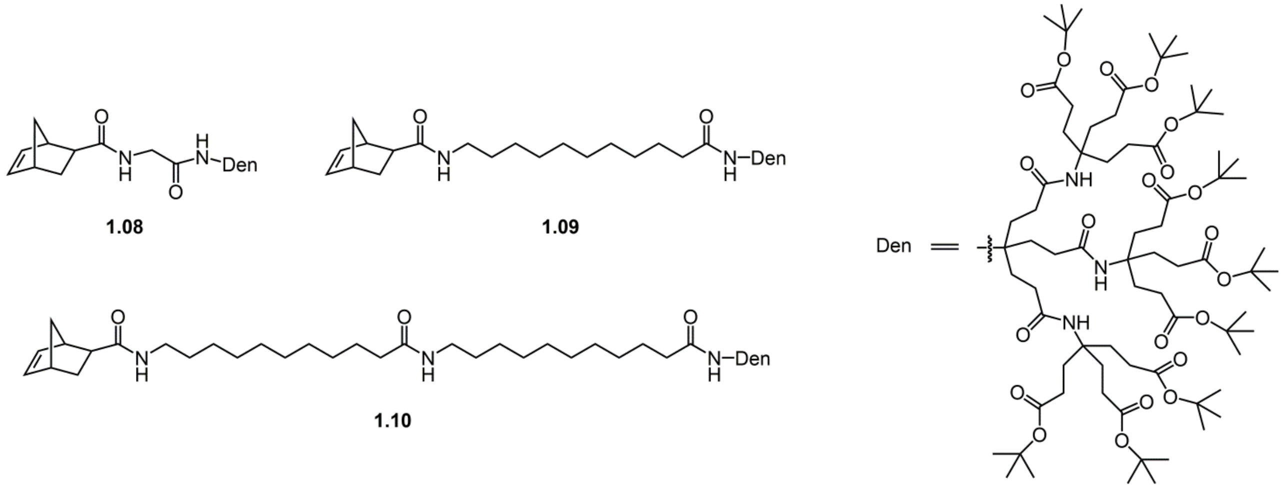

Figure 1.10. Steric congestion around the olefin functionality of **1.08** hindered polymerization. Increasing the linker length between the polymerizable norbornene and dendronized ligand alieviated the steric congestion and allowed high molecular weight polymers to be generated.

Steric effects can also interfere with ROMP. This problem surfaced in the preparation of dendronized polymers.[109] Efforts to generate these materials were driven by their potential utility in drug delivery, as the polymer backbone adopts a fully elongated conformation to accommodate the bulky side chains. When norbornene monomer **1.08** was exposed to ruthenium carbene **1.05** (Figure 1.10), only oligomers were obtained, presumably because the sterically demanding substituents blocked reaction at the alkene. This possibility was tested by varying the linker length between the polymerizable norbornene and the dendrimer substituent. An increase in linker length by 10 (**1.09**) or 20 (**1.10**) atoms led to large gains in the efficiency of polymerization. Although the biological activity of these polymers has not been assessed, their preparation provides guidance for the use of ROMP in generating polymers substituted with macromolecules, such as whole proteins.[110,111]

1.3.4. Routes to Functionalized ROMP Polymers

The results presented in Section 1.3.3 emerged in response to the challenges that arose when using pre-functionalized monomers. If this route is chosen for biological structure–function investigations, every type of polymer requires the synthesis of an appropriate pre-functionalized monomer, which then can be used in individual polymerization reactions to vary ligand composition, length, or density. To compare different polymers generated from different monomers, reaction conditions must be optimized, as monomers will vary in functionality and solubility and, therefore, reactivity. These differences in polymerization conditions can give rise to variations in polymer PDIs, degree of polymerization, or level of binding group substitution. Such variation can complicate comparison of polymer biological activities. With a post-polymerization modification (PPM) strategy, polymers displaying different ligands or different levels of ligand substitution can be generated from a single backbone and therefore compared directly (Figure 1.3). Still transformations carried out on the polymers must be high yielding and chemoselective. Accordingly, a variety of strategies for polymer conjugation have surfaced.

The initial application of PPM of polymers generated by ROMP exploited the reactivity of succinimidyl esters.[17] These activated esters are stable to the polymerization conditions and, in the presence of amines, are transformed efficiently into amides. Subsequently, other chemoselective reactions have been employed for PPM, including conjugate addition of thiols to maleimides, hydrazone or oxime formation from ketones or aldehydes, thiolate displacement of α-chloroacetamide groups, Diels-Alder reaction of maleimide-bearing polymers, and the azide-alkyne [3+2] cycloaddition.[21,112] There are some useful guidelines for applying these reactions. For the majority of the chemoselective reactions, it is beneficial if the polymer backbone displays the electron-deficient reactive group. In this configuration, the monomer does not contain nucleophilic groups that can coordinate to the catalyst. In the succinimidyl ester case, for example, it is preferable to install the activated ester in the monomer, as amines can hinder polymerization (vida supra). Similarly, polymers bearing maleimides or α-chloroacetamide groups have been generated from the corresponding monomers,[20,24,112] because monomers with thiol groups would be deleterious to the polymerization.[20,24,115] When oxime or hydrazone formation is used for conjugation, the backbone is generated such that it displays the carbonyl compound and not the nucleophile. Although both aldehydes and ketones can be used in this capacity, aldehyde-functionalized ROMP polymers tend to be only sparing soluble in organic solutions, rendering ketones are the more used electrophiles.[21]

The azide-alkyne [3+2] cycloaddition (AAC) is widely used in bioconjugate chemistry because this click reaction has exquisite chemoselectivity and efficiency.[113] AAC has been used with ROMP to create tailored polymers for biological applications,[57,112,117,118] however priming polymers for this reaction is not trivial because both azides and alkynes are incompatible with ruthenium catalysts.[114,115,116,117] Azides react with ruthenium to form a deactivated metalltetrazole species[119,120] while alkynes undergo metathesis themselves, which leads to increased polydispersity of the polymer products.[118,119] As a result, neither functional group used in AAC can be innocuously appended to a ROMP monomer, yet some strategies to combine ROMP and AAC have been developed.[114] One technique is to perform the AAC bioconjugation reaction before polymerization (Figure 1.11A).[57] The resultant triazole does not interact with the catalyst and the pre-functionalized monomer readily undergoes polymerization. If a PPM strategy is preferred, an alkyl bromide can be subjected to polymerization and the bromide substituents in the resulting polymer can be converted to alkyl azides, which can be further elaborated (Figure 1.11B).[21] In addition, azide-containing enol ether capping agents can be used.[56] Alternatively, a monomer containing a protected trimethylsilyl alkyne can be polymerized (Figure 1.11C).[112] The silyl group protects the alkyne from metathesis, and polymers with reasonable polydispersities (1.3-1.5) are obtained. After polymerization, the silyl group can be removed and AAC can be carried out.

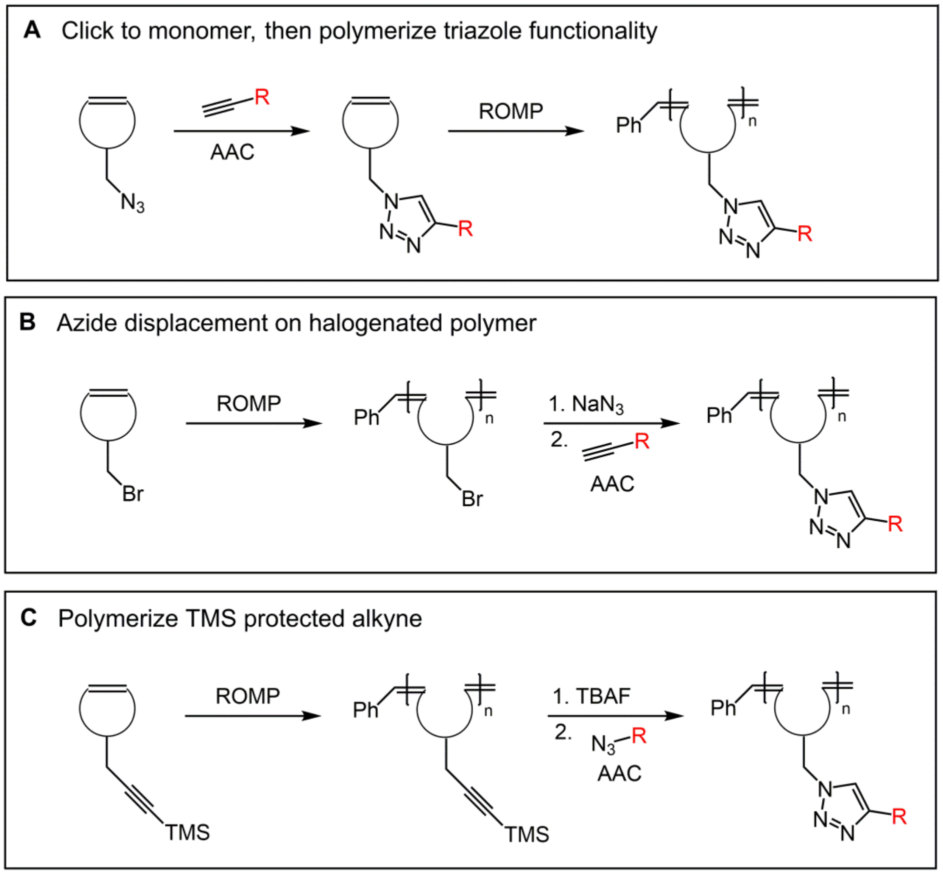
A Click to monomer, then polymerize triazole functionality
R
AAC
N3
ROMP
N
N
N
R
Ph
n
N
N
N
R
B Azide displacement on halogenated polymer
ROMP
Br
Ph
n
Br
1. NaN3
2.
R
AAC
Ph
n
N
N
N
R
C Polymerize TMS protected alkyne
ROMP
TMS
Ph
n
TMS
1. TBAF
2.
N3–R
AAC
Ph
n
N
N
N
R

Figure 1.11. Strategies to combine AAC and ROMP: A) A pre-functionalized monomer that contains a metathesis-compatible triazole can be employed. B) Post-polymerization modification of a halogenated polymer with sodium azide and furthur elaboration with AAC yields modified polymers. C) A monomer bearing a TMS-protected alkyne can be polymerized and the silyl group can be removed to reveal a polymer amenable to AAC. (TMS = trimethylsilyl, TBAF = tetrabutyl ammonium fluoride).

Most polymers used for PPM present a single reactive functional group. However, the copolymerization of differentially functionalized ROMP monomers is also facile and efficient (Figure 1.2).[20,23,112,120] If the polymer is to present multiple recognition epitopes, a mixture of monomers bearing chemoselective nucleophilic handles can be randomly copolymerized to afford polymers that present different reactive sites on the polymer. This approach offers no control over the regiochemistry of the recognition elements. On the other hand, block copolymers can be used to segment different binding groups to each half of a polymer chain.[121-124] This mode of epitope presentation contrasts with that offered with alternating or random copolymers, in which the binding epitopes are intermixed.[125,126] In one example, differentially reactive block copolymers were prepared as precursor scaffolds to yield polymers in which each domain has a distinct biological activity (i.e., a cell uptake domain appended to a protein binding domain).[23] In addition, reactive block copolymers have been exploited to rapidly generate a collection of functionalized polymers by a catch and release strategy. Specifically, a copolymer containing a succinimidyl ester block and maleimide block was generated. The maleimide block was used to immobilize the polymer on furan-functionalized beads, which aided in polymer isolation and purification, while the amine reactive block was used to conjugate recognition elements.[20] Finally, Gradient copolymers can also be synthesized by controlling the ratio of two different binding epitopes (or a binding and non-binding epitope) in the polymer modification reaction.[127]

In addition to covalent modifications, non-covalent ligand conjugation can also be employed. One non-covalent functionalization strategy relies on hydrogen bonding partners, such as the Hamilton wedge[128,129] or DNA duplex[130]. Because hydrogen bonding networks typically are not stable in aqueous solutions, the major applications for ROMP polymers functionalized with hydrogen-bonding groups are in the realm of diagnostic devices that interact with biological molecules *in vitro*.[130] A related strategy is to exploit metal chelation,[123,128,131] as illustrated by the generation of biocompatible quantum dots for *in vivo* imaging. Although metal-ligand interactions are more stable in aqueous media than hydrogen bonds, free metals are often highly toxic, which limits the use of ROMP scaffolds bearing metal complexes with low affinities.

1.4. ROMP Polymers as Imaging Agents

Fluorescent imaging methods have transformed our understanding of many aspects of biology, but there are many barriers to using fluorescence for *in vivo* imaging in mammals. Some probes are not water soluble or only exhibit high quantum yields when in a hydrophobic environment. Ohe and Sleimann have separately shown that these limitations can be circumvented by incorporating fluorescent dyes into polynorbornene nanoparticles (Figure 1.12A).[132-135] The hydrophobic core of these particles allows the dyes to shine brightly while the polyethylene glycol (PEG) grafts solubilize the aggregate in aqueous media. In addition, incorporation of reactive succinimidyl esters along the hydrophilic block provides the means to conjugate functional moieties. Fluorescent polymer **1.11** has valuable attributes for clinical imaging applications because it relies on near-IR radiation, which can penetrate through skin.[132,133]

Positron emission tomography (PET) imaging is a powerful imaging modality that is used widely in medical clinics. A challenge to generating materials for PET imaging is that they must be equipped with short-lived radioisotopes, such as ^{18}F. Thus, any synthetic route must have a means of rapidly installing the radioisotope. Matson and Grubbs demonstrated that ROMP can readily be adapted to generate PET imaging probes.[90] They generated an amphiphilic block copolymer **1.12** that self assembles into polymeric micelles in water (Figure 1.12B). These micelles can be covalently cross-linked through their photo-reactive cinnamoyl group. The key feature of the resulting nanoparticles is that they bear mesylate groups, so ^{18}F can be introduced via nucleophilic displacement. The ability to introduce the radiolabel on a short time scales and in the final synthetic step are assets for clinical applications.[136,137] In addition, the size of the stabilized nanoparticles should allow them to passively accumulate in tumors.[138]

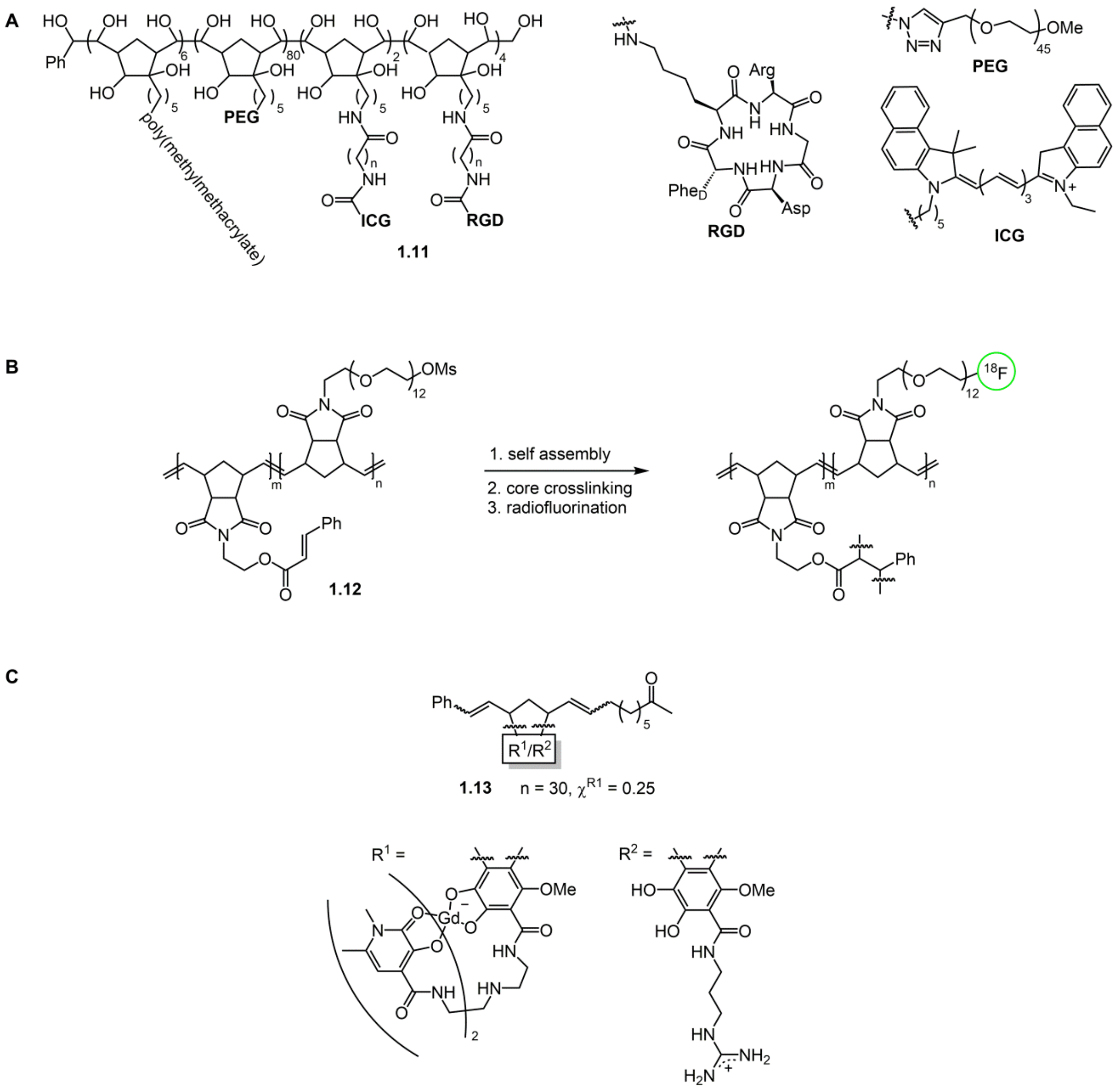
A
poly(methylmethacrylate)
PEG
ICG
RGD
1.11
Arg
Asp
Phe_D
B
OMs
12
1. self assembly
2. core crosslinking
3. radiofluorination
18F
1.12
C
Ph
R1/R2
1.13 n = 30, χR1 = 0.25
R1 =
R2 =
Gd
OMe

Figure 1.12. Polynorbornene *in vivo* imaging agents A) Near-IR indocyanine green (ICG) fluorophore conjugate. B) UV cross-linked polymer nanoparticle functionalized with PET emitting ^{18}F isotope. C) Multivalent gadolinium chelate for MRI imaging.

Magnetic resonance imaging (MRI) is an indispensable tool for identifying structural abnormalities in soft tissue that occur as a result of tumors or ligament damage. MRI relies on detecting differences in the relaxivity of ^1H_2O between tissue types.[139] Because the inherent relaxivity of ^1H_2O is slow, gadolinium(III) contrast agents are administered to increase relaxivity rates and sharpen the images.[140,141] Commercial MRI contrast agents contain a single Gd^{3+} per molecule, but ligands that possess multiple Gd^{3+} further augment relaxivity.[142-144] To this end, Allen et al. demonstrated that polynorbornene **1.13**, containing hydroxypyridonate ligands, could chelate multiple Gd^{3+} ions (Figure 1.12C).[131] As designed, this polymer had a molecular relaxivity 30-times greater than contrast agents currently administered.[145] Because the polymer contained a ketone at the chain-end, it could be elaborated to append a tissue targeting ligand to further sharpen the MRI images. Together, these examples highlight the potential of polynorbornene ROMP-polymers as imaging agents in fluorescence, PET, and MRI applications.

1.5. ROMP Polymers as Probes of Biological Processes.

Many biologically relevant interactions are multivalent, i.e. they involve multiple binding groups interacting with multiple binding sites.[2,5,146] Mammalian antibodies are oligomeric, as are many carbohydrate-binding proteins that participate in cell adhesion or host–pathogen interactions. By virtue of their ability to occupy multiple binding sites simultaneously, multivalent ligands can bind avidly to oligomeric proteins or even cell surfaces. In this way, they can serve as potent *inhibitors*. Additionally, polymers can act as *effectors* by clustering membrane bound proteins and, thereby, activating specific signaling pathways.

An intriguing feature of multivalent ligands is their ability to use different binding modes to optimize their specificity and activity (Figure 1.13).[2,147] The ability of a multivalent ligand to exploit these mechanisms depends upon its structure as well as that of the receptor of interest.[148] Variables such as the valency of the display, the density and orientation of the displayed epitopes, the distance between those epitopes and the distance between receptor binding sites may all affect how a multivalent ligand interacts with its receptor. Furthermore, multivalent ligands rarely utilize a single binding mechanism. For example, ligands that act via the chelate effect may also be able to cluster receptors under the appropriate conditions. In a study comparing the ability of different multivalent scaffolds to operate via distinct binding modes, Gestwicki et al. found that polymers generated by ROMP were especially effective at clustering proteins.[27] This attribute renders them well-suited to serve not only as inhibitors but also as biological activators.

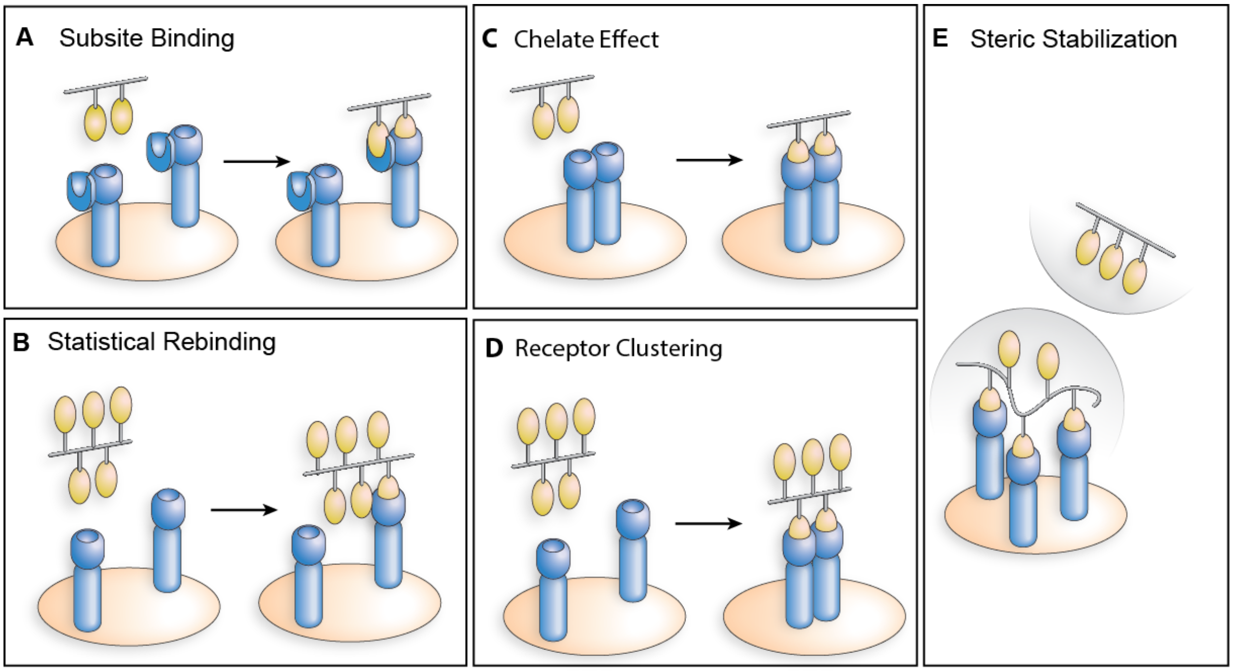

Figure 1.13. Multivalent ligands can engage a target receptor through different binding modes: (A) Subsite binding, (B) statistical rebinding, (C) chelate effect, (D) receptor clustering, (E) steric stabilization. Adapted from reference 3.

Polymers are outstanding platforms for generating multivalent ligands, as their repeating structures are naturally suited for presenting multiple binding groups. The level of control over polymer architecture and size afforded by ROMP provides a means to assess structure-activity relationships.[27] The following section highlights examples of how ROMP polmers can yield insights into multivalent interactions in biology.

1.5.1. ROMP Polymers as Inhibitors

The first protein-binding ROMP polymers were multivalent carbohydrate derivatives.[69] These compounds blocked the ability of the tetrameric glucose-binding protein concanavaline A (ConA) to cluster cells and were >1000-fold more potent than a monovalent glucose derivative. Intriguingly, the polymers were not only highly active but also exhibited high selectivity.[149] These studies underscored that ROMP could yield polymers that potently inhibit cell–cell interactions. Spurred by this result, our lab and others have applied bioactive ROMP polymers to other systems in which they act as inhibitors of biological processes. Polymers generated by ROMP that display sulfated carbohydrates have been used to inhibit glycoprotein–lectin interactions that occur in the inflammatory/immune response.[66,243,244] In addition, the Hsieh-Wilson group demonstrated that polycyclooctene conjugated to a chondroitin sulfate E (CS-E) tetrasaccharide is sufficient to mimic natural CS-E functionalized glycosaminoglycans when immobilized on a surface.[150-153] Interestingly, the polymer inhibited neurite outgrowth with the same potency as the natural polysaccharide even though the morphologies of the two inhibitors are different.[29] Finally, the Sampson lab showed that multivalent displays of a short peptide sequence, Glu-Cys-Asp (ECD), isolated from the protein fertilinβ, found on sperm cells, can serve as a ligand for the $\alpha_6\beta_1$ integrin, displayed on the surface of eggs.[154,155] These peptide-functionalized ROMP polymers blocked gamete fertilization,[31,108,156] leading to the conclusion that interactions between fertilinβ and $\alpha_6\beta_1$ contribute to sperm-egg adhesion.[156]

1.5.2. ROMP Polymers as Effectors

To explore how a ligand's structure influences its mechanism of action, Gestwicki et al. synthesized a series of diverse scaffolds and assessed their interaction with a single protein using four different assays.[27,148] These studies were devised to investigate how the architecture of a ligand influences its ability to inhibit or cluster receptors. Specific aspects of ligand-promoted clustering were tested including the rate of cluster formation, the size of the cluster and the distance between the individual receptors within a cluster. The ligands tested included a series of polymers generated by ROMP that differed in their degree of polymerization, small molecules, globular proteins, dendrimers, and polydisperse polymers (polyethylene maleic anhydride-substituted, PEMA). While ROMP polymers again proved to be effective inhibitors, ligand-conjugated proteins and polydisperse PEMA were equally potent in these inhibition assays. On the other hand, compared to all other ligands, the polymerrs generated by ROMP are especially well-suited for controlling various aspects of receptor clustering. They were superior to the other ligands tested at rapidly clustering receptors and they were the most effective at bringing receptors into close proximity. Because these factors are critical for transducing signals, polymers generated by ROMP are especially useful as effectors of receptor clustering and signal transduction.[26,157-161]

An example of where polymeric effectors have been used is in immune cell signalling. Immune cells must distinguish host cells from pathogens to appropriately trigger immune responses.[162,163] On B cells, which are capable of differentiating into antibody producing cells, the B cell antigen receptor (BCR) serves as a critical regulator of immune activation. When an antigen binds the cell surface BCR, this binding induces a signaling cascade that either leads to clonal expansion and antibody production (i.e., immunity) or tolerance.[162] To study directly how antigen valency influences output through the BCR, Kiessling and co-workers used bioactive ROMP polymer **1.14**, decorated with the immunogenic dinitrophenyl (DNP) hapten (Figure 1.14).[28,164] One downstream effect of antigen-induced signaling in B cells is an increase in intracellular calcium ion concentration. When B cells are exposed to polymer **1.14**, calcium flux occurs.[28] The increases in intracellular calcium levels depend on polymer valency, and longer polymers are more potent inducers of signaling. Interestingly, non-participatory receptors were recruited to the clusters, suggesting that this may be a general mechanism for signal amplification.[26,165,166]

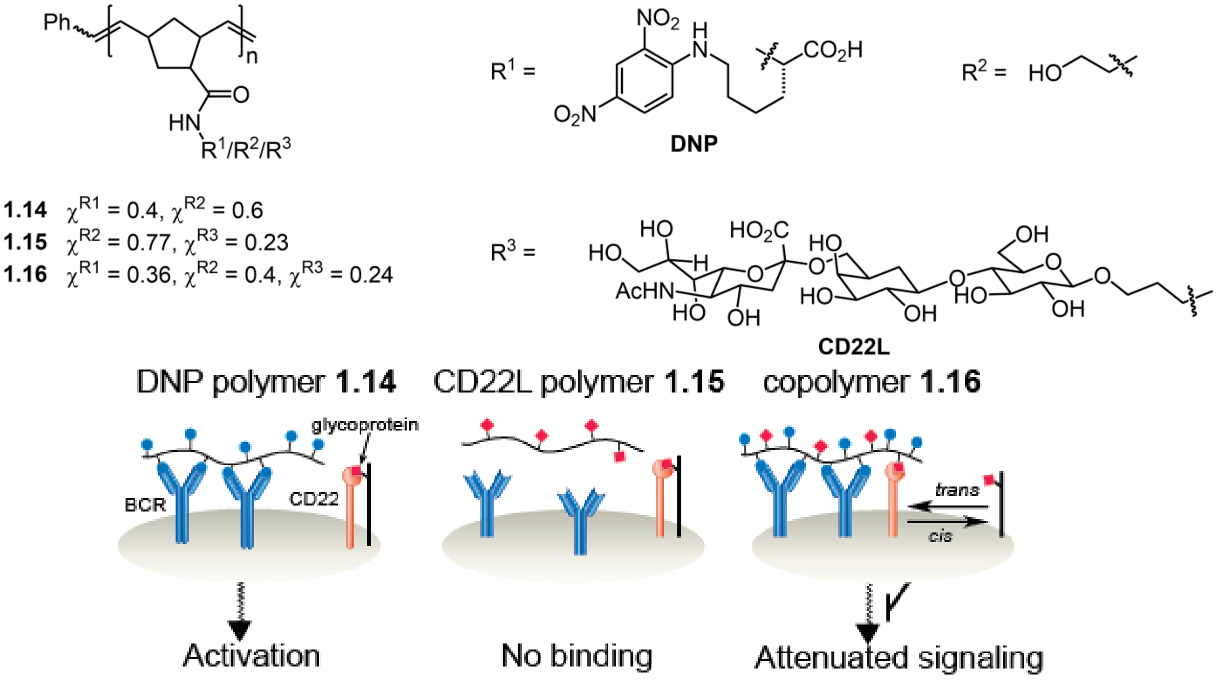
Ph
n
O
HN
$R^1/R^2/R^3$
1.14 $\chi^{R1} = 0.4$, $\chi^{R2} = 0.6$
1.15 $\chi^{R2} = 0.77$, $\chi^{R3} = 0.23$
1.16 $\chi^{R1} = 0.36$, $\chi^{R2} = 0.4$, $\chi^{R3} = 0.24$
R^1 =
NO_2
H
N
CO_2H
O_2N
DNP
R^2 = HO
R^3 =
HO
HO_2C
HO
OH
HO
H
O
O
O
O
O
AcHN
HO
OH
HO
OH
HO
OH
CD22L
DNP polymer **1.14**
CD22L polymer **1.15**
copolymer **1.16**
glycoprotein
BCR
CD22
trans
cis
Activation
No binding
Attenuated signaling

Figure 1.14. ROMP polymers can serve as synthetic antigens to study immune cell signaling.

1.5.3. Cell Penetrating ROMP Polymers

Polymers are effective tools for studying biological processes that occur in the extracellular milieu or on the cell surface, but the size of these macromolecules prevents cell internalization by passive means. This barrier has limited the investigation of biological processes inside cells using polymers. A general strategy to facilitate polymer uptake into the cytoplasm could provide novel therapeutic strategies and illuminate signaling processes.

1.5.3.1. ROMP Polymers as Artificial Translocation Domains

Certain proteins, such as HIV-TAT, contain arginine-rich domains that allow non-specific translocation of large particles across cell membranes (Figure 1.15).[167-171] Internalization is believed to occur through association of guanidinium groups on the protein with negatively charged sulfate groups of cell-surface glycosaminoglycans (GAGs).[172] Inspired by these protein transduction domains (PTD), Kolonko et al. demonstrated that guanidinium functionalized polynorbornenes were transported through eukaryotic membranes (Figure 1.15, **1.17**, **1.18**).[23,82] Using the length control afforded by ROMP, the authors determined that the optimum number of guanidinium repeats for polymer internalization mirrored the number of arginine residues found in natural PTDs.[173]

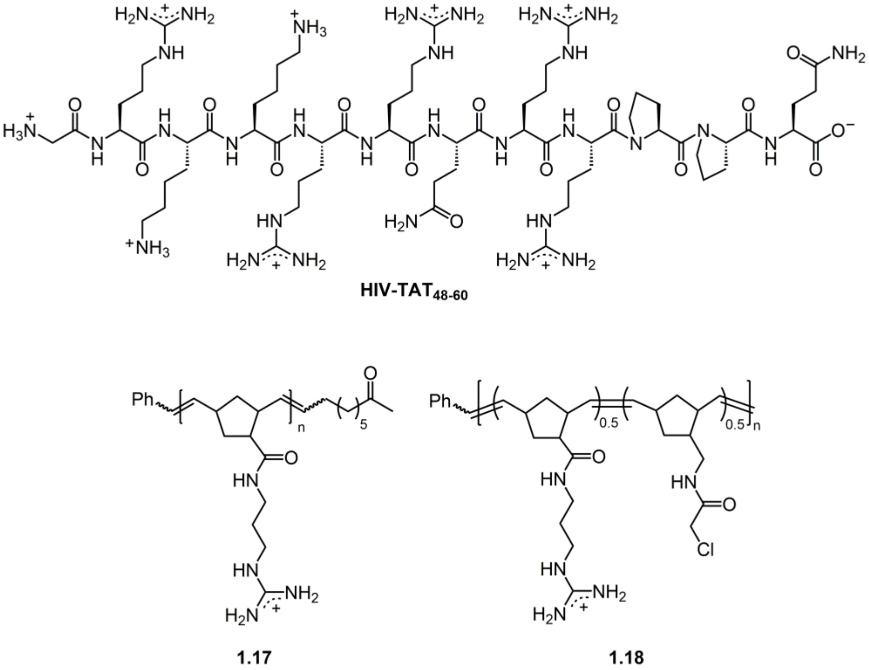

HIV-TAT$_{48\text{-}60}$

1.17 **1.18**

Figure 1.15. ROMP polymers decorated with a polyguanidinium block mimic protein transduction domains and promote polymer internalization into mammalian cells.

To expand the utility of cell penetrating ROMP polymers, modifications were envisioned to allow their multi-functionalization. End-functionalized polymer **1.17** and block copolymer **1.18** were generated, as each can be elaborated via PPM.[23,82] Polymer **1.17** allows a single moiety to be appended to the chain-end of the polymer.[82] This reactivity allows control over the regiochemistry of the desired ligand. If multiple copies of a ligand are needed, however, polymer **1.18** can be used.[23] This entity was generated by reaction of a succinimidyl ester block with an amine. The chloroacetamide block, which reacts more slowly with amines, can subsequently be modified by thiol alkylation to afford tailored ROMP polymers. Both functionalized polymers can pass through mammalian cell membranes. Therefore, these polymers can deliver molecules to the cell's interior.

1.5.3.2. Targeted Delivery: B Cell Internalization

The polymers described in Section 1.5.3.1. indiscriminately cross mammalian cell membranes. Polymers can also be designed to be internalized only by specific cell types or through specific receptors. For instance, in addition to signaling, the B-cell receptor can internalize antigen.[174,175] Accordingly, the DNP-functionalized polymer **1.19** can be internalized by B cells (Figure 1.16). This process was able to be tracked because polymer **1.19** was functionalized at the chain-end with a profluorophore developed by Raines and co-workers.[56,176,177] The profluorophore contains an esterase-sensitive trimethyl lock that is unraveled by cellular esterases to unmask the rhodamine fluorophore.[178] As a zero-background reporter for polymer internalization that eliminates the need for subsequent washing steps, this polymer labeling strategy affords a highly effective probe of uptake. Typically, receptor internalization (rather than cargo internalization) is assessed through staining the receptors on the exterior of the cell. By comparing the fluorescence of a cell at a given time point to the initial fluorescence of the cell, the number of receptors internalized can be quantified. On the other hand, the ability to track polymer **1.19**'s internalization is of high value for applications such as drug delivery or gene therapy, a need that compound **1.19** addresses.[1,179-183] This application also highlights the utility of end-capping polymers with fluorophores for cellular imaging. These studies open the door for tissue-specific cargo delivery to immune cells.

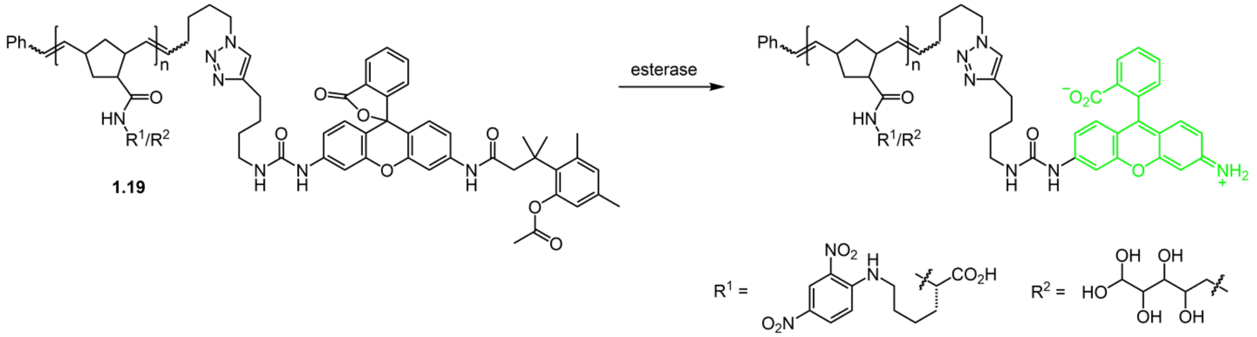

Figure 1.16. A caged fluorophore was used to monitor internalization of ROMP polymers by B cells. When exposed to intracellular esterases, the fluorophore is revealed.

1.5.4. Assembling Multi-Protein Complexes

Many accounts document that ROMP polymers can serve as both inhibitors and effectors of cell surface receptors (vida supra). Still, the aforementioned polymers interact with but a single type of receptor. These studies illuminate on the molecular mechanisms of multivalent interactions. Another frontier is to affect the organization of multi-protein complexes in physiological settings. In this way, insight into the *regulation* of signaling pathways can be gleaned. This objective requires synthetic multivalent ligands that interact with multiple distinct proteins simultaneously. As multiple ligands can be conjugated to a single ROMP backbone,[17] the synthesis of multifunctional polymers that cluster variegated cell surface receptors is attainable and this strategy offers a new powerful strategy to tune polymer activity and specificity.

Signaling events involved in regulating the immune system often rely on the use of co-receptors to augment or diminish a given response. As an example, the lectin CD22 is a co-receptor for the BCR that has been shown to down-regulate BRC activity.[184,185] CD22 binds glycoconjugates with terminal sialic acid residues. Ligands of this type can be found on the B-cell surface or on antigens.[186,187] Therefore, CD22 can be engaged by glycoproteins on its own surface (*cis* interactions) or on an antigen (*trans* interactions). While *cis* interactions have been established to be important for modulating immunity,[186] it was not clear if signal suppression could happen *in trans*. This issue is important in understanding whether sialic acid containing glycans aid in suppressing immune responses. Addressing this question not only provides insight into mechanisms of mammalian immunity and tolerance but also into the design of effective vaccines.

Multifunctional polymer **1.16** represented the first well defined antigen that could answer this question (Figure 1.14).[164] Specifically, the ability to decorate ROMP polymers with both DNP and the CD22 ligand Neu5Acα2,6Galβ1,4Glc (CD22L) with control over ligand density was exploited to obtain a definitive answer. Exposure of polymer **1.16** to B cells lead to signal attenuation relative to DNP-containing homopolymer **1.14**. Additionally, a mixture of **1.14** and polymer **1.15**, conjugated to CD22L but not DNP, produced a robust signal. These findings indicate that sialic acid containing antigens can indeed engage CD22 *in trans*, and that co-clustering the BCR and CD22 attenuates BCR signaling. Thus, the display of sialylated glycans that bind CD22 on self-cells could be a mechanism to suppress B cell activation and regulate autoimmunity. In addition, the results with polymer **1.16** open the door to create similar copolymers that generate complex protein assemblies that induce a unique response. In this way, mechanisms can be explored that regulate signal strength or even deliver new types of chemical signals to cells.

1.6. Outlook

In summary, the applications of ROMP polymers to biology have grown exponentially since their first use. We anticipate that the rapid advances in creative catalyst design combined with the development of new synthetic methods will provide the infrastructure to implement imaginative applications of ROMP to biology. In addition, there have also been recent efforts in the design of novel ROMP derived biomaterials for tissue engineering and cell culture. While this emerging field was not the focus of this chapter, it is expect to also have a widespread impact in the coming years.

Chapter 2: Synthesis of a Functionalizable and Degradable Polymer by ROMP

Portions of this work have been published in:

Fishman, J.M.; Kiessling, L.L. Synthesis of functionalizable and degradable polymers by ring-opening methathesis polymerization. *Angew. Chem. Int. Ed.* **2013**, *52*, 5061.

2.1. Identification of Bicyclic Oxazinones as Substrates for ROMP

A valuable approach for creating synthetic polymers is the ring-opening metathesis polymerization (ROMP).[188-190] Well-defined metal carbene catalysts have been devised that afford control over the polymer chain length and architecture.[11,191-194] In addition, ruthenium carbene intiators have been developed with excellent air stability and functional group tolerance.[88,194] These catalysts enable the synthesis of polymers with a range of functionality,[5,28,49,62,108,164,195,196] thereby providing access to polymers for diverse applications.[128,196-198]

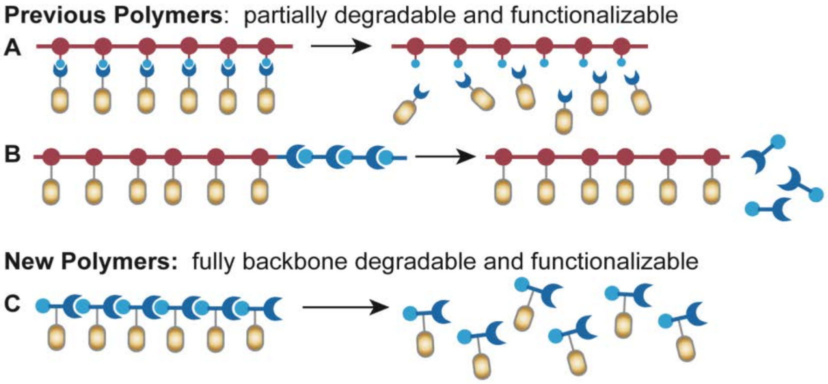
Previous Polymers: partially degradable and functionalizable
A
B
New Polymers: fully backbone degradable and functionalizable
C

Figure 2.1. Strategies to synthesize functionalizable and degradable ROMP polymers: a) ligand attachment via a cleavable linker, b) copolymerization with a sacrificial monomer, and c) homopolymerization of a functionalizable, heterocyclic oxazinone.

Extant polymers from ROMP, like the majority of synthetic polymers, are non-degradable. They therefore lead to refuse accumulation. A functional and degradable polymer from ROMP would allow the synthetically useful traits of ROMP reactions to be combined with the growing need for new degradable polymer scaffolds. To date, efforts to prepare degradable materials using ROMP have afforded polymers that are either functional or partially hydrolysable, but not both (Figure 2.1). For example, cargo can be attached via a linker such that it can be released from the polymer backbone by photolysis or hydrolysis in acid.[99,101,196,199] Still, the polymeric backbone persists. Alternatively, partially degradable polymers have been generated. A block copolymer can be generated from a modifiable monomer and a sacrificial dioxepine or dithiepine monomer.[49,200,201] In this scenario, one block is composed of a non-hydrolysable backbone and the degradable block contains acid-labile acetals or thioacetals that can be cleaved by hydrogenation. Polymers of this type only undergo partial degradation, as one block persists. Therefore, the current state-of-the-art demands a compromise between generating polymers that can be customized and polymers that can be easily degraded.

Applying ROMP to synthesize a modifiable homopolymer with a degradable backbone requires a monomer with three important attributes. First, it must be a strained cyclic or bicyclic olefin, so that it undergoes polymerization.[202] Second, it must contain core functionality that gives rise to a polymer that can be degraded. Third, a means to append desired functionality onto the monomer or polymer is needed to enable polymer diversification. Monomers with all of these attributes have been elusive. Many strained olefinic heterocycles spontaneously aromatize.[203,204] In addition, attempts to incorporate handles for diversification can further increase monomer instability.[205] Thus, traditional monomers used in ROMP cannot be simply modified to instil polymer degradability.

We sought a new class of monomers that would give rise to degradable materials. The generation of substrates with an 8-*oxo*-2-azabicylo[3.2.1]oct-6-en-3-one framework through a novel *aza*-[4+3] cycloaddition was recently reported (Scheme 2.1A).[105] We postulated that this bicyclic oxazinone would be a substrate for ROMP. Calculations suggest that this framework has a ring strain of 13.4 kcal/mol, which is comparable to that of *trans*-cyclooctene (a monomer that has favourable kinetics of polymerization using ROMP).[202,206] Reports of successful ring-opening cross metathesis on architecturally analogous 8-*oxo*-bicyclo[3.2.1.]oct-6-en-3-ones provided additional impetus.[207,208] Significantly, if the bicyclic oxazinone serves as a monomer in ROMP, the resulting framework should be both acid and base labile (Scheme 2.1B). Moreover, we postulated that we could modify this core monomer at a site distal to the polymerizable moieties and bridgehead carbons. Thus, without destabilizing the heterocycle, we could tailor the properties of the resulting materials. Methods to polymerize bicyclic oxazinones by ROMP and routes to functionalize the polyoxazinone backbone are discussed. Additionally, the propensity for the hydrolysable backbone to degrade is explored.

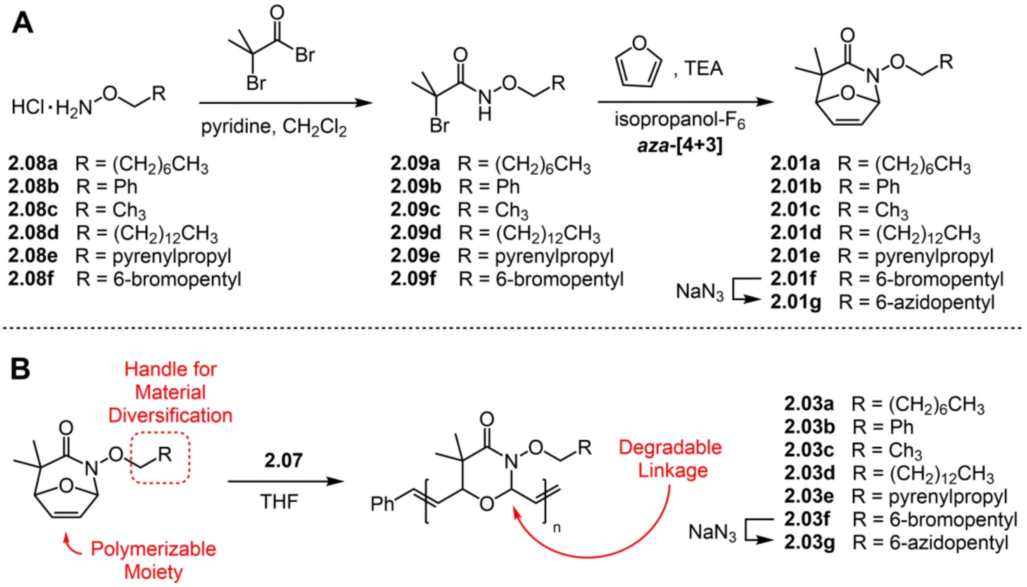
A
HCl·H2N–O–R
pyridine, CH2Cl2
, TEA
isopropanol-F6
aza-[4+3]
2.08a R = (CH2)6CH3
2.08b R = Ph
2.08c R = Ch3
2.08d R = (CH2)12CH3
2.08e R = pyrenylpropyl
2.08f R = 6-bromopentyl
2.09a R = (CH2)6CH3
2.09b R = Ph
2.09c R = Ch3
2.09d R = (CH2)12CH3
2.09e R = pyrenylpropyl
2.09f R = 6-bromopentyl
2.01a R = (CH2)6CH3
2.01b R = Ph
2.01c R = Ch3
2.01d R = (CH2)12CH3
2.01e R = pyrenylpropyl
2.01f R = 6-bromopentyl
NaN3
2.01g R = 6-azidopentyl
B
Handle for Material Diversification
Polymerizable Moiety
2.07
THF
Degradable Linkage
2.03a R = (CH2)6CH3
2.03b R = Ph
2.03c R = Ch3
2.03d R = (CH2)12CH3
2.03e R = pyrenylpropyl
2.03f R = 6-bromopentyl
NaN3
2.03g R = 6-azidopentyl

Scheme 2.1. Synthesis of a library of bicyclic oxazinone monomers that undergo ROMP to afford degradable polyoxazinones.

2.2. Polymerization of Bicylic Oxazinones

Despite our optimism that bicyclic oxazinones would serve as a monomer, we had concerns that its polymerization would yield highly oxygenated polymer products that would facilitate backbiting.[209,210] Our initial results confirmed our suspicions. The reaction of **2.01a** using Grubbs' second generation catalyst (**2.02**)[74] in chloroform afforded polymer **2.03a** (Table 2.2, entry 1), but we observed a concomitant increase in the PDI and decrease in the number averaged molecular weight (M_n) of the products as the polymerization progressed (Table 2.1).

Furthermore, after polymerization had arrested, dimer **2.04** began to evolve (Scheme 2.2). This species represents the elimination of the penultimate and terminal repeats of polymer **2.03a** by backbiting.

Table 2.1. Evidence for backbiting during the polymerization of oxazinone monomers.

entry[a]	time [h]	conv [%][b]	$M_n^{theo\,[c]}$ [g/mol]	$M_n^{GPC\,[d]}$ [g/mol]	PDI [M_n/M_w]
1	1	41	1100	13800	1.7
2	3	66	1700	11700	1.8
3	7	92	2400	9400	2.0
4	13	92	2400	8800	2.1
5	20	97[e]	2500	2600	2.6

[a] [**2.01b**]$_o$ = 1M in $CHCl_3$, [**2.01b**]$_o$/[**2.02**] = 10/1, 20 °C. [b] based off of ^{1}H-NMR integrations of monomer olefin signals to polymer olefin signals. [c] theoretical yield based off of monomer conversion. [d] calibrated with polystyrene standards, eluted in THF. [e] 15-20% cyclic dimer.

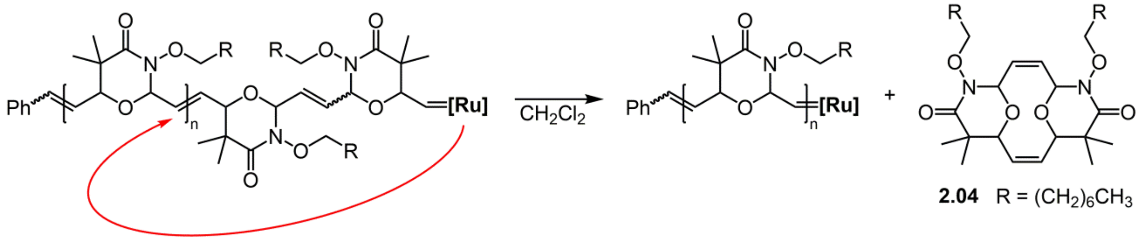

Scheme 2.2. Backbiting during the polymerization of bicyclic oxazinones led to the formation of cyclic dimers.

One strategy to mitigate backbiting is to raise the reaction temperature to disrupt dative bonds.[211-213] However, in our system, an increase in temperature did not reduce backbiting (Table 2.2, entry 2). Alternative conditions were screened to supress backbiting. Changing the solvent did not affect the polymerization of bicyclic oxazinones with catalyst **2.02** (Table 2.2, entries 3-5). In fact, some solvents, such as chlorobenzene or pyridine completely suppressed initiation. Screening different ROMP catalysts had varied effects on the polymerization of bicyclic oxazinones. Using catalysts with only phosphorous containing dative ligands, such as Grubbs' first generation catalyst (**2.05**) or Hoveyda-Grubbs' first generation catalyst (**2.06**), lead exclusively to the formation of dimer (Table 2.2, entry 6-7). Therefore, the rate of propagation for these catalysts is much less than the rate of ring-closing dimerization, which exacerbated backbiting. We then employed catalyst **2.07**,[88] which has superior polymerization kinetics to those obtained with the other catalysts. Indeed, this catalyst led to monodisperse polymer product with a PDI of 1.5 (Table 2.2, entry 8). Further enhancement of the PDI was observed when using catalyst **2.07** in oxygenated solvents, such as tetrahydrofuran (THF).[214] These changes afforded heightened control during the polymerization of **2.01a**. Under the optimized conditions, the molecular weight increased proportionally to monomer conversion during the polymerization (Figure 2.3). In addition, the M_n increased linearly with respect to the monomer to catalyst loading and the degree of polymerization (DP) agreed well with monomer conversion (Table 2.1, entry 9-13). We propose that the controlled polymerization of **2.01a** was achieve due to the synergy of the reaction kinetics of catalyst **2.07**, which promoted fast and complete monomer initiation, with the ability of oxygenated solvents to complete with the polydentate polymer ligand for catalyst coordination sites, which mitigated backbiting. Thus, bicyclic oxazinones are viable ROMP substrates that produce polymer scaffolds with a repeating oxazinane backbone.

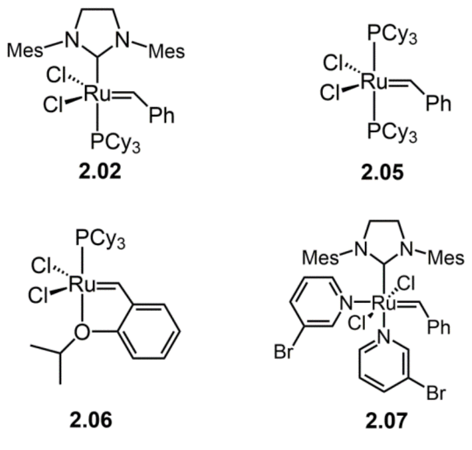

Figure 2.2. **C**atalysts screened while optimizing the polymerization of bicyclic oxazinones.

Table 2.2. Polymerization of bicyclic oxazinones by ROMP.

entry	**$[M]_o/[I]$**	**[M]**	**catalyst, I**	**solvent[a]**	**temp [^oC]**	**time [h]**	**conv [%][b]**	**Yield[c,d]**	**M_n^{theo} [g/mol]**	**$M_n^{NMR\ [e]}$ [g/mol]**	**$M_n^{GPC\ [f]}$ [g/mol]**	**PDI [f] [M_n/M_w]**
1	100/1	**2.01a**	**2.02**	$CHCl_3$	20	1	84	72	23600	103800	63200	2.8
2	100/1	**2.01a**	**2.02**	$CHCl_3$	45	18	81[g]	49	22800	26000	24900	2.6
3	10/1	**2.01b**	**2.02**	Benzene-Cl_6	20	1	nr	--	--	--	--	--
4	25/1	**2.01b**	**2.02**	THF	20	1	86	72	6750	unk	24800	2.6
5	10/1	**2.01b**	**2.02**	CH_2Cl_2	20	13	92	unk	2700	unk	8800	2.1
6	10/1	**2.01b**	**2.05**	CH_2Cl_2	20	1	dimer	n/a	--	--	--	--
7	10/1	**2.01b**	**2.06**	CH_2Cl_2	20	1	dimer	n/a	--	--	--	--
8	10/1	**2.01b**	**2.07**	CH_2Cl	20	1	96	96	2500	unk	3600	1.5
9	25/1	**2.01a**	**2.07**	THF	20	1	87	57	6100	6500	9300	1.4
10	50/1	**2.01a**	**2.07**	THF	20	1	85	71	12000	12500	16300	1.4
11	100/1	**2.01a**	**2.07**	THF	20	1	81	80	23100	22000	21600	1.4
12	100/1	**2.01a**	**2.07**	THF	20	18	81	85	23100	22100	22300	1.4
13	200/1	**2.01a**	**2.07**	THF	20	1	73	83	41000	45200	50300	1.5
14	25/1	**2.01b**	**2.07**	pyridine	20	15	nr	--	--	--	--	--

[a] $[M]_o$ = 1M. [b] based off of ^{1}H-NMR integrations of monomer olefin signals to polymer olefin signals. [c] isolated. [d] theoretical yield based off of monomer conversion. [e] based off ^{1}H-NMR integrations of polymers olefin signals and chain-end phenyl signals, when visible. [f] calibrated with polystyrene standards, eluted in THF, [g] additional 10-15% cyclic dimer.

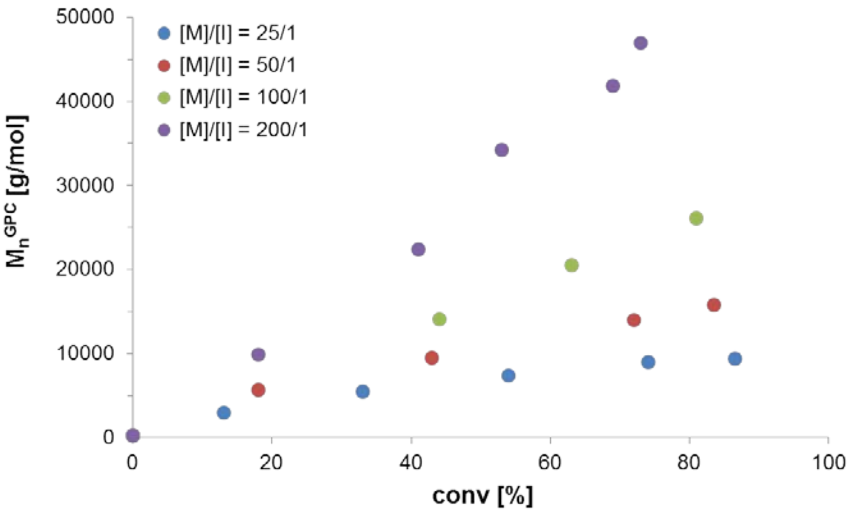

Figure 2.3. Polymerization of monomer **2.01a** under optimal conditions: [**2.01a**]$_o$ = 1 M in THF, catalyst = **2.07**, rt. The molecular weight linearly increases as a function of monomer conversion

Table 2.3. Polymerization of benzyl substituted monomer **2.01b**.

entry	**$[M]_o/[I]$[a]**	**Solvent**	**additive[b]**	**Temp [°C]**	**time [h]**	**conv [%][c]**	**yield[d,e]**	**M_n^{theo} [g/mol]**	**M_n^{GPC} [g/mol][f]**	**PDI [M_n/M_w]**
1	100/1	THF	--	20	1	80	n/a	20700	20500	3.3
2	25/1	$THF:CHCl_3$[g]	--	20	1	85	79	5500	8500	1.5
3	50/1	$THF:CHCl_3$[g]	--	20	1	78	85	10100	11300	1.7
4	100/1	$THF:CHCl_3$[g]	--	20	1	64	60	16700	18900	2.1
5	200/1	$THF:CHCl_3$[g]	--	20	1	57	66	29600	28500	2.1
6	100/1	$THF:CHCl_3$[g]	BCy_2Cl	20	1	92	69	23800	8400	1.7
7	200/1	$THF:CHCl_3$[g]	BCy_2Cl	20	1	93	73	48200	16000	1.8
8	500/1	$THF:CHCl_3$[g]	BCy_2Cl	20	1	84	66	108800	34700	2.2

[a] [**2.01b**]$_o$ = 1M, **I** = **2.07,** [b] 10 mol% (wrt **2.01b**), [c] based off of ^{1}H-NMR integrations of monomer olefin signals to polymer olefin signals, [d] isolated, [e] theoretical yield based off of monomer conversion, [f] calibrated with polystyrene standards, eluted in THF, [g] 1:1 (v/v).

The optimal polymerization conditions for monomer **2.01a** were found be applicable to other bicyclic oxazinone substrates that also possess alkyl hydroxyamic esters (vida infra). However, the same conditions were less effective at polymerizing bicyclic oxazinones with benzyl functionality, such as **2.01b** (Table 2.3, entry 1). The observed inflation in PDI when using benzyl substituted monomers is proposed to occur because of a decreased solubility of benzyl polyoxazinones in THF. This insolubility led to an observed increase in the viscosity of the polymerization milieu when using monomer **2.01b**, which prevented complete mixing of the monomers during the reaction. Therefore, oxygenated solvents may not be compatible with benzyl polyoxazinones at high concentrations. Solubility was enhanced by using a mixed solvent system of chloroform and THF. Unfortunately, the reduction in the number of THF molecules present allowed the growing polyoxazinone to again chelate to the catalyst, which reduced the monomer conversion (Table 2.3, entries 2-5). Catalytic activity has been restored in other systems where metathesis substrates contain hydroxamic esters that curtail reaction conversion by the addition of lewis acids that coordinate to the hydroxamic ester functionality, thereby blocking chelation to the catalyst.[215] In these studies, chloro dicyclohexylborane (BCy_2Cl) was the most effective additive to augment metathesis turnover. Indeed, the polymerization of **2.01b** was improved through the addition of 10 mol% BCy_2Cl (wrt monomer **2.01b**). This lewis acid increased monomer conversion while maintaining good control over molecular weight and polydispersity, even up to a monomer to catalyst loadings of 500:1 (Table 2.3, entries 6-8). The lewis acid loading of 10 mol% was found to be optimal for polymerization as increasing the concentration of this additive led to monomer decomposition (Table 2.4). Therefore, bicyclic oxazinone monomers with alkyl or benzyl functionality can now be polymerized efficiently using ROMP.

Table 2.4. Effect of BCy_2Cl on the polymerization of benzyl substituted monomer **2.01b**.

BCy_2Cl [mol% wrt 2.01b][a]	**conv to polymer [%]**
0	79
10	92
20	72
50	10
100	0[b]

[a] [**2.01b**]$_o$/[**2.07**] = 100/1, [**2.01b**]$_o$ = 1 M in 1:1 chloroform:THF. [b] all monomer decomposition.

2.3. Covalent Modification of Polyoxaziones

2.3.1. Functionalization of Polyoxazinones through Monomer Synthesis

Bicylic oxazinones can be used to access a new class of ROMP polymers called polyoxazinones. Substituents can be added to influence a polymer's bioactivity[5,28,62,76,108,164,196,197] as well as its materials[198,216-218] or electronic[219,220] properties. To enable the generation of specific polyoxazinones for variegated applications, our initial synthetic strategy was to use a library of bicyclic oxazinone monomers with differentially functionalized hydroxamic ester moieties (Scheme 2.1). Upon polymerization, each unique monomer produces a polymer with distinct physical or biological properties governed by the nature of the hydroxamic ester side chain. Importantly, modification of the hydroxamic ester alters the monomer as a site distal to the stained bicyclic core. Thus, we could tailor the properties of the resulting materials without destabilizing the heterocyclic compounds.

The aforementioned library of monomers was accessed by taking advantage of a two-step reaction sequence (Scheme 2.1A). A range of *O*-functionalized hydroxylamine precursors (compounds **2.08**) were esterified with α-bromoisobutyryl bromide (BIBB) and then the hydroxamic ester intermediates (compounds **2.09**) were converted to the corresponding bicyclic oxazinone monomers via an *aza*-[4+3] cycloaddition with furan. To illustrate the generality of our strategy, we generated polymers conjugated to ligands capable of influencing the physical, optical, or biological properties of the materials.

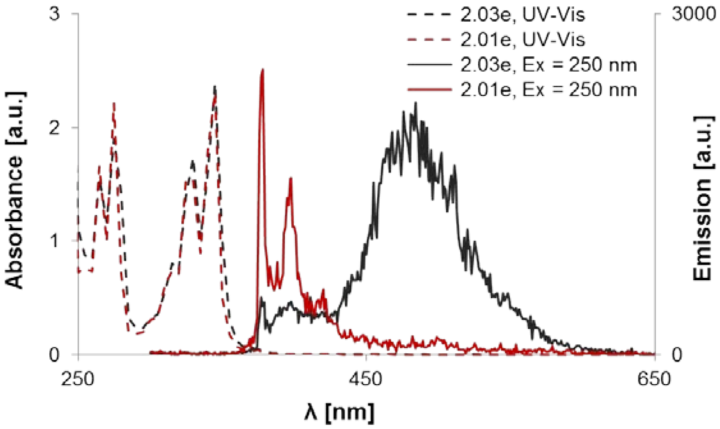

Figure 2.4. Optical properties of pyrene conjugates **2.03e** (polymer) and **2.01e** (monomer). [pyrene] = 80 μM. $[\mathrm{em}(480\ \mathrm{nm})/\mathrm{em}(377\ \mathrm{nm})]_{\mathrm{monomer}}$ = 0.038, $[\mathrm{Em}(480\ \mathrm{nm})/\mathrm{Em}(377\ \mathrm{nm})]_{\mathrm{polymer}}$ = 3.5.

Hydroxylamine precursors with hydrocarbon functionality were used to influence the physical properties of polyoxaziones (see Chapter 4). Both alkyl and aromatic functionality was tolerated during monomer synthesis and subsequent polymerization using the conditions described in Section 2.2. Specifically, octyl (**2.08a**), benzyl (**2.08b**), ethyl (**2.08c**), and tetradecyl (**2.08d**) substituted hydroxylamine starting materials were used to access polymers **2.03a**, **2.03b**, **2.03c**, and **2.03d**, respectively, with modified polymer side chains (Scheme 2.1A). Additionally, pyrene conjugate **2.08e** was leveraged to assemble polymer **2.03e**, which served as an optical sensor of polymer formation.[221] Polymer **2.03e** exhibited a red-shifted fluorescence spectrum indicative of pyrene excimer emission. Excimers form when two pyrene molecules dimerize due to π-stacking.[222] This only occurs at millimolar concentrations of pyrene. However, even when the absolute concentration of pyrene was 80 μM, polymer **2.03e** continued to produce excimers (Figure 2.4). This phenomenon did not occur when monomer **2.01e** was excited at an equal concentration of pyrene. On the other hand, the absorbance spectra for the monomer and polymer were superimposable, which indicates the chage in fluorescence was due to physical interactions between pyrene ligands and not do to chemical changes to the fluorophore itself. Therefore, pyrene incorporation along the polyoxazinone chain was confirmed because the backbone enforces a high local concentration of pyrene in solution, leading to excimer formation at low absolute pyrene concentrations.

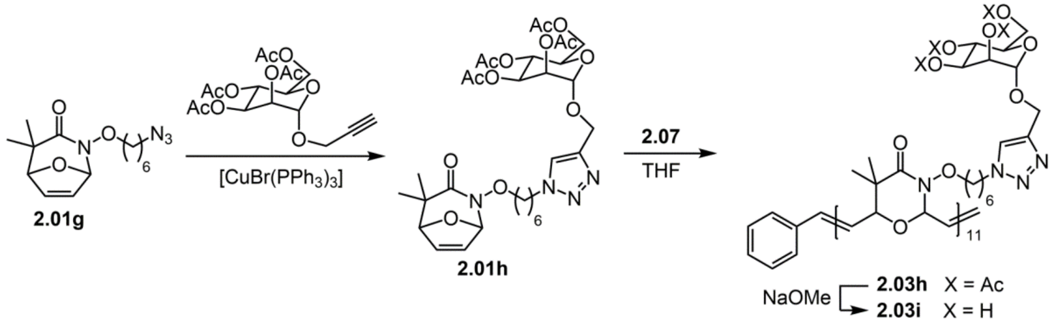

Scheme 2.3. Synthesis of a mannosylated polyoxazinone using CuAAC.

To expand the utility of our functionalization strategy, we devised a bicyclic oxazinone that can be elaborated at a late stage in monomer synthesis with compositionally complex ligands. We envisioned a facile and modular strategy to impart new functionality in this manner was to employ a bicyclic oxazinone containing a click reaction handle. The azide-alkyne [3+2] cycloaddition (AAC) was targeted for this purpose due its high yields, mild reaction conditions, and use as a handle for bioconjugation of ligands to macromolecules.[113,114,223,224] Starting with bromine functionalized hydroxylamine **2.08f**, monomer **2.01f** was accessed using the synthetic strategy discussed previously (Scheme 2.1A). Monomer **2.01f** can be elaborated through nucleophilic displacement of its alkyl bromide functionality with sodium azide to yield compound **2.01g**, which is a substrate for AAC. Azides, however, have been found to be incompatible with ruthenium catalysts.[199,225] Therefore, as a proof of concept, compound **2.01g** was conjugated to 1-propargyl-α-*D*-mannose-2,3,4,6-tetraacetate using a copper-catalyzed AAC

(CuAAC) to afford monomer **2.01h** (Scheme 2.3). The functionalized monomer that resulted could undergo ROMP to afford polymer **2.03h**. The acetate groups were subsequently hydrolyzed to produce mannose-substituted polymer **2.03i**. The bioactivity and biocompatibility of this polyoxazione glycopolymer is explored in Chapter 3; however, the synthesis of polymer **2.03i** demonstrates that monomer **2.01g**, which possess a pendant azide, can be used to add complex functionality at a late stage in monomer synthesis using CuAAC.

As can be seen, by taking advantage of various *O*-functionalized hydroxylamine precursors, a library of bicyclic oxazinone monomers was generated. Each substrate discussed was able to be synthesized in good yield using a facile two step synthesis. Upon polymerization, the functionality appended to the monomer's hydroxamic ester moiety was transferred to the polymer product. Therefore, polyoxaziones can be elaborated with functionality known to influence the mechanical, optical, or biological properties of polymers.

2.3.2. Functionalization of Polyoxazinones through Post-polymerization Modification

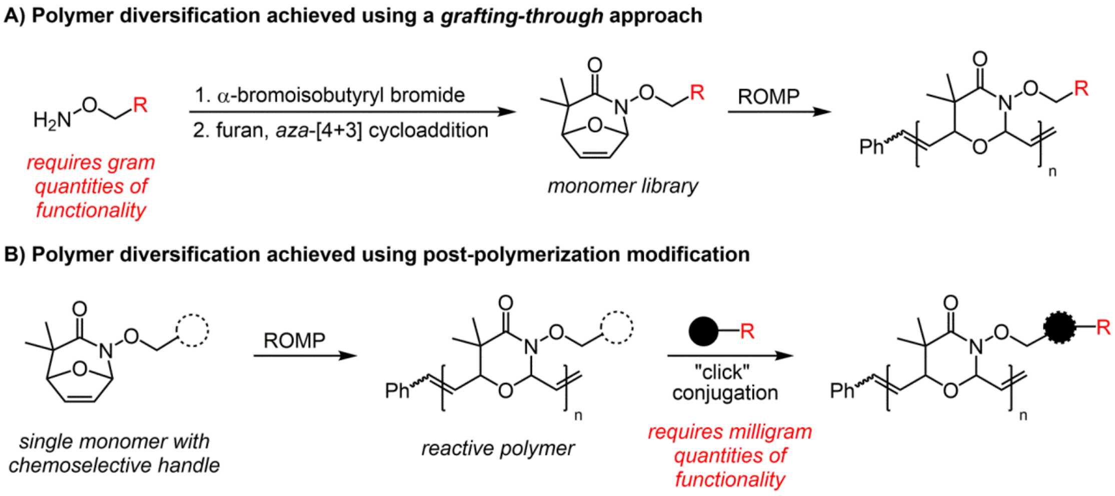
A) Polymer diversification achieved using a *grafting-through* approach
H2N
O
R
requires gram quantities of functionality
1. α-bromoisobutyryl bromide
2. furan, *aza*-[4+3] cycloaddition
O
N
O
R
monomer library
ROMP
Ph
O
N
O
R
n
B) Polymer diversification achieved using post-polymerization modification
single monomer with chemoselective handle
ROMP
reactive polymer
R
"click" conjugation
requires milligram quantities of functionality
Ph
n
R

Figure 2.5. Strategies to diversify polyoxazinones: A) *grafting-through* using a library of pre-functionalized monomers, B) post-polymerization modification of a reactive polymer species.

Modification through monomer synthesis is one method to alter the functionality displayed on polymers. Although facile, this approach requires gram quantities of each unique hydroxylamine precursor to obtain enough monomer to run the polymerizations at manageable reaction volumes. For many applications, especially when biological in nature, the requisite hydroxylamine starting material is only available in milligram quantities. Therefore, the *grafting-through* strategy described above is prohibitively expensive for generating functional polymers with valuable cargo, such as bioactive ligands or water-soluble fluorophores (Figure 2.5A). This represents an important obstacle for many polymer scaffolds. To circumvent this issue, synthetic macromolecules are often functionalized using post-polymerization modification (PPM), whereby ligands are covalently attached to a single, reactive polymer scaffold containing a chemoselective handle on a small scale.[115,226-228] To this end, we sought to construct a polyoxazinone scaffold that is amenable to PPM (Figure 2.5B).

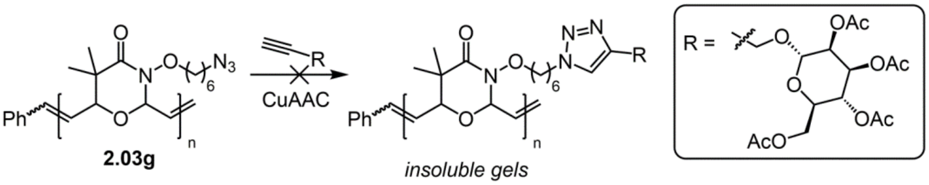

Scheme 2.4. Performing CuAAC on azido-polyoxazinone **2.03g** led to undesired gelation.

The synthesis of bicylic oxazinone monomer **2.01f**, bearing an alkyl halide functionality, was just discussed. This electrophilic monomer was converted to the corresponding azide, which enabled the conjugation of a peracetylated proparyl mannoside ligand using CuAAC, providing monomer **2.01h** (see Section 2.3.1.). Therefore, it was envisioned that CuAAC could also be used on polyoxazione substrates with azido functionality. To this end, monomer **2.01f** was polymerized directly and the resulting material was exposed to sodium azide to yield polyoxazinone **2.03g**, which appeared poised for PPM via CuAAC with ligands containing alkynyl functionality (Scheme 2.1B).[21,56,199] However, in our hands, this transformation led to an insoluble polymer gel instead of the desired polymer conjugate when using the same propargyl mannoside ligand (Scheme 2.4). This result was unexpected because performing CuAAC on monomer **2.01g** did not lead to gelation or other undesired side products. Therefore, while CuAAC is a viable way increase polymer diversity through pre-polymerization monomer functionalization, we sought a polyoxazinone scaffold containing an alternative chemoselective handle for PPM.

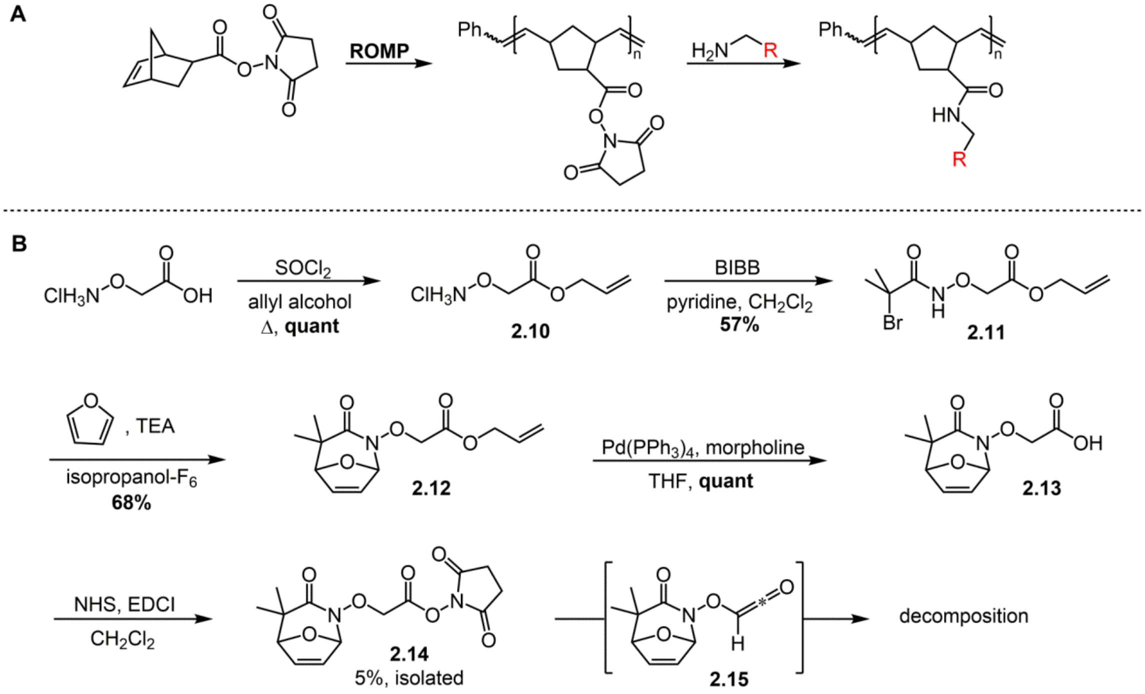
A
ROMP
Ph
n
H_2N R
Ph
n
HN
R
B
ClH_3N O OH
$SOCl_2$
allyl alcohol
Δ, quant
ClH_3N O
2.10
BIBB
pyridine, CH_2Cl_2
57%
Br N H O
2.11
, TEA
isopropanol-F_6
68%
2.12
$Pd(PPh_3)_4$, morpholine
THF, quant
OH
2.13
NHS, EDCI
CH_2Cl_2
2.14
5%, isolated
H
2.15
decomposition

Scheme 2.5. A) Polynorbonene ROMP polymers that display reactive NHS esters are amenable to PPM using amine containing ligands. B) A synthetic route to a bicyclic oxazinone decorated with an NHS ester. Polymerization of monomer **2.14** was thought to lead to amine reactive polyoxazinones; however, **2.14** was unstable and decomposed before isolation.

The Kiessling lab has pioneered the use of polynorbornene substrates decorated with *N*-hydroxyl succinimidyl (NHS) esters for generating compositionally complex macromolecules (Scheme 2.5A).[17,164,229] NHS esters facilitate the multi-functionalization of macromolecules by PPM through amide bond formation with amine-containing ligands. Therefore, access to an analogous bicyclic oxazione monomer containing an NHS ester was sought (Scheme 2.5B). To this end, *O*-(carboxymethyl) hydroxylamine was esterified with allyl alcohol, leading to hydroxylamine precursor **2.10**. Esterification of the free carboxylic acid was necessary to allow intermediate **2.10** to dissolve in organic solvents. Compound **2.10** was then acylated with BIBB leading to hydroxamic ester **2.11** and bicyclic oxazinone **2.12** was subsequently generated using an *aza*-[4+3] cycloaddition with furan. The selective removal of the allyl ester in the presence of the bicyclic olefin was achieved using tetrakis(triphenylphosphine) palladium and morphline, affording intermediate **2.13** with a free carboxylic acid. Unfortunately, re-esterification with NHS led to low isolated yields of the desired monomer **2.14**. It is hypothesized that **2.14** indeed forms in good yield, as all **2.13** was consumed by TLC, but the activated ester spontaneously eliminates the NHS group to form a reactive ketene intermediate, **2.15**. The ketene can participate in side reactions, such as cycloaddition with the bicyclic olefin, which erodes the isolated yield. This mode of ketene formation has been observed in other systems were a carboxylic acid alpha to an electron withdrawing heteroatom was activated with thionyl chloride.[230] Therefore, the strategy of using a bicyclic oxazinone monomer with NHS ester functionality to produce an amine reactive polyoxazinone substrate was abandoned.

Proteins engineered to contain the unnatural amino acid *p*-acetyl phenylalanine undergo chemoselective oxime formation when exposed to hydroxyalmines.[231-233] Inspired by these studies, we focused on synthesizing a polyoxazinone displaying the reactive acetophenone motif of this amino acid. To this end, we used the methodology of Terent'ev and co-workers to prepare protected hydroxylamine **2.16** (Scheme 2.6).[234] Because compound **2.16** is readily accessible in gram quantities, this substrate is an attractive starting material to generate acetophenone containing bicylic oxazinones and then polyoxazinones.

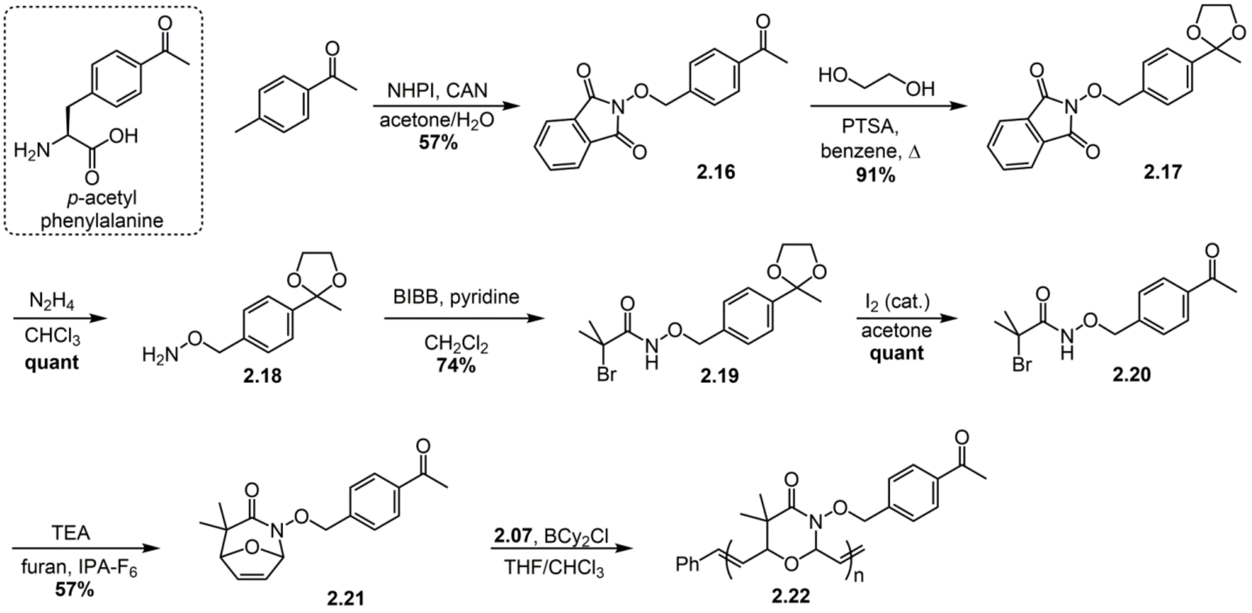
p-acetyl phenylalanine
NHPI, CAN
acetone/H2O
57%
2.16
HO OH
PTSA,
benzene, Δ
91%
2.17
N2H4
CHCl3
quant
2.18
BIBB, pyridine
CH2Cl2
74%
2.19
I2 (cat.)
acetone
quant
2.20
TEA
furan, IPA-F6
57%
2.21
2.07, BCy2Cl
THF/CHCl3
2.22

Scheme 2.6. Synthesis of reactive polymer **2.22**, a mimic of poly(*p*-acetyl phenylalanine).

This synthetic strategy proved effective. Upon generating compound **2.16**, conversion of the ketone to a 1,3-dioxane was necessary to prevent polymerization of the free hydroxylamine liberated upon deprotection of **2.17** in the next step. Subsequently, intermediate **2.18** was converted to the α-bromo hydroxamic ester **2.19** using BIBB. At this stage, the dioxane group was removed using catalytic iodine in acetone.[235] Importantly, these neutral conditions were necessary to generate **2.20** without deleterious side reactions, since α-bromohydroxamic esters rapidly decompose to acrylamides in mild acid or basic solutions. Finally, bicylic oxazinone monomer **2.21**, displaying an acetophenone moiety, was successfully produced via an *aza*-[4+3] cycloaddition with furan.

Initial attempts to polymerize monomer **2.21** were performed in a mixed solvent system of THF and chloroform using catalyst **2.07**. These conditions led to polyoxazinone **2.22**, but monomer conversion low (Table 2.5, entry 6). The polymerization of **2.21** was improved through the addition of 10 mol% BCy_2Cl (wrt monomer **2.21**) (see Section 2.2).[215] This lewis acid increased polymerization conversion while maintaining good control over molecular weight and polydispersity over a range of monomer to catalyst loading ratios (Table 2.5, entries 1-5). Therefore, access to a polyoxazinone scaffold with a click handle was achieved.

Table 2.5. Polymerization of monomer **2.21** by ROMP.

entry	$[M]_o/[I]$[a]	conv [%][b]	M_n^{theo} [g/mol]	M_n^{GPC} [g/mol][c]	PDI[c]
1	15/1	83	3700	7800	1.3
2	25/1	87	6500	13700	1.5
3	50/1	87	13100	16000	1.5
4	100/1	89	26800	23400	1.4
5	200/1	84	50600	40000	1.9
6	200/1[d]	24	14400	25800	2.0

[a] **M** = **2.21**, **I** = **2.07**, [**2.21**]$_o$ = 1 M in 1:1 chloroform:THF, 10% BCy_2Cl (wrt **2.21**). [b] based on ^{1}H-NMR integrations of monomer olefin signals to polymer olefin signals. [c] calibrated with polystyrene standards, eluted 1.0 mg/mL in THF. [d] w/o BCy_2Cl.

With acetophenone-functionalized polymer **2.22** in hand, we investigated methods to elaborate this scaffold with hydroxylamine ligands to form covalent oxime ethers. Conjugations of hydroxylamine ligands to biomacromolecules, such as proteins[66], or small molecules[69] usually proceed in acetate buffer. These conditions are incompatible with polyoxazinones because of the low aqueous solubility of polyoxazinone **2.22** and the acid lability of the oxazinone linkages along the polymer backbone. Alternative PPM conditions were screened using an oligoethylene glycol ligand terminated with a hydroxylamine (**2.23**) (Scheme 2.7). Compound **2.23** was successfully ligated to polymer **2.22** in a mixture of dimethyl sulfoxide (DMSO) and pyridine to produce oxime conjugate **2.24**.[236] A slight excess of ligand **2.23** (1.5-2.0 eq) led to quantitative conversion of all ketones ($H^a = \delta$ 7.8 ppm; $H^b = \delta$ 2.6 ppm) to oximes ($H^a = \delta$ 7.6 ppm; $H^b = \delta$ 2.2 ppm) within 24 h as observed by ^{1}H-NMR (Figure 2.6). In addition, gel permeation chromatography (GPC) confirmed a shift in retention time to a shorter elution volume after functionalization while the polydispersity of the sample remains unaffected (Figure 2.7). These observations indicate successful PPM of polymer **2.22** with ligand **2.23**.

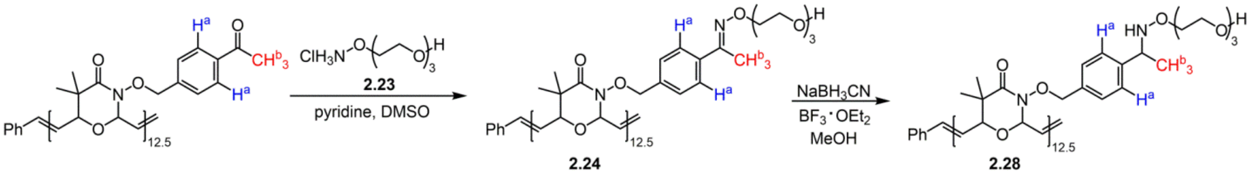
Hª
O
CHᵇ₃
Hª
N
O
O
O
Ph
12.5
ClH₃N
O
O
H
3
2.23
pyridine, DMSO
2.24
NaBH₃CN
BF₃·OEt₂
MeOH
HN
2.28

Scheme 2.7. Reactive polymer **2.22** can be elaborated via PPM with hydroxylamine ligands. The resulting oxime conjugates, **2.24**, can be further reduced to stabilize the labile oxime linkage.

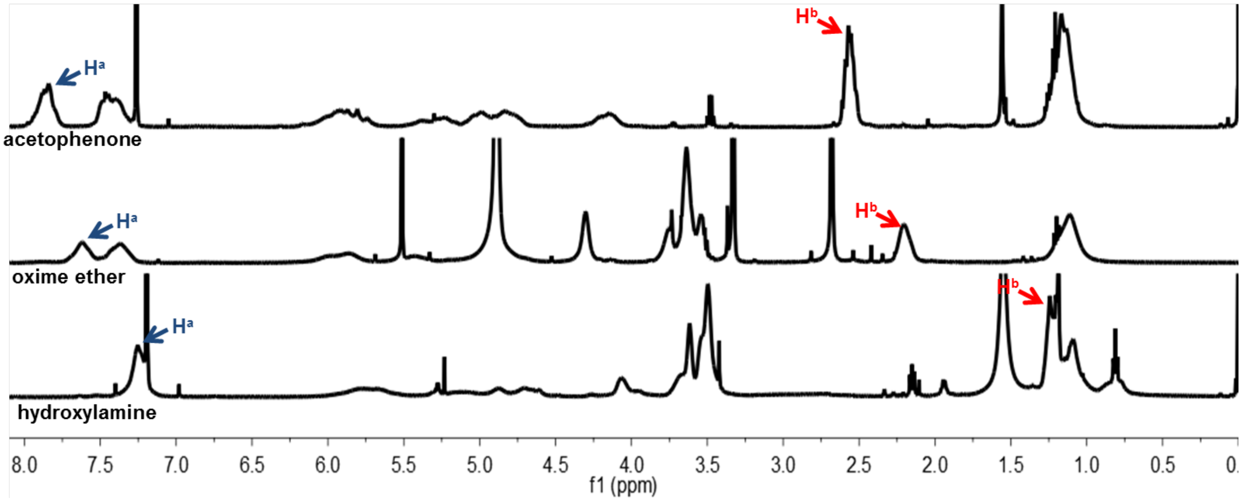

Figure 2.6. Quantitative conversion of acetophenone-functionalized polymer **2.22** to oxime conjugate **2.24** and subsequent reduction to polymer **2.28** was followed by ^{1}H-NMR. Functional group interconversion was monitored by following the ortho hydrogens (H_a, blue arrows) and α-methyl hydrogens (H_b, red arrows) of the acetophenone moiety, which appear as isolated peaks in each spectrum.

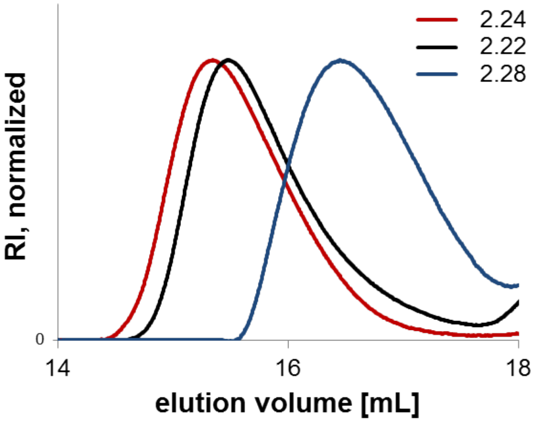

Figure 2.7. GPC analysis of polymers **2.22**, **2.24**, and **2.28**.

A second test to confirm the successful covalent modification of polyoxazinone **2.22** was carried out through conjugation of *O*-(4-pyrenylbutyl) hydroxylamine, **2.08e**, which bears the fluorophore pyrene (Scheme 2.8). As discussed previous, a property of pyrene is that dimerization occurs at high concentrations, enabled by π-stacking, which leads to excimers.[222] Excimer formation manifests as a broad fluorescent emission band centred at 480 nm, which alters the ratio of excimer to monomer emission [Ex(480)/Ex(378)]. Indeed, the fluorescence spectrum of polymer conjugate **2.25** has a higher Ex(480)/Ex(378) ratio than either small molecule conjugate **2.26** or free hydroxylamine ligand **2.08e** at 50 μM pyrene (Figure 2.8). Furthermore, over a range of concentrations tested, the Ex(480)/Ex(378) ratio does not change for any of the three species. These results indicate that the excimer signal of **2.25** occurs because of a constant, but enriched, relative concentration of pyrene, enforced by covalent attachment to the polymer backbone, and not due to concentration dependent pyrene aggregation. Therefore, the observed increase in pyrene stacking further verifies successful oxime formation with **2.22**. Interestingly, the maximum Ex(480)/Ex(378) ratio for the pyrene oxime conjugate **2.25** (0.8) is lower than that of pyrene conjugate **2.03e** (3.5), which was generated through monomer modification (see Section 2.3.1). This indicates that the environments for the pyrene ligands are different depending on how they are attached to the polyoxazinone backbone. Specifically, PPM using the acteophenone handle disfavors ligand-ligand interactions as compared to direct functionalization of the polymer backbone. At the present time, this observation is idiosyncratic; however it may prove useful in systems where control over the interaction between polymer ligands is desired.

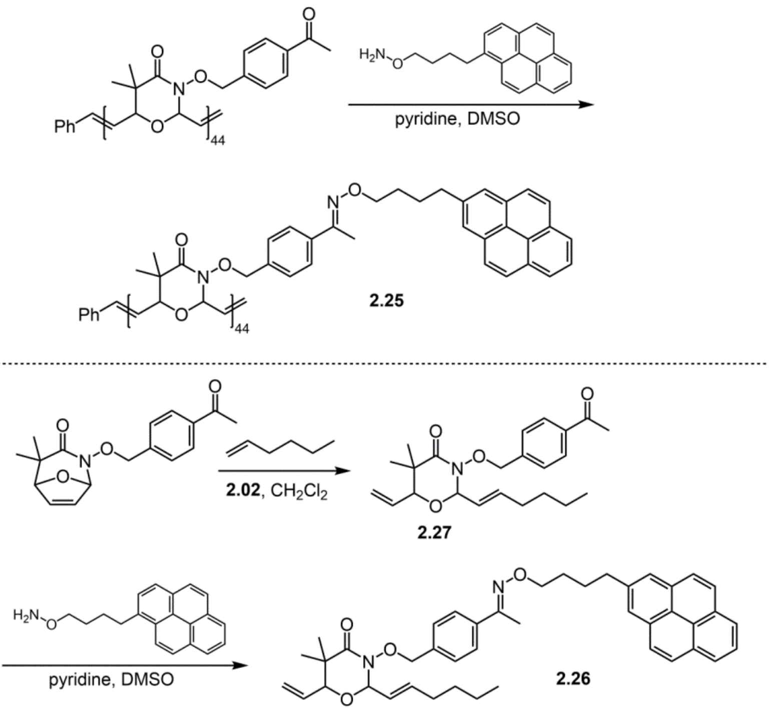

Scheme 2.8. Synthesis of pyrene-oxime conjugates: polymer **2.25** and 1-mer **2.26**.

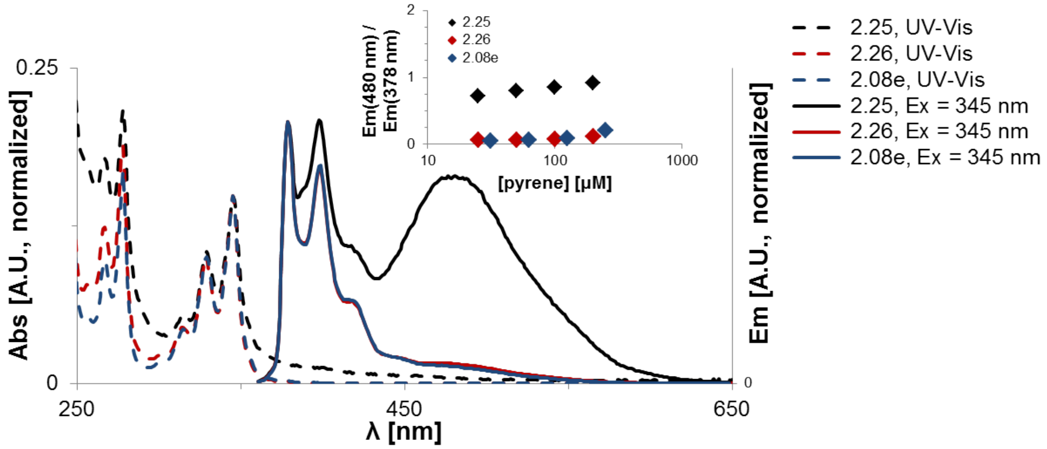

Figure 2.8. Absorbance and emission spectra for pyrene conjugates **2.25** and **2.26** and ligand **2.08e**. [pyrene] = 50 μM. The ratio of pyrene excimer to monomer emission does not change greatly between 25 and 200 μM (inset).

A significant advantage of using PPM is that multiple ligands can be conjugated to a given polymer scaffold in a single step to make random copolymers. This synthetic flexibility is often useful when preparing polymer conjugates for biological systems. In addition to fluorophores, bioactive ligands are often conjugated to marcomolecules through PPM to elicit specific physiological responses.[228] Indeed, multifunctional polyoxazinones can be accessed. The synthesis and biological application of these compositionally complex species are the focus of Chapter 3.

2.3.3. Reduction of Polyoxazione-Oxime Conjugates

Using PPM, the functional properties of polymer **2.22** can be tuned via oxime formation. Oxime formation constitutes a covalent modification, but this bond is hydrolysable in acidic media.[237] If this reversibility is undesired, oximes can be reduced to hydrolytically stable *N*-substituted hydroxylamines. To achieve this transformation, we required a means to reduce the oxime in the presence of oxazinone functionality. Encouragingly, oxime reduction has been achieved in previous syntheses in the presence of carbonyl groups as well as cyclic acetals.[238,239] Attempts to reduce **2.24** in DMSO were unsuccessful, which meant that oxime formation and subsequent reduction of polyoxazinone **2.22** could not be achieved in a one pot, two step sequence. Nevertheless, the selective reduction of **2.24** to polymer **2.28** was achieved using sodium cyanoborohydride as a reducing agent in methanol in the presence of the lewis acid boron trifluoride diethyl etherate, which was found to increase the rate of reduction (Scheme 2.7). Quantitative conversion of all oximes to hydroxylamines was assessed using ^{1}H NMR ($H^a = \delta$ 7.3 ppm; $H^b = \delta$ 1.3 ppm) (Figure 2.6). Both individual reactions leading to polymer **2.28** proceeded to complete conversion and both polymers were isolated in greater than 80% yield. This method of reduction was found to be general and was effective on polymer conjugate **2.25** as well. Therefore, the lability of the oxime ether conjugates to polyoxazinones is restrictable through reduction, leading to irreversible side chain linkages.

2.3.4. PPM Summary and Outlook

The covalent functionalization of macromolecules using post-polymerization modification is a powerful method to generate functional materials when the requisite ligands are only attainable in small quantities. To facilitate the PPM of polyoxazinones, a novel bicylic oxazinone monomer was synthesized containing an acetophenone moiety. Upon polymerization of this monomer, a polymer was generated that displayed repeating copies of a reactive acetophenone handle, which enabled side chain elaboration by oxime formation with various hydroxylamine ligands. Upon oxime formation, this hydrolyzable bond was stabilized through reduction. Thus the properties of polyoxazinones are now tunable through covalent post-polymerization modification, an economical and modular method to diversify a macromolecule's function.

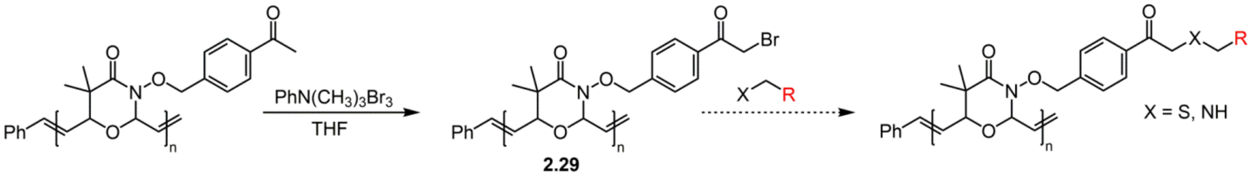

Scheme 2.9. Proposed route to amine and thiol reactive polyoxazinones.

Table 2.6. Unequal halogenation of the residues of polymer **2.29** occurs during bromination using $PhN(CH_3)_3Br_3$**.**

Entry	$Ph(CH_3)_3Br_3$ [wrt ketone]	Solvent	Unsubstitued repeats	Mono-brominated repeats	Di-brominated repeats
1	1.5 eq	THF	15%	60%	25%
2	1.5 eq	CH_2Cl_2	33%	47%	10%

PPM via oxime formation was enabled by acetophenone polymer **2.22**. However, in the future, it may be necessary use to ligands with alternative functionality to hydroxylamines. Therefore, modifications to polyoxazinone **2.22** can be envisioned to allow multi-functionalization with ligands that bear non-hydroxylamine functionality. For instance, α-halo ketones are amenable to nucleophilic addition by amines and thiols. Preliminary results indicate that the acetophenone functionality of polymer **2.22** can be transformed to an α-bromo ketone, polymer **2.29**, through the use of trimethylphenyl ammonium bromide (Scheme 2.9). Importantly, this reagent is able to halogenate the acetophenone moiety in the presence of olefin functionality without destabilizing the oxazinone ring. However, optimization of this reaction is needed to prevent the over halogenation of repeats that are more accessible to the brominating reagent (Table 2.6). Additionally, it remains to be shown whether polymer **2.29** is indeed amenable to PPM with amine and thiol containing ligands.

2.4. Degradation of Polyoxazinones

We next investigated the degradability of the new polyoxazinone scaffold. Small molecule oxazinones have been used to generate β-hydroxy carboxylic acids,[240,241] but the conditions used for ring opening have been harsh (i.e. extreme pH and high temperatures). We assessed more mild conditions. Utilizing gel permeation chromatography (GPC), we monitored the decomposition of polymer **2.03b** under a range of acidic and basic conditions at room temperature (Figure 2.9). No appreciable breakdown occurred at pH values between 4.5 and 9.0 over 48 h. This observation indicates that the oxazinone backbone is able to withstand exposure to a wide range of conditions, thereby facilitating polymer handling or modification. Indeed, this window of stability was crucial to allow polymer **2.22** to be decorated via PPM. Still, the polymers are vulnerable under specific conditions. At pH values less than 1.0, degradation is fast with complete decomposition occurring in under an hour. The acid-catalyzed backbone decomposition also occurs readily at pH 2.5, with 66% of the polymer mass lost in 6 h. At pH values up to 4.5, slower degradation occurs. We also observed polymer backbone cleavage under basic conditions. Thus, either acid or base can promote degradation of polymers with an *N*-alkoxy oxazinone backbone. Additionally, these data indicate that oxazinone-containing ROMP polymers represent a unique class of backbone degradable polymers that are stable at neutral pH values but labile in either acidic or basic environments.

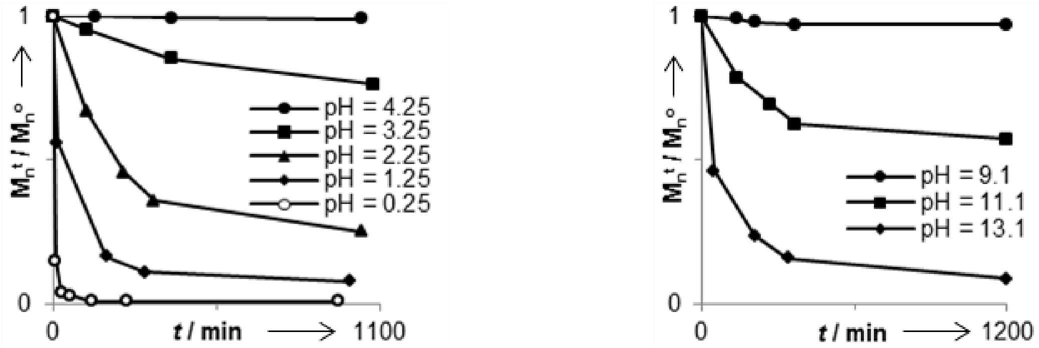

Figure 2.9. Degradation profile of polymer **2.03b** under acidic and basic conditions. M_n^o = 18,500 g/mol.

Further studies were conducted to characterize the degradation products. Because isolating the necessary quantities of specific polymer degradation fragments for characterization is difficult, we employed a model. Specifically, compound **2.01b** was subjected to a ring-opening cross metathesis reaction with 1-hexene to yield heterocycle **2.30**. When the product was exposed to an acidic methanol solution, ring-cleavage occurred to afford hydroxamic acid **2.31** (Scheme 2.10).[240] This mode of reactivity would promote fragmentation of the polyoxazinone backbone causing polymer degradation. It is expected that hydroxamic ester **2.31** undergoes further hydrolysis to a β-hydroxy carboxylic acid, however this species was not isolated.

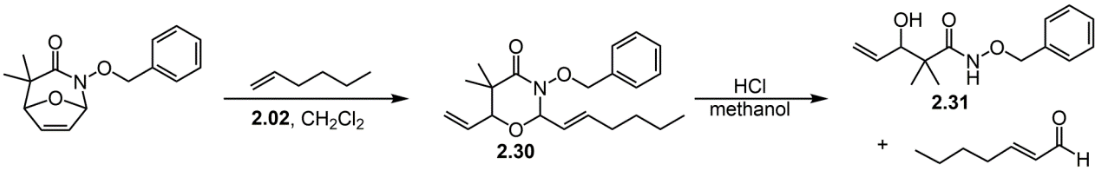

Scheme 2.10. Ring-opening cross metathesis of monomer **2.01b** and subsequent hydrolysis of 3-alkoxy-1,3-oxazin-4-one **2.30** under acidic conditions.

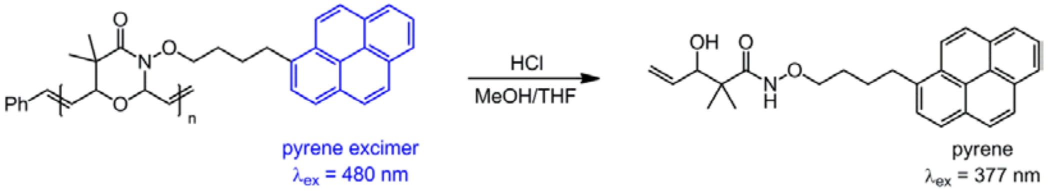

Scheme 2.11. Degradation of polymer **2.03e** releases monomeric pyrene fragments into the solution, thereby decreasing excimer emission over time. The decomposition product is a proposed structure.

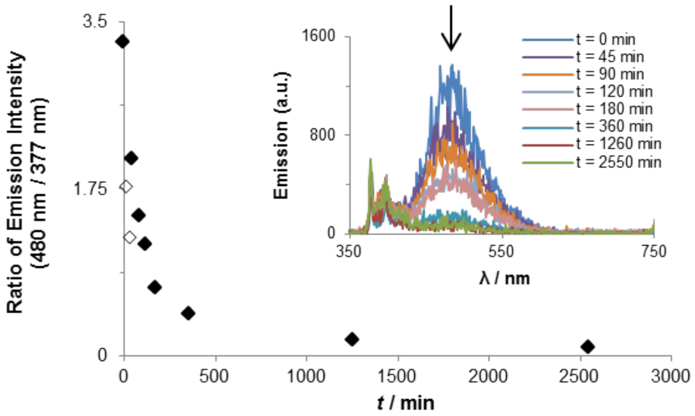

Figure 2.10. Degradation of **2.03e** was monitored by comparing the ratio of polymeric pyrene exiplex emission (λ_{max} = 480 nm) to monomeric pyrene emission (λ_{max} = 377 nm). λ_{ex} = 250 nm, pH = 0.25 (3:1 THF:MeOH). Unfilled diamonds represent low emission ratios due to initial low polymer solubility; polymer completely dissolved in solution within 40 min.

In addition to monitoring the degradation of polyoxazinones chromatographically, polymer decomposition was followed spectroscopically. This was enabled by the use of polymer **2.03e**, which induces concentration dependent pyrene excimer formation (see Section 2.3.1). When polymer **2.03e** undergoes hydrolytic degradation, a monomeric pyrene derivative is released from the backbone, thereby diminishing excimer emission (Scheme 2.11). Changes in the ratio of fluorescence intensity of monomeric pyrene emission (λ_{max}=377 nm) to polymeric exciplex emission (λ_{max}=480 nm) over time report on the extent of backbone hydrolysis. We followed this spectral change to reveal that exposure to acidic conditions for 3 h resulted in approximately 80% polymer degradation (Figure 2.10). This rate of polymer decomposition observed spectroscopically validated the rate of degradation obtained using GPC.

2.5. Conclusions

In conclusion, ROMP can be used to synthesize a new class of degradable polymer called polyoxazinones. These polymers possess a backbone that is labile under either acidic or basic conditions. Additionally, the polymers can be decorated through a modular monomer synthesis or through PPM. The process we describe affords functional and degradable polymers that can be used in specific applications. We envision that polymers of this type may yield new degradable plastics or resins. ROMP can be used on an industrial scale to generate new materials; therefore, the strategy described here could generate consumables with properties that complement those currently generated by ROMP.[188] In this way, ROMP can give rise to stable species or materials that can be broken down to simple building blocks. Furthermore, degradable and functional polymers can serve as scaffolds for directed drug delivery or regenerative medicine.[196,242,243] Therefore, we foresee that these polymers may find utility as novel biomaterials as well.

2.6. Materials and Methods

2.6.1. General Methods

All commercially available reagents were purchased from Sigma-Aldrich (St. Louis, MO). Compounds **2.09b** and **2.01b** were synthesized as described by Jeffrey and coworkers.[105] 4-(1-pyrenyl)butyl methanesulfonate was synthesized as described by Cicchi and coworkers.[244] *N*-Boc-*O*-(6-bromohexyl) hydroxylamine was synthesized as described by Francis and coworkers.[245] Compound **2.16** was synthesized as described by Terent'ev and coworkers.[234] 2-(2-

(2-(N-Boc aminoxy)ethoxy)ethoxy)ethanol was synthesized as described by Jones and coworkers.[246] Catalyst **2.07** was synthesized as described previously by Grubbs and coworkers.[88] Tris(triphenylphosphine) copper(I) bromide was synthesized as described previously by Gujadhar and coworkers.[247] Tetrahydrofuran (THF) was distilled over sodium/benzophenone. Methanol was distilled over magnesium filings. Dichloromethane and triethylamine were distilled over calcium hydride. Dimethylsulfoxide (DMSO), *N*,*N*-dimethyl formamide (DMF), diethyl ether, hexanes, and ethyl acetate (EtOAc) were used as received. Deionized (milliQ) water and PD-10 Desalting Columns (GE Healthcare; Little Chalfont, UK) were used to purify water soluble polymers. All reactions were run under an inert atmosphere of N_2 unless otherwise specified. Reactions were stirred using Teflon coated magnetic stir bars. All glassware and stir bars were stored in oven before use. Cold baths were prepared using water/ice (0 ^{o}C) or ethylene glycol/CO_2 (-10 ^{o}C).

Analytical thin layer chromatography (TLC) was carried out on E. Merck (Darmstadt) TLC plates pre-coated with silica gel 60 F254 (250 μm layer thickness). Analyte visualization was accomplished using a UV lamp and by charring with potassium permanganate stain (Fischer, 1.5 g in 300 mL water with 6.5% K_2CO_3 (w/v) and 5 mL 5% NaOH (w/v)). Flash column chromatography was performed on SiliaFlash® P60 (Silicycle; Quebec City, Canada; 40-63 μm particle size).

^{1}H and ^{13}C nuclear magnetic resonance (NMR) spectra were obtained using a Bruker AC-300 MHz spectrometer (for small molecules) or Varian Inova-500 MHz spectrometer (for polymers). Chemical shifts are reported relative to tetramethylsilane or residual solvent peaks in parts per million ($CHCl_3$: ^{1}H: δ 7.26, ^{13}C: δ 77.23). Peak multiplicity is reported as singlet (s), doublet (d), doublet of doublets (dd), doublet of doublet of doublets (ddd), doublet of doublet of triplets (ddt), triplet (t), doublet of triplets (dt), quartet (quart), pentet (pent), multiplet (m), AB quartet (ABX_2). When visible, the degree of polymerization (DP) was based upon integration of the phenyl protons at the chain end relative to the polymer olefin protons. High resolution electrospray ionization mass spectra (HRESI-MS) were obtained on a Micromass LCT mass spectrometer. Room temperature GPC-SEC analysis (Viscotek GPC max) was performed on 300 x 7.5 mm PolyPor 5 μm mixed columns from Polymer Laboratories. Data was analyzed using OmniSEC software (Viscotek Inc.). Polymers were eluted with THF (1.0 mL/min, 40 ^{o}C) to determine M_n, M_w, and polydispersity index (M_n/M_w). Columns were calibrated with 10 narrow polystyrene standards (Polymer Laboratories S-M2-10 kit). UV-Vis absorption spectra were obtained on a Varian Cary 50-Scan UV-Visible Spectrophotometer and fluorescence emission spectra were obtained on a Hitachi F-4500 Fluorescence Spectrophotometer. All optical measurements were taken in a quartz cuvette.

2.6.2. Synthesis of Small Molecules

Compound 2.32a

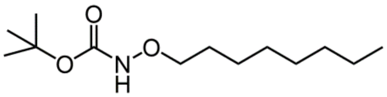

To a stirring solution of *N*-Boc hydroxylamine (1.40 g, 10.6 mmol) in DMF (7.0 mL) was added 1,8-diazabicyclo[5.4.0]undec-7-ene (DBU, 1.6 mL, 10.6 mmol) followed by DMF (3.5 mL). Then 1-bromooctane (1.6 mL, 9.5 mmol) was added to the solution followed by DMF (3.5 mL). The reaction was stirred at rt for 2 h, then DBU (0.8 mL) was added to the reaction and the solution was moved to an oil bath and stirred at 50 ^{o}C. After 20 h, dichloromethane (90 mL) was added to the reaction and the solution was washed with 15% aqueous citric acid solution (3 x 22 mL). The organic layer was dried over Na_2SO_4. The drying agent was removed by filtration and the solvent was removed under reduced pressure. The residue was purified by flash column chromatography (5 → 15% EtOAc/hexanes). **2.32a** was obtained as an oil (1.01 g, 43%). ^{1}H-NMR ($CDCl_3$, 500 MHz): δ 7.12 (s, 1H), 3.86 (t, *J* = 6.7 Hz, 2H), 1.63 (pent, *J* = 7.0 Hz, 2H), 1.50 (s, 9H), 1.43-1.21 (m, 10 Hz), 0.89 (t, *J* = 6.9 Hz, 3H). ^{13}C-NMR ($CDCl_3$, 125 MHz): δ 156.9, 81.6, 77.0, 31.8, 29.4, 29.2, 28.2, 28.0, 25.9, 22.7, 14.1. HRESI-MS calcd for $C_{11}H_{27}NO_3$ $[M+H]^+$ 263.2330; found 263.2324.

Compound 2.08a

To a stirring solution of **2.32a** (1.01 gg, 4.1 mmol) in dichloromethane (20 mL) at 0 ^{o}C was added trifluoroacetic acid (10.0 mL). Stirring continued for 1 h at 0 ^{o}C. The volatile compounds were removed under reduced pressure and the excess acid was removed by azeotroping with toluene (3 x 20 mL). **2.08a** was obtained as a clear oil (1.01 g, quant.), which was carried on without further purification. ^{1}H-NMR ($CDCl_3$, 500 MHz): δ 11.00-9.50 (broad s, 3H), 4.04 (t, *J* = 6.6 Hz, 2H), 1.66 (pent, *J* = 7.0 Hz, 2H), 1.50-1.12 (m, 10H), 0.90 (t, *J* = 6.7 Hz, 3H). ^{13}C-NMR ($CDCl_3$, 125 MHz): δ 162.8 (q, *J* = 36.7 Hz), 116.1 (q, *J* = 290.5 Hz), 76.0, 31.7, 29.1, 29.1, 27.5, 25.4, 22.6, 14.0. HRESI-MS calcd for $C_8H_{20}NO$ $[M-TFA]^+$ 146.1540; found 146.1537.

Compound 2.09a

To a stirring solution of **2.08a** (1.06 g mg, 4.1 mmol) in dichloromethane (15.5 mL) at 0 ^{o}C was added triethylamine (0.4 mL, 4.2 mmol) in one portion followed by α-bromoisobutyryl bromide (0.5 mL, 4.1 mmol) dropwise. Stirring continued for 15 min at 0 ^{o}C. Pyridine (0.5 mL, 4.7 mmol) was added and the reaction was allowed to slowly warm to rt. After 20 h, the reaction was diluted with dichloromethane (15 mL) and washed with H_2O (2 x 15 mL). The organic phase was dried over Na_2SO_4. The drying agent was removed by filtration and the solvent was removed under reduced pressure. The residue was purified by flash column chromatography (5 → 10% EtOAc/hexanes). **2.09a** was obtained as an oil (710 mg, 59%). ^{1}H-NMR ($CDCl_3$, 400 MHz): δ 9.22 (s, 1H), 3.96 (t, *J* = 6.7 Hz, 2H), 1.99 (s, 6H), 1.70 (pent, *J* = 7.0 Hz, 2H), 1.55-1.20 (m, 10H), 0.91 (t, *J* = 6.9 Hz, 3H). ^{13}C-NMR ($CDCl_3$, 100 MHz): δ 169.7, 76.9, 59.7, 32.5, 31.8, 29.4, 29.2, 28.0, 25.8, 22.7, 14.1. HRESI-MS calcd for $C_{12}H_{24}BrNO_2$ $[M+H]^+$ 311.1329; found 311.1318.

Monomer 2.01a

To a stirring solution of **2.09a** (705 mg, 2.4 mmol) in 1,1,1,3,3,3-hexafluoroisopropanol and furan [1:1 (v/v) 0.25 M] at 0 ^{o}C was added triethylamine (0.68 mL, 4.8 mmol) dropwise over 5 min. Stirring continued at 0 ^{o}C for 5 min, then the reaction was allowed to warm to rt over 25 min. The volatile compounds were removed under reduced pressure and the residue was purified by flash column chromatography (7 → 15% EtOAc/hexanes). Compound **2.01a** was obtained as a light yellow oil (443 mg, 66%). ^{1}H-NMR ($CDCl_3$, 500 MHz): δ 6.73 (broad d, *J* = 5.5 Hz, 1H), 6.49 (broad d, *J* = 5.5 Hz, 1H), 5.49 (broad s, 1H), 4.52 (broad s, 1H), 3.93 (ABX_2, J_{AB} = 9.2 Hz, J_{AX} = 6.7Hz, J_{BX} = 7.3 Hz, 2H), 1.73-1.60 (m, 2H), 1.50 (s, 3H), 1.45-1.20 (m, 10H), 1.06 (s, 3H), 0.89 (t, *J* = 7.1 Hz, 3H). ^{13}C-NMR ($CDCl_3$, 125 MHz): δ 175.9, 135.5, 134.7, 90.8, 87.4, 75.9, 49.0, 31.8, 29.4, 29.2, 28.2, 27.0, 25.9, 22.7, 19.8, 14.1. HRESI-MS calcd for $C_{16}H_{27}NO_3$ $[M+H]^+$ = 282.2064; found 282.2075.

Compound 2.09c

To a stirring solution of *O*-ethyl hydroxylamine hydrochloride (700 mg, 7.2 mmol) in dichloromethane (30 mL) at 0 ^{o}C was added triethylamine (1.00 mL, 7.2 mmol) in one portion followed by α-bromoisobutyryl bromide (0.89 mL, 7.2 mmol) dropwise. Stirring continued for 15 min at 0 °C. Pyridine (0.67 mL, 8.3 mmol) was added and the reaction was allowed to slowly warm to rt. After 20 h, the reaction was diluted with dichloromethane (30 mL) and washed with H_2O (2 x 30 mL). The organic phase was dried over Na_2SO_4. The drying agent was removed by filtration and the solvent was removed under reduced pressure. The residue was purified by flash column chromatography (25% EtOAc/hexanes). **2.09c** was obtained as a light yellow oil (1.24 mg, 81%). ^{1}H-NMR ($CDCl_3$, 500 MHz): δ 9.10 (broad s, 1H), 3.93 (q, *J* = 7.1 Hz, 2H), 1.90 (s, 6H), 1.23 (t, *J* = 7.1 Hz, 3H). ^{13}C-NMR ($CDCl_3$, 125 MHz): δ 169.8, 72.3, 59.8, 32.5, 13.4. HRESI-MS calcd for $C_6H_{12}BrNO_2$ $[M+H]^+$ 210.0125; found 210.0127.

Monomer 2.01c

To a stirring solution of **2.09c** (1.17 g, 5.5 mmol) in 1,1,1,3,3,3-hexafluoroisopropanol and furan [1:1 (v/v) 0.25 M] at 0 °C was added triethylamine (1.6 mL, 11.1 mmol) dropwise over 5 min. Stirring continued at 0 °C for 5 min, then the reaction was allowed to warm to rt over 25 min. The volatile compounds were removed under reduced pressure and the residue was purified by flash column chromatography (25% EtOAc/hexanes). Monomer **2.01c** was obtained as an oil (720 mg, 69%). ^{1}H-NMR ($CDCl_3$, 500 MHz): δ 6.66 (broad d, *J* = 6.6 Hz, 1H), 6.42 (broad d, *J* = 6.4 Hz, 1H), 5.41 (s, 1H), 4.44 (s, 1H), 3.93 (m, 2H), 1.45 (s, 3H), 1.21 (t, *J* = 7.1 Hz, 3H), 0.98 (s, 3H). ^{13}C-NMR ($CDCl_3$, 125 MHz): δ 175.8, 135.5, 134.7, 90.9, 87.4, 71.8, 49.0, 26.9, 19.8, 13.8. HRESI-MS calcd for $C_{10}H_{15}NO_3$ $[M+H]^+$ 198.1125; found 198.1130.

Compound 2.32d

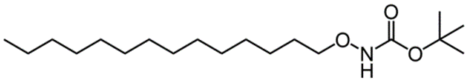

To a stirring solution of *N*-Boc hydroxylamine (1.094 g, 8.2 mmol) in DMF (5.4 mL) was added DBU (1.25 mL, 8.2 mmol) and DMF (2.7 mL). 1-bromotetradecane (2.056 g, 7.4 mmol) was added followed by DMF (2.7 mL). The solution was stirred at rt for 3 h and then excess DBU (1.25 mL) was added. The solution was stirred at rt for 4 h, then at 50 °C for 18 h. The solution was cooled to rt an then diluted with dichloromethane (70 mL) and washed with 15% citric acid solution (3 x 25 mL). The organic phase was dried and concentrated. The crude residue was purified by silica column chromatography (1→10% EtOAc/hex) to afford **2.32d** (1.06 g, 44%). ^{1}H-NMR ($CDCl_3$, 500 MHz): δ 7.08 (s, 1H), 3.84 (t, *J* = 6.7 Hz, 2H), 1.62 (pent, *J* = 7.1 Hz, 2H), 1.48 (s, 9H), 1.43-1.47 (m, 22H), 0.48 (t, *J* = 6.9 Hz, 3H). ^{13}C-NMR ($CDCl_3$, 125 MHz): δ 156.9, 81.6, 77.0, 31.9, 29.7, 29.7, 29.7 (2), 29.6, 29.6, 29.5, 29.4, 28.2 (3), 28.0, 25.9, 22.7, 14.2. HRESI-MS calcd for $C_{19}H_{39}NO_3$ $[M+NH_4]^+$ 347.6269; found 347.3254.

Compounds 2.08d and 2.09d

Compound **2.32d** (1.055 g, 3.2 mmol) was dissolved in 4 M HCl in 1,4-dioxane (26 mL, 104 mmol). The solution was stirred at rt for 45 min, then concentrated. Excess acid was azeotroped with toluene (3 x 5 mL). Crude **2.08d** (807 mg, 95%) was taken on without further purification.

To a stirring solution of **2.08d** (807 mg, 3.04 mmol) in dichloromethane (12 mL) at 0 °C was added pyridine (0.54 mL, 6.68 mmol) followed by BIBB (0.38 mL, 3.00 mmol), dropwise. The solution was stirred at rt for 17 h and then diluted with dichloromethane (12 mL). The solution was washed with water (2 x 12 mL) and the organic phase was dried and concentrated.

The residue was purified by silica column chromatography (15% EtOAc/hex) to afford compound **2.09d** (990 mg, 87%). ^{1}H-NMR ($CDCl_3$, 500 MHz): δ 9.16 (s, 1H), 3.93 (t, *J* = 6.7 Hz, 2H), 1.97 (s, 6H), 1.67 (pent, *J* = 7.2 Hz, 2H), 1.45-1.18 (m, 22H), 0.88 (t, *J* = 6.9 Hz, 3H). ^{13}C-NMR ($CDCl_3$, 1.25 MHz): δ 169.7, 76.9, 59.8, 32.5 (2), 31.9, 29.7, 29.7, 29.7 (2), 29.6, 29.5, 29.4, 29.4, 28.0, 22.7, 14.1. HRESI-MS calcd for $C_{18}H_{36}BrNO_2$ $[M+NH_4]^+$ 395.2268; found 395.2273.

Monomer 2.01d

To a stirring solution of **2.09d** (970 mg, 2.56 mmol) in 1,1,1,3,3,3-hexafluoroisopropanol and furan [1:1 (v/v) 0.25 M] at 0 °C was added triethylamine (0.73 mL, 5.13 mmol) dropwise over 5 min. Stirring continued at 0 °C for 5 min, then the reaction was allowed to warm to rt over 30 min. The volatile compounds were removed under reduced pressure and the residue was purified by flash column chromatography (10% EtOAc/hexanes) to afford monomer **2.01d** (740 mg, 79%). ^{1}H-NMR ($CDCl_3$, 500 MHz): δ 6.72 (broad d, *J* = 6 Hz, 1H), 6.84 (dd, *J* = 6.0 Hz, 1.7 Hz, 1H), 5.48 (d, *J* = 1 Hz, 1H), 4.51 (d, *J* = 1.7, 1H), 3.92 (ABX_2, J_{AB} = 9.3, J_{AX} = J_{BX} = 6.8 Hz, 2H), 1.70 – 1.60 (m, 2H), 1.49 (s, 3H), 1.45-1.20 (m, 22 H), 1.05 (s, 3H), 0.88 (t, *J* = 7.0 Hz, 3H). ^{13}C-NMR ($CDCl_3$, 1.25 MHz): δ 175.6, 135.5, 134.7, 90.7, 87.4, 75.9, 48.9, 31.9, 29.7, 29.7, 29.7 (2), 29.6, 29.5, 29.4, 29.4, 28.2, 26.9, 25.9, 22.7, 19.7, 14.2. HRESI-MS calcd for $C_{22}H_{39}NO_3$ $[M+H]^+$ 366.3003; found 366.3010.

Compound 2.32e

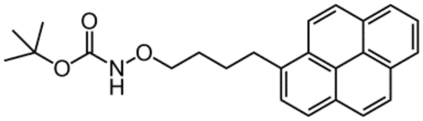

To a stirring solution of 4-(1-pyrenyl)butyl methanesulfonate (415 mg, 1.18 mmol) and *N*-Boc hydroxylamine (235 mg, 1.77 mmol) in DMF (1.3 mL) was added DBU (0.26 mL, 1.77 mmol) in DMF (0.65 mL). The reaction was allowed to stir for 20 h at 50 ^{o}C. The reaction was then concentrated and the residue was purified on a flash chromatography column (20% EtOAc/Hexanes). **2.32e** was isolated as an oil (236 mg, 51%). ^{1}H-NMR ($CDCl_3$, 300 MHz): δ 8.19 (dd, *J* = 9.3 Hz, 1H), 8.12-8.06 (m, 2H), 8.05-8.00 (m, 2H), 7.98-7.88 (m, 3H), 7.77 (d, *J* = 7.9 Hz, 1H), 7.21 (broad s, 1H), 3.86 (t, *J* = 6.6 Hz, 2H), 3.30 (t, *J* = 7.4 Hz, 2H), 1.96-1.82 (m, 4H), 1.82-1.68 (m, 4H), 1.44 (s, 9H). ^{13}C-NMR ($CDCl_3$, 75 MHz): δ 157.1, 136.6, 131.5, 131.0, 129.9, 128.7, 127.6, 127.3, 127.3, 126.7, 125.9, 125.2, 125.1, 124.9, 124.9, 124.8, 123.5, 81.7, 76.6, 33.3, 28.3, 28.2, 27.7. HRESI-MS calcd for $C_{25}H_{31}NO_3$ $[M+NH_4]^+$ 407.2333; found 407.2348.

Compound 2.08e

To a stirring solution of **2.32e** (117 mg, 0.30 mmol) in dichloromethane (1.5 mL) at 0 ^{o}C was added trifluoroacetic acid (0.75 mL). Stirring continued for 1 h at 0 ^{o}C. The volatile compounds were removed under reduced pressure and the excess acid was removed by azeotroping with toluene (3 x 20 mL). Compound **2.08e** was obtained as an oil (121 mg, quant.), which was carried on without further purification. ^{1}H-NMR ($CDCl_3$, 300 MHz): δ 10.09 (broad s, 3H), 8.00-7.50 (m, 8H), 7.35 (d, *J* = 8.1 Hz, 1H), 3.92 (broad t, *J* = 5.5 Hz, 2H), 2.82 (broad t, *J* = 7.0 Hz, 2H), 1.70-130 (m, 4H). ^{13}C-NMR ($CDCl_3$, 75 MHz): δ 135.8, 131.5, 130.9, 129.9, 129.3, 128.5, 127.5, 127.3, 126.9, 126.7, 125.7, 125.6, 125.0, 125.0, 124.8, 123.1, 75.9, 32.6, 27.5, 27.3. HRESI-MS calcd for $C_{20}H_{20}NO$ $[M\text{-}TFA]^+$ 290.1540; found 290.1532.

Compound 2.09e

To a stirring solution of **2.08e** (120 mg, 0.30 mmol) in dichloromethane (1.05 mL) at 0 ^oC was added triethylamine (38 μL, 0.30 mmol) in one portion followed by α-bromo isobutyryl bromide (36 μL, 0.30 mmol) dropwise. Stirring continued for 15 min at 0 ^oC. Pyridine (30 μL, 0.35 mmol)) was added and the reaction was allowed to slowly warm to rt. After 20 h, the reaction was diluted with dichloromethane (5 mL) and washed with H_2O (2 x 4 mL). The organic phase was dried over Na_2SO_4. The drying agent was removed by filtration and the solvent was removed under reduced pressure. The residue was purified by flash column chromatography (20% EtOAc/hexanes). Compound **2.09e** was obtained as an oil (68 mg**,** 53%). ^1H-NMR ($CDCl_3$, 300 MHz): δ 9.14 (broad s, 1H), 8.23 (d, *J* = 9.1 Hz, 1H), 8.16-8.10 (m, 2H), 8.00-7.91 (m, 3H), 7.82- (d, *J* = 7.7 Hz, 1H), 3.94 (t, *J* = 6.6 Hz, 2H), 3.35 (t, *J* = 7.4 Hz, 2H), 2.04-1.86 (m, 8H), 1.86-1.74 (m, 2H). ^{13}C-NMR ($CDCl_3$, 75 MHz): δ 169.9, 136.5, 131.6, 131.1, 130.0, 128.8, 127.7, 127.5, 126.8, 126.0, 125.2, 125.2, 125.0, 125.0, 124.9, 123.5, 76.7, 59.6, 33.3, 32.5, 28.0. ESI-MS calcd for $C_{48}H_{53}BrN_2O_4$ $[2M\text{-}HBr]^+$ calcd 795.7; found 796.4. **2.09e** was found to dimerize upon ionization, eliminating 1 eq of HBr.

Monomer 2.01e

To a stirring solution of **2.09e** (120 mg, 0.28 mmol) in 1,1,1,3,3,3-hexafluoroisopropanol and furan [1:1 (v/v) 0.25 M] at 0 ^oC was added triethylamine (73 μL, 0.59 mmol) dropwise over 5 min. Stirring continued at 0 ^oC for 5 min, then the reaction was allowed to warm to rt over 40 min. The volatile compounds were removed under reduced pressure and the residue was purified by flash column chromatography (20% EtOAc/hexanes). Compound **2.01e** was obtained as an orange solid (96 mg, 82%). ^{1}H-NMR ($CDCl_3$, 300 MHz): δ 8.25 (d, *J* = 9.0 Hz, 1H), 8.18-8.11 (m, 2H), 8.11-8.05 (m, 2H), 8.02-7.93 (m, 3H), 7.84 (d, *J* = 7.8 Hz, 1H), 6.65 (dd, *J* = 5.8, 0.9 Hz, 1H), 6.43 (dd, *J* = 6.1, 1.8 Hz, 1H), 5.42 (d, *J* = 1.1 Hz, 1H), 4.46 (d, *J* = 1.7 Hz, 1H), 3.98 (ABX_2, J_{AB} = 9.3 Hz, J_{AX} = J_{BX} = 6.5 Hz, 2H), 3.36 (t, *J* = 7.6 Hz, 2H), 2.05-1.72 (m, 4H), 1.47 (s, 3H), 1.03 (s, 3H). ^{13}C-NMR ($CDCl_3$, 75 MHz): δ 175.9, 136.7, 135.6, 134.9, 131.7, 131.1, 130.0, 128.9, 127.7, 127.5, 127.5, 126.8, 126.0, 125.3, 125.3, 125.1, 125.0, 124.9, 123.6, 91.0, 87.6, 75.7, 49.2, 33.4, 28.5, 28.3, 27.1, 20.0. HRESI-MS calcd for $C_{28}H_{27}NO_3$ $[M+H]^+$ 426.2064; found 426.2063.

Compound 2.08f

To a stirring solution of *N*-Boc-*O*-(6-bromohexyl) hydroxylamine (954 mg, 3.22 mmol) in dichloromethane (16 mL) at 0 ^{o}C was added trifluoroacetic acid (8.0 mL). Stirring continued for 1 h at 0 ^{o}C. The volatile compounds were removed under reduced pressure and the excess acid was removed by azeotroping with toluene (3 x 20 mL). Compound **2.08f** was obtained as a clear oil (998 mg, quant.), which was carried on without further purification. ^{1}H-NMR ($CDCl_3$, 300 MHz): δ 10.41 (broad s, 3H), 4.05 (broad t, *J* = 6.2 Hz, 2H), 3.40 (t, *J* = 7.0 Hz, 2H), 1.85 (pent, *J* = 6.7 Hz, 2H), 1.68 (broad pent, *J* = 6.3 Hz, 2H), 1.51-1.33 (m, 4H). ^{13}C-NMR ($CDCl_3$, 75 MHz): δ 33.7, 32.6, 27.8, 27.6, 24.2. HRESI-MS calcd for $C_6H_{15}BrNO$ $[M+H]^+$ 196.0332; found 196.0332.

Compound 2.09f

To a stirring solution of **2.08f** (945 mg, 3.05 mmol) in dichloromethane (11.5 mL) at 0 ^{o}C was added triethylamine (0.38 mL, 3.1 mmol) in one portion followed by α-bromoisobutyryl bromide (0.37 mL, 3.05 mmol) dropwise. Stirring continued for 15 min at 0 ^{o}C. Pyridine (0.29 mL, 3.45 mmol) was added and the reaction was allowed to slowly warm to rt. After 20 h, the reaction was diluted with dichloromethane (12 mL) and washed with H_2O (2 x 12 mL). The organic phase was dried over Na_2SO_4. The drying agent was removed by filtration and the solvent was removed under reduced pressure. The residue was purified by flash column chromatography (20% EtOAc/hexanes). **2.09f** was obtained as a light yellow oil (600 mg, 57%). ^{1}H-NMR ($CDCl_3$, 300 MHz): δ 9.59 (broad s, 1H), 3.95 (t, *J* = 6.7 Hz, 2H), 3.42 (t, *J* = 6.8 Hz, 2H), 1.97 (s, 6H), 1.87 (pent, *J* = 7.0 Hz, 2H), 1.68 (pent, *J* = 6.9 Hz, 2H), 1.53-1.38 (m, 4H). ^{13}C-NMR ($CDCl_3$, 75 MHz): δ 169.5, 76.2, 58.6, 33.8, 32.5, 32.1, 27.8, 27.7, 24.9. HRESI-MS calcd for $C_{10}H_{19}Br_2NO_2$ $[M+H]^+$ 343.9856; found 343.9851.

Monomer 2.01f

To a stirring solution of **2.09f** (665 mg, 1.93 mmol) in 1,1,1,3,3,3-hexafluoroisopropanol and furan [1:1 (v/v) 0.25 M] at 0 ^{o}C was added triethylamine (0.46 mL, 3.85 mmol) dropwise over 5 min. Stirring continued at 0 ^{o}C for 5 min, then the reaction was allowed to warm to rt over 40 min. The volatile compounds were removed under reduced pressure and the residue was purified by flash column chromatography (20% EtOAc/hexanes). Compound **2.01f** was obtained as a light yellow oil (406 mg, 63%). ^{1}H-NMR ($CDCl_3$, 300 MHz): δ 6.73 (dd, *J* = 6.0, 1.0 Hz, 1H), 6.48 (dd, *J* =6.0, 1.8 Hz, 1H), 5.48 (d, *J* = 1.0 Hz, 1H), 4.51 (d, *J* = 1.8 Hz, 1H), 3.92 (ABX_2, J_{AB} = 9.6 Hz, J_{AX} = J_{BX} = 6.8 Hz, 2H), 3.41 (t, *J* = 6.8 Hz, 2H), 1.87 (broad pent, *J* = 6.8 Hz, 2H), 1.67 (m, 2H), 1.49 (s, 3H), 1.46 (m, 4H), 1.05 (s, 3H). ^{13}C-NMR ($CDCl_3$, 75 MHz): δ

175.6, 135.4, 134.7, 90.7, 87.3, 75.4, 48.9, 33.8, 32.6, 28.0, 27.9, 26.9, 25.1, 19.8. HRESI-MS calcd for $C_{14}H_{22}BrNO_3$ $[M+H]^+$ = 332.0856; found 332.0840.

Monomer 2.01g

To a stirring solution of **2.01f** (100 mg, 0.302 mmol) in DMF (10 mL) was added sodium azide (98 mg, 1.51 mmol). The solution was allowed to stir at 65 ^{o}C for 17 h. After cooling to rt, the solution was diluted with water (10 mL) and extracted with EtOAc (3 x 15 mL). The combined organic phase was dried over Na_2SO_4. The drying agent was removed by filtration and the solvent was removed under reduced pressure to afford **2.01g** as a clear oil (73 mg, 83%). Intermediate **2.01g** was taken on immediately without further purification, as it was found to be unstable. ^{1}H-NMR ($CDCl_3$, 300 MHz): δ 6.70 (dd, *J* = 5.8, 1.0 Hz, 1H), 6.49 (dd, *J* = 6.0, 1.7 Hz, 1H), 5.47 (d, *J* = 1.1 Hz, 1H), 4.50 (d, *J* = 1.6 Hz, 1H), 3.92 (ABX_2, $J_{AX} = J_{BX}$ = 6.7 Hz, J_{AB} = 9.2 Hz, 2H), 3.27 (t, *J* = 7.0 Hz, 2H), 1.71-1.56 (m, 4H), 1.48 (s, 3H), 1.48-1.39 (m, 4H), 1.04 (s, 3H). ^{13}C-NMR ($CDCl_3$, 75 MHz): δ 175.4, 135.3, 134.6, 90.6, 87.1, 75.3, 51.2, 48.8, 28.5, 27.9, 26.7, 26.3, 25.3, 19.6. HRESI-MS calcd for $C_{14}H_{22}N_4O_3$ $[M+H]^+$ 295.1765; found 295.1758.

Monomer 2.01h

To a stirring solution of **2.01g** (37 mg, 0.126 mmol) and 1-propargyl-α-*D*-mannose-2,3,4,6-tetraacetate (49 mg, 0.126 mmol)[2] in toluene (0.25 mL) was added tris(triphenylphosphine) copper(I) bromide (2.7 mg, 0.0063 mmol). The reaction was allowed to stir at room temperature over night. The reaction was then directly loaded onto a silica flash chromatography column for purification (60 → 90% EtOAc/hexanes). Compound **2.01h** was isolated as an oil (55 mg, 64%). ^{1}H-NMR ($CDCl_3$. 300 MHz): δ 7.60 (s, 1H), 6.72 (dd, *J* = 6.2, 1.0 Hz, 1H), 6.49 (dd, *J* = 6.0, 1.7 Hz, 1H), 5.47 (d, *J* = 1.0 Hz, 1H), 5.36-5.24 (m, 3H), 4.96 (d, *J* = 1.4 Hz, 1H), 4.85 (d, *J* = 12.1 Hz, 1H), 4.68 (d, *J* = 12.1 Hz, 1H), 4.51 (d, *J* = 1.9 Hz, 1H), 4.37 (t, *J* = 7.4 Hz, 2H), 4.30 (dd, *J* = 12.4, 5.4 Hz, 1H), 4.13-4.06 (m, 3H), 3.96 (ABX_2, J_{AB} = 9.6, $J_{AX} = J_{BX}$ = 6.6 Hz, 2H), 2.16 (s, 3H), 2.12 (s, 3H), 2.04 (s, 3H), 1.99 (s, 3H), 2.00-1.90 (m, 2H), 1.71-1.60 (m, 2H), 1.53-1.34 (m, 6H), 1.05 (s, 3H). ^{13}C-NMR ($CDCl_3$. 75 MHz): δ 175.9, 170.8, 170.2, 170.0, 169.9, 143.6, 135.6, 134.9, 122.9, 97.0, 90.8, 87.5, 75.5, 69.6, 69.2, 68.8, 66.2, 62.3, 61.3, 50.4, 49.1, 30.3, 28.1, 27.0, 26.4, 25.4, 21.0, 20.9, 20.8. 20.8. 19.9. HRESI-MS calcd for $C_{31}H_{44}N_4O_{13}$ $[M+H]^+$ 681.2978; found 681.2986.

Compound 2.10

To a suspension of *O*-(carboxy) hydroxylamine hemichloride (2.00 g, 18.3 mmol) in allyl alcohol (36 mL) at 0 °C was added thionyl chloride (1.6 mL, 22.0 mmol), dropwise, over 15 min. The solution was moved to a 75 °C oil bath and stirred for 2 h. The solution was cooled to rt and the solvent was removed *in vacuo* to afford an orange-brown residue. The residue was taken up in methanol and treated with activated charcoal. After 15 min, the charcoal was removed by filtration and the solvent was removed *in vacuo* to afford compound **2.10** (3.18 g, quant), which was taken on without further purification. ^{1}H-NMR (MeOH-d_4, 300 MHz): δ 6.11 (ddt, *J* = 17, 11, 5 Hz, 1H), 5.51 (d, *J* = 17 Hz, 1H), 5.43 (d, *J* = 11 Hz, 1H), 5.06 (broad s, 4H). ^{13}C-NMR (MeOH-d_4, 75 MHz): δ 169.9, 132.8, 119.5, 71.6, 67.3.

Compound 2.11

To a stirring solution of compound **2.10** (2.94 g, 17.5 mmol) and pyridine (2.82 mL, 35.0 mmol) in dichloromethane (70 mL) at 0 °C was added BIBB (2.14 mL, 17.3 mmol), dropwise.

The solution was stirred for 15 h, then diluted with dichloromethane (35 mL) and then washed with water (2 x 70 mL). The organic phase was dried and concentrated and the crude residue was purified by silica column chromatography (25% EtOAc/hex) to afford compound **2.11** (2.81 g, 58%). ^{1}H-NMR ($CDCl_3$. 300 MHz): δ 9.9 (s, 1H), 5.93 (ddt, *J* = 17, 11, 5 Hz, 1H), 5.43-5.29 (m, 2H), 4.72 (dt, *J* = 6, 1 Hz, 2H), 4.55 (d, 2H), 1.96 (s, 6H).

Compound 2.12

To a stirring solution of **2.11** (1.00 g, 3.53 mmol) in 1,1,1,3,3,3-hexafluoroisopropanol and furan [1:1 (v/v) 0.25 M] at 0 °C was added triethylamine (1.00 mL, 7.06 mmol) dropwise over 5 min. Stirring continued at 0 °C for 5 min, then the reaction was allowed to warm to rt over 30 min. The volatile compounds were removed under reduced pressure and the residue was purified by flash column chromatography (25% EtOAc/hexanes) to afford monomer **2.12** (648 mg, 68%). ^{1}H-NMR ($CDCl_3$, 300 MHz): δ 6.76 (dd, *J* = 5.9, 1.0 Hz, 1H), 6.51 (dd, *J* = 5.9, 2.9 Hz, 1H), 6.00 (d, *J* = 1.2 Hz, 1H), 5.94 (ddt, *J* = 17.4, 10.6, 5.6 Hz, 1H), 5.36 (dq, *J* = 17.4, 1.4 Hz, 1H), 5.29 (dq, *J* = 10.8, 1.4 Hz, 1H), 4.70 (m, 2H), 4.55 (s, 2H), 4.50 (d, 1.8 Hz, 1H), 1.48 (s, 3H), 1.06 (s, 2H).

Compound 2.13

To a solution of **2.12** (200 mg, 0.75 mmol) and morpholine (0.32 mL, 3.77 mmol) in THF (20 mL) was added $Pd(PPh_3)_4$ (83 mg, 0.075 mmol). The solution was stirred at rt for 1 h and then the reaction was concentrated *in vacuo*. The residue was dissolved in sat. $NaHCO_3$ (25 mL) and washed with dichloromethane (3 x 20 mL). The aqueous solution was acidified to pH = 2 with 1 M HCl and the solution was extracted with EtOAc (4 x 50 mL). The combine EtOAc phase was dried and concentrated to afford compound **2.13** (174 mg, quant), which was taken on without further purification. ^{1}H-NMR ($CDCl_3$, 300 MHz): δ 9.74 (s, 1H, -OH), 6.78 (dd, *J* = 5.9, 0.8 Hz, 1H), 6.59 (dd, *J* = 6.1, 2.9 Hz, 1H), 5.79 (d, *J* = 1.0 Hz, 1H), 4.58 (AB quartet, *J* = 17.3 Hz, 2H), 4.58 (d, *J* = 2.8 Hz, 1H), 1.51 (s, 3H), 1.10 (s, 3H). ^{13}C-NMR ($CDCl_3$, 75 MHz): δ 179.7, 170.8, 135.6, 135.2, 91.7, 87.0, 73.4, 49.1, 26.8, 19.6.

Compound 2.14

To a stirring solution of **2.13** (471 mg, 2.07 mmol) in dichloromethane (2.5 mL) was added *N*-hydroxysuccinimide (337 mg, 2.94 mmol) and EDCI (442 mg, 2.86 mmol). The solution was stirred at rt for 15 h. The reaction was diluted with dichloromethane (10 mL) and washed with 5% citric acid solution (2 x 20 mL), sat. $NaHCO_3$ (3 x 20 mL), and brine (1 x 20 mL). The organic phase was dried and concentrated. The residue was purified by silica column chromatography (75% EtOAc/hex) to afford compound **2.14** (35 mg, 5%). ^{1}H-NMR ($CDCl_3$, 300 MHz): δ 6.70 (dd, *J* = 6.5, 1.0 Hz, 1H), 6.51 (dd, *J* = 6.5, 2.0 Hz, 1H), 5.90 (d, *J* = 1.0 Hz, 1H), 4.87 (s, 2H), 4.50 (d, 2.0 Hz, 1H), 2.88 (s, 4H), 1.50 (s, 3H), 1.06 (s, 3H). ^{13}C-NMR ($CDCl_3$, 75 MHz): δ 178.3, 168.8, 165.4, 135.4, 135.2, 92.5, 87.2, 70.61, 50.0, 26.8, 19.9, 25.7.

Compound 2.17

To a solution of ketone **2.16** (1.95 g, 6.53 mmol) in benzene (25 mL) was added ethylene glycol (1.35 mL, 24.2 mmol) and *p*-toluene sulfonic acid monohydrate (12 mg, 0.063 mmol). The solution was then refluxed under Dean-Stark conditions for 15 h and then cooled to rt. The solution was diluted with dichloromethane (80 mL) and washed with brine (2 x 60 mL) followed by DI water (2 x 60 mL). The organic layer was dried over Na_2SO_4, filtered, and concentrated to afford **2.17** as a white solid (2.13 g, 95%). ^{1}H-NMR ($CDCl_3$, 500 MHz): δ 7.85-7.80 (m, 2H), 7.77-7.72 (m, 2H), 7.56-7.48 (m, 4H), 5.21 (s, 2H), 4.06-4.00 (m, 2H), 3.78-3.71 (m, 2H), 1.64 (s, 3H). ^{13}C-NMR (CDCl$_3$, 125 MHz): δ 163.5, 144.5, 134.5, 133.2, 129.7, 128.9, 125.6, 123.5, 108.7, 79.7, 64.4, 27.5. HRESI-MS calcd for $C_{19}H_{17}NO_5$ [M+H]$^+$ 340.1180; found 340.1176.

Compound 2.18

To a stirring solution of **2.17** (517 mg, 1.52 mmol) in $CHCl_3$ (4.7 mL) was added hydrazine (0.11 mL, 3.35 mmol, anhydrous). The solution was stirred for 1.5 h at rt, during which time a white precipitate appeared. The solution was diluted with $CHCl_3$ (2 mL) and the insoluble solids were filtered off. The filtrate was concentrated and the resultant yellow oil, **2.18**, was taken on without further purification (322 mg, quant). ^{1}H-NMR (CDCl$_3$, 500 MHz): δ 7.52-7.45 (m, 2H), 7.37-7.31 (m, 2H), 5.41 (broad s, 2H, -NH$_2$), 4.69 (s, 2H), 4.07-3.97 (m, 2H), 3.81-3.73 (m, 2H), 1.65 (s, 3H). ^{13}C-NMR (CDCl$_3$, 125 MHz): δ 143.1, 137.0, 18.2, 125.5, 108.8, 77.7, 64.4, 27.6. HRESI-MS calcd for $C_{11}H_{15}NO_3$ [M+H]$^+$ 210.1125; found 210.1118.

Compound 2.19

To a stirring solution of **2.18** (315 mg, 1.51 mmol) in dichloromethane (6 mL) at 0 ^{o}C was added pyridine (0.26 mL, 3.24 mmol) followed by α-bromoisobutyryl bromide (0.19 mL, 1.51 mmol), which was added dropwise. The solution was stirred for 1 h at rt. The solution was diluted with dichloromethane (10 mL) and washed with DI water (2 x 9 mL). The organic layer was dried over Na_2SO_4, filtered, and concentrated. The resultant residue was purified by flash column chromatography (35% EtOAc/hexanes). Compound **2.19** was obtained as an off-white solid (400 mg, 74%). ^{1}H-NMR (CDCl$_3$, 500 MHz): δ 9.09 (s, 1H, NH), 7.55-7.48 (m, 2H), 7.43-7.36 (m, 2H), 4.93 (s, 2H), 4.09-3.99 (m, 2H), 3.81-3.71 (m, 2H), 1.94 (s, 6H), 1.65 (s, 3H). ^{13}C-

NMR ($CDCl_3$, 125 MHz): δ 169.6, 144.2, 134.3, 129.4, 125.7, 108.7, 78.0, 64.5, 59.4, 32.4, 27.6. HRESI-MS calcd for $C_{15}H_{20}BrNO_4$ $[M+H]^+$ 358.0649; found 358.0643.

Compound 2.20

To a stirring solution of **2.19** (937 mg, 2.61 mmol) in acetone (10.8 mL) was added iodine (66 mg, 0.26 mmol). The solution was stirred for 10 min at rt, then concentrated to ~¼ total volume. The remaining solution was diluted with dichloromethane (26 mL) and washed with 5% $Na_2S_2O_3{\bullet}5H_2O$ (1 x 26 mL) and DI water (2 x 26 mL). The organic layer was dried over Na_2SO_4, filtered, and concentrated to afford **2.20** as a white solid (823 g, quant). ^{1}H-NMR ($CDCl_3$, 500 MHz): δ 9.32 (s, 1H, NH), 7.92-7.86 (m, 2H), 7.47-7.41 (m, 2H), 4.92 (s, 2H), 2.53 (s, 3H), 1.86 (s, 6H). ^{13}C-NMR ($CDCl_3$, 125 MHz): δ 197.8, 169.9, 140.0, 137.2, 129.2, 128.6, 77.4, 58.9, 32.2, 26.7. HRESI-MS calcd for $C_{13}H_{16}BrNO_3$ $[M+H]^+$ 314.0387; found 314.0377.

Monomer 2.21

To a stirring solution of **2.20** (89.5 mg, 0.28 mmol) in furan (0.57 mL) and 1,1,1,3,3,3-hexafluoroisopropanol (0.57 mL) at 0 ^{o}C was added triethylamine (79 μL, 0.57 mmol) dropwise. The solution was then stirred at rt for 30 min and then concentrated. The resultant residue was purified by flash column chromatography (40% EtOAc/hexanes). Compound **2.21** was obtained as a clear oil (50 mg, 58%). ^{1}H-NMR ($CDCl_3$, 500 MHz): δ 8.02-7.90 (m, 2H), 7.58-7.49 (m, 2H), 6.63 (dd, *J* = 6.0, 1.0 Hz, 1H), 6.48 (dd, *J* = 6.0, 1.8 Hz, 1H), 5.28 (d, *J* = 1.1 Hz, 1H), 4.98 (AB quartet, *J* = 11.3, 2H), 4.49 (d, *J* = 1.8 Hz, 1H), 2.61 (s, 3H), 1.48 (s, 3H), 1.06 (s, 3H). ^{13}C-NMR ($CDCl_3$, 125 MHz): δ 197.7 (C), 176.1 (C), 140.7 (C), 137.2 (C), 135.2 (CH), 134.8 (CH), 129.5 (CH), 128.5 (CH), 91.3 (CH), 87.3 (CH), 77.0 (CH_2, under solvent), 49.3 (C), 26.9 (CH_3), 26.7 (CH_3), 19.7 (CH_3). HRESI-MS calcd for $C_{17}H_{19}NO_4$ $[M+H]^+$ 302.1387; found 302.1391.

Ligand 2.23

2-(2-(2-(N-Boc aminoxy)ethoxy)ethoxy)ethanol (24 mg, 0.09 mmol) was dissolved in a 4M solution of hydrochloric acid in 1,4-dioxane (0.79 mL). The solution was stirred for 1 h at rt and then concentrated. Excess acid was azeotroped with dichloromethane (3 x 0.5 mL). Compound **2.23** was isolated as a clear oil (20 mg, quant). ^{1}H-NMR (MeOH-d$_4$, 500 MHz): δ 4.24-4.16 (m, 2H), 3.90-3.80 (m, 2H), 3.73-3.65 (m, 6H), 3.61-3.56 (m, 2H). ^{13}C-NMR (CDCl$_3$, 125 MHz): δ 72.8, 72.2, 70.6, 70.1, 69.2, 60.8. HRESI-MS calcd for $C_6H_{16}NO_4$ [M-Cl]$^+$ 166.1074; found 166.1076.

Compound 2.27

To a stirring solution of **2.21** (75 mg, 0.25 mmol) and 1-hexene (0.15 mL, 1.24 mmol) in dichloromethane (0.63 mL) was added Grubbs' 2nd Generation catalyst (**2.02**, 21 mg, 0.025 mmol) in dichloromethane (0.27 mL). The solution was stirred for 2 h at rt and then the reaction was quenched by the addition of ethyl vinyl ether (0.4 mL). After an additional hour of stirring, the solution was concentrated *in vacuo* and the crude residue was purified by flash column chromatography (20% ethyl acetate/hexanes). Products **2.27** (66 mg, 69%) was isolated as a pure brown solid which was separable from disubstituted product, **2.27'**, (20 mg, 18%). **2.27:** ^{1}H-NMR (CDCl$_3$, 400 MHz): δ 7.93 (d, *J* = 8.3 Hz, 2H), 7.48 (d, *J* = 8.3 Hz, 2H), 5.99 (dt, *J* = 15.4, 6.8 Hz, 1H), 5.79 (ddd, *J* = 17.2, 10.6, 6.5 Hz, 1H), 5.51 (ddt, *J* = 15.4, 7.7, 1.4 Hz, 1H), 5.38-5.26 (m, 2H), 5.16 (d, *J* = 7.7 Hz, 1H), 5.07 (d, *J* = 10.2 Hz, 1H), 4.82 (d, *J* = 10.2 Hz, 1H), 4.00 (d, *J* = 6.4 Hz, 1H), 2.59 (s, 3H), 2.15-2.05 (m, 2H), 1.42-1.27 (m, 4H), 1.23 (s, 3H), 1.14 (s, 3H), 0.88 (t, *J* = 7.1 Hz, 3H). ^{13}C-NMR (CDCl$_3$, 100 MHz): δ 197.8, 173.9, 140.4, 139.9, 137.3, 132.0, 129.3, 128.5, 125.4, 119.5, 91.6, 82.8, 76.7, 45.1, 32.0, 30.9, 26.8, 22.4, 21.0, 20.6, 14.0. HRESI-MS calcd for $C_{23}H_{31}NO_4$ [M+H]$^+$ 386.2326; found 386.2328. **2.27':** ^{1}H-NMR (CDCl$_3$, 400 MHz): δ 7.92 (d, *J* = 8.3 Hz, 2H), 7.48 (d, *J* = 8.3 Hz, 2H), 5.97 (dt, *J* = 15.4, 6.7 Hz, 1H), 5.73 (dt, *J* = 15.4, 6.7 Hz, 1H), 5.50 (ddt, *J* = 15.4, 7.8, 1.3 Hz, 1H), 5.42 (ddt, *J* = 15.5, 7.4, 1.3 Hz, 1H), 5.15 (d, *J* = 7.8 Hz, 1H), 5.07 (d, *J* = 10.2 Hz, 1H), 4.82 (d, *J* = 10.2 Hz, 1H), 2.59 (s, 3H), 2.15-2.01 (m, 4H), 1.44-1.21 (m, 11H), 1.09 (s, 3H), 0.93-0.84 (m, 6H). ^{13}C-NMR ($CDCl_3$, 100 MHz): δ 197.8, 174.2, 140.5, 139.8, 137.2, 137.1, 129.3, 128.3, 125.8, 124.7, 91.6, 83.0, 76.6, 45.3, 32.3, 31.9, 31.2, 30.8, 26.8, 22.4, 22.3, 21.1, 20.8, 14.0, 14.0. HRESI-MS calcd for $C_{27}H_{39}NO_4$ $[M+H]^+$ 442.2952; found 442.2962.

Compound 2.26

Compound **2.27** (4.8 mg, 12.5 μmol) was taken up in a 252 μL of a 19.0 mg/mL solution of *O*-pyrenyl hydroxylamine hydrochloride in DMSO. The solution was stirred at rt for 24 h and then diluted with dichloromethane (1.5 mL). The solution was washed with brine (3 x 1 mL), dried, and concentrated. The crude residue was purified by flash column chromatography (15 → 25% ethyl acetate/hexanes). Compound **2.26** was isolated as a brown oil (4 mg, 49%). ^{1}H-NMR ($CDCl_3$, 500 MHz): δ 8.29 (d, *J* = 9.3 Hz, 1H), 8.15-7.95 (m, 7H), 7.89 (d, *J* = 7.8 Hz, 1H), 7.61 (d, *J* = 8.2 Hz, 2H), 7.36 (d, *J* = 7.8 Hz, 2H), 5.95 (dt, *J* = 15.4, 6.7 Hz, 1H), 5.79 (ddd, *J* = 17.2, 10.7, 6.5 Hz, 1H), 5.49 (ddt, *J* = 15.4, 7.7, 1.5 Hz, 1H), 5.36-5.28 (m, 2H), 5.11 (d, *J* = 7.4 Hz, 1H), 5.04 (d, *J* = 9.8 Hz, 1H), 4.79 (d, *J* = 9.8, 1H), 4.29 (t, *J* = 6.4 Hz, 2H), 3.98 (d, *J* = 6.5 Hz, 1H), 3.41 (t, *J* = 7.4 Hz, 2H), 2.21 (s, 3H), 2.15-2.07 (m, 2H), 2.03-1.89 (m, 4H), 1.42-1.32 (m, 4H), 1.23 (s, 3H), 1.15 (s, 3H), 0.90 (t, *J* = 7.2 Hz, 3H). ^{13}C-NMR ($CDCl_3$, 125 MHz): δ 154.0, 139.7, 137.3, 137.0, 135.9, 132.1, 131.6, 131.1, 130.5, 129.9, 129.7, 128.0, 127.7, 127.6, 127.4, 127.3, 126.7, 126.1, 125.9, 125.5, 125.0, 124.9, 124.8, 123.6, 119.4, 91.5, 82.7, 74.1, 45.1, 34.8, 33.4, 32.0, 30.9, 29.4, 29.2, 28.4, 25.4, 21.0, 20.7, 12.8, 11.6. HRESI-MS calcd for $C_{43}H_{48}N_2O_4$ $[M+H]^+$ 657.3687; found 657.3690.

Compound 2.30

To a stirring solution of **2.01b** (100 mg, 0.388 mmol) in dichloromethane (1.0 mL) was added 1-hexene (0.24 mL, 1.95 mmol) and then catalyst **2.02** (33 mg, 0.0388 mmol) in dichloromethane (0.3 mL). The reaction was allowed to stir at room temperature for 1.45 h and was then quenched by the addition of ethyl vinyl ether (150 μL). The solution was allowed to stir for an additional hour. The volatiles were removed under reduced pressure and the residue was purified by flash column chromatography (5 → 18% EtOAc/hexanes). Compound **2.03** was isolated as a red oil (59 mg, 44%). ^{1}H-NMR ($CDCl_3$, 300 MHz): δ 7.45-7.30 (m, 5H), 5.95 (dt, *J* = 15.5, 7.0 Hz, 1H), 5.79 (ddd, *J* = 17.4, 10.5, 6.5 Hz, 1H), 5.49 (ddt, *J* = 15.5, 7.8, 1.5 Hz, 1H), 5.32 (dt, *J* = 17.5, 1.5 Hz, 1H), 5.30 (dt, *J* = 10.5, 1.5 Hz, 1H), 5.08 (d, *J* = 7.8 Hz, 1H), 4.90 (AB quartet, J_{AB} = 9.5 Hz, 2H), 3.96 (broad d, *J* = 6.0 Hz, 1H), 2.12 (broad quart, *J* = 6.8 Hz, 2H), 1.49-1.31 (m, 4H), 1.23 (s, 3H), 1.14 (s, 3H), 0.91 (t, *J* = 7.2 Hz, 3H). ^{13}C-NMR ($CDCl_3$, 75 MHz): δ 173.4, 139.7, 135.3, 132.2, 129.8, 128.9, 128.5, 125.5, 119.4, 91.5, 82.7, 77.3, 45.0, 31.98, 30.9, 22.5, 21.0, 20.7, 14.9. HRESI-MS calcd for $C_{21}H_{29}NO_3$ $[M+H]^+$ 344.2; observed 344.2. The regiochemistry of **2.30** was determined by the coupling between signals at δ 5.49 to δ 5.08 and coupling between signals at δ 5.79 to δ 3.96. NMR spectrum showed that is single isomer was isolated.

Compound 2.31

To a stirring solution of **2.30** (20 mg) in methanol (0.50 mL) was added 1 mL of a 2.27 M HCl solution in methanol. The solution was allowed to stir at 45 °C for 17 h. The solution was neutralized by elution through a plug of Aberlite® IRA 400(OH) basic resin and the volatiles were removed under reduced pressure. The residue was purified by flash column chromatography (the column was packed with 10% EtOAc/hexanes and eluted with a gradient to

20% EtOAc/hexanes). A low R_f fraction was isolated to afford a clear oil characterized as **2.31**. ^{1}H-NMR ($CDCl_3$, 500 MHz): δ 8.85 (s, 1H, NH), 7.60-7.25 (m, 5H), 5.82 (ddd, *J* = 17.1, 10.3, 6.8 Hz, 1H), 5.28 (dt, *J* = 17.2, 1.0 Hz, 1H), 5.23 (dd, 10.3, 1.0 Hz, 1H), 4.91 (s, 2H), 3.99 (broad d, *J* = 6.9 Hz, 1H), 1.21 (s, 3H), 1.08 (s, 3H). ^{13}C-NMR ($CDCl_3$, 125 MHz): δ 174.7, 136.1, 135.3, 129.3, 128.8, 128.6, 118.5, 78.6, 78.0, 45.0, 23.8, 20.4. HRESI-MS calcd for $C_{14}H_{19}NO_3$ $[M+Na]^+$ 272.1288; observed 272.1266.

2.6.3. Synthesis of polymers

General Procedure A: Synthesis of Polyoxazinones by ROMP

To a stirring solution of monomer (0.20 mmol) in THF (0.1 mL) under an atmosphere of Ar was added, if necessary, a 1 M solution of BCy_2Cl in hexanes (20 μL, 0.02 mmol) followed by catalyst **2.07** in either chloroform or THF (0.1 mL). The reaction was allowed to stir for 30 min at rt, then the reaction was quenched with ethyl vinyl ether (100 μL). The solution was allowed to stir over night at rt. The reaction mixture was triturated using Et_2O or MeOH (30 mL) and the resulting solid was isolated via centrifugation.

Polymer 2.03a

Polymer **2.03a** was synthesized following general procedure A using monomer **2.01a**. The polymer was collected by trituration into MeOH. ^{1}H-NMR ($CDCl_3$, 500 MHz): δ 6.25-5.60 (m, 2H), 5.50-5.20 (m, 1H), 4.35-3.55 (m, 3H), 1.75-1.00 (m, 18H), 1.90-1.80 (broad t, *J* = 6.7 Hz, 3H).

Polymer 2.03b

Polymer **2.03b** was synthesized following general procedure A using monomer **2.01b** in a 1:1 THF:$CHCl_3$ solution with BCy_2Cl. Polymer **2.03b** was collected by trituration into Et_2O. ^{1}H-NMR ($CDCl_3$, 500 MHz): δ 7.50-7.20 (broad s, 5H), 6.10-5.60 (m, 2H), 5.20-4.60 (m, 3H), 4.15-3.90 (broad d, 1H), 1.35-1.00 (broad s, 6H).

Polymer 2.03c

Polymer **2.03c** was synthesized following general procedure A using monomer **2.01c**. Polymer 2**.03c** was collected by trituration into Et_2O. ^{1}H-NMR ($CDCl_3$, 500 MHz): δ 6.30-5.60 (m, 2H), 5.60-5.10 (m, 1H), 4.70-3.50 (m, 3H), 1.50-0.90 (m, 9H).

Polymer 2.03d

Polymer **2.03d** was synthesized following general procedure A using monomer **2.01d**. Polymer **2.03d** was collected by trituration into MeOH. ^{1}H-NMR ($CDCl_3$, 500 MHz): δ 6.20-5.65 (m, 2H), 5.40-5.15 (m, 1H), 4.25-4.10 (m, 1H), 3.95-3.85 (m, 1H), 3.85-3.70 (m, 1H), 1.65-1.50 (m, 2H), 1.45-1.10 (m, 28H), 0.95-0.80 (m, 3H).

Polymer 2.03e

Polymer **2.03e** was prepared following the general procedure using monomer **2.01e**. Polymer was collect via trituration into Et_2O. ^{1}H-NMR ($CDCl_3$, 500 MHz): δ 8.40-7.40 (m, 9.1H), 6.00-2.80 (m, 7H), 1.90-1.30 (m, 5H), 1.30-0.50 (m, 6H).

Polymer 2.03f

Polymer **2.03f** was synthesized following the general procedure using monomer **2.01f**. Polymer was collected by trituration into cold MeOH. ^{1}H-NMR ($CDCl_3$, 500 MHz): δ 7.50-7.30 (m, 0.18 H), 7.00-6.80 (m, 0.04H), 6.20-5.70 (m, 2H, olefin), 5.45-5.25 (m, 1H), 4.30-3.70 (m, 3H), 3.40 (broad t, *J* =6.1 Hz, 2H), 1.85 (broad s, 2H), 1.70-1.35 (m, 6H), 1.30-1.05 (m, 6H).

Polymer 2.03g

Polymer **2.03f** (5 mg) and sodium azide (5 mg, 5 equiv with respect to bromine) were taken up in 1.0 mL DMF. The solution was stirred at 65 °C overnight. The reaction was allowed to cool and the solvent was removed under reduced pressure. The residue was taken up in 2.0 mL of dichloromethane and the solution was separated from the insoluble material. The solvent was removed under reduced pressure to afford polymer **2.03g**. ^{1}H-NMR ($CDCl_3$, 500 MHz): δ 7.60-7.40 (m, 0.10H), 6.20-5.75 (m, 2H), 5.50-5.25 (m, 1H), 4.30-3.70 (m, 3H), 3.26 (broad t, 2H), 1.75-1.00 (m, 16H).

Polymer 2.03h

Polymer **2.03h** was synthesized following general procedure A using monomer **2.01h**. Polymer **2.03h** was collected by trituration into Et_2O. ^{1}H-NMR ($CDCl_3$, 500 MHz): δ 7.62 (broad s, 1H), 7.50-7.43 (m, 0.18H), 7.40-7.30 (m, 0.21H), 6.20-5.70 (m, 2H), 5.50-5.15 (m, 4H), 4.96 (broad s, 1H), 4.85 (broad d, 1H), 4.68 (broad d, 1H), 4.50-4.00 (m, 6H), 4.00-3.75 (m, 2H), 2.15 (broad s, 3H), 2.11 (broad s, 3H), 2.04 (broad s, 3H), 1.98 (broad s, 3H), 2.00–1.90 (m, 2H), 1.50-0.80 (m, 14H).

Polymer 2.03i

To a stirring solution of polymer **2.03h** (7.0 mg) dissolved in DMSO (1.0 mL) was added a solution of sodium methoxide in MeOH (50 μL, 0.5 M). The solution was stirred at rt for 45 min and then directly loaded onto a PD-10 desalting column to remove the DMSO and methoxide. The water was removed by lyophilization to obtain polymer **2.03i** as an off white solid (5.0 mg). ^{1}H-NMR (DMSO-d$_6$, 500 MHz): δ 8.15 (s, 1H), 7.59 (s, 0.13H), 7.36 (s, 0.21H), 6.20-5.60 (m, 2H), 5.00-4.20 (m, 10H), 4.10-3.70 (m, 5H), 1.83 (s, 2H), 1.80-1.00 (m, 16H).

Polymer 2.22

Polymer **2.22** was synthesized following general procedure A using BCy_2Cl in 1:1 chloroform:THF using monomer **2.21**. Polymer **2.22** was isolated by trituration into Et_2O. ^{1}H-NMR ($CDCl_3$, 500 MHz): δ 8.03-7.70 (m, 2H), 7.60-7.30 (m, 2H + end group Ph Hs), 6.30-5.60 (m, 2H), 5.55-5.12 (m, 1H), 5.12-4.60 (m, 2H), 4.40-3.85 (m, 1H), 2.67-2.40 (m, 3H), 1.35-0.92 (m, 6H). Note: monomer **2.21** was re-purified before each polymerization.

General Procedure B: Synthesis of Polyoxazinone Oxime Conjugates

Polymer **2.22** (n eq. wrt acetophenone) was taken up in a solution of hydroxylamine ligand (1.5n eq) in DMSO so the final concentration of acetophenone is 40 mM. Pyridine (8n eq) was added and the solution was stirred at rt for 24 h. Benzaldehyde (n x 1.5 eq) was added and the solution was stirred for 1 h (benzealdehyde caps any unreacted hydroxylamine and aids in separation from polymer in next step). The solution was triturated into 1.25 mL diethyl ether and the solids were collected by centrifugation. Trituration was repeated until all small molecules were removed as determined by NMR.

Polymer 2.24

Polymer **2.24** was synthesized following general procedure B using **2.23** as the ligand. ^{1}H-NMR (MeOH-d_4, 500 MHz): δ 7.75-7.20 (m, 4H + end group Ph Hs), 6.35-5.65 (m, 2H), 5.55-5.25 (m, 1H), 5.15-4.60 (m, 2H, under solvent), 4.45-4.10 (m, 3H), 3.85-3.45 (m, 10H), 2.30-2.05 (m, 3H, 1.30-0.85 (m 6H).

Polymer 2.25

Polymer **2.24** was synthesized following general procedure B using **2.08e** as the ligand. ^{1}H-NMR ($CDCl_3$, 500 MHz): δ 8.30-7.45 (m, 11H), 7.45-7.15 (m, 2H, under solvent peak), 6.10.4.50 (m, 6H), 4.30-3.80 (m, 3H), 3.45-3.10 (m, 2H), 2.60-2.35 (m, 1H, OH), 2.25-2.05 (m, 3H), 2.0-1.75 (m, 4H), 1.15-1.00 (m, 6H).

General Procedure C: Reduction of Polyoxazinone Conjugates

To a solution of polymer (n eq wrt oxime) and sodium cyanoborohydride (75n eq wrt oxime) in methanol (0.25 mL) at 0 ^{o}C was added boron trifluoride diethyl etherate (50n eq wrt oxime). The solution was stirred for 30 mins at 0 ^{o}C and at rt for an 1 h. The reaction was quenched with saturated sodium bicarbonate solution (0.5 mL). The solution was diluted with chloroform (0.5 mL) and the biphasic mixture was separated. The aqueous phase was extracted with chloroform (2 x 0.5 mL) and the combined organic layer was dried over Na_2SO_4, filtered, and concentrated.

Polymer 2.28

Polymer **2.28** was synthesized following general procedure C. ^{1}H-NMR ($CDCl_4$, 500 MHz): 7.45-7.05 (m, 4H, overlap with solvent), 6.15-4.40 (m, 6H), 4.30-3.82 (m, 3H), 3.78-3.15 (m, 10H), 1.30- 1.00 (m, 9H).

Polymer 2.29

Polymer **2.22** (2.57 mg, 8.5 mmol wrt acetophenone) was taken up in THF or dichloromethane (0.125 mL) and cooled to 0 ^oC. Phenyl trimethyl ammonium tribromide (3.34 mg, 8.9 mmol) was added in one portion and the solution was stirred for 1.25 h at 0 ^oC, then 0.5 h at rt. The solution was diluted with dichloromethane (1 mL) and washed with water (3 x 1 mL). The organic phase was dried and concentrated. The crude residue was dissolved in dichloromethane (0.2 mL) and triturated into diethyl ether (1.25 mL). The solids were isolated by centrifugation. Trituration was repeated 2x. Reaction conversion was assess by ^{1}H-NMR in $CDCl_3$ by comparing the ratio of the acetophenone methyl (δ = 2.57 ppm) to the α-bromoacetophenone methylene (δ = 4.44 ppm to the α,α-dibromoacetophenone methyne (δ = 6.73 ppm) which all appeared as isolated bands.

2.6.4. Monitoring the Degradation of Polymers

Monitoring the Acidic Degradation of the ROMP Derived Polymers:

A stock solution of HCl in methanol (2.27 M) underwent four 10x dilutions to afford methanol solutions with [H^+] between 2.27 M and 0.27 μM. Polymer (2.4 mg) was taken up in THF (0.75 mL) and allowed to dissolve over 1 h. The polymer solution was passed through a syringe driven filter (Millex® - GV, PVDF – 0.22 μm) and an initial M_n reading was acquired by

GPC. Acidic methanol solution (0.25 mL) was added to the polymer solution and degradation at each [H^+] concentration was monitored by analyzing aliquots of solution (100 μL) over 48 h by GPC.

Monitoring the Basic Degradation of the ROMP Derived Polymers:

A commercially available stock solution of sodium methoxide in methanol (0.50 M) underwent four 10x dilutions to afford methanol solutions with [$^-$OMe] between 0.5 M and 0.05 μM. Polymer (2.4 mg) was taken up in THF (0.75 mL) and allowed to dissolve over 1 h. The polymer solution was passed through a syringe driven filter (Millex® - GV, PVDF – 0.22 μm) and an initial M_n reading was acquired by GPC. Basic methanol solution (0.25 mL) was added to the polymer solution and degradation was monitored at each [$^-$OMe] concentration by analyzing aliquots of solution (100 μL) over 48 h by GPC.

Monitoring the Degradation of Polymer 2.03e via Pyrene Fluorescence:

Polymer **2.03d** (2.4 mg) was taken up in THF (0.75 mL) and allowed to dissolve over 1 h. The polymer solution was passed through a syringe driven filter (Millex® - GV, PVDF – 0.22 μm) and then acidified methanol (0.25 mL, 2.27 M) was added to the solution. The solution was allowed to stir at room temperature. Periodically, aliquots of the solution (14.3 μL) were drawn and diluted with THF (1.0 mL). The fluorescence emission spectrum of the sample was taken (λ_{ex} = 250 nm) and the ratio of pyrene exciplex emission (λ_{em} = 480 nm) to monomeric pyrene emission (λ_{em} = 377 nm) was calculated. Decomposition was monitored by following this ratio over time.

Chapter 3: Assessing the Bioactivity and Biocompatibility of Polyoxazinones

Contributions:

Biological experiments were performed by L.R. Prost and D.B. Zwick

3.1. Impetus for a Degradable and Bioactive ROMP Polymer

The use of synthetic polymers as prophylactic biomaterial is an area of active research spurred by the seminal studies of Langer and co-workers.[248-251] In these early studies, it was demonstrated that embedding therapeutic molecules into a polymer matrix is a biocompatible way to control the *temporal* release of drugs. Besides finding utility as a bulk depot for the controlled release of therapeutics, soluble polymers conjugated to bioactive molecules have also been explored as a method to control the *spatial* accumulation of drugs.[1,252-254] First proposed by Ringsdorf, the ideal polymer-drug conjugate is composed of a macromolecular carrier that is covalently attached to both therapeutic agents and a tissue specific ligand.[255] The tissue specific ligand steers the ensemble to cells that contain cognate surface receptors, leading to accumulation in or around that tissue. Then, an exogenous stimulus, such as a change in pH or presence of a hydrolytic enzyme, is co-opted to release the therapeutic via cleavage of a degradable polymeric backbone or side chain linkage. If all of Ringsdorf's criteria are satisfied, a drug can theoretically be delivered directly to its desired target while minimizing interactions with healthy cells, thereby increasing potency and decreasing side effects.

Although proposed 40 years ago, there are few examples of polymer-drug conjugates that have fully met all of Ringsdorf's criteria. This paucity stems from the dearth of robust methods available to synthesize macromolecules that are defined, compositionally complex, and degradable. Historically, only macromolecules conjugated to a single functional element have been synthetically tractable.[243,256] Therefore, most embodiments contain only a therapeutic agent and rely on passive delivery guided by the enhanced permeability and retention (EPR) or extravasation through leaky vasculature and the subsequent inflammatory cell-mediated sequestration (ELVIS) effects.[257-259] These phenomena rely on the fact that the vasculature network in tumors or sites of inflammation are often malformed, which allows nano-sized particles to diffuse through them. However, this strategy is only effective when targeting to these locations is desired. Therefore, a platform that is amenable to broad multi-functionalization and is also degradable is needed to fully satisfy Ringsdorf's vision.

ROMP, as well as other living polymerization methodologies, has enabled the synthesis of specialty polymers with high compositional complexity. Due to the functional group tolerance of ruthenium catalysts, well-defined ROMP polymers conjugated to bioactive ligands have been synthesized.[30,62,108,196,199] In addition, ROMP polymers that are amenable to post-polymerization modification have been used successfully to conjugate both therapeutics and targeting ligands to a single polymeric backbone.[132,196] While ROMP has assuaged the multi-functionalization problem, all current scaffolds are non-degradable. Therefore, if used clinically, only renal clearance can be used to prevent unwanted bioaccumulation.[260,261] This size constraint is an issue when using targeting moieties that must be displayed multivalently, which increases the length of polymer needed to effectively bind the particle's target receptors.[3,5] We envisioned that polyoxazinone ROMP polymers that 1) undergo pH-dependent degradation and 2) can be functionalized with targeting ligands could bypass such defects. Towards this aim, we sought to demonstrate that polyoxazinone ROMP polymers can be rationally decorated to target specific routes of intracellular uptake and can undergo pH-sensitive degradation *in cellulo*. If successful, these capabilities offer promise as scaffolds for next-generation drug delivery and regenerative medicine.

3.2. Generation of Multivalent Polyoxazinone Antigens

3.2.1. Introduction

The use of polyoxazinones for directed drug delivery was envisioned to augment the success of non-degradable ROMP platforms by providing a mechanism for polymer degradation *in vivo*. To this end, the ability to target specific uptake mechanisms using bioactive polyoxazinone ligand displays was paramount to ensure the polymer was delivered to cellular compartments with a reduced pH. A potential complication, however, is that polyoxazinones differ from other classes of bioactive ROMP polymers in that they possess a heteroatom-rich polymer backbone, in contrast to the simple hydrocarbon chains found in polynorbornenes, polycyclooctenes, and polybutenes.[3,39,62,196] The oxazinone repeats were anticipated to provide a mechanism for polyoxazinone degradation, but it was unknown if they would also engage in off-target cellular interactions, thus occluding entry through specific internalization pathways. Therefore, the polyoxazinone backbone was decorated with bioactive ligands known to promote the internalization of non-degradable polymer conjugates by either receptor-mediated or non-specific endocytosis (Figure 3.1). Additionally, uptake of polymers can require either hydrophobic or hydrophilic ligand displays. By targeting polyoxazinones to receptors of each class, the impact of polymer hydrophobicity on uptake can be investigated as well.

Diverse multi-functionalization was enabled using the post-polymerization oxime reaction discussed in Chapter 2. To be exact, a variety of hydroxylamine ligands conjugated to bioactive moieties and water-soluble fluorophores were interchangeably attached to the oxazinone backbone to rapidly tailor the biological and spectral properties of the polymer probes to match that of previously used bioactive ROMP polymers (Figure 3.1*)*. After functionalization, the polymers were exposed to cells that express the cognate receptors to investigate whether targeted delivery is indeed tractable with this new scaffold.

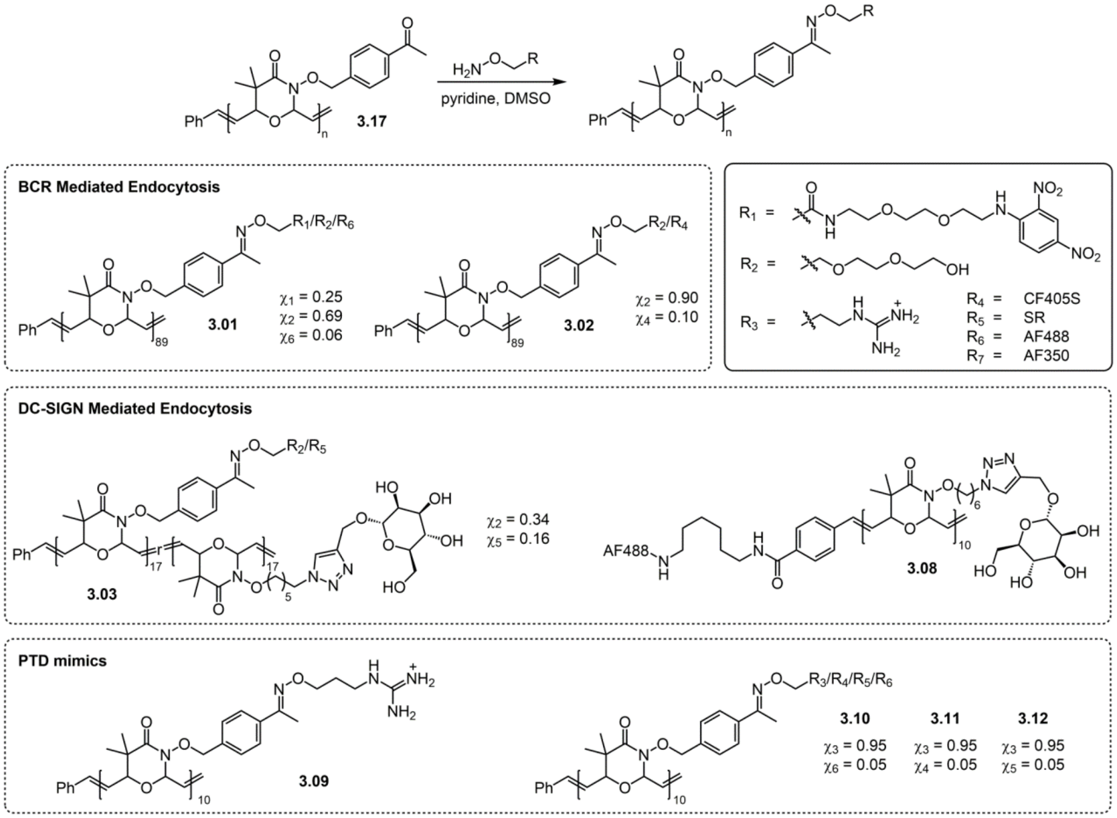
3.17
pyridine, DMSO
BCR Mediated Endocytosis
3.01
χ_1 = 0.25
χ_2 = 0.69
χ_6 = 0.06
3.02
χ_2 = 0.90
χ_4 = 0.10
R_1 =
R_2 =
R_3 =
R_4 = CF405S
R_5 = SR
R_6 = AF488
R_7 = AF350
DC-SIGN Mediated Endocytosis
3.03
χ_2 = 0.34
χ_5 = 0.16
AF488
3.08
PTD mimics
3.09
3.10
χ_3 = 0.95
χ_6 = 0.05
3.11
χ_3 = 0.95
χ_4 = 0.05
3.12
χ_3 = 0.95
χ_5 = 0.05

Figure 3.1. Structures of polyoxazinones used in cellular internalization assays. SR = sulforhodamine, AF488 = AlexaFluor 488.

3.2.2. Interactions with the B-cell Receptor

B cells are key players of the adaptive immune system.[262] If a B cell encounters a pathogenic antigen, a signaling cascade is turned on that leads to T cell recruitment. The T cells then induce clonal expansion of the naïve B cell population to both plasma B cells, which produce antibodies, and memory B cells. Antigen recognition is facilitated by a membrane bound cell-surface receptor termed the B-cell receptor (BCR).[263] The BCR is composed of two domains, an extracellular antibody fragment and an intracellular signal transduction domain. Each B cell's BCR is unique and contains an antibody fragment that allows antigen specific binding. After binding, BCR signaling is activated by receptor clustering caused by multivalent interactions between the antigen and the BCR.[28,162,163] Among other effects, BCR activation results in antigen internalization and trafficking to endosomes, where the antigen can be digested, processed, and presented to T cells. Both natural and non-natural antigens can cause BCR mediated B cell activation. We have shown that synthetic ROMP polymers can induce B cell activation because the repeating nature of the macromolecular backbone leads to a multivalent display of BCR binding ligands.[28,30,229] Therefore, we posited that polyoxazinones possessing the same antigenic displays would similarly promote B cell activation and subsequent trafficking to intracellular endosomes.

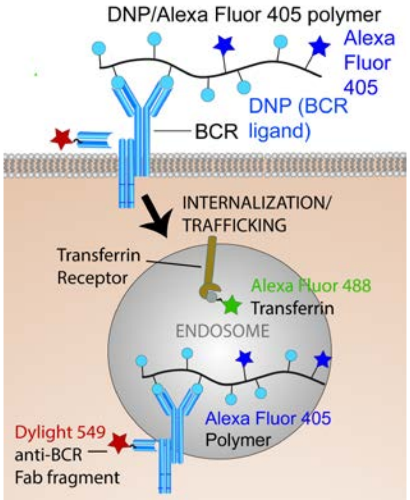
DNP/Alexa Fluor 405 polymer
Alexa Fluor 405
DNP (BCR ligand)
BCR
INTERNALIZATION/ TRAFFICKING
Transferrin Receptor
Alexa Fluor 488 Transferrin
ENDOSOME
Alexa Fluor 405 Polymer
Dylight 549 anti-BCR Fab fragment

Figure 3.2. Upon binding DNP-conjugate **3.01**, the surface exposed BCRs of A20HL B cells are internalized and routed to early endosomes. By fluorescently labeling polymer **3.01**, the BCR, and the early endosomal marker transferrin, this process can be followed using microscopy. Image courtesy of Dan Zwick.

Antigen possessing a multivalent display of the 2,4-dinitrophenyl hapten (DNP) can engage DNP-specific BCRs expressed by the A20HL B cell line and activate the B cells (Figure 3.2).[264-266] Upon antigen engagement with the BCR, both the ligand and the bound receptors are internalized and rapidly directed to early endosomal compartments.[267,268] We have previously shown that polynorbornenes conjugated to DNP are selectively internalized by A20HL cells and are trafficked to early endosomes.[28,30,229] It was important, therefore, to verify that polyoxazinone scaffolds also promote the same responses. To see how polyoxazinones performed in cell-based assays we generated polymer **3.01**, which is conjugated to the immunogenic epitope DNP and the blue fluorophore CF405S (Figure 3.1). After synthesis and purification, polymer **3.01** was incubated with A20HL cells for 30 minutes at 37 ^{o}C or 4 ^{o}C. As BCR mediated endocytosis is an energy dependent process, internalization should only occur at 37 ^{o}C. The cells were then washed and internalization was assessed using confocal microscopy (Figure 3.3A). Uptake of polymer **3.01** occurred at 37 ^{o}C as visualized by the presence of intracellular fluorescent puncta. Additionally, the internalized polymer was found to co-localize with the BCR, which indicates that this receptor played a role in internalization (Figure 3.3D). Further staining of the cells for the early endosomal marker transferrin confirmed that both the internalized polymer and the BCR co-localized with this marker, demonstrating that the polymeric antigen was inducing trafficking to the expected intracellular compartment (Figure 3.3E).[229] Internalization was ablated when polymer **3.01** was incubated with the A20HL cells at 4 ^{o}C, indicating an active mode of cell penetration. Taken together, polymer **3.01** was able to engage the BCR in a physiologically relevant manner.

To further show that the oxazinone backbone is biologically inert, polymer **3.02**, conjugated to only a fluorophore and a non-immunogenic triethylene glycol ligand, was not internalized when incubated with A20HL cells at either 4 or 37 ^{o}C (Figure 3.3B). In this case, no intracellular fluorescence is observed at either temperature and the polymer does not co-localize with either the BCR or transferrin (Figure 3.3D/E). The fluorescence that is observed on the polymer channel is localized to the outside of the cell and is likely due to non-specific cell sticking. However, this association did not promote polymer uptake. In addition, polymer **3.03**, conjugated to the carbohydrate mannose, was not internalized by A20HL cells either (Figure 3.3C). Mannose is an immunogenic ligand, but is not recognized by the cell-surface receptor suite found on A20HL cells. Therefore, it was not recognized as antigenic by the A20HL cells. These results indicate the non-natural oxazinone functionality of polyoxazinones is insufficient to promote the uptake of the polymer by B cells. Therefore, polyoxazinones can be selectively decorated to promote BCR mediated endocytosis through judicious choice of side chain functionality.

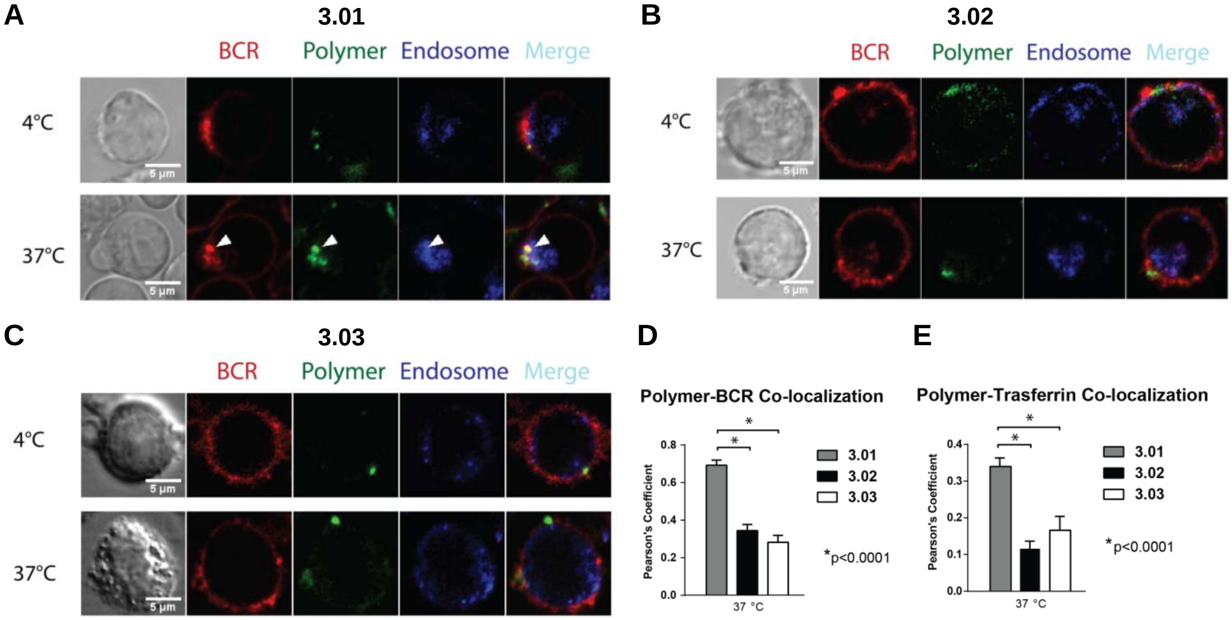
A
3.01
BCR
Polymer
Endosome
Merge
4°C
37°C
5 µm
B
3.02
C
3.03
D
Polymer-BCR Co-localization
Pearson's Coefficient
0.0
0.2
0.4
0.6
0.8
37 °C
*
3.01
3.02
3.03
*p<0.0001
E
Polymer-Trasferrin Co-localization
0.0
0.1
0.2
0.3
0.4

Figure 3.3. Confocal imaging of A20HL B cells exposed to A) DNP conjugate **3.01**, B) triethylene glycol conjugate **3.02**, and C) mannose conjugate **3.03** at 4 ^{o}C and 37 ^{o}C. Co-localization of polymers **3.01**, **3.02**, and **3.03** at 37 ^{o}C with D) the DNP-specific BCR and E) the early endosomal marker transferrin in A20HL cells. Arrow points to intracellular puncta. Scale bar = 5 μm.

3.2.3. Interactions with DC-SIGN

Dendritic cells (DC) are professional antigen-presenting cells that serve as a link between the body's innate and adaptive immune systems.[269-271] Present in regions of the body that are in contact with the external environment, such as mucosal membranes and the gastrointestinal track, DCs use an arsenal of cell-surface receptors that sense highly conserved non-self epitopes, called pathogen-associated molecular patterns (PAMPs), to constantly sample their environment.[272,273] When antigen is encountered that displays a PAMP, the entity is internalized, processed, and then presented on the DCs surface to promote T cell activation and begin an adaptive immune response.

One class of PAMPs are glycans found on viruses and bacteria.[273] These motifs are recognized through carbohydrate binding receptors called lectins.[274] One such lectin that has garnered much attention is the receptor dendritic cell-specific ICAM-3-grabbing non-integrin (DC-SIGN).[275,276] DC-SIGN is a Ca^{2+}-dependent lectin that is able to bind highly mannosylated and fucosylated glycans. Interestingly, DC-SIGN has been shown to interact with both host and foreign glycans that contain these carbohydrates.[277-280] In addition, there are reports that suggest that DC-SIGN can differentiate host from foreign glycans to induce either a tolerance or immunological response, respectively.[279] However, well defined probes are needed to test the validity of these observations and understand the underlying physiology.

We have previously used ROMP polymers as probes of DC-SIGN function.[281,282] Well-defined mannosylated glycopolymers of different chain lengths were generated and exposed to Raji B cells transfected to express DC-SIGN.[283] Raji cells were used instead of DCs because DCs have multiple receptors that can bind mannose. B cells have no other mannose binding receptors, so the polymer’s effect on DC-SIGN could be unequivocally assigned with this cell line. By taking advantage of this cell line, it was confirmed that mannosylated poly(*oxo*-norbornene) ROMP polymers can indeed stimulate DC-SIGN and lead to antigen internalization in a valency dependent fashion (Figure 3.4). Therefore, we were curious to know whether changing backbone architecture from a poly(*oxo*-norbornene) to a polyoxazinone motif would impact internalization. It is notable that just because polyoxazionones induced BCR mediated uptake when functionalized with DNP there was no guarantee that functionalization with mannose would ensure successful polymer uptake by DC-SIGN. One reason for this skepticism stems from the fact that while poly(*oxo*-norbornene) glycopolymers were successfully internalized by DC-SIGN expressing Raji cells, structurally analogous polynorborene glycoconjugates were not.[282] Therefore, interactions with DC-SIGN may be sensitive to polymer architecture. Additionally, although both A20HL cells and Raji cells are both B-cells, they express different cell surface receptors. This presents new opportunities for the oxazione backbone to engage in off-target interactions that might lead to non-DC-SIGN mediated uptake.

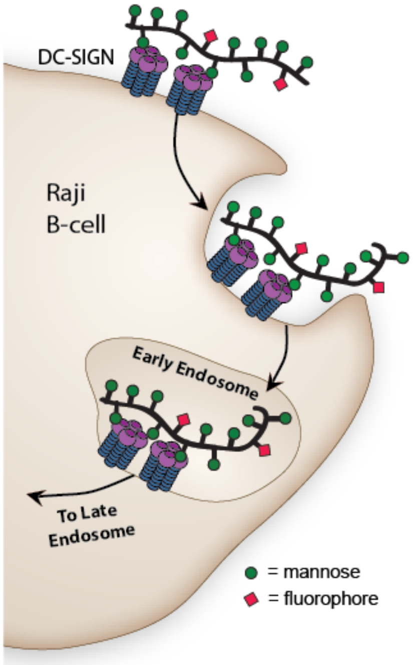

Figure 3.4. Mannosylated polymeric antigen is internalized by Raji B cells that express the cell surface receptor DC-SIGN. Image courtesy of Joe Grim.

To assess whether polyoxazinone antigen can induce DC-SIGN specific polymer uptake, the scaffold required functionalization with both mannose, to promote uptake, and a fluorophore, to visualize uptake. The synthesis of bicyclic oxazinone monomer **3.04**, conjugated to a peracetyl mannose moiety, has been established and was shown to be a viable ROMP substrate (see section 2.3.1). Furthermore, the end-labeling of ROMP polymers with fluorophores has previously been used to visualize polymers using microscopy.[56,66,82] One method to end-label ROMP polymers is the modification of the alkylidene ligand of metathesis catalysts.[128,209,284,285] Upon polymerization initiation, the alkylidene is transferred to the nascent polymer chain-end along with any pendant functionality. To this end, we generated catalyst **3.06**, which attached a chemoselective *N*-hydroxysuccinimide ester to the end of polyoxazinone glycopolymer **3.07** (Scheme 3.1). This handle was then used to regioselectively conjugate a single fluorophore to the polymer. Hydrolysis of the acetate groups from the mannose ligands afforded fluorescently tagged glycoconjugate **3.08**.

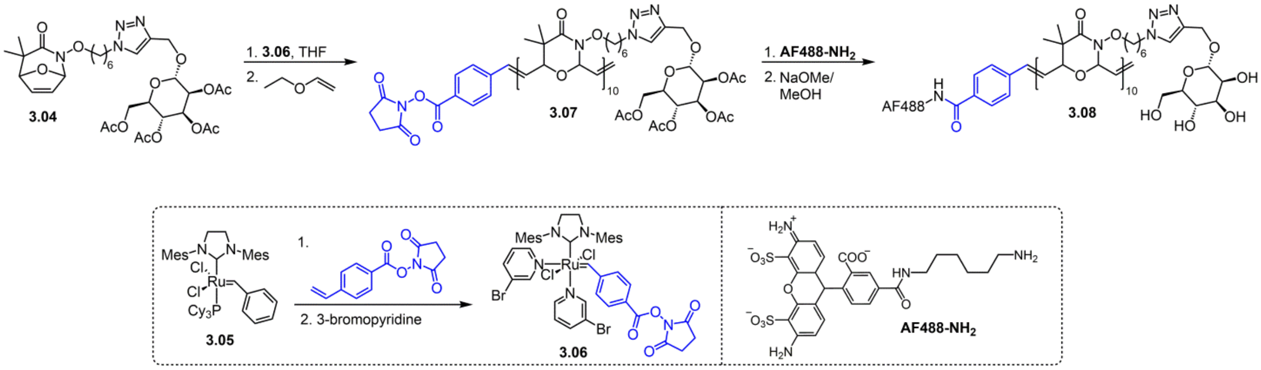

Scheme 3.1. Installation of an amine reactive end group at the chain-end of polyoxazinone **3.07** was achieved through modification of the metathesis catalyst's alkylidene ligand.

With polymer **3.08** in hand, we examined whether polyoxazinone glycopolymers could be internalized by cells expressing DC-SIGN. To test this, we exposed **3.08** to the Raji B cells discussed above. A positive result is indicated by intracellular fluorescence due to polymer internalization. As a control, **3.08** was also exposed to Raji cells that do not express DC-SIGN. After incubating the cells for 40 minutes at 37 ^{o}C with **3.08**, the cells were washed and internalization was assessed via confocal microscopy. The results of these experiments are shown in Figure 3.5. When the polymer was added to the DC-SIGN-expressing Raji cells, the polymers were internalized and punctate intracellular fluorescence was observed. On the other hand, no fluorescence was observed in Raji cells that do not express DC-SIGN, indicating that the polymers undergo receptor-specific cellular internalization. Additionally, the internalization using polymer **3.08** mirrored the results of the assay using mannosylated Bovine Serum Albumin (**ManBSA**), which is known to induce DC-SIGN mediated endocytosis.[281] This shows that the internalization of **3.08** was caused by its multivalent display of mannose and not due to off-target interactions between the polymer and the cells. Therefore, mannosylated polyoxazinones can induce polymer uptake through interactions with the receptor DC-SIGN. In addition, the oxazinone backbone did not promote non-specific internalization of the polymer probe by Raji B cells.

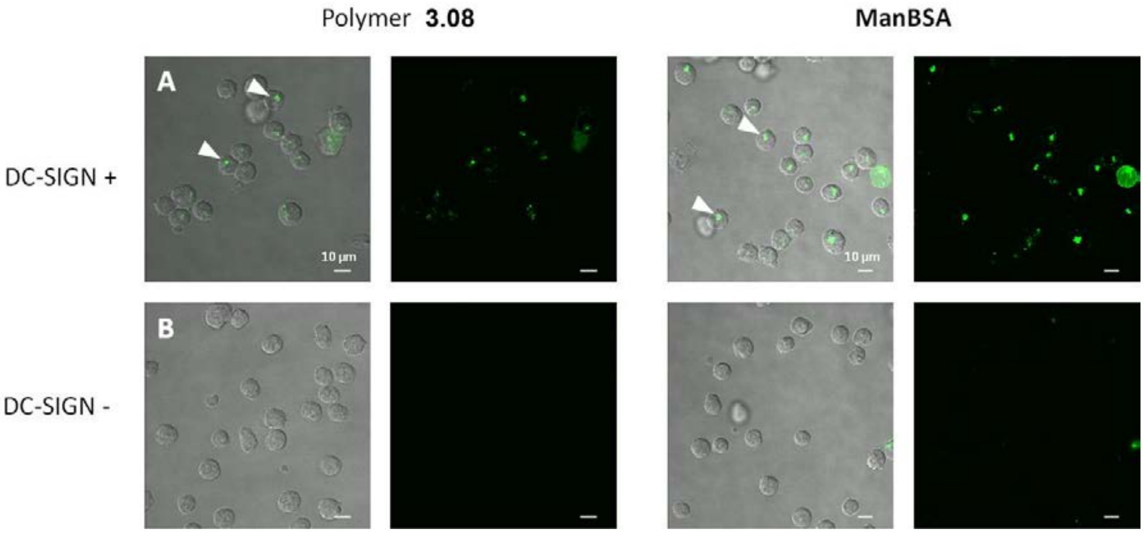

Figure 3.5. Selective internalization of polymer **3.08** and **ManBSA** by the surface receptor DC-SIGN. Internalization is observed in A) DC-SIGN expressing Raji cells but not in B) Raji cells that do not expressing DC-SIGN. Arrows point to examples of internalized polymer. Scale bar = 10 µM.

3.2.4. Non-specific Uptake of Polyoxazinone Conjugates

A challenge associated with using polymer-based drug delivery platforms is overcoming the macromolecule's inability to penetrate cell membranes. Therefore, intracellular delivery of therapeutics is often stymied by the size constraints of the biomaterial. One solution to this problem is conjugation of a ligand to the polymer that triggers receptor-mediated endocytosis, as described in the previous two subsections. This strategy is tissue specific. However, indiscriminate cell uptake may also be useful if multiple tissue types require delivery of a therapeutic but do not express the same surface receptors. Additionally, receptor-mediated endocytosis routes the internalized polymer to endosomes, but delivery of a polymer conjugate to other areas of the cell, such as the cytosol, might also be necessary for some applications. A method to facilitate the non-specific uptake of synthetic polymers is the incorporation of a protein transduction domain (PTD) mimic.[170,171,286] PTDs are small, arginine rich amino acid sequences of proteins that are able to complex with negatively charged sulfated glycosaminoglycans (GAGs), a standard component of cell membranes, which induces non-specific uptake of the entire protein (see Section 1.5.3.1).[172,287,288] The exact mechanism for internalization is unknown, but the process has been shown to be energy-dependent and relies on deformations in the curvature of the membrane.[173] To mimic PTDs, ROMP polymers have been functionalized with a polyguanidinium artificial transduction domain (ATD) to enable non-specific internalization by cells.[23,82,173] Therefore, polyoxazinones were decorated with guanidinium ligands to assess their ability to catholically enter cells as well.

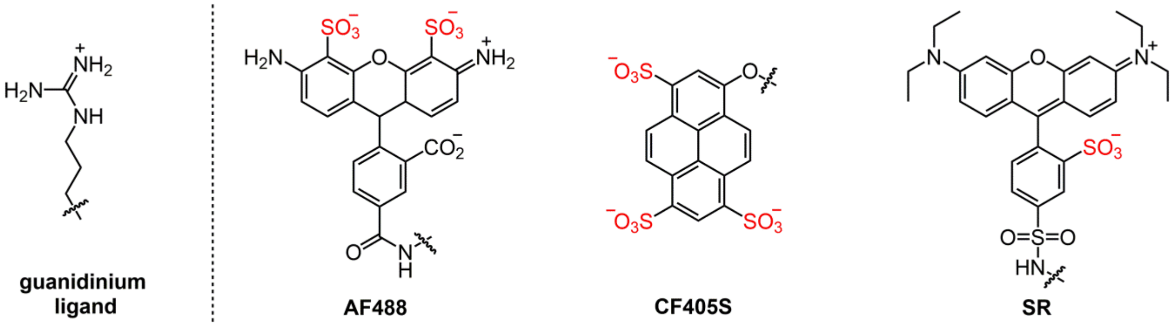

guanidinium ligand **AF488** **CF405S** **SR**

Figure 3.6. Structures of the guaninidum ligand and the fluorophores conjugated to PTD mimics **3.10**, **3.11**, and **3.12**. Conjugation of AF488 and CF405s led to insoluble material.

Polyoxazinone **3.09** was generated with an ATD using a guanidinium functionalized hydroxylamine ligand (Figure 3.1). Besides an ATD, conjugation of a fluorescent tag was needed to visualize the internalization of the polyguanidinium conjugates. Unexpectedly, guanidinium/AF488 co-polymer **3.10** was only sparingly soluble in both water and DMSO after isolation. This result was surprising as neither polyguanidinium homopolymer **3.09** nor the other AF488 conjugates described previously (polymers **3.01** and **3.08**) had solubility issues. Changing to the dye CF405s (which was also previously used without issue) led to a completely insoluble polymer product, **3.11**. Fortunately, use of the dye sulforhodamine led to a fully soluble polymer, **3.12**. The cause of this fluorophore dependent solubility is unknown; however, qualitatively, the decrease in solubility correlates with an increase in the number of a fluorophore's sulfate groups (Figure 3.6). As PTDs use arginine to bind to sulfate groups on GAGs, it is possible that salt bridges formed between the guanidinium functionality and the sulfate groups on polymers **3.10** and **3.11** when the material was isolated. These salt bridges can serve as non-covalent crosslinks that prevent polymer solvation and lead to the observed insolubility. Sulforhodamine, however, only has a single sulfate group that is sterically hindered, potentially preventing crosslinking for polymer **3.12**.

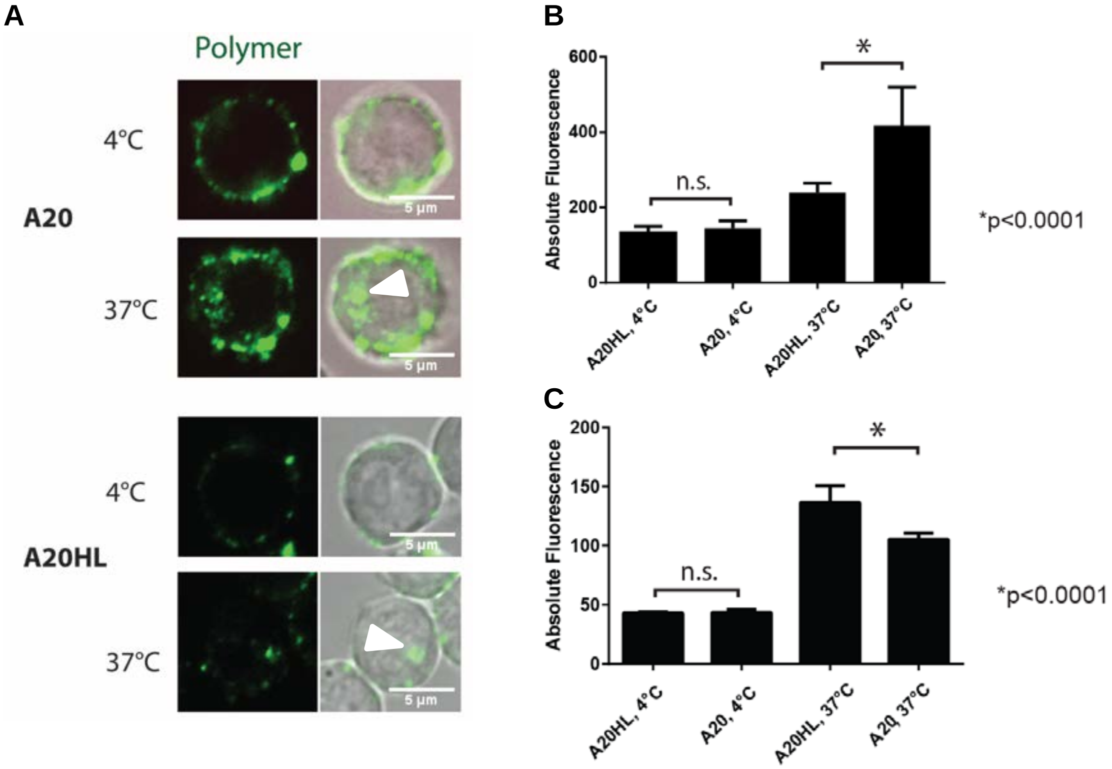

Figure 3.7. A) Polymer **3.12**, a polyguanidinium PTD mimic, was internalized by both A20HL and A20 B-cells at 37 ^{o}C but not at 4 ^{o}C. Arrows point to examples of intracellular polymer. Scale bar = 5 μM. B) Uptake of polymer **3.12**; this polymer was internalized to a greater extent by A20 cells than A20HL cells at 37 ^{o}C. C) Uptake of polymer **3.01**; this polymer was internalized to a greater extent by A20HL cells than A20 cells at 37 ^{o}C.

With soluble and fluorescent polyguanidinium **3.12** in hand, the cell-permeability of this PTD mimic was tested. Polymer **3.12** was exposed to both A20HL B-cells, which express a DNP-specific BCR, and A20 cells, which do not. Successful internalization was observed after exposure of **3.12** to both cell lines for 30 min at 37 ^{o}C (Figure 3.7). Uptake was not seen after incubation at 4 ^{o}C for 30 mins, although non-specific association with the outer membrane was seen. The temperature-dependence of polymer internalization indicates an active mode of cell penetration, as reported previously. Interestingly, polymer **3.12** was internalized to a greater extent by A20 cells than by A20HL cells (Figure 3.7B). Although the cause of this difference is currently unknown, the result suggests that polymer **3.12** was not internalized through interactions with the BCR as DNP conjugate **3.01** was internalized more efficiently in A20HL cells (Figure 3.7C). Nevertheless, these combined results shown that polyoxazinones can be specifically functionalized to promote either receptor-mediated or non-specific endocytosis.

3.2.5. Conclusions

The results of this section demonstrate that polyoxazinone ROMP polymers are able to be taken up by cells when decorated with specific bioactive ligands. Additionally, the heteroatom rich oxazinone repeats of polyoxazinones are insufficient to promote the internalization of these polymers. Both receptor-mediated and non-specific entry into cells was achieved through judicious choice of side chain functionality. In addition, both hydrophobic and hydrophilic ligands were able to be used without causing deleterious off-target interactions. Thus, polyoxazinones are a bioinert multivalent scaffold that can be applied to both chemical biology and regenerative medicine applications in the future.

3.3. Design of a Fluorescent Polyoxazinones Probe to Detect Degradation Inside Cells

3.3.1. Methods to Detect Polymer Decomposition

Most synthetic biodegradable polymers are polyesters, polycarbonates, or polyanhydrides.[289-293] To prove their degradability, a polymer disk is cast and submerged in different physiologically relevant buffers. At various time points, the disk is removed from the solution and weighed to dryness. As the polymer hydrolyses, the wafer decreases in weight, which is correlated to polymer decomposition.[292,294] This strategy is effective when the polymer of interest can be obtained on a large scale. However, for specialty polymers, obtaining the large quantity of material need for bulk degradation assays is tedious and expensive. To obtain rates of hydrolysis of these precious materials, chromatographic techniques are used to monitor the change in molecular weight of a polymer solution over time.[57] These assays can report on the rates of polymer hydrolysis in aqueous buffer. However, for applications in regenerative medicine, not only is the *in vitro* rate of hydrolysis important, but the degradation rate of polymers inside living cells is essential as well.

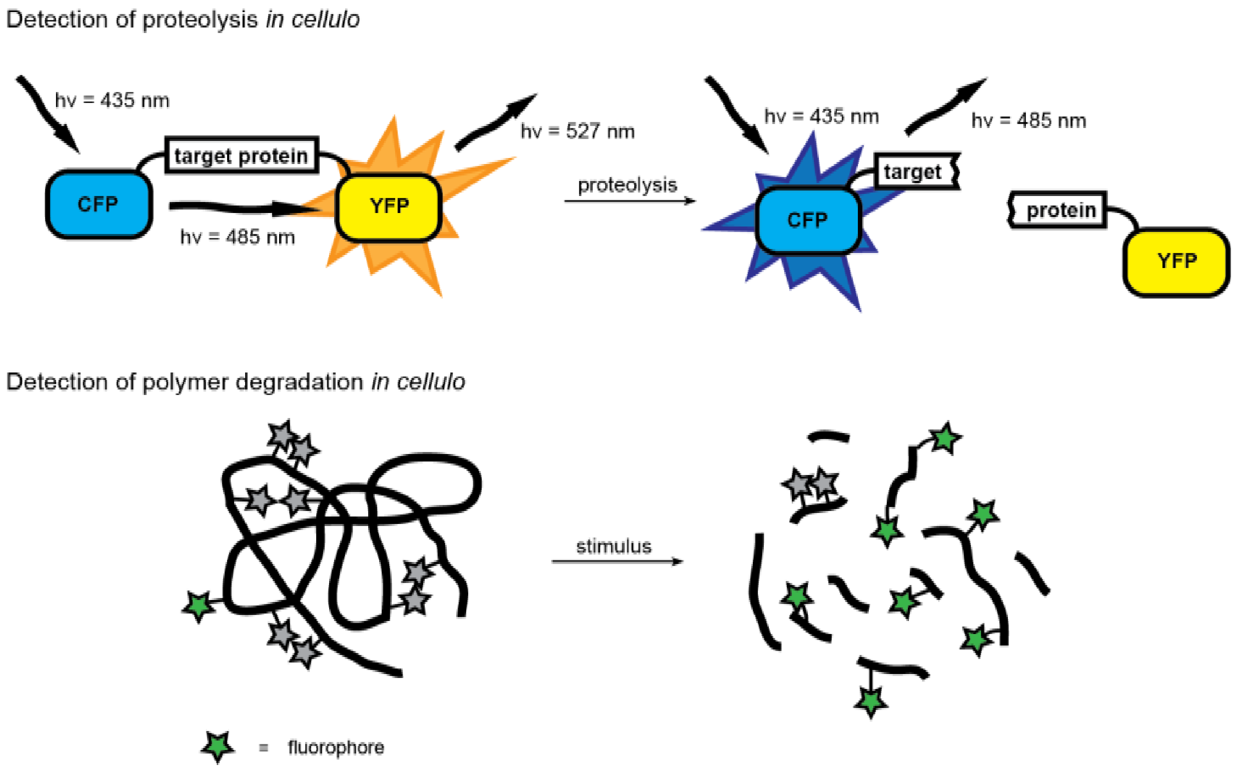

Detection of proteolysis *in cellulo*

Detection of polymer degradation *in cellulo*

Figure 3.8. Proteolysis can be monitored *in cellulo* through the construction of a fusion protein composed of a protease sensitive target protein flanked by two fluorescent proteins that are FRET partners. Monitoring changes in the spectral signature of the construct directly reports on the state of the bioconjugate. Multi-functionalization of a polymer scaffold with small molecule fluorophores possessing concentration dependent spectra properties was envisioned to allow the degradation of synthetic polymer scaffolds to be monitored *in cellulo* as well.

To the best of our knowledge, an assay that directly monitors polymer decomposition inside living cells has never been performed with synthetic polymer substrates. However, the degradation of proteins *in cellulo* has been monitored using assays based on fluorescence spectroscopy.[295-297] Experimentally, a construct is made containing of a protease sensitive protein or peptide flanked by two fluorescent proteins that are Förester Resonance Energy Transfer (FRET) partners (Figure 3.8). FRET is a through space, radiationless energy transfer that occurs when the emission of a donor fluorophore is able to excite a nearby acceptor fluorophore, which causes a red-shift in the overall emission of the construct. Since FRET intensity is inversely related to the distance between the fluorophores, when the construct is intact FRET can occur. However, as the protein of interest is degraded the fluorescent proteins are detached and diffuse away from each other, which restores the native fluorescence of the FRET donor. Changes in the spectral properties of the bioconjugate can be monitored in real time and directly correlate to the concentration of intact protein remaining. In this way, rates of proteolysis have been monitored *in cellulo*.[296,297] The use of analogous fluorescence-based assays to monitor the biodegradation of synthetic polymers has not yet been reported. However, the ease in multi-functionalization of polyoxazinones by PPM provided an opportunity to apply this technology to artificial scaffolds. To this end, we set out to synthesize a polyoxazinone probe capable of fluorescently reporting on the integrity of its backbone inside cells.

3.3.2. Synthesis of Fluorescent Polyoxazinone Probes to Detect Degradation in Cells

Polyoxazinones functionalized with the molecule pyrene have previously been shown to induce excimer formation when the fluorophore is covalently attached to the polymer backbone (see section 2.3). Excimer formation causes a 100 nm red shift in maximum fluorescence and loss of this signal was used to monitor the decomposition of a pyrene homopolymer spectroscopically, *in vitro* (see section 2.4). Therefore, it was envisioned that this excimer to monomer transition could be used to measure biodegradation *in cellulo* as well. To this end, a pyrene-mannose copolymer **3.14** was synthesized (Scheme 3.2). Polymer **3.14** was derived from the copolymerization of mannosylated monomer **3.04** and pyrenyl monomer **3.15**. Monomer **3.04** was chosen as a copolymerization partner to theoretically promote the internalization of the fluorescent probe by DC-SIGN to observe degradation in DCs (see section 3.2.3). Encouragingly, preliminary spectral characterization of intermediate copolymer **3.14** showed a similar emission spectrum as homopolymer **3.13**, confirming excimer formation (Figure 3.9A). However, when the acetate groups were removed, polymer **3.16** was found to be insoluble in aqueous media. This was unexpected as glycosylation usually confers high water solubility; unfortunately, the hydrophobic pyrene ligands of **3.16** counterbalanced the hydrophilicity of the mannosylated repeats. Therefore, an alternative fluorophore was needed.

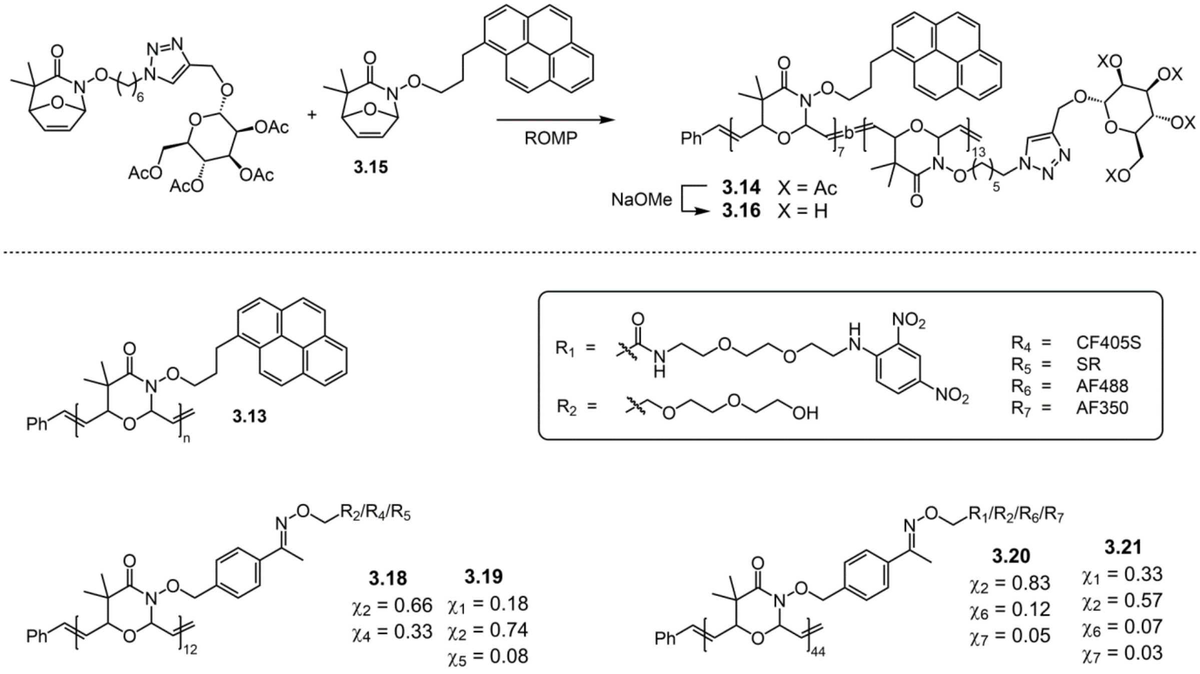

3.15
ROMP
NaOMe
3.14 X = Ac
3.16 X = H
3.13
R1 =
R2 =
R4 = CF405S
R5 = SR
R6 = AF488
R7 = AF350
R2/R4/R5
R1/R2/R6/R7
3.18
χ2 = 0.66
χ4 = 0.33
3.19
χ1 = 0.18
χ2 = 0.74
χ5 = 0.08
3.20
χ2 = 0.83
χ6 = 0.12
χ7 = 0.05
3.21
χ1 = 0.33
χ2 = 0.57
χ6 = 0.07
χ7 = 0.03

Scheme 3.2. Structures of polyoxazinones conjugated to fluorophores with concentration dependent spectral properties.

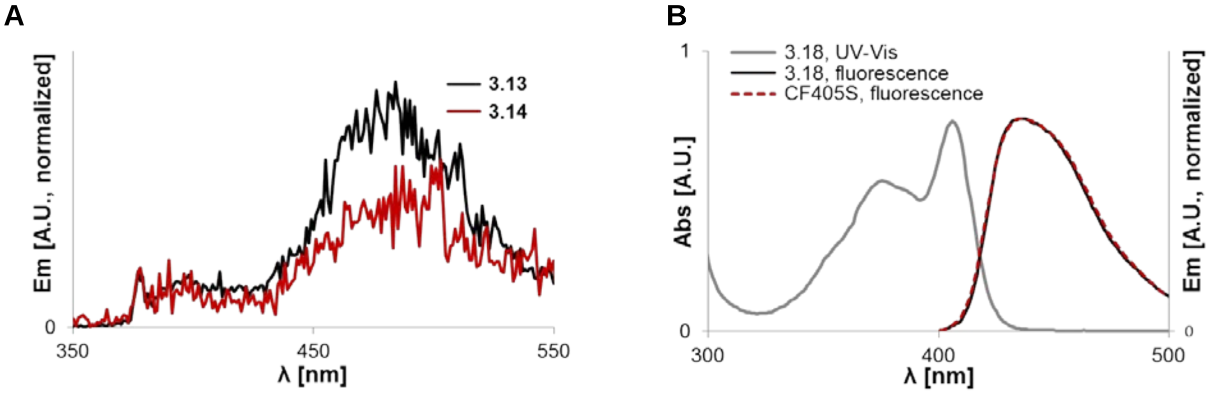

Figure 3.9. A) Both pyrene copolymer **3.14** and pyrene homopolymer **3.13** lead to excimer formation. Ex = 250 nm; [pyrene] = 80 μM; spectra are normalized to pyrene monomer emission at 377 nm. B) The sulfopyrene conjugate **3.18** did not form excimers.

Pyrene can be functionalized with sulfate groups to enhance its water solubility. The polar sulfate groups solvate the polyaromatic fluorophore and provides a handle for bioconjugation. A hydroxylamine derivative of the sulfopyrene dye CF405s was reacted with polymer **3.17** to see if this fluorophore would enhance the water solubility of polyoxazinone conjugates and still form excimers. Indeed, polymer **3.18** was highly water soluble, even without glycosylation (Scheme 3.2). However, unlike the pyrene derivatives **3.13** or **3.14**, this fluorophore did not undergo concentration dependent excimer formation (Figure 3.9B). Therefore, the free dye and the polymer conjugate have overlapping emission spectra, which disallows the use of this fluorophore for detecting polymer degradation *in cellulo*. Therefore, CF405S is also not a viable dye to detect the biodegradation of polyoxazinones.

At this point, the strategy of using a single fluorophore with concentration dependent spectral shifts was abandoned and attention was turned to other methods of fluorescence modulation. Contact quenching has been used to monitor molecular confirmation changes *in cellulo*.[298] During contact quenching, fluorescence is extinguished through direct contact between a fluorophore and a quenching moiety, which form an intramolecular non-fluorescent complex.[299] Therefore, quenching only occurs when the fluorophore and quencher are close enough in space to physically interact. DNP is a contact quencher of sulforhodamine (SR).[298] As polyoxazinone conjugates to either DNP or SR have been generated previously, we thought a new polyoxazinone variant conjugated to both moieties would be useful to explore whether contact quenching would occur. To test this hypothesis polymer **3.19** was synthesized (Scheme 3.2). After synthesizing **3.19**, the polymer was taken up in a pH = 1.25 solution known to lead to oxazinone hydrolysis, *in vitro*. After 24 h, GPC analysis revealed complete decomposition of the polymer; however, only a modest change in fluorescence intensity was observed (Figure 3.10). The 1.5-fold change in SR fluorescence upon polymer degradation was far below the 100-fold enhancement of fluorescence observed in other systems where the dye and quencher are only separated by a few angstroms.[298] It is proposed that although polymer **3.19** was conjugated to both SR and DNP, the rigidity of the polyoxazinone backbone restricts direct interaction between the dye and the quencher, preventing robust contact quenching. If this is the case, the geometry of the polyoxazinone backbone prevents efficient complexation between DNP and SR, which bars useful fluorescence turn-on ratios.

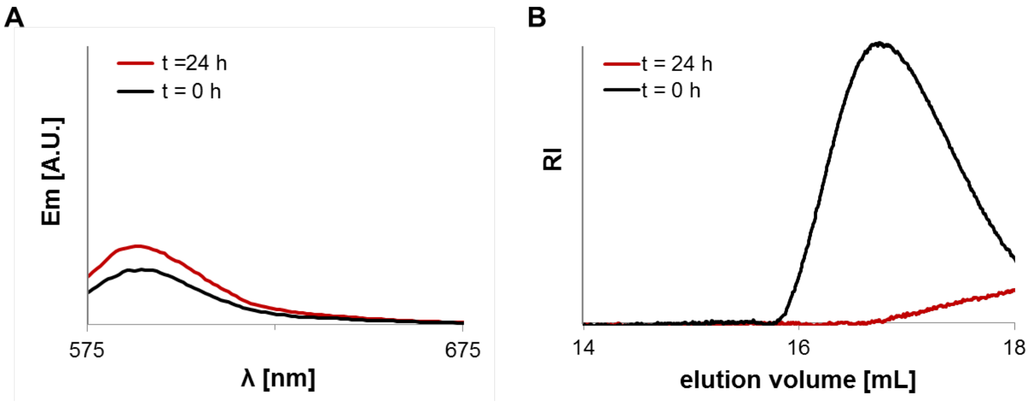

Figure 3.10. Polymer **3.19**, conjugated to the dye SR and the contact quencher DNP does not undergo significant fluorescence turn-on upon oxazinone degradation at pH = 1.25. A) Emission spectrum of polymer **3.19** before and after degradation. B) GPC analysis showed complete polymer degradation within 24 h after exposure to acidic solution. Ex = 558 nm; [polymer] = 32 μg/mL.

Probes used to detect proteolysis inside living cells are conjugated to fluorescent proteins that are FRET partners.[295-297] As mentioned previously, FRET is a through space interaction, so the two dyes do not need to physically touch, yet only occurs on length scales of 10-100 Å. Therefore, upon proteolysis, the two dyes diffuse away from each other and the FRET signal is lost. An additional benefit of using FRET as the diagnostic response is that the acceptor dye can be excited directly or through FRET. This provides an internal standard to monitor polymer uptake and can be used to differentiate poor degradation from poor polymer uptake, which was not the case with the fluorescent strategies discussed previously. To this end, the FRET pair AlexaFluor 350 (AF350, donor, Ex = 350 nm, Em = 444 nm) and AF488 (acceptor, Ex = 495 nm, Ex = 520 nm) were conjugated to polymer **3.17** to obtain multifunctional polymer **3.20** (Scheme 3.2). When polymer **3.20** was excited at 350 nm a maximum emission at 520 nm, and not 444 nm, was observed (Figure 3.11). This wavelength corresponds to AF488 excitation by FRET from AF350. It should be noted that AF488 has a minor absorbance band at 350 nm; therefore, it is weakly excited when exposed to 350 nm light, regardless of the presence of AF350. However, there is an enhancement in fluorescence at 520 nm when both AF350 and AF488 are conjugated to polymer **3.20**. On the other hand, when polymer **3.20** was excited by 495 nm light, only AF488 emission was observed. Upon successful FRET with polymer **3.20**, the polyoxazinone scaffold was further elaborated with the bioactive ligand DNP to afford polymer **3.21**, which can be recognized by A20HL B cells (Scheme 3.2). This polymer also produced a FRET signal when excited by 350 nm light (Figure 3.12). Finally, a proof of concept *in vitro* degradation test confirmed a loss of FRET overtime as polymer **3.21** degraded (Figure 3.12). Therefore, the use of the FRET pair AF350/AF488 is a viable candidate for use in the detection of polyoxazinone degradation *in cellulo*.

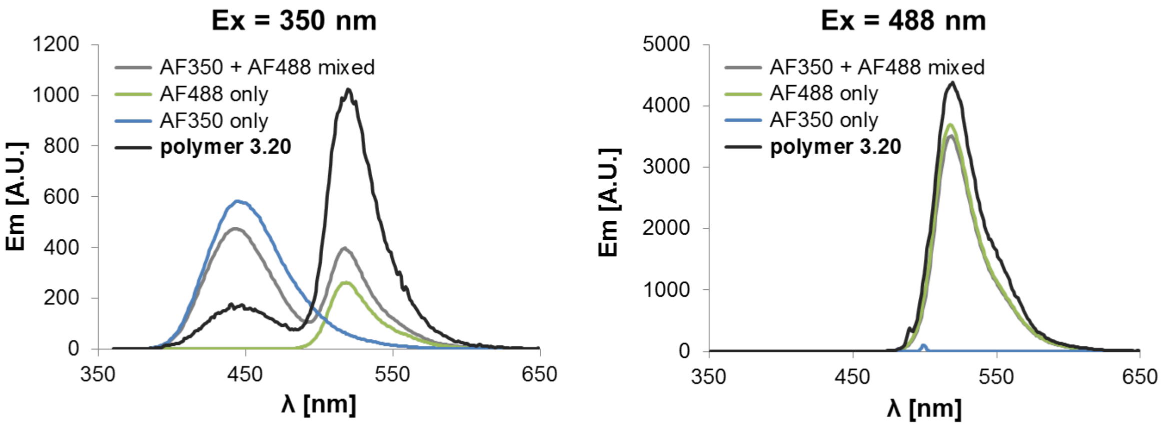

Figure 3.11. Emission spectra for polymer **3.20** and fluorophores AF350 and AF488 in water. [AF488] = 14.9 μM, [AF350] = 7.95 μM.

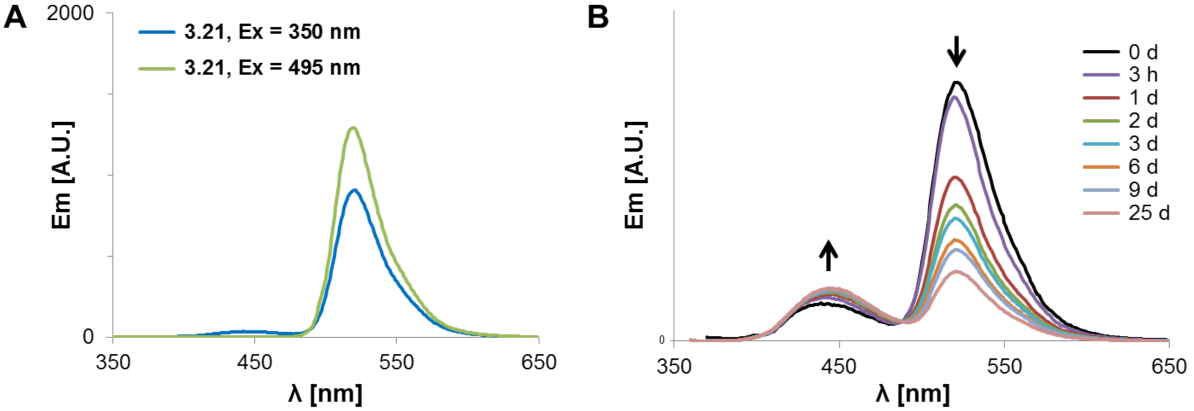

Figure 3.12. A) Emission spectra for polymer **3.21** at excited at 350 nm and 495 nm. [AF488] = 18 μM, slit width 350 nm = 5.0 nm, slit width 495 nm = 2.5 nm. B) Exposure of polymer **3.21** pH = 2.0 buffer results in a loss of FRET signal at 520 nm. Ex = 350 nm, [AF488]$_{o}$ = 14.9 μM.

3.4. Future Directions – Assessing the Degradation of Polyoxazinones in Living Cells

Polyoxazinones represent a novel ROMP polymer scaffold that contain a pH sensitive backbone and can be readily functionalized through monomer synthesis or post-polymerization modification. Decorating the polyoxazinone backbone with ligands specific for cell-surface receptors expressed on immune cells led to polymer internalization through different endocytic pathways. On the other hand, polymers that were not functionalized with the correct ligands were barred entry. Additionally, the polyoxazinone backbone was transformed into an ATD by the conjugation of guanidinium ligands to the scaffold. This modification induced the non-specific uptake of the polymer conjugates in a surface receptor independent manner. Therefore, the results presented in this chapter demonstrate that polyoxazinones are bioinert, but further studies are needed to determine if they are biodegradable as well.

To determine if polyoxazinones are able to degrade inside living systems, polymer **3.21** was generated. Polymer **3.21** is co-functionalized with the bioactive ligand DNP and the FRET pair AF350/AF488. DNP was added to facilitate BCR mediated endocytosis because BCR trafficking ultimately routes antigen to late endosomes, which are acidic (Figure 3.13). Subsequently, the FRET pair can report on polyoxazinone degradation fluorescently: as the polymer degrades, FRET transfer should diminish. A20HL B cells with DNP-specific BCRs were exposed to polymer **3.21** and the cells were incubated at 37 ^{o}C for 10 h. Aloquots of the cell culture were taken at various time points and the cellular fluorescence was assessed using flow cytometry, which allows changes in fluorescence to be observed on a single cell level. In addition to using the FRET probe **3.21**, polymer **3.01**, conjugated to DNP and AF488 but not AF350, was also used to ensure changes in the AF488-FRET channel were due to interactions between the FRET partners and not due to the absorbance of AF488 at 350 nm. A20HL cells were also exposed to polymer **3.21** in the presence of the small molecule chloroquine, which prevents endosomal acidification. This control reports on whether any observed degradation was indeed acid promoted, as expected. With these controls in hand, the anticipated results were that cells exposed to polymer **3.21** would undergo a decrease in their FRET ratio [Ex = 350 nm, Em(520 nm)/Em(450 nm)] over time while the cells exposed to polymer **3.01** or **3.21** plus chloroquine would not. On the other hand, all probes used should behave similarly when the cellular fluorescence was monitored on the AF488 home channel [Ex = 488 nm, Em(520 nm)], as this read out is not effected by proximity of AF488 to AF350.

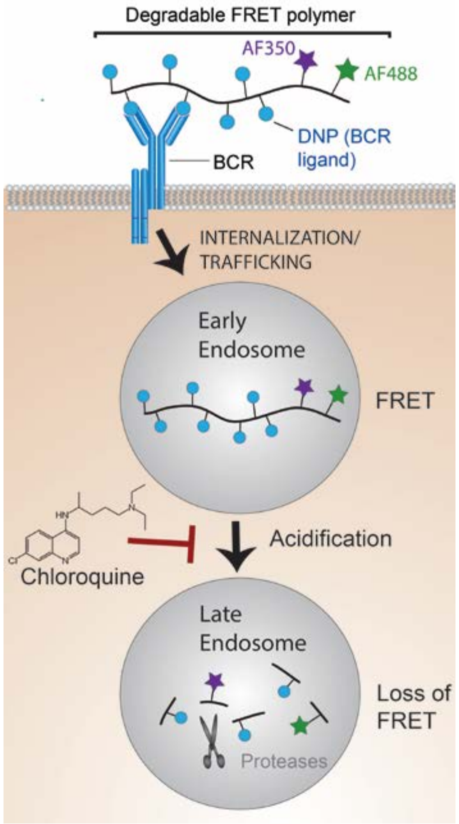
Degradable FRET polymer
AF350
AF488
DNP (BCR ligand)
BCR
INTERNALIZATION/ TRAFFICKING
Early Endosome
FRET
Chloroquine
Acidification
Late Endosome
Loss of FRET
Proteases

Figure 3.13. Assay for detecting polyoxazinone degradation inside live cells. DNP conjugate **3.21** induces BCR-mediated uptake and trafficking to acidic late endosomes, resulting in polymer hydrolysis. Hydrolysis is detected by a loss of cellular FRET signal.

The results of the *in cellulo* degradation assay are inconclusive at this point. While the flow cytometer was able to detect differences in fluorescence between unstimulated B cells and cells exposed to the polymers on either of the AF488 channels, there was no significant difference between the unstimulated cells and the polymer exposed cells on the AF350 home channel (Figure 3.14). The cause of the high baseline on the AF350 home channel is not known, but it may be that the autofluorescence of the cells when excited at 350 nm is much greater than the fluorescence of AF350 at this wavelength. Alternatively, the 450 nm light that AF350 emits is not efficiently reaching the detector either through quenching that is occurring in the cell or because of a low quantum yield. Either way, polymer **3.21** did not produce a signal for AF350 that was above the baseline inside cells, which makes conclusions based on the observed changed in the FRET ratio ambiguous. An additional complication that has to be addressed is that the signal from AF488 on all probes tests decayed by ~60% over the 10 h of the experiment. This was unexpected because AF488 is reported to have high photostability inside cells. However, prior experiments that have used FRET to investigate proteolysis in cells only incubate the fluorescent probes for an hour or two inside the cells, a much shorter time period than was required by our system.[297] Therefore, AF488 may be decomposing inside the cells over the time period of our experiments. To address these issues, alternative FRET pairs need to be screened to obtain higher signal on each fluorophore’s home channels and longer photostability when exposed to the intracellular milieu for extended periods of time.

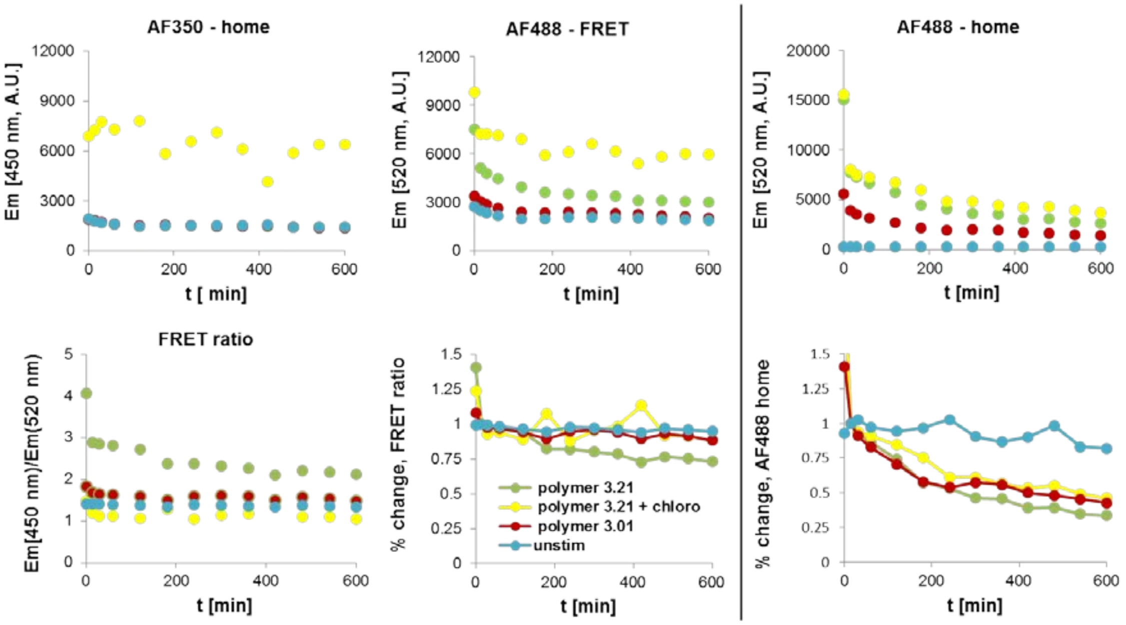

Figure 3.14. The degradation of polyoxazinones in cells was followed by flow cytometry over time. Data collected on the AF350-home channel (Ex = 350 nm, Em = 450 nm) and the AF488-FRET channel (Ex = 350 nm, Ex = 520 nm) were used to calculate the FRET ratio [Ex = 350 nm, Em(520 nm)/Em(450 nm)] over time. The percent change in the FRET ratio is normalized to t = 15 min. Data collected on the AF488-home channel reports on the stability of AF488 itself over the time course of the experiment. The percent change on the AF488-home channel is normalized to t = 15 min.

If a robust FRET pair can be found that is easily detected by flow cytometry and has good long term photostability, the rate of degradation of polyoxazinones in cells can be assessed definitively. Once this value has been estabilished, methods to modulate this rate can be investigated by changing the functionality around the oxazinone repeats through monomer synthesis. As outlined in Chapter 2, monomers are generated in a two-step reaction sequence: a range of *O*-functionalized hydroxylamine precursors are esterified with α-bromoisobutyryl bromide (BIBB) and then the hydroxamic ester intermediates are converted to the corresponding bicyclic oxazinone monomers via an *aza*-[4+3] cycloaddition with furan. Modifications to this scheme can be envisioned to alter the hydrolyzability of the oxazinone core (Figure 3.15). First, the heteroatom at the hemi-amidal position of polyoxazinones can be modified by changing the heteroatom at the monomer's bridgehead position. This can be achieved by using an alternate heteroaromatic diene during the *aza*-[4+3]-cycloaddition step. If thiophene or pyrrole are used instead of furan[300,301], the oxygen atom will be replaced with a sulfur or nitrogen, respectively. Alternatively, the *gem*-dimethyl substituents next to the carbonyl compound may be restricting oxazinone hydrolysis due to annular strain induced by the Thorpe-Ingold effect. If alternative acylating agents are used instead of BIBB, then the substituents at this position can be modified as well. A caveat to this modification is that the *gem*-dimethyl groups may increase the ring strain of the monomers, which enables the monomers to be polymerized efficiently using ROMP. Nevertheless, certain modifications at this position may lead to an altered rate of degradation. By investigating the synthetic changes described above, the hydrolyzability of oxazinones may be able to be tuned for specific applications.

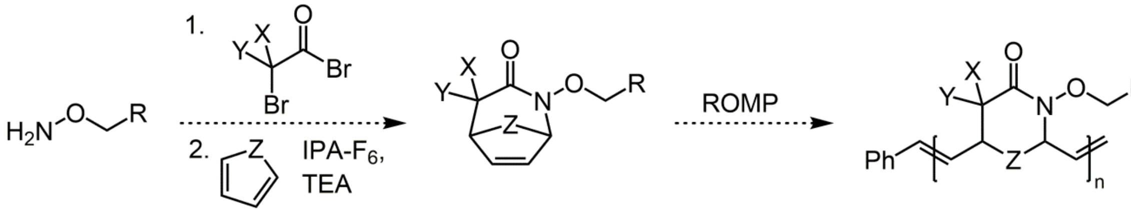

Figure 3.15. Proposed modifications to the synthesis of bicyclic oxazinone monomers to alter the rate of degradation of polyoxazinones.

3.5. Materials and Methods

3.5.1. General Methods

All commercially available reagents were purchased from Sigma-Aldrich (St. Louis, MO), Invitrogen (Grand Island, NY), or Biotium (Hayward, CA) and used as received unless otherwise noted. Monomers **3.04**, **3.15**, **3.22**, polymer **3.17**, and PEG$_3$OH ligand **3.23** were synthesized as described in Chapter 2. *N*-Boc, *O*-(3-aminopropyl) hydroxylamine[302], intermediate **3.24**[298], and catalyst **3.35**[88] were synthesized as described previously. All reactions were run under an inert atmosphere of N_2 unless otherwise specified. Reactions were stirred using Teflon coated magnetic stir bars. All glassware and stir bars were stored in oven before use.

^1H and ^{13}C nuclear magnetic resonance (NMR) spectra were obtained using an Avance-500 or Avance-400 MHz spectrometer. Chemical shifts are reported relative to tetramethylsilane or residual solvent peaks in parts per million ($CHCl_3$: ^1H: δ 7.26, ^{13}C: δ 77.23; MeOH-d_4: ^1H: δ 3.31, ^{13}C: δ 49.00). Peak multiplicity is reported as singlet (s), doublet (d), doublet of doublets (dd), triplet (t), doublet of triplets (dt), quartet (q), quartet of doubles (qd), pentet (pent), multiplet (m). When possible, the degree of polymerization (DP) was assessed by comparing the ratio of polymer olefin signals to phenyl end-group. When possible, the conversion of ketone to oxime by PPM was determined by comparing the acetophenone signal at 2.55 ppm to the oxime signal at 2.20 ppm. Multifunctional polymers contain many broad overlapping signals; therefore, the peaks that can unequivocally be assigned to either the backbone or a specific ligand are reported, along with the full spectrum in the references section.

High resolution electrospray ionization mass spectra (HRESI-MS) were obtained on a Micromass LCT mass spectrometer. Room temperature GPC-SEC analysis (Viscotek GPC max) was performed on 300 x 7.5 mm PolyPor 5 μm mixed columns from Polymer Laboratories. Data was analyzed using OmniSEC software (Viscotek Inc.). Polymers were eluted with THF (1.0 mL/min, 40 ^oC) to determine M_n, M_w, and polydispersity index (M_n/M_w). Columns were calibrated with 10 narrow polystyrene standards (Polymer Laboratories S-M2-10 kit). UV-Vis absorption spectra were obtained on a Varian Cary 50-Scan UV-Visible Spectrophotometer. Optical measurements were taken in a quartz cuvette.

3.5.2. Synthetic procedures

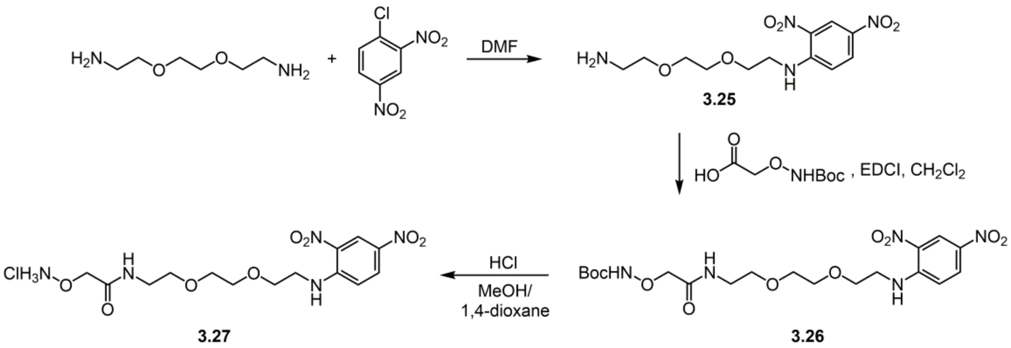

Compound 3.25

To a solution of 2,2’-(ethylenedioxy) bis(ethylenediamine) (1.0 mL, 6.80 mmol) in DMF (1.5 mL) was added 1-chloro-2,4-dinitrobenzene (138 mg, 0.68 mmol) in DMF (6 mL), dropwise. The solution was then stirred for 30 min at rt. The solution was diluted with dichloromethane (20 mL) and was washed with DI water (2 x 26 mL). The organic layer was dried over Na_2SO_4, filtered, and concentrated to afford **3.25** as a yellow oil (197 mg, 92%). ^{1}H-NMR ($CDCl_3$, 400 MHz): δ 9.13 (d, *J* = 2.7 Hz, 1H), 8.82 (s, 1H, NH), 8.27 (dd, *J* = 9.5, 2.6 Hz, 1H), 6.96 (d, *J* = 9.5 Hz, 1H), 3.85 (t, *J* = 5.3 Hz, 2H), 3.76-3.65 (m, 4H), 3.61 (q, *J* = 5.1 Hz, 2H), 3.53 (t, *J* = 5.3 Hz, 2H), 2.88 (t, *J* = 5.2 Hz, 2H), 1.44 (s, 2H, NH_2). ^{13}C-NMR ($CDCl_3$, 100 MHz): δ 148.4, 136.1, 130.5, 130.3, 124.3 114.0, 73.6, 70.8, 70.3, 68.6, 43.3, 41.8. HRESI-MS calcd for $C_{12}H_{18}N_4O_6$ $[M+H]^+$ 315.1300; found 315.1290.

Compound 3.26

To a stirring solution of **3.25** (25 mg, 0.08 mmol) and (*N*-Boc-aminoxy)acetic acid (19 mg, 0.10 mmol) in dichloromethane (5 mL) was added 1-ethyl-3-(3-dimethylaminopropyl)carbodiimide hydrochloride (EDCI, 48 mg, 0.25 mmol). The solution was stirred for 16 h at rt. The solution was diluted with dichloromethane (4 mL) and washed with DI water (1 x 6 mL) and brine (1 x 6 mL). The organic layer was dried over Na_2SO_4, filtered, and concentrated. The resultant residue was purified by flash column chromatography (48% acetone/hexanes) to afford compound **3.26** (29 mg, 75%). ^{1}H-NMR ($CDCl_3$, 400 MHz): δ 9.15 (d, *J* = 2.6 Hz, 1H), 8.82 (broad s, 1H, NH), 8.28 (dd, *J* = 9.5, 2.3 Hz, 1H), 7.95 (broad s, 1H, NH), 7.57 (s, 1H, NH), 6.95 (d, *J* = 9.5 Hz, 1H), 4.33 (s, 2H), 3.86 (t, *J* = 5.3 Hz, 2H), 3.76-3.65 (m, 4H), 3.60 (q, *J* = 5.3 Hz, 4H), 3.53 (q, *J* = 5.4 Hz, 2H), 1.47 (s, 9H). ^{13}C-NMR ($CDCl_3$, 100 MHz): δ 168.8, 157.4, 148.4, 136.1, 130.5, 130.3, 124.5, 114.0, 82.9, 76.1, 70.7, 70.4, 69.7, 68.5, 43.3, 38.8, 28.1. HRESI-MS calcd for $C_{19}H_{29}N_5O_{10}$ $[M+H]^+$ 488.1988; found 488.1987.

Compound 3.27

To a stirring solution of **3.26** (29 mg, 0.06 mmol) in methanol (0.2 mL) was added a 4 M solution of hydrochloric acid in 1,4-dioxane (0.5 mL). The solution was stirred for 1 h at rt and then concentrated. Excess acid was azeotroped with chloroform (3 x 0.5 mL). Compound **3.27** was isolated as a yellow oil (25 mg, quant). ^{1}H-NMR (MeOH-d_4, 500 MHz): δ 9.06 (d, *J* = 2.7 Hz, 1H), 8.32 (dd, *J* = 9.5, 2.7 Hz, 1H), 7.24 (d, *J* = 9.6 Hz, 1H), 4.57 (s, 2H), 3.83 (t, *J* = 5.2 Hz, 2H), 3.73-3.63 (m, 6H), 3.61 (t, *J* = 5.5 Hz, 2H), 3.45 (t, *J* = 5.4 Hz, 2H). ^{13}C-NMR (MeOH-d_4, 125 MHz): δ 168.2, 148.4, 135.7, 130.2, 129.7, 123.3, 114.7, 70.7, 70.2, 69.9, 69.0, 68.4, 42.6, 38.7. HRESI-MS calcd for $C_{14}H_{22}N_5O_8$ $[M-Cl]^+$ 388.1465; found 388.1463.

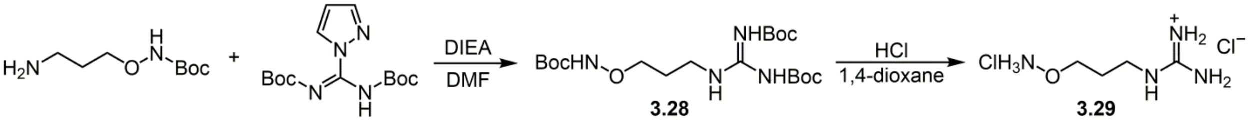

Compound 3.28

To a stirring solution of *N*-Boc, *O*-(3-aminopropyl) hydroxylamine (310 mg, 1.0 mmol) and *N, N'*-di-Boc-*1H*-pyrazole-1 carboxamidine (475 mg, 2.50 mmol) in DMF (8.7 mL) was added DIEA (0.35 mL, 2.0 mmol). The solution was stirred at rt for 18 h and then concentrated. The residue was suspended in water (20 mL) and extracted successively with dichloromethane (3 x 15 mL) and ethyl acetate (4 x 15 mL). The combined organic phase was dried and concentrated. The residue was purified by silica column chromatography (50% EtOAc/hex). Compound **3.28** was isolated was a white solid (370 mg, 85%). ^{1}H-NMR ($CDCl_3$, 500 MHz): δ 11.47 (s, 1H), 8.50 (s, 1H), 7.66 (s, 1H), 3.94 (t, *J* = 5.7 Hz, 2H), 3.57 (q, *J* = 6.3 Hz, 2H), 1.87 (pent, *J* = 6.2 Hz, 2H), 1.51 (s, 9H), 1.49 (s, 9H), 1.48 (s, 9H). ^{13}C-NMR ($CDCl_3$, 125 MHz): δ 163.4, 156.9, 156.3, 153.2, 83.2, 81.5, 79.4, 74.0, 37.8, 28.3, 28.3, 28.1, 27.9.

Compound 3.29

Compound **3.28** (365 mg, 0.84 mmol) was dissolved in a 4 M solution of HCl in 1,4-dioxane (6.8 mL) at 0 ^{o}C. The solution was stirred and allowed to warm to rt over 20 h. The solution was concentrated and excess acid was azeotroped with toluene (3 x 6 mL) to afford compound **3.29** as a white solid (140 mg, 81%). ^{1}H-NMR (MeOH-d_4, 500 MHz): δ 4.16 (T, *J* = 6.1 Hz, 2H), 3.34 (t, *J* = 7.1 Hz, 2H, under solvent), 2.01 (pent, *J* = 6.5 Hz, 2H). ^{13}C-NMR (MeOH-d_4, 125 MHz): δ 157.3, 72.0, 37.6, 26.9. HRESI-MS calcd for $C_4H_{13}N_4O$ $[M]^+$ 133.1084; found 133.1079.

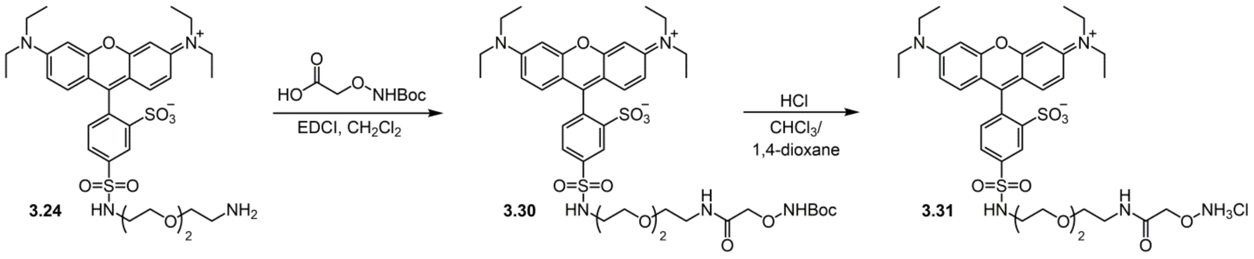

Compound 3.30

(*N*-Boc-aminoxy)acetic acid (13.9 mg, 73 μmol), **3.24** (40 mg, 58 μmol), and EDCI (35 mg, 183 μmol) were dissolved in dichloromethane (3.75 mL) and stirred at rt for 6 h. The solution was concentrated and the residue was purified by silica column chromatography (8% MeOH/CH$_2$Cl$_2$) to afford compound **3.30** (16 mg, 32%). ^{1}H-NMR (MeOH-d$_4$, 500 MHz): δ 8.69 (d, *J* = 1.8 Hz, 1H), 8.15 (dd, *J* = 7.9, 1.8 Hz, 1H), 7.53 (d, *J* = 8.0 Hz, 1H), 7.15 (d, *J* = 9.5 Hz, 2H), 7.02 (dd, *J* = 9.5, 2.4 Hz, 2H), 6.95 (d, *J* = 2.4 Hz, 2H), 4.25 (s, 2H), 3.74-3.57 (m, 16H), 3.46 (t, *J* = 5.5 Hz, 2H), 3.25 (t, *J* = 5.4 Hz, 2H), 1.48 (s, 9H), 1.32 (t, *J* = 7.1 Hz, 12H). ^{13}C-NMR (MeOH-d$_4$, 125 MHz): δ 171.6, 159.6, 159.4, 157.9, 157.2, 147.2, 144.2, 135.4, 133.7, 132.4, 129.3, 127.7, 115.3, 115.0, 97.0, 83.0, 76.4, 71.4, 70.8, 70.4, 49.9, 46.8, 44.1, 39.9, 28.5, 12.8.

Compound 3.31

To a stirring solution of **3.30** (16 mg, 18.6 μmol) in chloroform (0.6 mL) was added a 4 M solution of HCl in 1,4-dioxane (0.6 mL). The solution was stirred at rt in the dark for 1 h. The solution was concentrated and excess acid was azeotroped with dichloromethane (3 x 0.5 mL) to afford compound **3.31** as a purple solid (16 mg, quant). ^{1}H-NMR (MeOH-d$_4$, 500 MHz): δ 8.67 (d, *J* = 1.8 Hz, 1H), 8.13 (dd, *J* = 7.9, 1.8 Hz, 1H), 7.53 (d, *J* = 7.9 Hz, 1H), 7.12 (d, *J* = 9.5 Hz, 2H), 7.00 (dd, *J* = 9.5, 2.2 Hz, 2H), 6.95 (d, *J* = 2.2 Hz, 2H), 4.55 (s, 2H), 3.68 (q, *J* = 7.1 Hz, 8H), 3.64-3.53 (m, 8H), 3.46 (t, *J* = 6.3 Hz, 2H), 3.24 (t, *J* = 6.3 Hz, 2H), 1.30 (t, *J* = 7.1 Hz, 12H). ^{13}C-NMR (MeOH-d$_4$, 125 MHz): δ 169.5, 159.4, 157.7, 157.2, 147.1, 144.2, 135.4, 133.6, 132.5, 129.4, 127.7, 115.3, 115.0, 97.0, 72.3, 71.3, 70.6, 70.4, 49.9, 46.8, 44.1, 40.1, 12.8. HRESI-MS calcd for $C_{35}H_{47}N_5O_{10}S_2$ $[M+Na]^+$ 784.2657; found 784.2667.

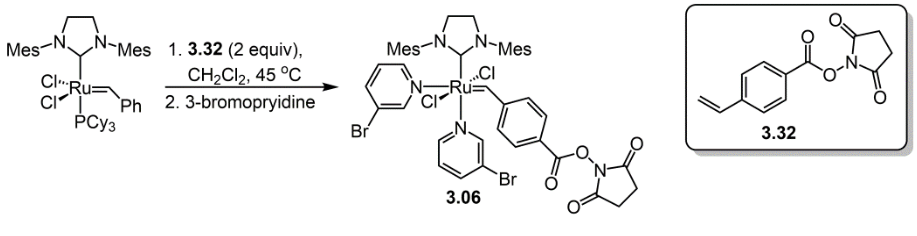

Compound 3.32

To a stirring solution of 4-vinyl benzoic acid (33.0 mg, 0.225 mmol) in dichloromethane and DMF [9:1 (v/v), 0.39 mL] was added *N*-hydroxysuccinimide (34.0 mg, 0.394 mmol) and EDCI (58.0 mg, 0.401 mmol). The solution was stirred for 22 h at rt. The reaction was diluted with dichloromethane (5.0 mL) and washed with a 5% citric acid solution (2 x 3 mL). The organic phase was dried and concentrated. The solid residue was purified by flash column chromatography (25% EtOAc/hexanes) to afford **3.32** as white solid (36.5 mg, 66%). ^{1}H-NMR (CDCl$_3$, 300 MHz): δ 8.08 (d, *J* = 8.3 Hz, 2H), 7.52 (d, *J* = 8.3 Hz, 2H), 6.76 (dd, *J* = 17.5, 11.1 Hz, 1H), 5.92 (d, 17.6 Hz, 1H), 5.45 (d, *J* = 11.1 Hz, 1H), 2.91 (s, 4H). ^{13}C-NMR (CDCl3, 75 MHz): δ 169.5, 161.8, 144.2, 135.8, 131.1, 126.7, 124.2, 188.1, 25.9. HRESI-MS calcd for $C_{13}H_{11}NO_4Na$ $[M+Na]^+$ 268.0581; found 268.0578.

(H_2IMes)(3-bromopyridine)$_2$Cl$_2$Ru=HCPh-4-(NHS ester), Catalyst 3.06

To a stirring solution of catalyst **3.05** (10 mg, 0.012 mmol) in dichloromethane (0.6 mL) was added **3.32** (5.6 mg, 0.024 mmol). The reaction was stirred for 1 h at 45 ^{o}C. The precipitate was pelleted via centrifugation and the supernatant was decanted and concentrated under reduced pressure (without heating). The residue was taken up in 3-bromopyridine (0.15 mL) and allowed to stir for 5 min. Pentanes (2.5 mL) were layered on top of the solution and the bifurcated mixture was stored in a -20 ^{0}C freezer for 24 h. The solid precipitate was collected via vacuum filtration and washed with cold pentanes (3 x 2 mL) to afford catalyst **3.06** as a purple-green solid (3.4 mg, 28%). ^{1}H-NMR ($CDCl_3$, 500 MHz): δ 19.65 (s, 1H), 8.16 (d, *J* = 8.5 Hz, 1H), 8.12 (d, *J* = 8.5 Hz, 1H), 7.84 (d, *J* = 8.4 Hz, 1H), 7.76 (d, *J* = 8.6 Hz, 1H), 7.67 (d, *J* = 8.5 Hz, 1H), 7.63 (d, *J* = 8.5 Hz, 1H), 7.55 (d, *J* = 7.2 Hz, 1H), 7.40 (t, *J* = 7.1 Hz, 1H), 7.35-7.27 (m, 2H), 7.17-7.05 (m, 2H), 6.97 (s, 1H), 6.90-6.75 (m, 2H), 4.70-3.7 (m, 4H), 2.91 (s, 4H), 2.63 (s, 3H), 2.43 (s, 3H), 2.43 (s, 3H), 2.40 (s, 3H), 2.32 (s, 3H), 3.29 (s, 3H), 2.22 (s, 3H).

General Procedure for the Synthesis of Polyoxazinone Oxime Conjugates

Polymer **3.17** (n eq. wrt acetophenone) was taken up in a solution of hydroxylamine ligands (1.75n eq) in DMSO so the final concentration of acetophenone is 40 mM. Pyridine (8n eq) was added and the solution was stirred at rt for 24 h. Benzaldehyde (1.5n eq) was added and the solution was stirred for 1 h at rt (benzealdehyde caps any unreacted hydroxylamine ligands and aides in ligand separation from the polymer in next step). The solution was triturated into 1.25 mL diethyl ether and the solids were collected by centrifugation. Trituration was repeated until all small molecules were removed as determined by NMR.

Polymer 3.01

Polymer **3.01** was synthesized following the general procedure using **3.27**, **3.23**, and AlexaFluor488 as ligands in a 0.5 : 0.42 : 0.08 ratio (mol/mol/mol). ^{1}H-NMR (500 MHz, DMSO-d_4): Set backbone signal at δ 6.30-5.60 ppm to 2H. Used signal at 8.34 (s, 1xH) to determine AF488 content. Used signal at 8.13 (m, 1xH) to determine DNP content. Found 95% conversion to oxime; 25% DNP, 6% AF488, 69% PEG_3-OH conjugation.

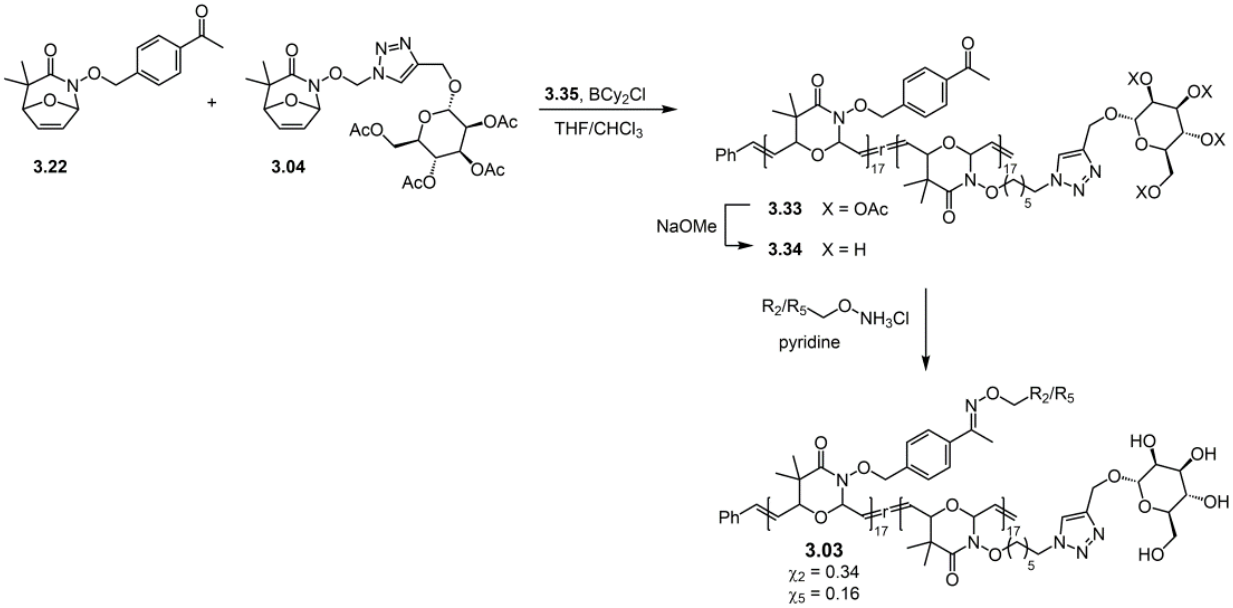

Polymer 3.33

To a solution of **3.22** (30 mg, 0.10 mmol) and **3.04** (68 mg, 0.10 mmol) in THF (0.1 mL) under at atmosphere of Ar was added BCy_2Cl from a 1 M solution in hexanes (20 μL) followed by a solution of **3.35** (4.43 mg, 5 μmol) in chloroform (0.08 ml). The solution was stirred for 50 min at rt and then the polymerization was quenched by the addition of ethyl vinyl ether (0.1 mL). The precipitated solids were re-dissolved in minimal chloroform and the solution was triturated into 30 mL diethyl ether. Intermediate polymer **3.33** was collected by centrifuge. ^{1}H-NMR (500 MHz, $CDCl_3$). Set backbone signal at δ 6.30-5.60 ppm to 2H. Used signals at 7.59 (broad s, 1xH, triazole-H) and 2.03 (s, 3xH, acetate) to determine Ac_4Mannose content. Used signals at 7.89 (m, 2xH) and 2.59 (broad s, 3xH, acetophenone methyl) to determine acetophenone content. Found 50% acetophenone, 50% Ac_4Mannose incorporation.

Polymer 3.34

To a stirring solution of **3.33** (5.1 mg, 4.4 μmol (wrt mannose)) in DMSO (0.2 mL) was added a 0.5 M solution of sodium methoxide in methanol (17.6 μL). The solution was stirred for 20 min at rt and then acidified with a 0.23 M solution of anhydrous HCl in methanol (45 μL). The neutralized solution was triturated into 1.25 mL diethyl ether and the solids were isolated via centrifugation. Intermediate polymer **3.34** was dissolved in DMSO-d_6 over 16 h before ^{1}H-NMR analysis. ^{1}H-NMR (500 MHz, DMSO-d_6). Set backbone signal at δ 6.25-5.35 ppm to 3H. Used signal at 8.09 (broad s, 1xH, triazole-H) and 1.77 (s, 2xH) to determine mannose content. Used signal at 7.90 (m, 2xH) to determine acetophenone content. Found 50% acetophenone, 50% mannose incorporation.

Polymer 3.03

To a solution of polymer **3.34** (0.96 mg, 1.17 μmol (wrt ketone)) in 100 μL DMSO was added **3.23** (0.24 mg, 0.88 μmol) from a 16.4 mg/mL stock solution in DMSO and **3.31** (0.73 mg, 0.88 μmol) from a 68.2 mg/mL stock solution in DMSO. Pyridine (1.131 μL, 10.4 μmol) was added and the solution was stirred at room temperature in the dark for 24 h. Benzaldehyde (1.79 μL, 1.76 μmol) was added and the solution was stirred for 1 h. The solution was triturated into 1.25 mL diethyl ether and the solids were collected by centrifugation. Trituration was repeated until all small molecules were removed as determined by NMR. ^{1}H-NMR (500 MHz, DMSO-d_6). Set backbone signal at δ 6.30-5.15 ppm to 3H. Used signals at 8.06 (broad s, 1xH, triazole-H) and 1.74 (broad s, 2xH) to determine mannose content. Used signals at 7.93 (broad s, 1xH) and 3.00 (broad s, 2xH) to determine SR content. Found 100% conversion to oxime; 50% mannose, 32% PEG$_3$OH, 16% SR conjugation.

Polymer 3.07

To a vial containing **3.04** (22.5 mg, 0.033 mmol) under at atmosphere of Ar at -10 ^{o}C was added **3.06** (1.7 mg, 0.0017 mmol) dissolved in THF (50 μL). The solution was stirred and allowed to warm to rt over 5.5 h, then the polymerization was quenched with ethyl vinyl ether. After 1 h, the solution was triturated into diethyl ether (4 mL) and the solids were collected by centrifuge. ^{1}H-NMR (500 MHz, $CDCl_3$): δ 8.12 (m, 0.16 H, 2x end-cap Ar), 7.62 (broad s, 1H, triazole-H), 6.40-5.60 (m, 2H, olefin), 5.45-5.15 (m, 4H), 4.96 (s, 1H), 4.90-4.77 (m, 1H), 4.75-4.60 (m, 1H), 4.45-3.70 (m, 8H), 2.93 (s, 0.69 H, 4x NHS), 2.20-2.10 (m, 6H), 2.03 (s, 3H), 2.02-1.86 (m, 5H), 1.40-1.05 (m, 14H). DP^{NMR} = 12. M_n^{GPC} = 7600, M_w^{GPC} = 10500, PDI = 1.39.

Polymer 3.08

To a solution of **3.07** (1 mg, 0.13 μmol) in DMSO (200 μL) was added *N*-methyl morpholine (0.72 μL, 6.5 μmol) neat and AlexaFluor 488 cadaverine (0.27 mg, 0.42 μmol) from a 10 mg/mL stock solution in DMSO. The solution was stirred on a rotisserie at rt in the dark for 15 h. The polymer was separated from excess small molecules using a PD-10 desalting column. The fluorescent eluent to elute before the DMSO band was collected and the intermediate polymer was isolated by lyophilization to afford an orange solid.

Dissolved isolated polymer in DMSO (0.45 mL) and added a 0.5 M solution of sodium methoxide in methanol (5 μL). The solution was stirred for 45 min at rt, then moved immediately to a PD-10 desalting column to remove excess small molecules. The fluorescent eluent to elute before the DMSO band was collected and polymer **3.08** was isolated by lyophilization

Polymer 3.09

Polymer **3.09** was synthesized following the general procedure using ligand **3.29**. Triturating the solution into diethyl ether did not remove all excess ligand. The polymer was purified using a PD-10 desalting column. ^{1}H-NMR (500 MHz, MeOH-d_4): δ 7.65-7.05 (m, 4H), 6.10-5.60 (m, 2H), 5.55-5.30 (m, 1H), 5.00-4.55 (m, 2H, under solvent), 4.40-3.85 (m, 3H), 2.10-2.00 (m, 3H), 1.95-1.80 (m, 2H), 1.15-0.85 (m, 6H).

Polymer 3.12

Polymer **3.12** was synthesized following the general procedure using **3.29** and **3.31** in a 97 : 3 ratio (mol:mol). Triturating the solution into diethyl ether did not remove all excess ligand. The polymer was purified using a PD-10 desalting column. ^{1}H-NMR (500 MHz, MeOH-d_4). Set backbone signal at δ 6.25-5.25 ppm to 3H. Used signal at 7.99 (s, 1xH) to determine SR content. Used signal at 1.89 (m, 2xH) to determine guanidinium content. Found 90% conversion to oxime; 95% guanidinium, 5% SR conjugation.

Polymer 3.14

In a 0.4 mL insert for a 0.5 dram vial was added monomer **3.15** (8 mg, 18.8 μmol) under and atmosphere for Ar. Catalyst **3.05** (3.2 mg, 3.8 μmol) was added in dichloromethane (200 μL) and the solution was stirred for 1.25 h at rt. Monomer **3.04** (51 mg, 75.2 μmol) was added in dichloromethane (75 μL) and the combined solution was stirred for an additional 5 h. The polymerization was quenched with ethyl vinyl ether and stirred for an additional 1 h. The solution was triturated into diethyl ether and the solids were collected via centrifugation. ^{1}H-NMR (500 MHz, $CDCl_3$): Ratio of pyrene to mannose was determined by the ratio of the signals at δ 8.20-7.75 (m, 7x H, pyrene) to 4.82 (m, 1x H, mannose). Found 33% pyrene, 66% mannose incorporation. DP^{NMR} = 20. M_n^{GPC} = 6900, M_w = 20200, PDI = 2.9.

Polymer 3.16

To a solution of polymer **3.14** (6 mg) in DMSO (0.67 mL) was added a 0.5 M solution of sodium methoxide in methanol (35 μL). The solution was stirred for 45 min at room and the passed through at PD-10 desalting column. Freeze-dried eluent to elute before DMSO band to afforded solids that were found to be insoluble in water.

Polymer 3.18

Polymer **3.18** was synthesized following the general procedure using **3.23** and CF405S in a 55 : 45 ratio (mol:mol). Product was not isolated by trituration but rather the polymerization milieu was diluted into 3 mL milliQ water and moved to a 3 mL, 7000 MWCO dialysis cassette. The solution was dialyzed against milliQ water for 24 h, changing water 3 times. Freeze-dried the contents of the dialysis cassette. ^{1}H-NMR (500 MHz, D_2O). Set backbone signals at δ 7.75 – 6.25 ppm to 4H. Used signals at 9.20-8.65 (m, 6x H, sulfopyrene) to determine CF405S content. PEG_3-OH signal fell under solvent peak. Found 33% CH405S conjugation.

Polymer 3.19

To a solution of polymer **3.17** (1.56 mg, 5.04 μmol (wrt ketone)) in DMSO (30.9 μL) was added **3.27**, **3.31**, and **3.23** in a 31 : 6 : 63 ratio (mol:mol:mol). ^{1}H-NMR (500 MHz, $CDCl_3$). Set backbone signal at δ 6.30-5.60 ppm to 2H. Used signal at 8.26 (m, 1xH) to determine SR content. Used signal at 8.16 (m, 1xH) to determine DNP content. Found 95% conversion to oxime; 8% SR, 18% DNP, 69% PEG_3-OH conjugation.

Polymer 3.20

Polymer **3.20** was synthesized following the general procedure using AF488, AF350, and **3.23** in a 33 : 17 : 50 ratio (mol:mol:mol). Polymer was isolated by diluting solution into 3 mL milliQ water and the excess small molecules were removed by dialysis in a 3 mL, 7000 MWCO dialysis cassette. The solution was dialyzed against milliQ water for 24 h, changing the water 3 times. Freeze-dried the contents of the dialysis cassette. ^{1}H-NMR (500 MHz, DMSO-d_6). Set backbone signals at δ 6.15-5.30 ppm to 3H. Used signal at 8.34 (m, 1xH) to determine AF488 content. Used signal at 2.91 (m, 2xH) to determine AF350 content. Found 99% conversion to oxime; 32% AF488, 22% AF350, 45% PEG_3-OH conversion.

Polymer 3.21

To a solution of polymer **3.17** (1.23 mg, 4.05 μmol (wrt ketone)) in DMSO (148.8 μL) was added **3.27** (5.15 mg, 12.2 μmol) from a 34.6 mg/mL stock solution in DMSO. Pyridine (7.86 μL, 97.6 μmol) was added and the solution was stirred at rt for 24 h. Benzaldehyde (0.5 μL) was added and the solution was stirred for 1 h. The solution was triturated into 1.25 mL diethyl ether and the solids were isolated by centrifuge to afford intermediate polymer **3.21’**. ^{1}H-NMR (500 MHz, 1:1 MeOH-d_4:$CDCl_3$): δ 8.97-8.82 (m, 0.33 H, DNP), 8.80-8.78 (m, 0.16 H, DNP N-H), 8.22-8.07 (m, 0.33 H, DNP), 8.00-7.72 (m, 1.33 H, acetophenone aryl), 7.56-7.20 (m, 3H), 7.02-6.90 (m, 0.33 H, DNP), 6.30-5.61 (m, 2H, olefin), 5.57-5.20 (m, 1H, oxazinone), 5.10-4.70 (m, 2H, benzyl), 4.40-4.16 (m, 1H, oxazinone), 3.80-3.41 (m, 4.6 H, PEG), 2.67-2.42 (m, 1.8H, acetophenone), 2.33-2.17 (m, 1.2 H, oxime), 1.25-1.05 (m 6H, *gem*-dimethyl).

Polymer **3.21’** (0.99 mg, 1.54 μmol (wrt ketone)) was dissolved in **3.23** (26.2 μL, 1.54 μmol) from a 16.4 mg/mL stock solution in DMSO, AF488 (0.34 mg, 0.39 μmol) from a 35.8 mg/mL stock solution in DMSO, and AF350 (0.11 mg, 0.19 μmol) from a 23.4 mg/mL stock solution in DMSO. Pyridine (1.364 μL, 16.9 μmol) was added and the solution was left in dark at rt for 48 h. The solution was diluted with DMSO (300 μL) and the polymer was separated from excess small molecules using a PD-10 desalting column, eluting with milliQ water. Collected fluorescent eluent to elute before DMSO band and freeze-dried solution. ^{1}H-NMR (500 MHz, DMSO-d_6). Set backbone signal at δ 6.05-5.30 to 3H. Used signal at 8.34 (m, 1xH) to determine AF488 content. Used signal at 8.13 (m, 1xH) to determine DNP content. Used signal at 2.89 (m, 2xH) to determine AF350 content. Found 97% conversion to oxime; 9% AF488, 3% AF350, 45% DNP, 43% PEG$_3$-OH conjugation.

3.5.3. Cell culture

Raji and Raji/DC-SIGN cells were obtained from the NIH AIDS Reference and Reagent Program.[283] Cells were maintained in RPMI media (Gibco) supplemented with 10% fetal bovine serum (FBS) and penicillin/streptomycin at 37 ^{o}C and 5% carbon dioxide.

A20 and A20/2J cells stably transfected with DNP/TNP-specific mIgM to generate the A20/2J HL$_{TNP}$ cell line were provided by A. Ochi (University Health Network, Toronto, ON, Canada).[266,303] A20/2J HL$_{TNP}$ cells were cultured in RPMI medium 1640 supplemented with 2 mM L-glutamine, 10% FBS, 50 μM 2-mercaptoethanol, 100 U mL^{-1} penicillin and 100 U mL^{-1} streptomycin.

3.5.4. Procedures for Selective Internalization of Polymer Probe ***3.08*** *and* ***ManBSA*** *by DC-SIGN expressing Raji Cells*

Raji cells were washed and resuspended in phosphate buffer solution containing $CaCl_2$ (Gibco) and 1% Bovine Serum Albumin at 1 million cells per mL. Polymer **3.08** was added to a final concentration of 1.85 μM and incubated with cells for 40 minutes at 37 °C. Cells were then washed and transferred to eight-chambered cover glass slides (Nunc). Cells were visualized on a Nikon Eclipse Ti-E confocal microscope with a 60x oil-immersion objective and the NIS Elements software package. Identical procedures were followed for **ManBSA**.

3.5.5. Procedures for the Internalization of Polymer Probes ***3.01****,* ***3.02****, and* ***3.12*** *by A20 and A20 HL Cells*

A20 and A20HL cells were resuspended at $1.5x10^6$ cells/ml in 1% BSA/RPMI and incubated for 30 min in the presence of 8.8 ug/ml Dylight 549 conjugated transferrin (Jackson Immunoresearch) at 37 °C. Cells were pelleted and resuspended on ice using the previous buffer, prechilled. Cell surface BCR was labeled using 15 ug/ml Alexa Fluor 647 conjugated goat anti mouse IgM mu chain specific Fab fragment for 20 min on ice. Cells were then pelleted and resuspended in PBS, pH 7.4 supplemented with 1 mM $CaCl_2$ and 0.5 mM $MgCl_2$ at 37 °C. Cells were then treated with synthetic antigens at 5 μg/mL at 37 °C and samples were placed on ice after 30 minutes. Cells were visualized in no. 1.5 borosilicate eight-well chambered coverglass (Nunc). Images were collected on a Nikon A1R confocal microscope using a 60x objective. Intensity and co-localization analysis was performed using ImageJ software (National Institutes of Health, NIH). The Pearson's Coefficient was calculated for individual cells using the colocalization threshold plugin in ImageJ. Images were despeckled to remove noise.

*3.5.6. In vitro degradation of polymer **3.21***

An aliquot of a solution of polymer **3.21** in DMSO (5 mg/mL) was diluted into a pH = 2 HCl/KCl buffer such that the [AF488] was 14.9 μM. The solution was stirred in the dark at 40 °C and fluorescence readings were taken a various time points, λ_{ex} = 350 nm. The change in the ratio of AF350 emission (λ_{em}^{max} = 444 nm) to AF488 emission (λ_{em}^{max} = 520 nm) over time was used to assess polymer decomposition. Note: As some of the solvent partitioned into the headspace over time, the overlaid spectra were normalized to λ_{em} = 488 nm to account for this change in concentration.

3.5.7. Procedures for Monitoring the Degradation of Polymers by FRET in Live Cells

A20HL cells were suspended at 10^6 cells per mL in ice cold PBS pH 7.4 supplemented with 1 mM $CaCl_2$ and 0.5 mM $MgCl_2$. Cells on ice were treated with 5 ug/ml polymer for 30 minutes. Cells were washed twice with ice cold 0.1% BSA/PBS pH 7.4 and resuspended at 10^6 cells per mL in 2.5% FBS/RPMI 1640 buffer (pre-chilled). Cells were transferred to a 37 °C water bath for the indicated time periods (or a tissue culture incubator for time points longer than 3 hours). At each indicated time point, 350 μL of cells were transferred to flow tubes on ice and analyzed by flow cytometry using the BD LSR II (UW Carbone Cancer Center at University of Wisconsin-Madison).

Chapter 4: Examination of the Thermal Properties of Polyoxazinones and the Synthesis of Oxazinone-Cyclooctadiene Copolymers

4.1 Thermal Characterization of Polyoxazinones

Plastics are utilized for many applications due to their toughness, durability, light weight, and ease of processability.[304-306] Lately, focus on the environmental impact of plastic derived refuse, as well as an ongoing interest in the use of polymers for drug delivery and regenerative medicine, has made the degradability of these materials an equally important characteristic.[289,304,307,308] However, the incorporation of a degradable linkage along a polymer backbone often alters the thermal or mechanical properties of the bulk material. For instance, changing from a polyamide to a polyester backbone enables facile polymers hydrolysis, yet significantly decreases the glass transition temperature (T_g).[305] Therefore, the identification of degradable scaffolds with thermal and mechanical properties equivalent to existing non-degradable resins is an area of active research.[309-315]

Two classes of non-degradable polymers that have good thermal stability are polystyrenes[316,317] and cyclic olefin copolymers (COCs)[318-322] (Figure 4.1). COC's are generated by the copolymerization of ethylene and a cyclic alkene. The incorporation of cyclic repeats into the linear polyethylene chain increases the rigidity of the backbone, leading to an increase in T_g. For instance, copolymerization with cyclopentene can raise the T_g of polyethylene from -90 ^oC to 5 ^oC (Figure 4.1, **COC-1**).[318] For many applications where COCs are used, a T_g of 150 ^oC or higher is required (vida infra).[322] This is achieved by increasing the sterics of the cyclic repeat; when exo-1,4,4a,9,9a,10-hexahydro-9,10-(1',2')-benzeno-1,4-methanoanthracene was used as a monomer, a T_g of 207 ^oC was reported (Figure 4.1, **COC-2**).[322] Polystyrene (PS) is also thermally stable. In this case, the ability of the aromatic side chains to interact with each other leads to glassy domains that engender the material with good thermal stability. We recently reported the synthesis of a new class of degradable polymer called polyoxazinones.[57] We noticed that polyoxazinone **4.01** has structural attributes that resembled both PS and COC's: aromatic functionality and a backbone with cyclic repeat units. Therefore, we postulated that these characteristics would engender this degradable material with favorable thermal properties as well.

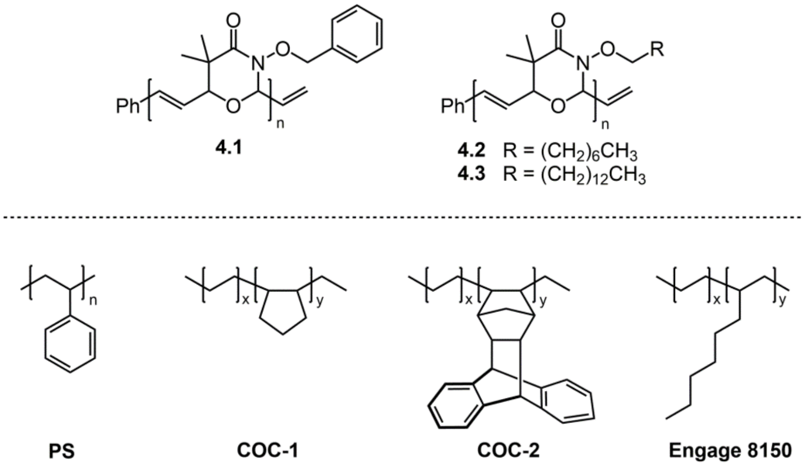

Figure 4.1. Structures of polyoxazinones with aromatic or alkyl functionality. Polyoxazinones have structural elements that resemble polystyrene, **PS**, and cyclic olefin copolymers, **COCs**.

A series of **4.01** was generated with molecular weights between 5 and 60 kDa and the thermal transitions were surveyed by Differential Scanning Calorimetry (DSC) (Figure 4.2a). Each sample tested had a T_g above 100 ^oC. Even the lowest molecular weight oligomer with a degree of polymerization (DP) of only 20 had a T_g equal to 105 ^oC. As the molecular weight of the benzyl polyoxazinones increases from 5 kDa to 30 kDa, the T_g of the materials also increased linearly to 145 ^oC. After this cutoff, the T_g of the polymers plateaued and an increase in molecular weight no longer greatly affected the T_g. We were not anticipating that every sample would have a T_g above 100 ^oC as polystyrene must have a molecular weight greater than 30 kDa (DP ~ 290) to pass this threshold (Figure 4.2b).[316,317] Nevertheless, this results demonstrates that benzyl substituted polyoxazinones are indeed high T_g degradable polymers.

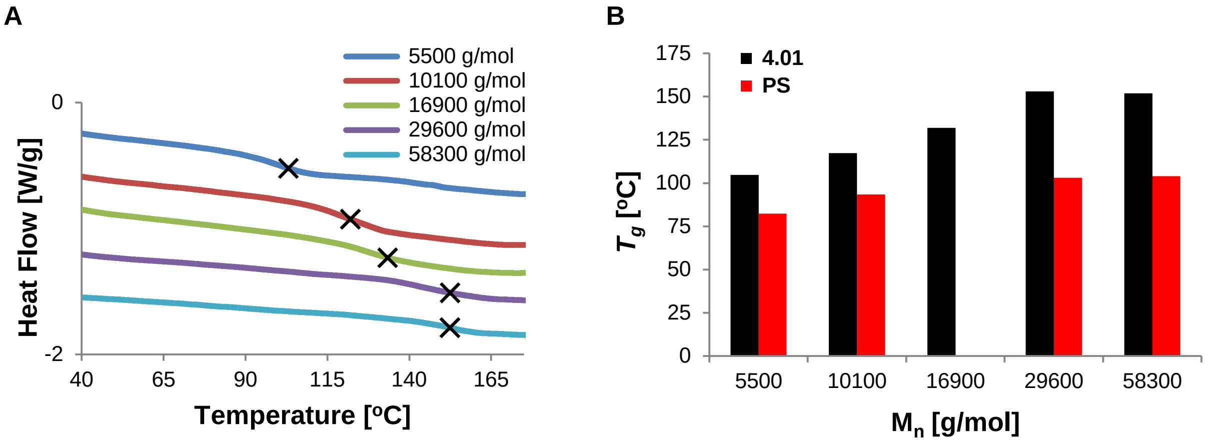

Figure 4.2. A) The glass transition temperature for polymer **4.01** as a function of molecular weight. The mid-point of the glass transition is marked by an "x". All measurements are of the third heating, ramp at 10 °C/min. B) At each molecular weight tested, the glass transition temperature of the polyoxazinone sample was greater than that of the corresponding polystyrene sample. Polystyrene glass transitions taken from Hitachi High-Tech Science Corporation, application brief TA no. 68.

To further prove that the high thermal transitions of the benzyl polyoxaziones were a result of both the aromatic functionality and backbone connectivity, the benzyl substituent was replaced with aliphatic functionality. The polyoxazinone backbone was decorated with two linear hydrocarbon chains of differing length [octyl (**4.02**) and tetradecyl (**4.03**)] and the glass transition temperatures for these polymers were assessed over a range of molecular weights (Figure 4.3). Two trends appear from the results. First, the T_g for **4.01** is consistently higher than the aliphatic polyoxazinones at a similar degree of polymerization (DP). For example, at a DP of ~75, polymers **4.01**, **4.02**, and **4.03** have T_g's of 132 °C, 70 °C, and 51 °C, respectively. Therefore, the ability of the aromatic side groups on **4.01** to interact is stabilizing the polymer chain. Second, increasing the chain length of the aliphatic side chain decreases the T_g. This trend is also observed in poly(α-olefin) systems were an increase in the length of the side chain decreases the T_g of the resultant polymer because the side group acts as a plasticizer.[305,323] However, it is notable that the aliphatic polyoxazinones have greater T_g's than their corresponding linear α-olefin counterpart. For instance, octyl substituted **4.02** has a T_g of 75 ^{o}C at a molecular weight of 77 g/mol. On the other hand, the commercial ethylene-*co*-1-octene polymer Engage 8150 (25 weight% 1-octene) has a T_g of only -43 ^{o}C at a molecular weight 162 kg/mol (Figure 4.1).[324] Therefore, the introduction of the cyclic oxazinone repeats is also contributing to observed thermal properties of polyoxazinones. Taken together, these result supported our hypothesis that both functionality and backbone structure are playing roles in the thermal properties of the polymers.

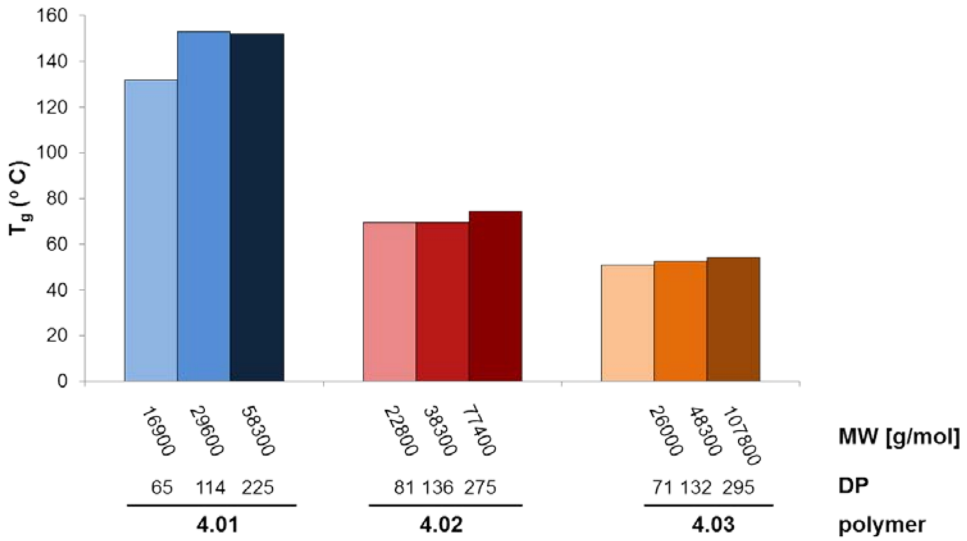

Figure 4.3. Effect of the side chain structure on the glass transition temperature of polyoxazinones.

In addition to the thermal phase transitions determined by DSC, it is also important to know the overall thermal stability of a polymer to determine how to process a polymer sample and what applications the resin is most useful for. The thermal stability of the polyoxazinone scaffolds were assessed using Thermogravometric Analysis (TGA). Representative TGA curves, as well as the corresponding derivative thermogravimetry (DTG) curves, are overlaid in Figure 4.4. Examining all curves shows that the decomposition of polymers **4.01**, **4.02**, and **4.03** look qualitatively the same, regardless of functionality. Each polymer has a maximum degradation temperature at about 280 °C and appears to combust at 450 °C. In addition, the polymers degrade in two stages, with a change in rate (T_{change}) between 315-345 °C. The mass loss after the first stage of degradation corresponds to the mass loss of the entire hydroxamic ester moiety (Table 4.1). This fragmentation pattern makes sense as the hydroxyamic ester contains the weakest bonds in the polymer. From this point, the remainder of the polymer decomposes at a constant rate until combustion at 450 °C. One potential limitation revealed by the TGA curves is that all samples have a low an onset degradation temperature ($T_{5\%}$, as defined by 5% mass loss), which was found to be between 200-225 °C. This is lower than other degradable resins, such as polyesters, which show negligible mass loss until 280-375 °C.[309,310,312] Therefore, polyoxazinones may not be amenable to molding processes that heat resins to temperatures above this its decomposition threshold.

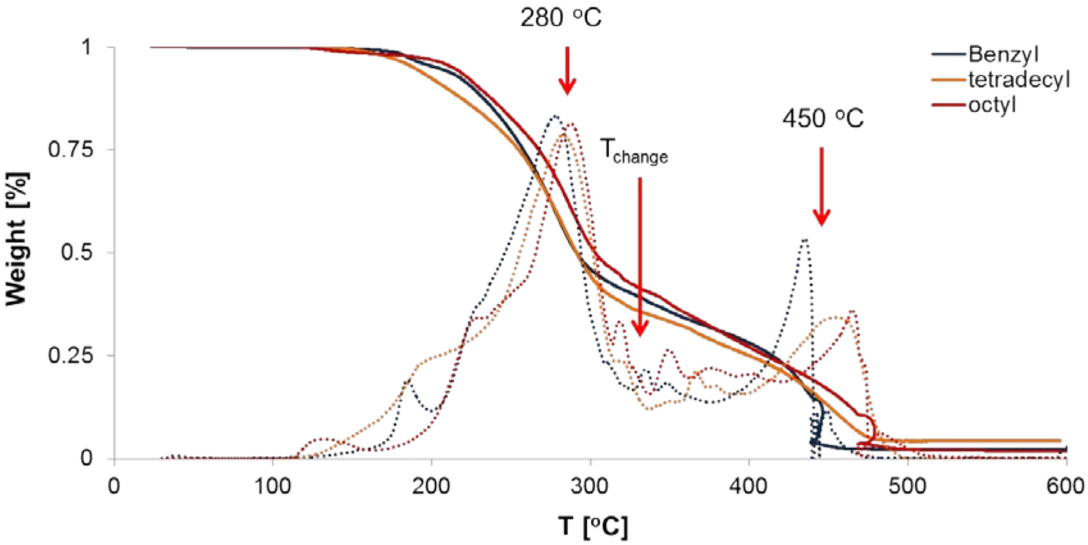

Figure 4.4. Thermal stability of polyoxazinones as determined by TGA. DTG traces are shown as dashed lines**.** Traces are representative of 3 sample replicates.

Table 4.1. Transitions in polymer mass loss from TGA

Polymer	**T, 5% decomp**	**T, change**	**W% @ T_{change}, theoretical[a]**	**W% @ T_{change}, observed**
4.01	215	316	42.6	42.7 ± 0.8
4.02	195	332	39.9	40.0 ± 1.9
4.03	193	344	30.3	33.1 ± 1.7

[a] **"**W% @ $T_{change,}$ theoretical" is the calculated mass loss from elimination of the hydroxyamic ester side chain.

In conclusion, polyoxazinones are a new class of degradable polymers with high glass transition temperatures. Benzyl functionalized **4.01** showed thermal transitions above 100 ^{o}C across all molecular weights tested. This high T_g is a result of the cyclic oxazinone repeat units in conjunction with the aromatic functionality of the benzyl side chain. If the aromatic functionality is replaced with linear, aliphatic functionality, the T_g of the polymer remains elevated, but decreases as the length of the side chain increases.

4.2. Synthesis of Oxazinone-Cyclooctadiene Copolymers

4.2.1. Introduction to Copolymers

Copolymers are a class of materials that are generated from the polymerization of two or more monomers.[305,323,325,326] The properties of copolymers often synergistically combine the individual traits of the corresponding homopolymers derived from each monomer, which cannot be achieved by mixing the two polymers.[327] For instance, qualitatively, polystyrene is glassy and brittle while polybutadiene is soft and gummy. However, when polymerized into an ABA triblock copolymer, the resulting material becomes a durable thermoplastic elastomer that is used to make car tires (SBS rubbers).[328] This will only happen if the polymers are covalently attached. If the homopolymers are mixed, phase separation will cause the two species to spontaneously segregate and the properties of the SBS copolymer will not be attained. However, due to the covalent attachment of block copolymers, phase separation is limited to the length scale of the blocks, which enforces equal distributions of both polymer components throughout the material. This leads to glassy polystyrene domains that physically crosslink the elastomeric polybutadiene midblock which contributes to the bulk properties of SBS rubbers.

In addition to block copolymers, random copolymers can also be used to generate materials with novel properties.[305,328] Unlike in block copolymers, the repeat units in random copolymers are interspersed along the entire polymer chain. Therefore, microphase separation does not occur and the properties of random copolymers are directly related to the composition of the polymer backbone. By altering features of the backbone, such as percent incorporation of each monomer type or the pattern of the repeat units, the physical properties of random copolymers can be finely tuned. For instance, the glass transition temperature of random copolymers is governed by the Fox equation:

$$1/T_g = w_1/T_{g,1} + w_2/T_{g,2} + \ldots + w_n/T_{g,n} \qquad \text{eq. 4.1}$$

where w_n is the weight fraction of each type of repeat along the backbone and $T_{g,n}$ is the corresponding glass transition temperature for that monomer if homopolymerized. An example of where this is used is in the design of polyacrylate copolymers used to make adhesives.[329,330] By changing the composition of the polyacrylate backbone, features of the polymer, such as glass transition, tack, and peel strength, can all be modified using a finite monomer pool.

The potential for making novel copolymers with unique properties may seem endless; however, choice of polymerization strategy dictates the type of monomers that can be used, what combination of monomers can be effectively copolymerized, and what functionality is tolerated. Therefore, expanding the monomer toolbox for a given methodology is a powerful way to access new copolymer compositions. ROMP is a robust way to make both block and random polymers.[50,331-333] Recently, even perfectly alternating copolymers have been generated.[43,334] Therefore, it was envisioned that bicyclic oxazinone monomers could be used to generate new ROMP copolymers. The benefits of incorporating polyoxazinone blocks into ROMP polymers was thought to be two fold. First, the presence of the oxazinone linkage along the copolymer backbone would provide a mechanism for polymer degradation while allowing the properties of the materials to be modified through manipulation of the hydroxamic ester side chain (see Section 2.3). This flexibility improves upon existing degradable ROMP copolymers, like dioxepine-cyclooctene copolymers, that contain hydrolysable moieties along the polymer backbone but are challenging to functionalize through either monomer synthesis or post-polymerization modification.[200] Second, polyoxazinones formed from monomer **4.04** have high glass transition temperatures relative to many degradable polymers. Other monomers that lead to degradable polymers with high T_g's are often ill-suited for block copolymerization.[312,313,315] Recently, there have there been reports of modified lactide monomers that can be incorporated into high T_g polymer blocks, but these molecules are tedious to make and slow to polymerize.[309,310] Therefore, the use of monomer **4.04** in copolymer synthesis could uniquely confer degradability, functionality, and thermal stability to its copolymers.

4.2.2. Synthesis of Poly(oxazinone-b-cyclooctadiene) Copolymers

The introduction of degradable linkages into polymers has been historically achieved though condensation polymerization, leading to linear polyesters. This methodology affords random or alternating copolymers, but cannot produce block copolymers.[10,11,13] Recent advances in living polymerization methods has allowed degradable block copolymers to be generated as well. In this way, polymers containing degradable polyester blocks have been synthesized from the ring-opening polymerization (ROP) of cyclic ester and lactide monomers.[314] In addition, fully degradable block copolymers have also been reported that contain hard polylactide blocks and soft poly(caprolactone) blocks, which leads to biodegradable elastomers for biomedical applications.[335-337] However, currently utilized degradable polymers do not possess the requisite thermal stability required for many applications outside of the biomedical field. Even the hard polylactide blocks described above have a relatively low glass transition temperature of ~60 °C. Therefore, it cannot be used to replace current non-degradable polymeric blocks in applications that require greater thermal stability. To solve this problem, some research groups have identified routes to modify polylactide monomers leading to higher T_g's, but these molecules are tedious to make and slow to polymerize.[309,310] As an alternative to these modified lactide monomers, bicyclic oxazinones could be used to generate thermally stable, yet degradable blocks copolymers through ROMP.

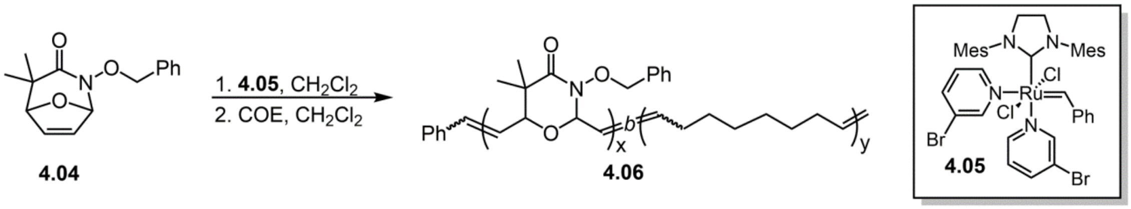

Scheme 4.1. Synthesis of block copolymers from **4.04** and *cis*-cyclooctene by ROMP.

Polyoxazinone containing block copolymers were initially generated from the sequential addition of monomer **4.04** and *cis*-cyclooctene (COE) using Grubbs-Love catalyst (**4.05**) and dichloromethane as a solvent (Scheme 4.1). It was found that the polyoxazinone block needed to be generated first, followed by the polycyclooctene (pCOE) block. This order is necessary because the optimal concentration for the polymerization of **4.04** is 1 M. By polymerizering **4.04** first, this concentration can be maintained. Monomer **4.04** was allowed to polymerize for 25 min and then COE was added in a solution of dichloromethane. If COE was added directly, the pre-formed polyoxazinone macroinitiator precipitated out of solution due to its insolubility in hydrocarbon solvents. Under these conditions, the conversion of monomer **4.04** was comparable to previously reported homopolymers (~85%). Quantitative conversion of COE was assessed by comparing the observed ^{1}H-NMR ratio of polyoxazinone to pCOE olefin signals to the expected ratio dictated by monomer feedstock compositions, which were found to be in good agreement.

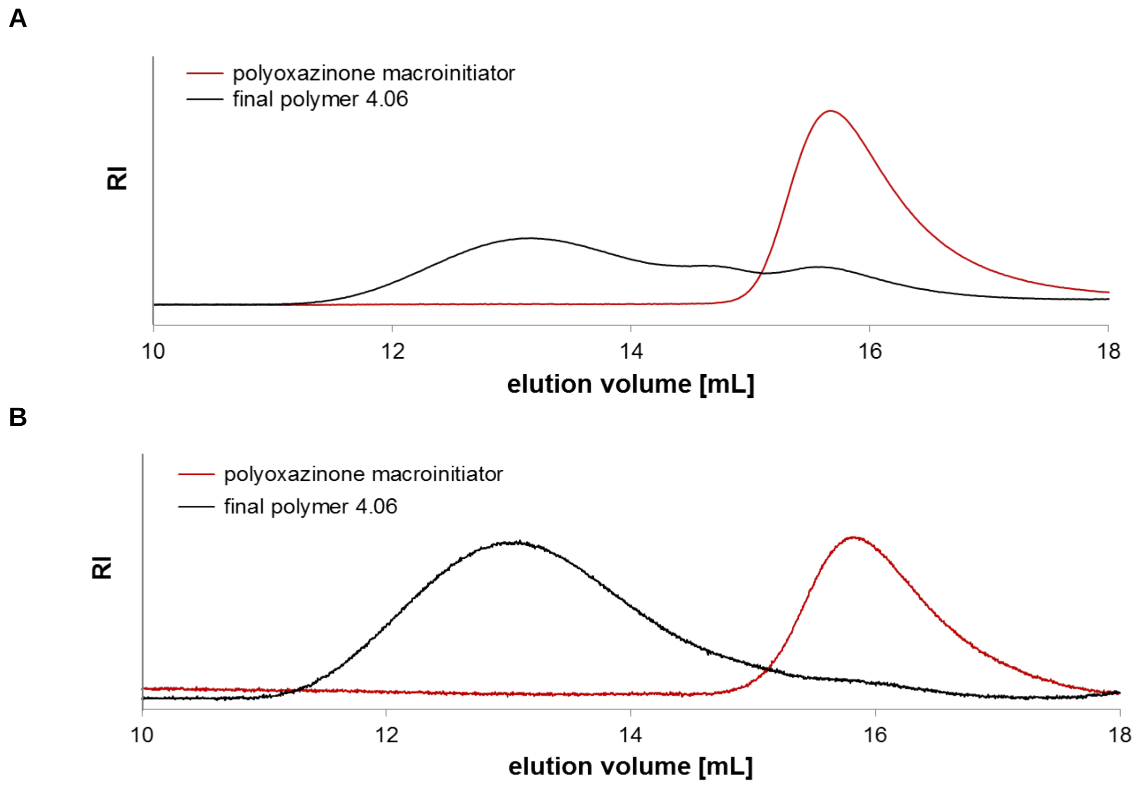

Figure 4.5. GPC analysis of the block copolymers generated from **4.04** and *cis*-cyclooctene. A) *Cis*-cyclooctene added 25 min after polymerization initiation. B) *Cis*-cyclooctene added 8 min after polymerization initiation. Both methods led to polydisperse material.

The promising NMR results belied complications revealed during GPC analysis (Figure 4.5A). An aliquot of the polymerization milieu immediately preceding COE addition revealed a monomodal distribution of molecular weights with a narrow PDI (1.3). However, after the COE monomer had been consumed, the GPC trace was multimodal and appeared to contain two populations of polymer. The observed multimodality could be explained by a number of factors. First, some of the catalyst is chelated to the polyoxazinone macroinitiator at the time of COE addition and does not initiate before the COE pool is consumed. Second, COE is a poor choice of co-monomer due it its polymerization kinetics. Finally, residual catalyst that did not initiate polymerization with monomer **4.04** forms a second population of pCOE homopolymers. The last scenario was deemed unlikely because the GPC trace of the macroinitiator polyoxazinone was monomodal with a narrow PDI, indicating complete initiation. Therefore, attention was turned to examine whether either of the first two possibilities were hampering copolymerization.

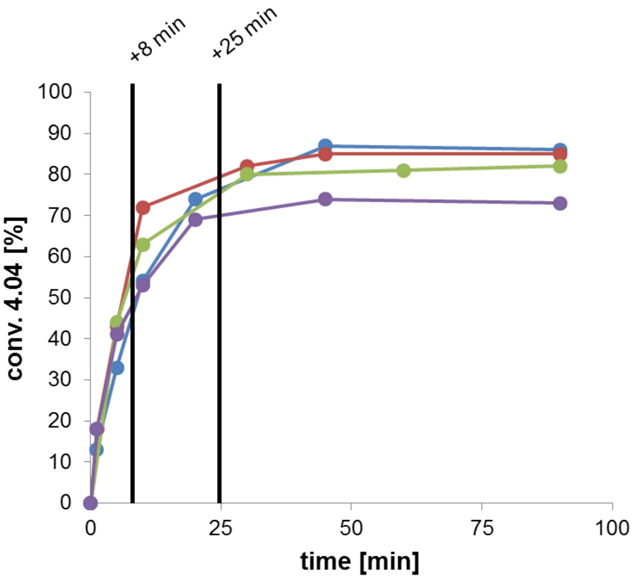

Figure 4.6. Reaction conversion of monomer **4.04** during ROMP. A linear increase in conversion is seen during the first 15 min of polymerization, which is curtailed by chelation of the catalyst to the polydentate polymer ligand by minute 20. [**4.04**]$_o$/[**4.05**] = 200:1 (purple), 100:1 (green), 50:1 (red), 25:1 (blue).

Monitoring the polymerization of **4.04** over time revealed that polymer growth increased linearly with time during the first fifteen minutes of the polymerization in an apparent living fashion. However, by minute twenty, monomer incorporation had arrested without reaching full conversion (Figure 4.6). This result indicates that by the time COE was added to the copolymerization milieu significant catalyst chelation was occurring, impeding further reaction progress. If catalyst chelation to the polyoxazinone macroinitiator was competitive with COE initiation then heterogeneous chain elongation would have occured. Therefore, it was reasoned that if the COE monomer was added during the first fifteen minutes of polymerization all growing chains should still have metathesis active chain ends and uniformly elongate with the COE charge. Consequently, the addition of COE was expedited from 25 min to 8 min post polyoxazinone initiation. GPC analysis revealed that the new chronology of monomer addition improved the initiation efficiency of the pCOE block, but small amounts of low molecular weight material still persisted (although reduced from 23% to 5% of the total area, Figure 4.5B). Therefore, catalyst chelation was hindering complete initiation of the pCOE block, but was not the sole factor.

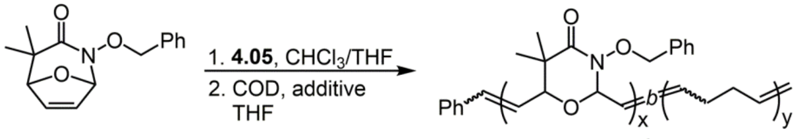

4.04

4.07

Scheme 4.2. Synthesis of block copolymers from **4.04** and 1,5-cyclooctadiene by ROMP.

Cis-cyclooctene is a viable ROMP substrate, but it cannot be homopolymerized in a living manner.[333] This is due to COE’s low ring strain (~7 kcal/mol) which reduces the rate of initiation relative to chain propogation and leads to statistical PDIs. Therefore, the reduced rate of initiation inherent to COE could have also been a factor leading to incomplete macroinitiation of the pCOE block. To address this issue, the co-monomer was changed to 1,5-cyclooctadiene (COD), a monomer that has higher ring strain than COE and has been reported to undergo living ROMP (Scheme 4.2).[338] Changing the co-monomer to COD achieved a copolymer, **4.07**, with a monomodal molecular weight distribution, which confirmed that COE’s slow rate of initiation was hindering uniform block copolymer synthesis (Figure 4.7). However, the GPC trace appeared to now have a high molecular weight shoulder, which suggested that while complete initiation was occurring, it was still not simultaneous. This result was not unsurprising as COD only polymerizes in a living manner when exposed to an excess of triphenyl phosphine (PPh_3), which slows the rate of polymerization.[338] Following these examples, the block co-polymerization of **4.04** and COD was performed with PPh_3 or 3-bromopyridine as additives (Table 4.2). This modification suppressed the generation of the high molecular weight shoulder and led to a monomodal and symmetric molecular weight distribution (Figure 4.7). Under optimal conditions, the final PDI was 1.65, which was acceptable as the PDI obtained for the polyoxazinone macroinitiator was 1.3. Therefore, the pCOD block only led to a modest increase in molecular weight polydispersity. Finally, it was demonstrated that the resulting material was indeed a block copolymer by dissolving the **4.07** in an acidic solution known to degrade polyoxazinones and monitoring the molecular weight over time (Figure 4.8). The resulting residue had a lower average molecular weight by GPC but was still monomodal. This would only occur if the non-degradable pCOD repeats were completely segregated to a single block along the polymer chain.

Table 4.2. Effect of additives on the block copolymerization of **4.04** and COD by ROMP.

Entry	Additive	$[4.04]_o$:$[COD]_o$:[4.05]	conv. 4.04 [%]	poly(4.04):pCOD^{NMR} (theoretical ratio)	M_n^{GPC} [g/mol]	PDI
1	--	25 : 460 : 1	40	1 : 66 (1 : 46)	129800	1.96
2	5 eq PPh_3	25 : 460 : 1	20	1 : 110 (1 : 92)	117000	1.73
3	60 eq PPh_3	25 : 460 : 1	50	1 : 38 (1 : 37)	117400	1.66
4	120 eq PPh_3	25 : 460 : 1	41	1 : 49 (1 : 46)	99600	1.66
5	60 eq 3-BP	25 : 460 : 1	39	1 : 48 (1 : 46)	117300	1.63

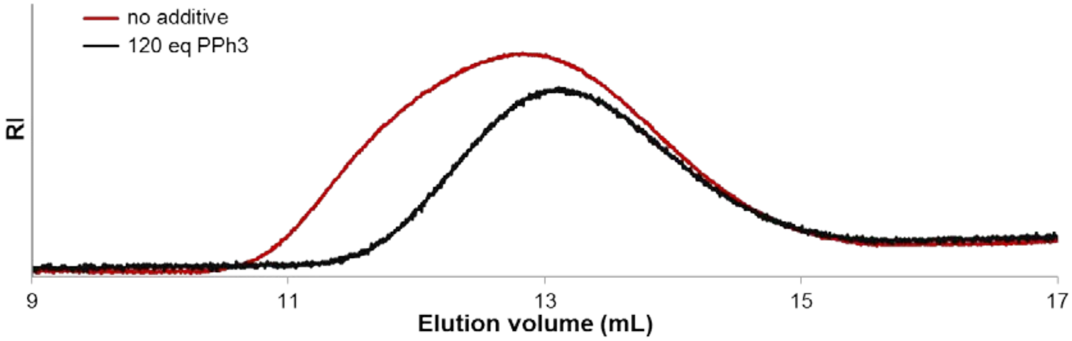

Figure 4.7. GPC analysis of block copolymers generated from **4.04** and 1,5-cyclooctadiene. Block copolymerization leads to a high molecular weight shoulder that could be removed by the addition of additives that slow the rate of COD polymerization

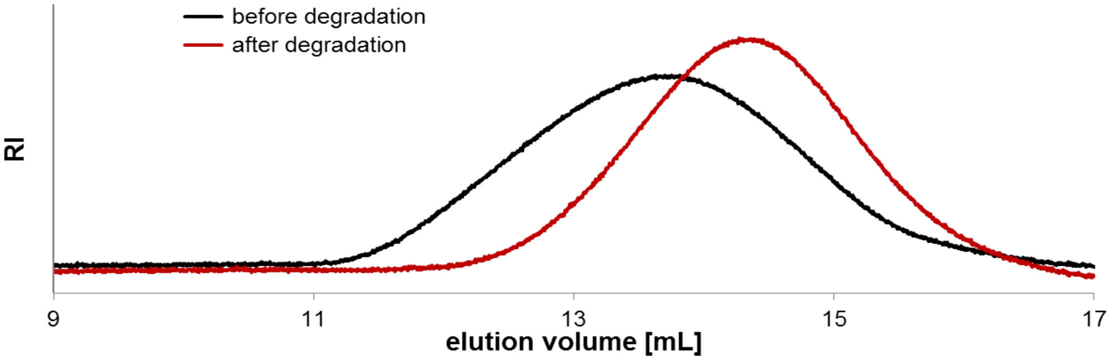

Figure 4.8. Exposure of **4.07** to a pH = 0.25 MeOH/THF solution leads to degradation of the polyoxazinone repeats. Block copolymerization is confirmed by the fact that the remaining pCOD material is a lower molecular weight species with a monomodal PDI.

Besides AB block copolymers, multi-block copolymers are also used as commercial resins. One of the most widely used multiblock copolymers are SBS rubbers, which are ABA block copolymers composed of a soft polybutadiene block flanked by glassy polystyrene blocks.[328] It was envisioned that monomer **4.04** and COD could be similarly enlisted to afford ABA block copolymers that also contained a hard-soft-hard motif that possessed a degradable hard block. This goal presented an immediate challenge: how to add the second polyoxazinone block. As discussed above, for effective polymerization of **4.04** the concentration of this monomer must be 1 M. However, after polymerization of the first two blocks, the concentration of **4.04** in the solution would be well below this value if added as a third monomer charge. Therefore, an alternate approach to sequential monomer addition was needed to generate the desired ABA oxazinone-cyclooctadiene copolymers.

An advantage of using ROMP is the ability to control the end group functionality.[49] This is achieved either through modification of the catalyst, which adds end group functionality upon initiation, or through the use of polymerization quenchers with distinct moieties, which modify the polymer chain upon termination. We posited that using the later approach would lead to ABX copolymers where the X group is a functional handle amenable to click conjugation. The installed reactive chain end would then be used in a second step to couple two ABX polymers together, with the net effect of generating an ABA analogue (if the linker is a small percentage by weight of the polymer composition).

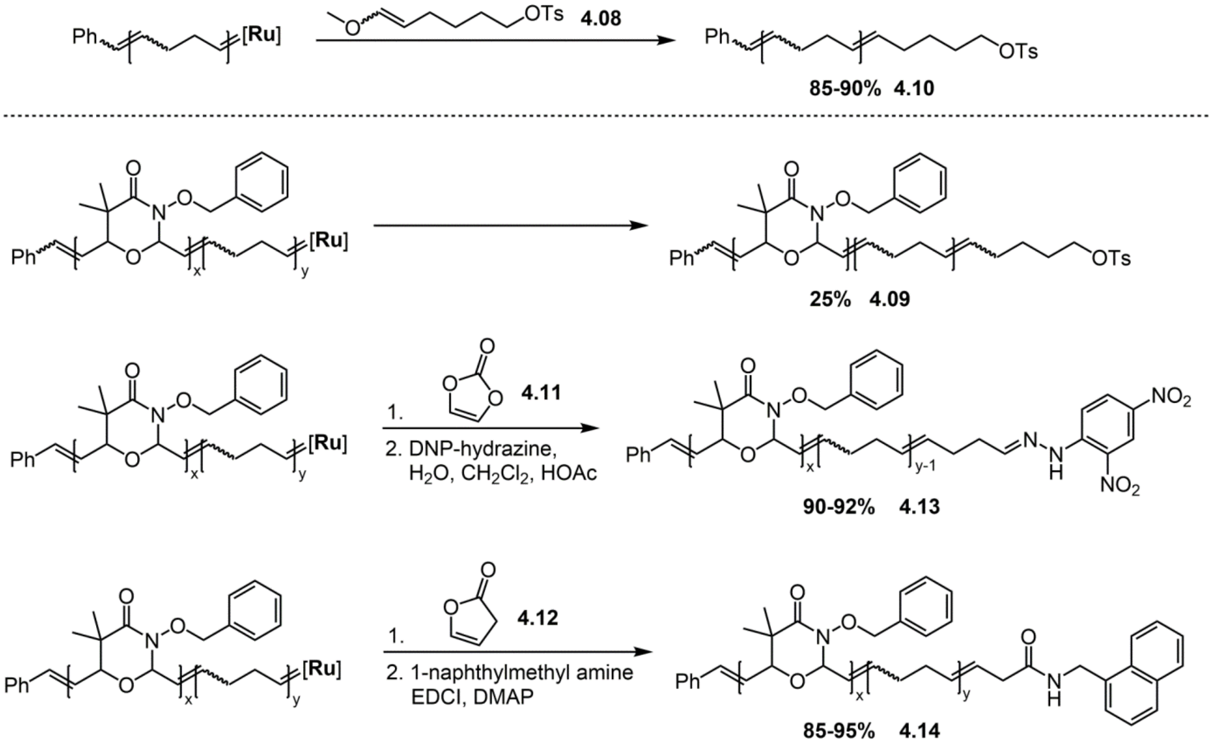
Ph
[Ru]
OTs
4.08
Ph
OTs
85-90% 4.10
O
N
O
Ph
O
x
y
[Ru]
OTs
25% 4.09
1.
4.11
2. DNP-hydrazine, H2O, CH2Cl2, HOAc
y-1
N
N
H
NO2
NO2
90-92% 4.13
1.
4.12
2. 1-naphthylmethyl amine EDCI, DMAP
85-95% 4.14

Scheme 4.3. Screen of end-capping efficiency for various vinyl ethers. Polymers terminated with cyclic vinyl ethers **4.11** and **4.12** were further elaborated with functionality amenable to end group analysis by ^{1}H-NMR.

There are multiple ways to add functional groups to the end of a ROMP polymer generated with ruthenium catalysts.[49] The most common method is the use of functional vinyl ethers (Scheme 4.3).[66] These capping agents concomitantly functionalize the polymer terminus and deactivate the dissociated ruthenium species via the formation of an inert Fischer carbene. Typically, linear vinyl ethers are used to terminate ROMP polymers. However, vinyl ether **4.08** led to incomplete capping when used to quench oxazinone-*b*-cyclooctadiene copolymers, **4.09**. This was unexpected as **4.08** led to high levels of end capping when cyclooctene was homopolymerized, **4.10**. Cyclic vinyl ethers, vinylene carbonate, **4.11**, and 3*H*-furanone, **4.12**, were found to be more effective at terminating the oxazinone-b-cyclooctadiene copolymer. These cyclic quenchers lead to a terminal aldehyde or carboxylic acid, for **4.11** and **4.12** respectively.[68] End capping efficiency was not directly quantified on the resultant material, but rather the polymers were elaborated further with either 2,4-dinitrophenyl hydrazine, **4.13,** or 1-naphthyl methylamine, **4.14**, to facilitate end-group analysis using ^{1}H-NMR. In this way, the end capping efficiency of **4.11** and **4.12** were both found to be ~90%. Therefore, oxazinone-*b*-cyclooctadiene copolymers were efficiently functionalized by use of cyclic vinyl ethers **4.11** and **4.12**.

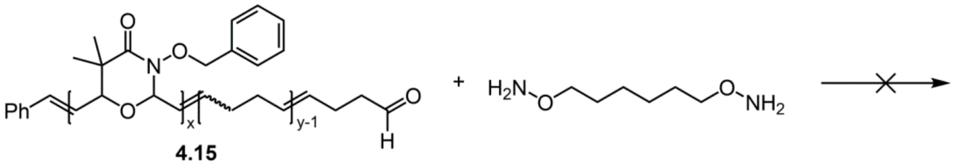

4.15

Scheme 4.4. Polymer **4.15** was unable to be conjugated to dihydroxylamine crosslinkers due to solubility incompatibilities

With ABX oxazinone-cyclooctadiene copolymers in hand, the coupling of two polymer chains was attempted. First, aldehyde terminated polymer **4.15** was mixed with an α,ω-dihydroxylamine crosslinking agent (Scheme 4.4). This strategy did not lead to successful chain growth. Conjugation was stymied because a solvent compatible with both the block copolymer and the small molecule crosslinker was not found. To address this issue, an alternative end cap with the ability to form dimers was desired. Dimerization would eliminate the need for the small molecule crosslinker and ensure all reactive handles were in solution. Coumarin was selected as a target motif because it is known to undergo photodimerization through a [2+2] cycloaddition.[339-341] Furthermore, this moiety has been used to crosslink polyacrylates together to form covalent polymer networks.[342-344] Using carboxylic acid functionalized polymer **4.16**, the small molecule coumarin ligand **4.17** was conjugated to the block copolymer in high conversion using EDCI to afford end labeled polymer **4.18** (Scheme 4.5). Following successful coumarin incorporation, a solution of polymer **4.18** in tetrahydrofuran was degassed and exposed to 350 nm UV light to generate a triblock copolymer. Aliquots of the reaction were taken at various time points to monitor the extent of dimerization by UV-Vis, which was assessed by monitoring the disappearance of the absorbance band of coumarin at 320 nm (Figure 4.9A). After exposure to UV light for 14 hours, complete disappearance of all coumarin signal was achieved. Additionally, coumarin consumption follows second order kinetics, which is expected for a dimerization process (Figure 4.9B). ^{1}H-NMR confirmed the successful photodimerization of polymer **4.18** as well through loss of the coumarin's olefin signals but retention of it aryl protons (Figure 4.10). Finally, GPC analysis of the final polymer product, **4.19**, showed a shift in retention volume but maintained a monomodal molecular weight distribution, indicating a uniform reaction (Figure 4.11). Taken together, this data indicates successful photodimerization of ABX oxazinone-cyclooctadiene copolymer **4.18**, where X is a coumarin moiety. Therefore, both AB and ABA block copolymers of polyoxazinones and polycycloooctadienes are accessible.

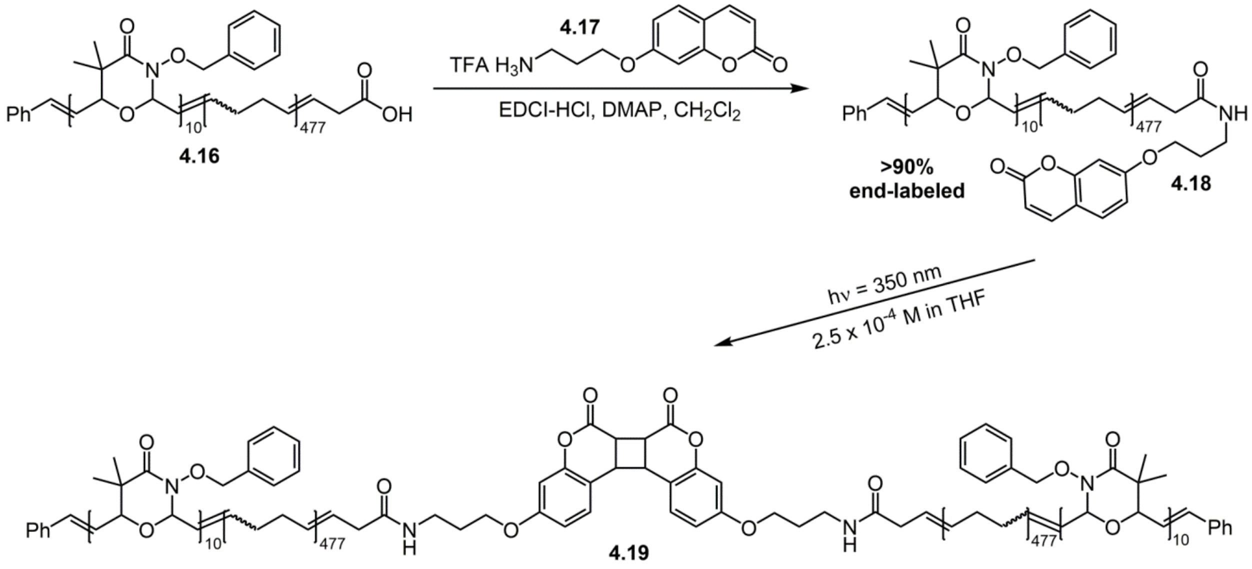
4.17
TFA H3N
EDCI-HCl, DMAP, CH2Cl2
Ph
O
N
O
OH
10
477
4.16
NH
>90%
end-labeled
4.18
hν = 350 nm
2.5 x 10-4 M in THF
N
H
4.19

Scheme 4.5. Polymer **4.16** was elaborated with a coumarin moiety at the pCOD terminus. Coumarin functionalization allowed photodimerization of polymer **4.18** with 350 nm light.

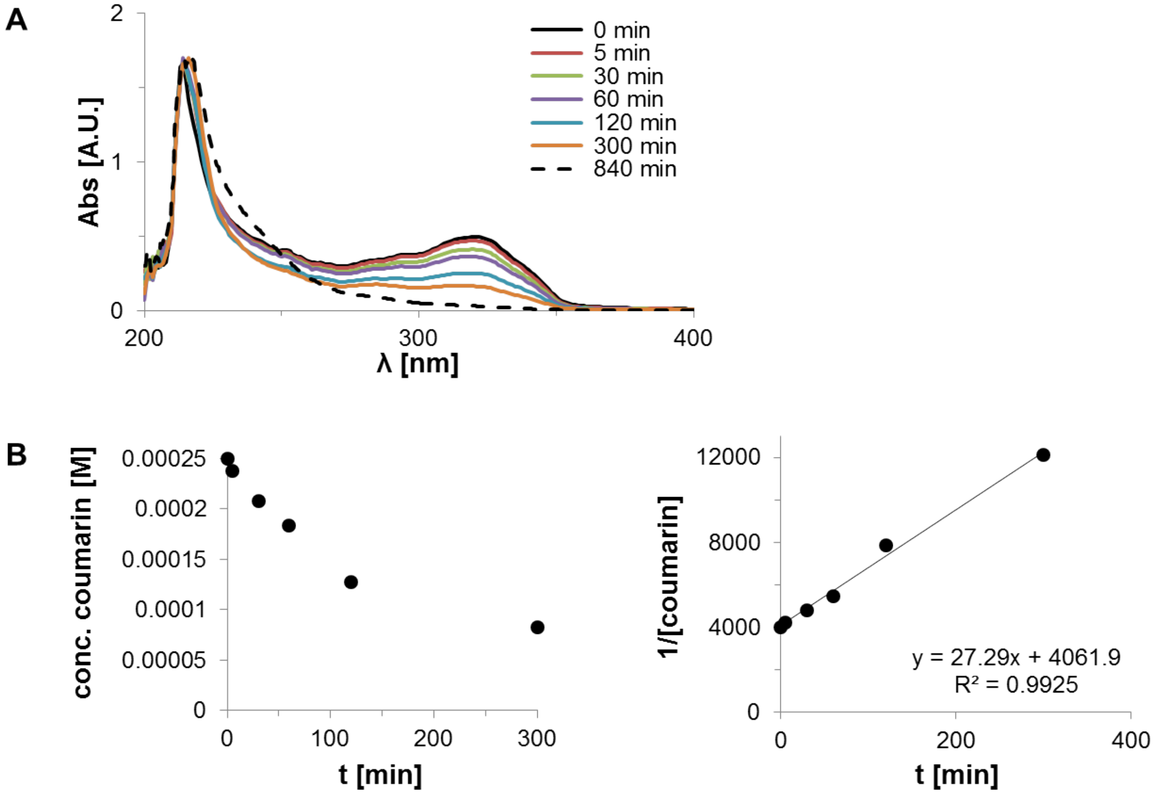

Figure 4.9. Photodimerization of polymer **4.18** with 350 nm light. A) Aliquots of the reaction were taken at various time points for UV-Vis analysis. Loss of the coumarin absorbance band at 320 nm was observed over time. B) The concentration of coumarin during the photodimerization of polymer **4.18** indicates a second order reaction.

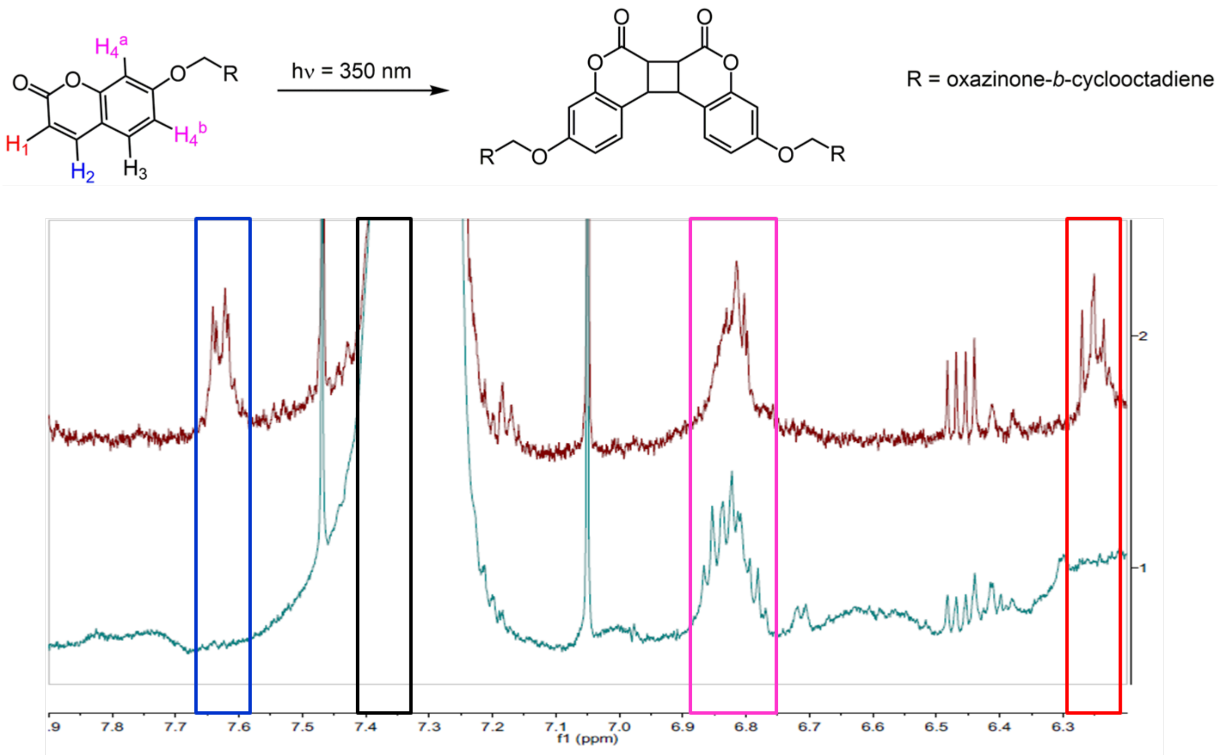

Figure 4.10. ^{1}H-NMR confirmed the successful photodimerization of polymer **4.18** through loss of H_1 (red) and H_2 (blue) olefin signals but retention of aromatic H_4 (pink). Aromatic H_3 (black) overlapped with the solvent peak, but is expected to remain unchanged.

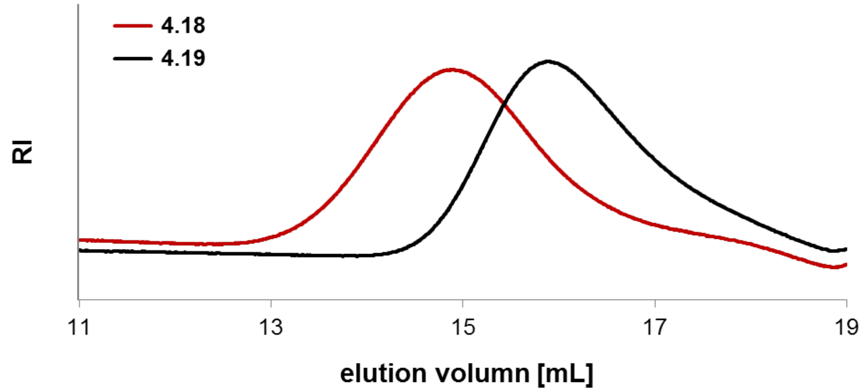

Figure 4.11. GPC analysis of the photodimerization of polymer **4.18** revealed a shift of elution time but retention of a monomodal molecular weight distribution, indicating complete dimerization.

4.2.3. *Synthesis of Poly(oxazinone-r-cyclooctadiene) Cyclic Olefin Copolymers*

A class of random copolymers are cyclic olefin copolymers (Figure 4.1).[318-322] A hallmark of COCs is their high glass transition temperatures and good transmittance of light.[320]

Therefore, COCs have found commercial applicability as heat-resistant materials for high clarity plastic lenses and optical storage media.[345] COCs are generated through the random copolymerization of ethylene and a cyclic olefin. Control over the cyclic olefin content is paramount in governing the properties of the polymers. This can be achieved by optimizing the polymerization conditions, such as partial pressure of ethylene, temperature, and catalyst structure.[48,49] However, optimal polymerization conditions often must be rescreened for each new co-monomer, which can differ greatly.

Alternatively, ROMP can be used to make COCs. Beneficially, ROMP eliminates the need to drastically rescreen polymerization conditions for each new monomer because a small cadre of catalysts are able to polymerize many substrates. Indeed, the homopolymerization of norbornene by ROMP leads to a perfectly alternating COC, which has been commercialized.[346,347] A limitation of using norbornene to make COCs by ROMP is that the cyclopentane content is fixed at 50 mol%. Ideally, the number of cyclic repeats could be reduced through copolymerization of norbornene with a monocyclic ROMP monomer, such as COD, to modulate the mechanical properties of the material. However, the difference in ring strains between norbornene (~27 kcal/mol) and COD (~13 kcal/mol) prevents random copolymerization due to mismatched rates of polymerization. On the other hand, bicylic oxazinones are calculated to have ring stains similar to COD (~13.5 kcal/mol).[206] Therefore, it was envisioned that COD and bicyclic oxazinone **4.04** could be randomly copolymerized to generate a new oxazinone containing COC with tunable cyclic backbone character.

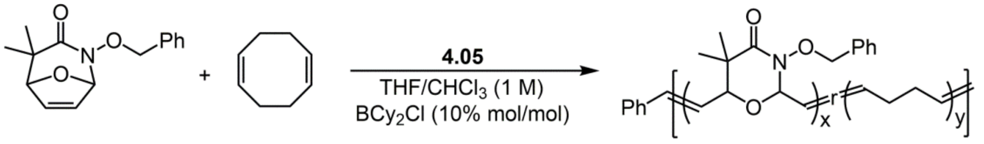

4.20

Scheme 4.6. Bicyclic oxazinone **4.04** and 1,5-cyclooctadiene could be copolymerized by ROMP to afford random copolymers.

Bicyclic oxazinone **4.04** was indeed able to be copolymerized with COD using the optimal polymerization conditions described previously to generate copolymer **4.20** (Scheme 4.6). The composition of the polymer backbone was assessed using ^{1}H-NMR by comparing the distinct olefin signals of the two types of repeats. Good agreement was observed between initial monomer feedstock ratio and final polymer composition across a range of feedstock ratios (Table 4.3). Steps were then taken to confirm the reaction produced random copolymers. GPC analysis of the isolated polymeric materials revealed a monodisperse population of polymers, with the PDI unaffected by polymer composition. Furthermore, DSC analysis revealed that each polymer sample possessed only one glass transition temperature (Figure 4.12A). Encouragingly, the glass transition temperature was found to be linearly proportional to polyoxazinone backbone content and was well described by the Fox equation (Figure 4.12B). Therefore, the copolymers were deemed to be random in composition.

Table 4.3. Random copolymerization results for bicyclic oxazinone monomer **4.04** and 1,5-cyclooctadiene.

$[4.04+COD]_o$/ [4.05]	$[4.04]_o/[COD]_o$	conv. 4.04 [%]	poly(4.04)/ $pCOD^{NMR}$	M_n^{GPC} [g/mol]	PDI
200/1	all 1	93	n/a	16000	1.8
200/1	9/1	85	11.7/1	9400	2
200/1	3/1	86	3.6/1	9900	1.9
200/1	1/1	88	1/1	9800	1.8
200/1	1/3	72	1/4.8	12200	2

Bicyclic oxazinone **4.04** was chosen as a co-monomer for polymerization with COD because polymer **4.01** has a high glass transition temperature. This property gave oxazinone-COD random co-polymers high glass transition temperatures as well. If all COD repeats are considered to be four ethylene equivalents and all oxazinone repeats contribute one additional ethylene unit, copolymers **4.20** with 80 and 92 mol% **4.04** incorporation can be thought of as ethylene/oxazinone COCs with 33 and 41 mol% oxazinone content. These ethylene/oxazinone COCs indeed have elevated glass transition temperatures (99 and 105 ^{o}C, respectively) as compared to unfunctionalized ethylene/cyclopentene COCs (-15 and 1 ^{o}C), at equivalent mol% cyclopentene.[348] Interestingly, the oxazinone-COD random copolymers have similar T_g's as bicyclic ethylene/norbornene COCs with the same mol% norbornene (76 and 102 ^{o}C).[321] Therefore, to the best of our knowledge, these oxazinone-COD random copolymers represent the highest T_g COCs that possess a monocyclic repeat.

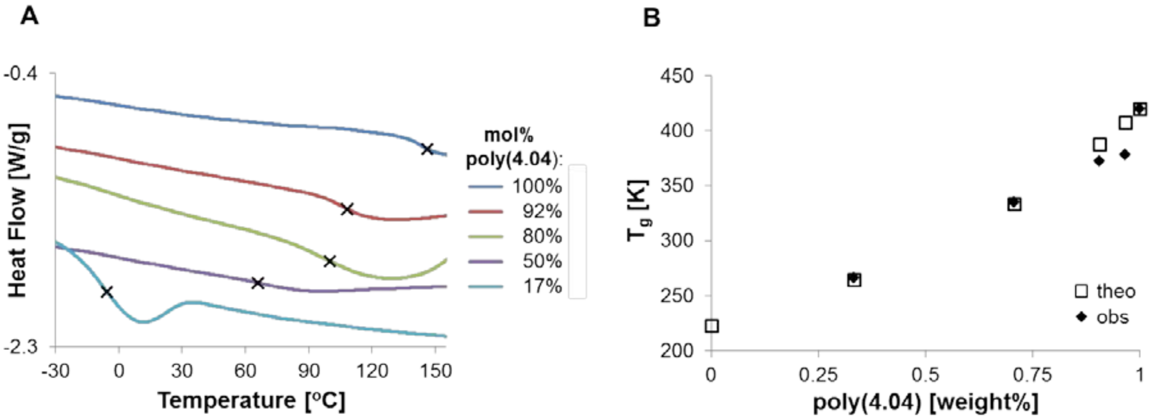

Figure 4.12. A) DSC analysis of poly(oxazinone-r-cyclooctadiene) at various mol% poly(**4.04**). B) The glass transition temperatures obtained by DSC are well described by the Fox equation.

Future modifications to oxazinone-cyclooctadiene COCs can be envisioned to investigate whether ever higher glass transition temperatures can be achieved at low levels of oxazinone incorporation. By taking advantage of the interchangeability of the hydroxamic ester side functionality, the benzyl substituent can be replaced with bulkier polyaromatic or polycyclic moieties known to increase the T_g's of existing hydrocarbon COCs. In addition, appending polar functional groups off of the hydroxamic ester may also increase the thermal stability of the material by engaging in strong non-covalent interactions, such as hydrogen bonds. Adding polar functionality to COCs by classical ethylene copolymerization is often challenging due to catalyst deactivation.[349] However, ROMP can tolerate polar functionality, which makes this modification tenable. By making modifications such as the ones suggested above, it may be possible to achieve thermal stabilities equal to currently utilized COCs while maintaining a low cyclic content, to maintain good mechanical strength.

4.2.4. Conclusions

In conclusion, bicyclic oxazinone monomers are able to be copolymerized with 1,5-cyclooctadiene to afford both block and random copolymers. Importantly, parity of the ring-strain inherent to both monomers allowed monomer **4.04** and COD to form random copolymers with backbone composition closely mirroring the initial monomer feedstock ratio. During block copolymerization, the timing of COD addition and the use of coordinating additives were found to be crucial for generating uniform blocks. Furthermore, multi-block ABA copolymers were achieved through the photodimerization of ABX diblock copolymers with coumarin end caps.

4.3. Future Directions

There are now synthetic pathways to access polyoxazinone containing homopolymers as well as diblock, triblock, and random copolymers. Future studies are now needed to perform mechanical characterization of these materials to see if these polymers are indeed able to supplement or replace extant thermally stable but non-degradable commodity materials. Of particular interest is whether the ABA oxazinone-cyclooctadiene copolymers are able to mimic the properties of SBS rubbers and random oxazinone-cyclooctadiene copolymer are able to improve on the brittleness of some COC variants. To do this, the tensile strength and elastic modulus will need to be evaluated.

It will also be interesting to see how benzyl polyoxazinone blocks in copolymers microphase separate. To answer this question, the block copolymers will need to be analyzed for ordered structure using scattering techniques such as small angle X-ray scattering. If benzyl polyoxazinones are found to microphase separate like polystyrene, tandem ROMP-ATRP catalysts can be utilized to make degradable poly(styrene-*b*-methylmethacryalte) (PS-PMMA) analogues.[284] PS-PMMA is widely studied due to its ability to microphase separate when annealed in thin films and has received recent attention in the electronic industry as a candidate for commercial polymer lithography applications.[350-353] A current goal of this field is to make PS-PMMA analogues with orthogonally degradable blocks to use as templates for substrate patterning.[354,355] It will be interesting to see if poly(**4.04**)-PMMA self assembles similarly to PS-PMMA and if the poly(**4.04**) block can be degraded away to reveal a PMMA pattern with high fidelity.

4.4. Materials and Methods

4.4.1. General Methods

All commercially available reagents were purchased from Sigma-Aldrich (St. Louis, MO) and used as received unless otherwise noted. Monomer **4.04** and polymers **4.01-4.03** were synthesized as described in Chapter 2. Catalyst **4.05** was synthesized following the procedures of Grubbs, *et. al.*[88] 3*H*-furanone (**4.12**) was generated from furfural following the procedures of Näsman, *et.al.*[356] High purity 1,5-cyclooctadiene (98% purity as received) was obtained using the "reactive distillation" method described by Macosko, *et.al.*, which removes the vinyl cyclohexane impurity.[357] 1-methoxy-6-hydroxy (*E*, *Z*)-hex-5-ene was synthesized following the procedures of Kiessling, *et. al.*[56]

^{1}H and ^{13}C nuclear magnetic resonance (NMR) spectra were obtained using an Avance-500 MHz spectrometer. Chemical shifts are reported relative to tetramethylsilane or residual solvent peaks in parts per million ($CHCl_3$: ^{1}H: δ 7.26, ^{13}C: δ 77.23; MeOH-d_4: ^{1}H: δ 3.31, ^{13}C: δ 49.00). Peak multiplicity is reported as singlet (s), doublet (d), doublet of doublets (dd), triplet (t), doublet of triplets (dt), quartet (q), quartet of doubles (qd), pentet (pent), multiplet (m). Conversion of monomer **4.04** during copolymerization was assessed by comparing the monomer olefin signals at 6.56 and 6.44 ppm to the polymer olefin signal at 5.80 ppm. High resolution electrospray ionization mass spectra (HRESI-MS) were obtained on a Micromass LCT mass spectrometer.

Room temperature GPC-SEC analysis (Viscotek GPC max) was performed on 300 x 7.5 mm PolyPor 5 μm mixed columns from Polymer Laboratories. Data was analyzed using OmniSEC software (Viscotek Inc.). Polymers were eluted with THF (1.0 mL/min, 40 ^{o}C) to determine M_n, M_w, and polydispersity index (M_n/M_w). Columns were calibrated with 10 narrow polystyrene standards (Polymer Laboratories S-M2-10 kit).

UV-Vis absorption spectra were obtained on a Varian Cary 50-Scan UV-Visible Spectrophotometer. Optical measurements were taken in a quartz cuvette with THF as the solvent (coumarin dimerization).

DSC thermatograms were obtained on a TA Instruments Q100 Modulated Differential Scanning Calorimeter. All measurements were taken in aluminum pans under a nitrogen atmosphere; between 2.5–5.0 mg of sample were used per pan. Ramp rate was set to 10 ^{o}C/min with 5 min isotherms. Polyoxazinone homopolymers were cycled between 20 – 200 ^{o}C and polyoxazinone-co-polycyclooctadiene copolymers were cycled between -60 – 185 ^{o}C. Duty cycles were repeated 3 times and T_g's were taken from the 3rd heating. TGA traces were obtained on a TA Instruments Q500 Thermogravimetric Analyzer. All measurements were taken in a platinum pan under an oxygen atmosphere; between 10-30 mg of sample was used per run. Ramp rate was set to 10 ^{o}C/min ending at 600 ^{o}C. Measurements were repeated 3 times. DSC and TGA data was analyzed using TA Universal Analysis software.

4.4.2. Synthetic Procedures:

Poly(oxazinone-r-cyclooctadiene) 4.20.

To a stirring solution of **4.20** and COD (total monomer = 0.40 mmol, 200 eq) in THF (volume such that [**4.20**]$_o$ = 2 M wrt THF) under an atmosphere of Ar was added a 1 M solution of chlorodicyclohexyl borane in hexanes (10 mol% wrt **4.04**) followed by **4.05** (1.77 mg, 2 μmol, 1 eq) in chloroform (0.1 mL). The solution was stirred for 30 min at rt. The reaction was quenched with ethyl vinyl ether (0.1 mL) and 4 drops methanol and the solution was stirred overnight. The solution was triturated into diethyl ether (15 mL) and the solids were collected by centrifugation. ^{1}H-NMR ($CDCl_3$, 500 MHz): δ 7.45-7.25 (m, 5x polyoxazinone H), 6.05-5.55 (m, 2x polyoxazinone H), 5.55-5.33 (m, 4x pCOD H), 5.17-4.55 (m, 3x polyoxazinone H), 4.07-3.85 (m, 3x oxazinone H), 2.25-1.95 (m, 8x pCOD H).

Compound 4.08.

1-methoxy-6-hydroxy (*E*, *Z*)-hex-5-ene (200 mg, 1.54 mmol) was dissolved in dichloromethane (3 mL). Triethylamine (0.47 mL, 3.39 mmol) was added followed by *p*-toluenesufonyl chloride (586 mg, 3.07 mmol) and DMAP (xtal). The solution was stirred for 1 h and then diluted with dichloromethane (7.5 mL) and washed with sat. $NaHCO_3$ (7 mL), water (7 mL), and brine (7 mL). The organic phase was dried and concentrated. The residue was purified by silica column chromatography (5 → 12% EtOAc/hex). Vinyl ether **4.08** was isolated as a clear oil (312 mg, 72%, ~3:1 E:Z). ^{1}H-NMR ($CDCl_3$, 500 MHz): δ 7.79 (m, 2H), 7.35 (m, 2H), 6.23 (dt, *J* = 12.6, 0.7 Hz, 0.75 H, E), 5.86 (dt, *J* = 6.2, 1.3 Hz, 0.25 H, Z), 4.62 (dt, *J* = 12.6, 7.3 Hz, 0.75 H, E), 4.24 (broad q, *J* = 7.0 Hz, 0.25 H, Z), 4.06-3.99 (m, 2H), 3.55 (s, 0.75 H, Z), 3.48 (s, 2.25 H, E), 2.45 (s, 2H), 2.00 (qd, *J* = 7.4, 1.2 Hz, 0.5 H, Z), 1.88 (qd, *J* = 7.3, 0.8 Hz, 1.5 H, E), 1.69-1.60 (m, 2H), 1.40-1.33 (m, 2H). ^{1}H-NMR ($CDCl_3$, 500 MHz): δ 147.6, 146.8, 144.8, 144.7, 133.4, 133.3, 130.0, 129.9, 128.0 (x2), 105.8, 102.1, 70.8, 70.6, 59.6, 56.0, 28.4, 28.2, 27.1, 26.5, 25.5, 23.1, 21.8 (x2). HRESI-MS calcd for $C_{14}H_{20}O_4S$ $[M+H]^+$ 285.1156; found 285.1159.

Polymer 4.10.

To a solution of 1,5-cyclooctadiene (87 μL, 710 μol, 460 eq) and 3-bromopyridine (8.9 μL, 93 μol, 60 eq) in tetrahydrofuran (0.5 mL) was added **4.05** (1.4 mg, 1.5 μmol, 1 eq) in tetrahydrofuran (0.15 mL). The solution was stirred for 12 min at rt and then **4.08** (21.3 mg, 75 μmol) was added. The solution was stirred for 24 h and then concentrated to ¼ total volume. The solution was triturated into cold MeOH (1.2 mL) and the solids were isolated by centrifugation. End-capping efficiency of **4.08** was assessed to be >91% by ^{1}H-NMR by comparing the tosyl signal at δ 7.80 ppm to the pCOD olefin signal at δ 5.38 ppm. ^{1}H-NMR ($CDCl_3$, 500 MHz): δ 7.80 (d, *J* = 8.2 Hz, tosyl end-cap, 2H), 5.38 (m, pCOD, 4x H), 2.08 (m, pCOD, 8x H).

Poly(oxazinone-b-cyclooctadiene) 4.07.

To a stirring solution of **4.04** (100 mg, 0.39 mmol, 30 eq) in THF (0.2 mL) under an atmosphere of Ar in a 30 °C bath was added **4.05** (11.5 mg, 13 μmol, 1 eq) in chloroform (0.19

mL). The solution was stirred for 3 min at 30 °C and then removed from the oil bath. COD (0.72 mL, 5.91 mmol, 455 eq) and PPh_3 (205 mg, 0.78 mmol, 60 eq) were added in THF (5 mL) and the solution was stirred at rt for 30 min. The reaction was quenched by the addition of an appropriate vinyl ether (0.2 mL) and the solution was stirred overnight. The solution was twice triturated into 32 mL cold methanol and the solids were isolated by centrifugation. The solids were dissolved in benzene (8 mL) spiked with Irganox 1076 (~15 mg, to prevent oxidative cross-linking) and freeze-dried. ^{1}H-NMR ($CDCl_3$, 500 MHz): δ 7.38-7.22 (m, 5x polyoxazinone H), 6.00-5.62 (m, 2x polyoxazinone H), 5.60-5.17 (m, 4x pCOD H), 5.15-4.60 (m, 3x polyoxazinone H), 4.10-3.90 (m, 1x polyoxazinone H), 2.30-1.85 (8x pCOD H), 1.25-1.05 (m, 6x polyoxazinone H).

Conjugation of 2,4-dinitrophenyl hydrazine to polymer 4.15

To a solution of polymer **A** (0.31 μmol) in chloroform (0.9 mL) was added HOAc (0.18 mL) and 2,4-dinitrophenyl hydrazine (7.6 mg, 38.5 μmol). The solution was stirred at 70 °C for 4 h. The solution was divided into 3 equal portions and triturated into 3 epitubes filled with 1 mL hot ethanol. The solids were isolated by centrifugation. The combined isolated material was dissolved in a minimal amount of dichloromethane and re-triturated, twice. The conjugation efficiency was assess by ^{1}H-NMR using the DNP signals at $\delta = 9.08$, 8.25, or 7.92 ppm against the signals for **4.07** given in above.

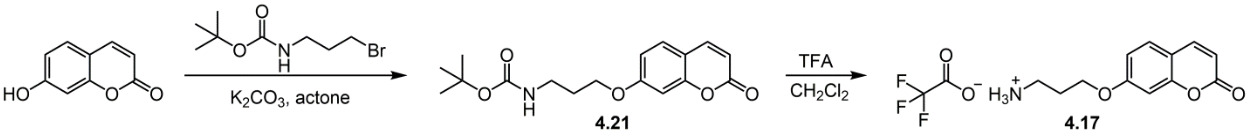

Compound 4.21.

A solution of 7-hydroxycoumarin (0.69 g, 4.26 mmol), 3-(Boc-amino)propyl bromide (1.12 g, 4.70 mmol), and potassium carbonate (0.93 g, 6.72 mmol) in acetone (30 mL) was refluxed for 24 h. The solution was cooled to rt and concentrated. The solids were suspended in dichloromethane (100 mL) and washed with water (2 x 50 mL). The combined aqueous phase was extracted with dichloromethane (75 mL). The combined organic phase was dried and concentrated. The residue was purified by silica column chromatography (30→50% EtOAc/hexanes). Compound **4.21** was isolated as an off white solid (1.13 g, 83%). ^{1}H-NMR ($CDCl_3$, 500 MHz): δ 7.64 (d, *J* = 9.5 Hz, 1H), 7.37 (d, *J* = 8.6 Hz, 1H), 6.84, (dd, *J* = 8.5, 2.3 Hz, 1H), 6.80 (d, *J* = 2.2 Hz, 1H), 6.25 (d, *J* = 9.5 Hz, 1H), 4.90-4.35 (broad s, 1H, NH), 4.08 (t, *J* = 6.0 Hz, 2H), 3.34 (broad q, *J* = 5.7 Hz, 2H), 2.03 (broad pent, *J* = 6.5 Hz, 2H), 1.45 (s, 9H). ^{13}C-NMR ($CDCl_3$, 125 MHz): δ 162.0, 161.2, 156.0, 155.8, 143.4, 128.8, 113.2, 112.8, 112.6, 101.4, 79.4, 66.3, 37.7, 29.4, 28.4. HRESI-MS calcd for $C_{17}H_{21}NO_5$ $[M+H]^+$ 320.1495; found 320.1493.

Compound 4.17.

Compound **4.21** (153 mg, 0.48 mmol) was dissolved in dichloromethane (2.5 mL) and set in 0 °C bath. Trifluoroacetic acid (1.2 mL) was added and the solution was stirred in a cold bath until the starting material was consumed by TLC. The solution was concentrated and the excess acid was azeotroped off with toluene (3 x 2.5 mL) to afford **4.17** (160 mg, quant). ^{1}H-NMR (MeOH-d_4, 500 MHz): δ 7.91 (d, *J* = 9.5 Hz, 1H), 7.58 (d, *J* = 8.5 Hz, 1H), 7.02-6.94 (m, 2H),

6.29 (d, *J* = 9.5 Hz, 1H), 4.24, (t, *J* = 5.8 Hz, 2H), 3.19 (t, *J* = 7.3 Hz, 2H), 2.21 (broad pent, *J* = 6.4 Hz, 2H). ^{13}C-NMR (MeOH-d_4, 125 MHz): δ 163.3, 163.2, 157.1, 145.7, 130.6, 114.4, 114.0, 113.8, 102.4, 66.9, 38.4, 28.2. HRESI-MS calcd for $C_{12}H_{14}NO_3$ $[M\text{-}TFA+H]^+$ 220.0969; found 220.0967.

Conjugation of amine ligands to polymer 4.16.

Polymer **4.16** (1.3 μmol) was dissolved in dichloromethane (1.16 mL) and was added to a round bottom flask containing an amine ligand (13 μmol), EDCI•HCl (27 mg, 142 μmol), and DMAP (27 mg, 225 μmol). The solution was stirred at rt for 24 h and then concentrated to ¼ the total volume. The concentrated solution was triturated into 1 mL MeOH at -78 ^{o}C. The solids were isolated by centrifugation. The isolated material was dissolved in chloroform (4 drops) and re-triturated into cold MeOH twice. The conjugation efficiency was assess by ^{1}H-NMR using the coumarin signals at δ = 7.63 or 6.82 ppm or the naphthalene signal at δ = 8.00 ppm against the signals for **4.07** given in above.

Photodimerization of polymer 4.18.

Polymer **4.18** was dissolved in THF such that $[\text{coumarin}]_o = 2.5 \times 10^{-4}$ M. The solution was sparged with N_2 for 30 mins and then the flask was set in a photoreactor. The flask was illuminated with 350 nm blue light for 14 h. Aliquots were taken over time to monitor the reaction progress (did not open flask to air). Concentrated the solution to 1/20th the original volume and triturated the solution into MeOH at -78 ^{o}C. The solids were isolated via centrifugation. Complete dimerization was assess by ^{1}H-NMR by the loss of coumarin signals at δ = 7.62 and 6.25 ppm.

4.4.3. Monitoring the polymerization of monomer ***4.04***

To a stirring solution of **4.04** (0.2 mmol) in THF (0.1 mL) under and atmosphere of Ar was added **4.05** at various monomer to catalyst loadings in chloroform (0.1 mL). Aloquots (5-10 μL) were taken at various time points over 1 h and concentrated. Crude material was taken up in $CDCl_3$ and monomer conversion was assess using ^{1}H-NMR by comparing the residual monomer olefin signals to the polymer olefin signal.

4.4.4. Degradation of polymer ***4.07***

Polymer **4.07** was taken up in a solution of THF/2.27 M HCl in MeOH (3:1) and allowed to stir at rt for 24 h. The solution was concentrated and the residue was taken up in THF and analyzed by GPC. GPC trace was compared to that of a native **4.07** sample.

Appendix A: Synthesis of Synthetic Antigens with Tunable Stiffness

A.1. Mechanosensing in the Immune System

Our bodies are continuously exposed to pathogens, from viruses to bacteria to fungi. It is the role of our immune system to identify and eliminate these invading microbes. Moreover, cells of the adaptive immune system are responsible for recognizing pathogens that our body has encountered before, either through natural exposure or vaccination. This immunological memory is the result of an elaborate communication network of B cells and T cells.[262] Specifically, when a B cell encounters a foreign antigen, the antigen is internalized and a signaling cascade is turned on that leads to T cell recruitment. The T-cells then induce clonal expansion of the naïve B cell population to both plasma B cells, which produce antibodies, and memory B cells.[263] However, there are notable cases when this line of defense fails. For instance, autoimmune diseases, such as rheumatoid arthritis[358,359], are brought on because immune cells interpret host tissue as pathogenic and then attempt to expunge healthy tissue. Unfortunately, the underlying causes of most immune malfunctions are still poorly understood and, therefore, hard to cure.

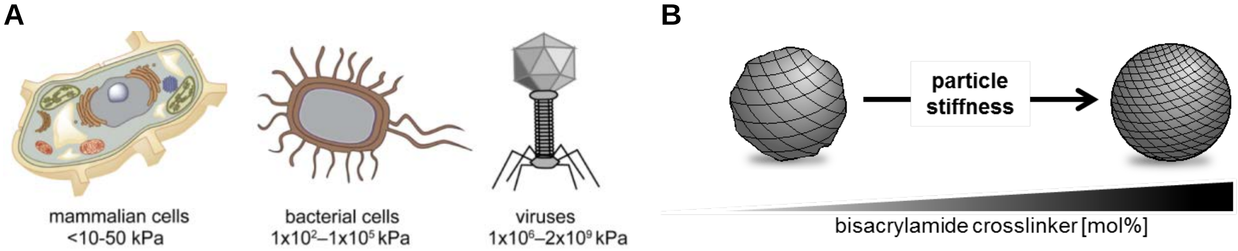

Figure A.1. A) The difference in stiffness between mammalian cells and pathogens spans nine orders of magnitude. B) The elasticity of hydrogel nanoparticles can be tuned to match that of mammalian cells or bacterial pathogens by varying the crosslink densities.

In order to treat immunological diseases we must understand the molecular mechanisms that govern how immune cells differentiate host cells from pathogens. One method immune cells use to delineate self from non-self is through the recognition of organism specific epitopes displayed on cell surfaces or viral capsids, such as glycans or proteins.[263] Indeed, chemically defined probes that can systematically study this aspect of immune activation have garnered much attention in recent years.[28,30,229,282,360-363] However, there is another anatomical feature that that immune cells may use to distinguish host tissue from pathogens: cell stiffness. Prokaryotic cells are stiffer than eukaryotic cells and viruses are stiffer still (Figure A.1).[364-367] In fact, the difference in stiffness between a human cell and a virus can be nine orders of magnitude. As mechanical cues have proven to be important in stem cell proliferation and differentiation[368-372], we posited that immune cells may similarly use mechanosensing to detect pathogens.

There have been recent reports demonstrating that the mechanical properties of synthetic biomaterials can influence the activation of macrophages[373,374], B cells[375,376], and T cells[377,378]. However, it is unclear whether the model systems used in these studies are physiologically relevant. For instance, one study used polyacrylamide hydrogel particles to demonstrate that differences in particle stiffness leads to differences in the extent and mechanism of particle internalization by macrophages.[374] However, the particles used were not functionalized with pathogenic biomarkers. As our lab has previously shown that ligand display is an important parameter for immune cell signaling, it is hard to know if the macrophages responded to these antigens in the same way as a natural pathogen. On the other hand, the studies on B cell activation did use a biomaterial decorated with immunogenic ligands; however, the ligands were immobilized onto surfaces of varying stiffness. While these experiments led to stiffness dependent immunological responses as well, this is also not a physiologically accurate system. B cells typically encounter soluble antigen in the body, which can be internalized and presented to T-cells to activate an adaptive immune response.[262] Therefore, this aspect of immune cell activation is lost when using static, but antigenic, surfaces. Nevertheless, these studies set the stage for the use of well-defined, soluble probes to investigate the role of mechanosensing in the immune system.

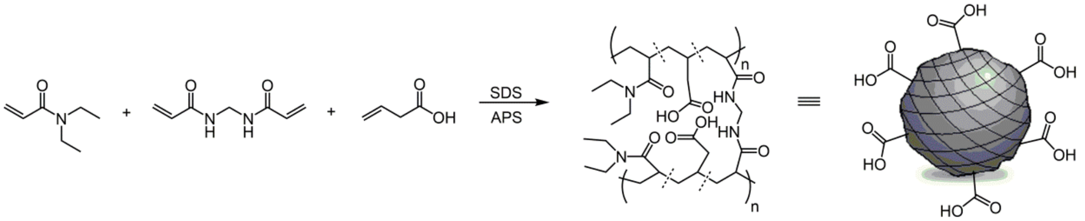

Scheme A.1. Synthesis of carboxylic acid containing polyacrylamide hydrogel nanoparticles.

To improve upon the probes used in the studies described above, alterations to the hydrogel platforms were needed to obtain synthetic antigens with the following characteristics: 1) tunable stiffness across a range of physiologically relevant elasticities; 2) chemical handles that enable modular decoration of the particles with bioactive ligands, and 3) control over the size of the antigen. To achieve these goals, polyacrylamide hydrogel nanoparticles were generated from diethyl acrylamide (DEA) and vinyl acetic acid (VAA) monomers using the covalent cross-linker methylene bisacrylamide (MBA) (Scheme A.1). The inclusion of vinyl acetic acid in the monomer feed led to nanoparticles with carboxylic acid functionality. This moiety facilitates the bioconjugation of immunogenic ligands to the surface of the particles through amide bond coupling.[379] Additionally, free radical copolymerization of acrylamides with VAA has been shown to incorporate the VAA monomer along the outer corona of the particle.[379] This compositional patterning places the majority of the carboxylic acid handles near the hydrogel surface, which enables high conjugation efficiencies. The same regiochemistry does not occur if other carboxylic acid containing monomers, such as acrylic acid, methacrylic acid, or furamic acid, are used. Furthermore, it was envisioned that the mechanical properties of the particles could be tuned by using different amounts of bisacrylamide cross-linker (Figure A.1). It has previously been demonstrated that a hydrogel particle's shape and size can be held constant while changing the cross-linker concentration if the co-monomer feed is unchanged between polymer batches[374]; although this phenomenon has not been shown for particles derived from

DEA and VAA. Therefore, we set out of make functionalizable hydrogel nanoparticles of varying cross-link densities.

A.2. Synthesis and Functionalization of Hydrogel Nanoparticles

Table A.1. Recipes used to generate DEA/VAA hydrogel nanoparticles with different stiffness.

	monomers in feed [mmol]						Particle Size [nm][a]	
% MBA	**DEA**	**VAA**	**MBS**	**SDS [mmol]**	**APS [mmol]**	**water [mL]**	**25 °C**	**37 °C**
2	1.65	0.464	0.043	0.011	0.059	20	141 ± 17	48 ± 1
2	1.65	0.464	0.043	0.017	0.059	20	75 ± 4	37 ± 1
2	1.65	0.464	0.043	0.023	0.059	20	77 ± 23	36 ± 1
4	1.65	0.464	0.088	0.023	0.059	20	202 ± 15	70 ± 1
8	1.65	0.464	0.184	0.023	0.059	20	141 ± 2	82 ± 1
15	1.54	0.518	0.364	0.023	0.059	20	113 ± 2	80 ± 1

[a] Determined using DLS, 0.1 mg/mL in milliQ water.

Polyacrylamide hydrogel nanoparticles were generated from an emulsion polymerization using a binary monomer feed of DEA and VAA. MBA was included as a covalent cross-linker (Scheme A.1). Sodium dodecyl sulfate (SDS) was used as the surfactant and ammonium persulfate (APS) was used as a radical initiator, which was activated thermally. Although hydrogel nanoparticles derived from acrylamide monomers and VAA have previously been generated[379,380], it was not known if changing the cross-link density would impact particle size or functional group density. Therefore, conditions were screened to assess whether this level of control is possible (Table A.1). A previously described synthesis of 5% cross-linked *N*-isopropyl acrylamide/VAA hydrogel particles was used as the basis for the screen.[379] The size of the particles at 37 °C fell within a narrow range (70-80 nm) for cross-link concentrations between 4-15%; however, the size of the 2% particles was lower under the same reaction conditions (35 nm). By decreasing the concentration of SDS, the size was elevated to approximately 50 nm. It is currently unknown if decreasing in the concentration of SDS even further will lead to 2%

particles with sizes comparable to the other particles, but this may be a way to obtain larger particles at low cross-link densities in the future. On the other hand, the average size of the particles was less uniform at 25 ^{o}C. The heterogeneity at 25 ^{o}C is acceptable, however, as the particles will be tested at the physiologically relevant temperature of 37 ^{o}C. Therefore, further optimization to control the size of the particles at 25 ^{o}C was not attempted.

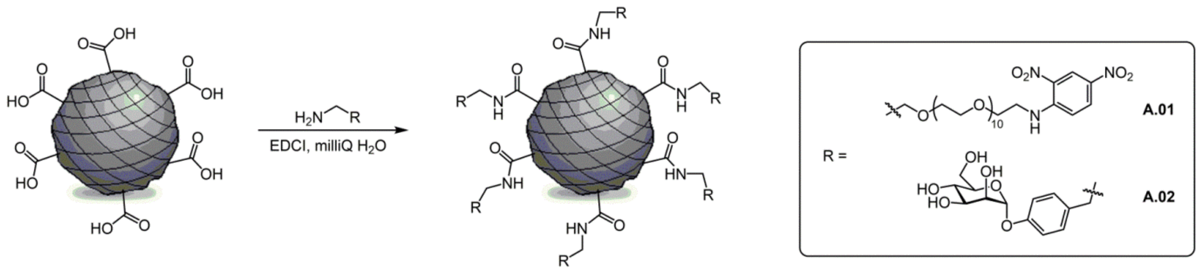

Scheme A.2. Functionalization of carboxylic acid containing polyacrylamide hydrogel nanoparticles.

After synthesizing DEA/VAA hydrogel nanoparticles, DNP ligand **A.01** was conjugated to the particles using EDCI as a coupling agent in water (Scheme A.2). DNP was chosen for two reasons. First, DNP functionalized synthetic macromolecules are able to activate A20HL B cells via interactions with the B cell receptors found on this cell line (see Section 3.2.2).[28,30,229] Therefore, the effect of particle stiffness on B cell activation can be probed. Second, conjugation of DNP to the particles can assist in quantifying the amount of VAA incorporated into the particles during hydrogel synthesis, which is challenging to quantify directly. The amount of DNP conjugated onto the particles is easily assessed using the absorbance of DNP at 360 nm (Figure A.2). As VAA containing hydrogels have previously been shown to enable conjugation efficiencies greater than 95%[379], the DNP content determined colorimetrically can be used to infer the amount of VAA incorporated into the hydrogels. By this measure, at a VAA feedstock loading of 21 mol%, the final DNP content was found to be 4.4 mol% (averaging across all cross-linking densities) (Table A.2). This corresponds to a VAA incorporation of 20%, which is in good agreement with the literature.[379,380] Additionally, conjugation of ligand **A.01** to the hydrogel particles led to an increase in particle size at 37 °C. This makes sense as ligand **A.01** contains a PEG_{11} linker between the amine and DNP functionality. The location of the carboxylic acid moieties should place the DNP ligands around the outer sphere of the particle; therefore, the addition of this water soluble oligomer should increase to the observed radius of gyration.

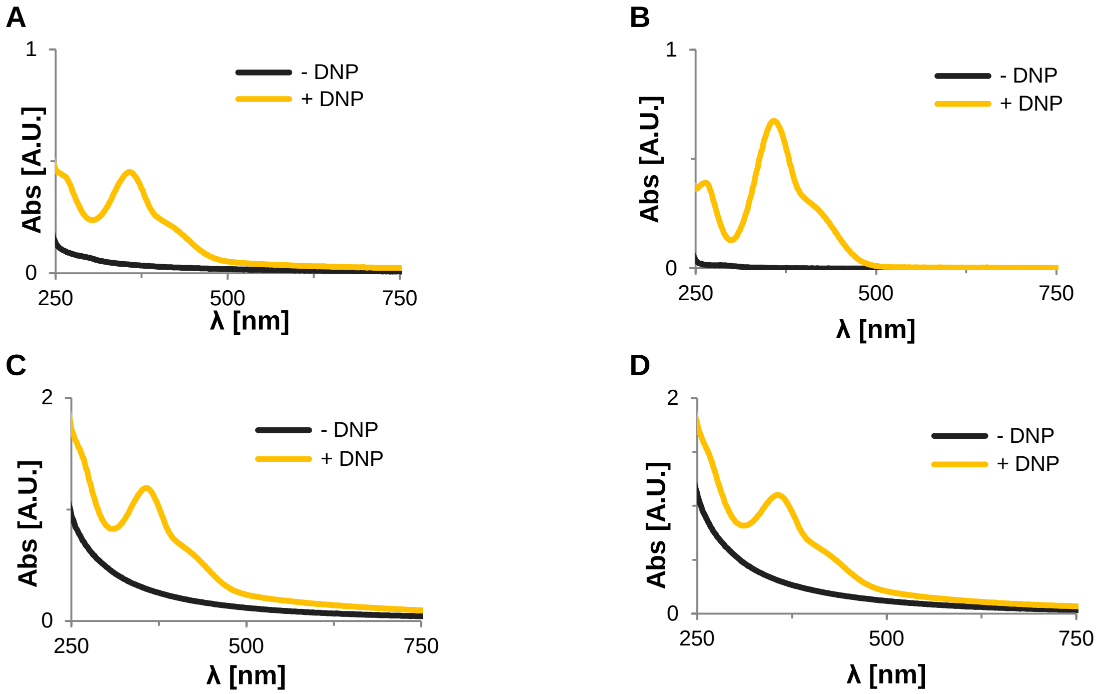

Figure A.2. The extent of DNP conjugated to carboxylic acid containing hydrogels was assessed using UV-Vis. A) 2%, [particle] = 1 mg/mL, B) 4%, [particle] = 0.68 mg/mL, C) 8%, [particle] = 1 mg/mL, D) 15%, [particle] = 0.83 mg/mL. ε^{DNP}(360 nm) = 17530 $M^{-1}cm^{-1}$, l = 5/32 cm. A360(DNP) was obtained by subtracting A360(-DNP) from A360 (+DNP).

Table A.2. DNP conjugation was used to quantify the –COOH content of the hydrogel particles.

	size, 37 °C [nm]			
% MBA	**- DNP**	**+ DNP**	**DNP content [μmol/mg dry gel]**	**-COOH content [mol%]**
2	48 ± 1	54 ± 1	0.245	3.5
4	70 ± 1	unk	0.222	4.7
8	82 ± 1	252 ± 12	0.330	4.5
15	80 ± 1	161 ± 12	0.347	4.9

In addition to DNP, the mannose ligand **A.02** was also attached to the hydrogel particles to facilitate the internalization of the hydrogel nanoparticles by dendritic cells and macrophages (see Section 3.2.3) (Scheme A.2). However, assessing the mannose content of the final glycosylated particles was less straightforward than with the DNP ligand. This is because mannose does not have a distinct absorbance band that can be used to quantify its incorporation colorimetrically. To work around this limitation, an early biochemical hexose assay was applied to this analytical problem.[381-384] Originally, this assay was used to quantify the carbohydrate content on the surface of bacteria. To assess this value, surface exposed carbohydrates are oxidized to 5-hydroxymethyl furfural by sulfuric acid (Scheme A.3). Then, cysteine is added which condenses with the aromatic intermediate to form a UV active chromophore that quantitatively reports on the amount of carbohydrates on the surface of the bacteria. Using ligand **A.02**, a calibration curve was generated for mannose. Importantly, the calibration was linear in the expected range of hydrogel functionalization (Figure A.3). Applying this assay to the mannosylated hydrogels was found to be effective for quantifying the mannose content conjugated to the nanoparticles (Table A.3). Therefore, polyacrylamide hydrogel nanoparticles can be generated from DEA and VAA to afford soluble particles that can be functionalized with bioactive ligands.

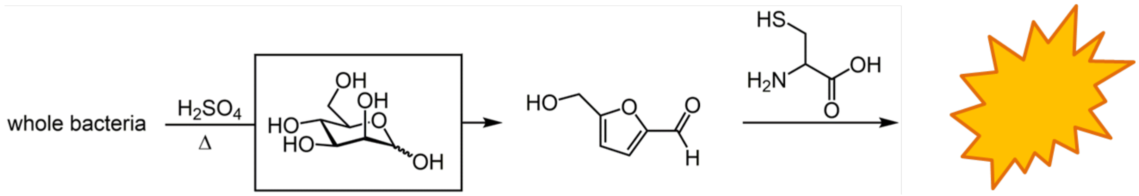

Scheme A.3. The hexose assay can be used to quantify the amount of surface exposed carbohydrates on bacteria or hydrogels.

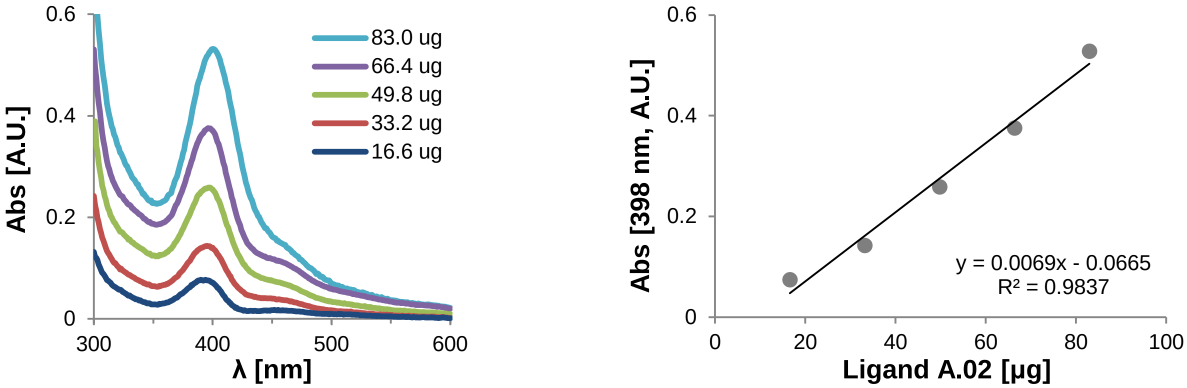

Figure A.3. The hexose assay was performed on mannose ligand **A.02** to generate a calibration curve used to assess the mannose content on the hydrogel nanoparticles

Table A.3. Mannose content of polyacrylamide hydrogels determined by the hexose assay.

% MBA	A398	mannose content [µg mannose/mg gel]
2	0.035	146
4	0.055	175
8	0.061	185
15	0.080	212

A.3. Characterization of the Stiffness of Polyacrylamide Hydrogel Nanoparticles

Atomic force microscopy (AFM) was used to characterize the stiffness of the polyacrylamide hydrogel nanoparticles. To prepare substrates for AFM analysis, the hydrogels were covalently conjugated to amine functionalized glass coverslips using an EDCI coupling (Scheme A.4). The particle stiffness was assessed in phosphate buffered saline solution (PBS). If measurements were taken in air, the exposed charges led to static buildup which interfered with data collection. Therefore, the treatment in PBS was necessary to neutralize the excess charges from the amine surface and the unreacted carboxylic acids on the particles. Scanning the substrate in contact mode revealed that the particles were spherical and the particle diameters were in good agreement with the DLS data (Table A.4). However, the height of the particles decreased as the cross-link density decreased, which made the particles less pronounced at lower cross-link densities (Figure A.4). Although this result was unanticipated, it was an early indication that changing the cross-link densities changed the particle's properties. Probing the elasticity of the 15% particles afforded an elasticity of 261 ± 100 kPa, in good agreement with other hydrogel particles of similar cross-link density.[374] Unfortunately, it is challenging to obtain reliable stiffness measurements on soft substrates below 50 nm in thickness.[385] Therefore, the collapsed nature of the 4% and 2% particles impeded the investigation of the mechanical properties of these substrates when force curves were taken. Therefore, while immobilizing the hydrogel particles on the coverslips allowed the particles to be imaged, it was not effective for obtaining definitive particle stiffness across all cross-link densities.

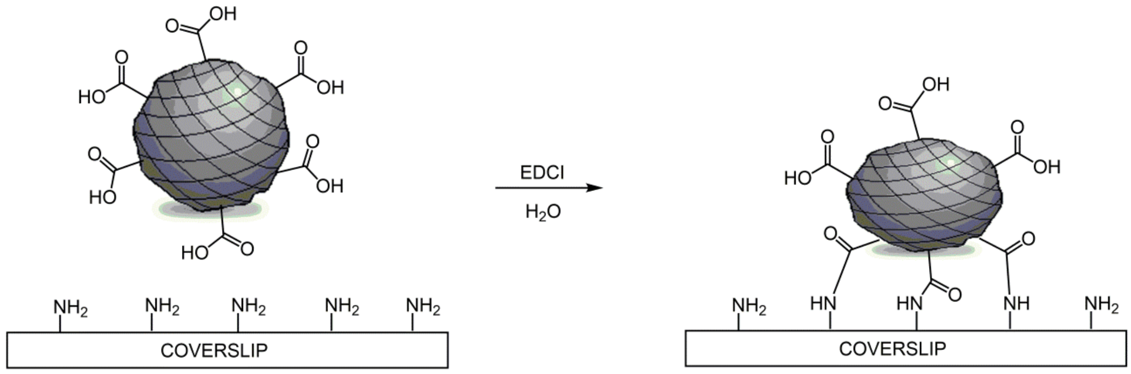

Scheme A.4. Functionalization of glass coverslips with hydrogel particles for AFM analysis.

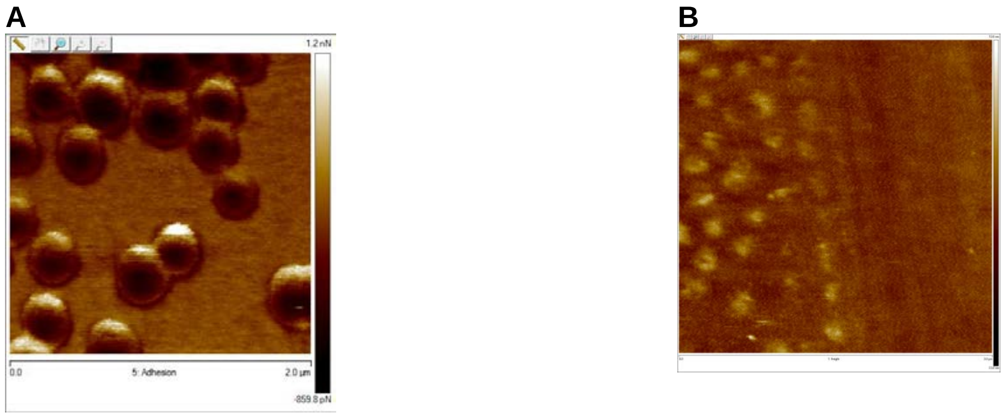

Figure A.4. AFM image of A) 15% particles immobilized on a glass coverslip, scale bar 2.0 µm and B) 4% particles immobilized on a glass coverslip, scale bar 3.0 µm.

Table A.4. Particle aspect ratios as determined by AFM.

% MBA	particle diameter [nm]	particle height [nm]
2	95	n/a
4	275	4
8	Unk	unk
15	315	100

To work around ambiguity of probing the stiffness of the hydrogel particles using AFM, uniform hydrogel sheets were generated from the same monomer feed stocks. Hydrogel sheets completely cover the glass substratum and have micrometer thicknesses. These features prevent the penetration of the AFM tip to the glass surface below. These surfaces serve as surrogates for the particles, and the elasticities of the surfaces will be used to approximate the elasticities of the particles. Analysis of the elasticities of these surfaces by AFM is still being investigated.

A.4. Future Directions

Although the exact stiffness of the hydrogel particles discussed in this appendix have not been quantified, initial biological evaluations have been performed. Importantly, both the DNP functionalized particles and the mannosylated particles were able to be taken up by cells that express DNP or mannose binding cell surface receptors, respectively. It is anticipated that further analysis of particle uptake will reveal that stiffer particles are taken up to a greater extent than softer particles, as pathogens are stiffer than mammalian cells (Figure A.1).[374] In addition, the mechanism by which the different particles are internalized will need to be assessed. This can be done by pre-treating the cells with inhibitors of different cellular machinery used during endocytosis. For instance, chloropromazine inhibits clatherin-mediated endocytosis[386] while nystatin inhibits caveolae-mediated processes[387]. These experiments will reveal *how* the particles get into the cells. Additionally, different endosomal compartments can be illuminated with various fluorescent dyes. As the hydrogel particles are amenable to co-functionalization with both bioactive ligands and amine-bearing fluorophores, co-localization analysis can be used to follow the trafficking of the particles once they are internalized.[229] Visualization of the particles in this way will show *where* the particles go once inside the cell. If particles of different stiffness are observed to be internalized and trafficked differently, this information can be used to understand how immune cells may use mechanical cues to discern host tissue from pathogens. Finally, in collaboration with the Broad Institute, the RNA expression profiles of macrophages exposed to mannosylated hydrogels of different stiffness will be sequenced to understand what genes are activated or suppressed when these cells encounter the different synthetic antigens.

A.5. Materials and Methods

A.5.1. General Methods

All commercially available reagents were purchased from Sigma-Aldrich (St. Louis, MO). ^{t}Boc-*N*-amido-dPEG$_{11}$-amine was purchased from Quanta Biodesign (Plain City, OH). Ligand **A.02** was graciously supplied by Cassie Jarvis, who generated the small molecule following the procedures found in Joseph C. Grim's thesis (Kiessling lab, 2014). DEA was purified by column chromatography (25% acetone/hexanes) before each use. SDS was recrystallized from ethanol once. Dialysis cassettes and SurfaSil siliconizing reagent were purchased from Thermo Scientific (Rockford, IL).

^{1}H and ^{13}C nuclear magnetic resonance (NMR) spectra were obtained using a Bruker Avance-500 spectrometer. Chemical shifts are reported relative to tetramethylsilane or residual solvent peaks in parts per million (CHCl$_3$: ^{1}H: δ 7.26, ^{13}C: δ 77.23). Peak multiplicity is reported as singlet (s), doublet (d), doublet of doublets (dd), triplet (t), quartet (q), multiplet (m). High resolution electrospray ionization mass spectra (HRESI-MS) were obtained on a Micromass LCT mass spectrometer. UV-Vis absorption spectra were obtained on a Varian Cary 50-Scan UV-Visible Spectrophotometer. DLS was performed using a Wyatt Mobius Mobility Instrument on 0.1 mg/mL solution of hydrogel particles.

Force curves were acquired with a Catalyst Bioscope scanning probe microscope (Bruker Corp, Santa Barbara, CA). Samples were hydrated 30 minutes in PBS prior to imaging in PBS. Silicon nitride cantilevers with a nominal spring constant of 0.06 N/m were used (ORC8, Bruker). Force curves were acquired in force-volume mode, with a total of 1024 force curves obtained per sample. Each force curve was taken at a rate of 2 μm/sec, with a 1 μm approach and a 1 μm retract.

A.5.2. Synthesis of Ligand ***A.01***

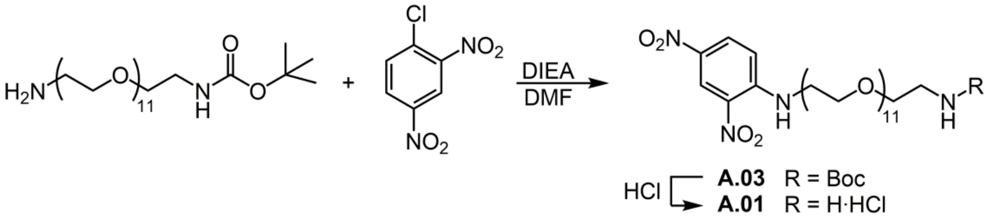

To a stirring solution of ^{t}Boc-*N*-amido-dPEG$_{11}$-amine (40 mg, 62 μmol) and 1-chloro-2,4-dinitrobenzene (15.7 mg, 77.6 μmol) in DMF (0.8 mL) was added DIEA (14.2 μL, 81.5 μmol). The solution was stirred for 1 h at rt and then concentrated. The crude residue was purified by silica column chromatography (1-5% MeOH/CH$_2$Cl$_2$) to afford intermediate **A.03** was a yellow oil (39 mg, 78%). ^{1}H-NMR (500 MHz, CDCl$_3$): δ 9.07 (d, *J* = 2.5 Hz, 1H), 8.63 (s, 1H), 8.20 (dd, *J* = 9.5, 2.4 Hz, 1H), 6.90 (d, *J* = 9.5 Hz, 1H), 4.97 (s, 1H), 3.77 (t, *J* = 5.2 Hz, 2H), 3.67-3.50 (m, 44H), 3.47 (t, *J* = 5.0 Hz, 2H), 3.24 (broad q, *J* = 4.7 Hz, 2H), 1.37 (s, 9H). ^{13}C-NMR (125 MHz, CDCl$_3$): δ 156.0, 148.3, 136.1, 130.5, 130.3, 124.3, 114.1, 79.1, 70.8, 70.7, 70.7, 70.6 (overlapping methylenes), 70.5,70.3, 70.2, 68.6, 50.9, 43.4, 40.4, 28.4. HRESI-MS calcd for $C_{35}H_{62}N_4O_{17}$ $[M+NH_4]^+$ 828.4449; found 828.4446.

To a stirring solution of intermediate **A.03** (40.5 mg, 49.9 μmol) in MeOH (1.1 mL) was added a 4 M solution of HCl in 1,4-dioxane (0.66 mL). The solution was stirred for 50 min at rt and then concentrated. Excess acid was removed by azeotrope with chloroform (3 x 1 mL) to afford ligand **A.01** (39 mg, quant). ^{1}H-NMR (500 MHz, MeOH-d_4): δ 8.94 (s, 1H), 8.20 (s, 1H), 7.15 (s, 1H), 3.80-3.45 (m, 46H), 3.09 (s, 2H). ^{13}C-NMR (125 MHz, MeOH-d_4): δ 149.9, 137.0, 131.6, 131.1, 124.7, 116.5, 71.8, 71.7, 71.7, 71.6, 71.6, 71.5, 71.5, 71.5 (overlapping methylenes), 71.4, 71.3, 71.3 (overlapping methylenes), 71.2 (overlapping methylenes), 71.2, 71.1, 70.8, 70.2, 68.2, 68.1, 44.4, 40.1. HRESI-MS calcd for $C30H54N_4O_{15}$ $[M+H]^+$ 711.3659; found 711.3660.

A.5.3. Synthesis of hydrogel particles

DEA, VAA, MBA, and SDS were dissolved in milliQ water following the recipe from Table A.01. The solution was heated to 70 °C while degassing with N_2 for 30 min. APS was added in milliQ water (1 mL) and the solution was stirred at 70 °C for 16 h. After cooling to rt, the solution was filtered through 2.0 μm TTTP Isopore membrane filters (Millipore) and the filtrate was moved to a 30 mL, 10k MWCO dialysis cassette. The solution was dialyzed for 1 week against milliQ water, changing the water at least 1x per day. The contents of the dialysis cassette were freeze-dried to afford the hydrogel particles as a white powder.

A.5.4. Functionalization of hydrogel particles

To a 1.0 mg/mL solution of unfunctionalized particles in milliQ water (1.0 mL) was added the appropriate ligand from a 1.0 mg/mL stock solution in milliQ water (0.5 mL) (NOTE: stock solutions of ligand **A.01** were neutralized with 1 equivalent of 1 M NaOH before addition). The solution was stirred for 30 min at rt. EDCI was added from a 15.8 mg/mL stock solution in milliQ water (31.6 μL) and the combined solution was stirred for 24 h at rt. The solution was moved directly to a 3 mL, 7k MWCO dialysis cassette and dialyzed against milliQ water for 24 h, changing the water 3x during this period. The contents of the dialysis cassette were freeze-dried to afford functionalized particles. The mannose content was determined by the hexose assay and the DNP content was determined by UV-Vis.

A.5.5. Hexose Assay

Cool 100 μL aliquots of standard solutions with [**A.02**] between 0.17 - 0.83 mg/mL to 0 ^{o}C. Add 900 μL 85% H_2SO_4 and let the solution sit at 0 ^{o}C for 1 min, then warm to rt over 2 min. The solution was moved to a 100 ^{o}C bath for 20 min, then immediately cooled to rt over 30-45 s. A 20 μL aliquot of a 3% (w/v) solution of cysteine in milliQ water was added. The solution was gently swirled to homogenize the mixture, and then left in the dark for 30 min at rt. A UV-Vis spectrum (300-600 nm) was taken immediately of each standard and the absorbance at 398 nm was used to generated a calibration curve.

To obtain the mannose content of functionalized DEA/VAA hydrogel nanoparticles, repeat the above procedures using a 100 μL aliquot from a 1.0 mg/mL stock solution of particles in milliQ. The final mannose content can be back calculated from the A398 vs [mannose] calibration curve.

A.5.6. Preparation of hydrogel substrates for AFM

A.5.6.1. Attachment of hydrogel particles

A glass coverslip (12 mm, #1) was etched with a 0.1 M NaOH solution for 3 min. The basic solution was aspirated off and aminopropyl triethyl silane (APTES) was added to the hydrophilic coverslip. The coverslip was incubated with APTES for 5 mins and then excess reagent was immediately removed. The coverslip was washed 3x with milliQ water. The amine coated coverslip was moved to a 6-well cell culture dish and submerged in a 1 mg/mL solution of hydrogel particles in milliQ water. EDCI was added from a 124 mg/mL stock solution in milliQ water (100 μL). After incubating for 24 h, the supernatant was removed and replaced with fresh milliQ water. The water was changed every 30 min for 2 h to removed unligated particles.

A.5.6.2. Synthesis of hydrogel surfaces

Table A.5. Recipes used to prepare hydrogel surfaces.

	Gel Composition (mol% MBA)			
Reagent	**2**	**4**	**8**	**15**
DEA (μL)	83	83	83	83
VAA (μL)	14	14	14	14
MBA (mL)[a]	0.118	0.237	0.473	0.887
water (mL)[b]	0.882	0.763	0.527	0.113
APS (μL)	70	70	70	70
TEMED (μL)	14	14	14	14

[a] 2% w/v in milliQ water, [b] 10% w/v in milliQ water

Hydrogel precursor solutions were prepared from DEA, VAA, MBA, and water using the amounts listed in Table A.04. Immediately before use, *N*,*N*,*N'*,*N'*-tetramethylenediamine (TEMED) and APS were added. The solution was briefly vortexed and a 75 μL aliquot was placed on the reactive coverslips described above. A separate glass coverslip (12 mm, #1) siliconized with SurfaSil was placed on top of the hydrogel solution. After 45 min, the siliconized coverslip was gently removed. The hydrogel coated substrate was soaked in milliQ water to removed unincorporated monomers.

A.5.7. Procedures for AFM

The force curves were analyzed using the Hertz model for a conical probe in contact with a flat surface as previously described.[385,388] Only force curves that exhibited a good fit with the theoretical model were included in the final analysis. To obtain an accurate modulus value, the optical sensitivity and the spring constant of each cantilever was determined. Optical sensitivity was measured as the slope of the force curve, taken in PBS, when the tip is in contact with a rigid surface. The optical sensitivity is used to convert cantilever deflection in volts to deflection in nanometers (x). Spring constants (k) were measured using the thermal tune method (Butt and Jaschke, 1998). The force can then be determined by F = kx. The Hertz model provides a relationship between the loading force and the indentation:

$$F = \frac{2}{\pi}\frac{E\delta}{1-\nu^2}{}^{2}\tan(\alpha) \qquad \text{eq. A.1}$$

where F is the loading force in Newtons, ν is Poisson's ratio (assumed to be 0.5), δ is the indentation depth, E is the elastic modulus in Pascals and α is the half opening cone angle. The values obtained from the force curve are z, z_o, d and $d_{o,}$ where z is the piezo displacement, d is the cantilever deflection, and z_o and d_o are the values at initial contact of the tip with the sample. These values can be used to calculate the indentation, which is given by:

$$\delta = (z-z_o)-(d-d_o) \qquad \text{eq. A.2}$$

Using these equations and knowing that $F = k(d-d_o)$, where k is the cantilever spring constant, gives the following equation for E:

$$E = \frac{\pi}{2}\frac{k(d - d_o)(1-\nu^2)}{\tan(\alpha)((z - z_o) - (d - d_o))^2} \qquad \text{eq. A.3.}$$

Appendix B: NMR Spectra

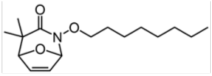

2.01a

^{1}H-NMR (CDCl$_3$, 500 MHz)

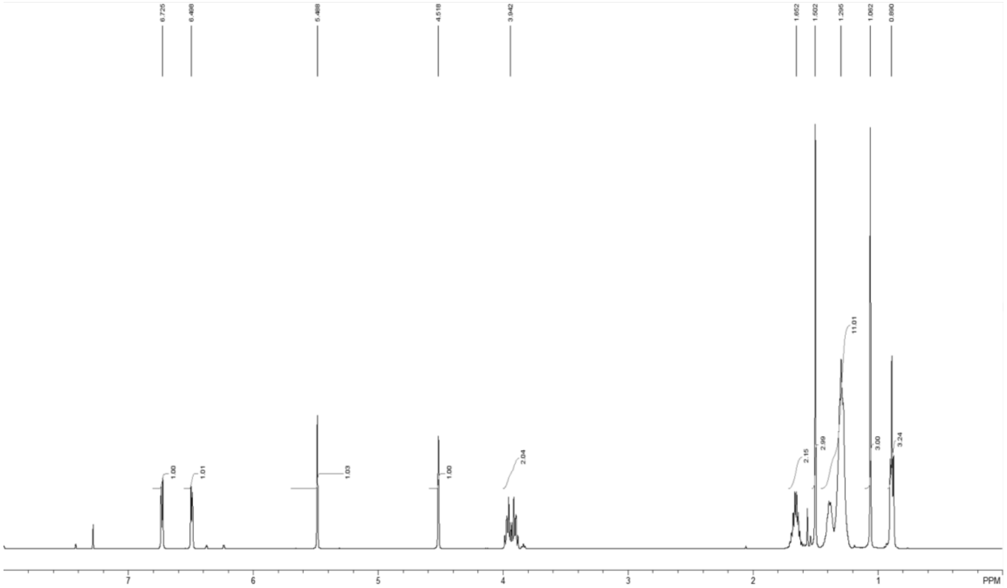

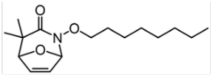

2.01a

^{13}C-NMR (CDCl$_3$, 125 MHz)

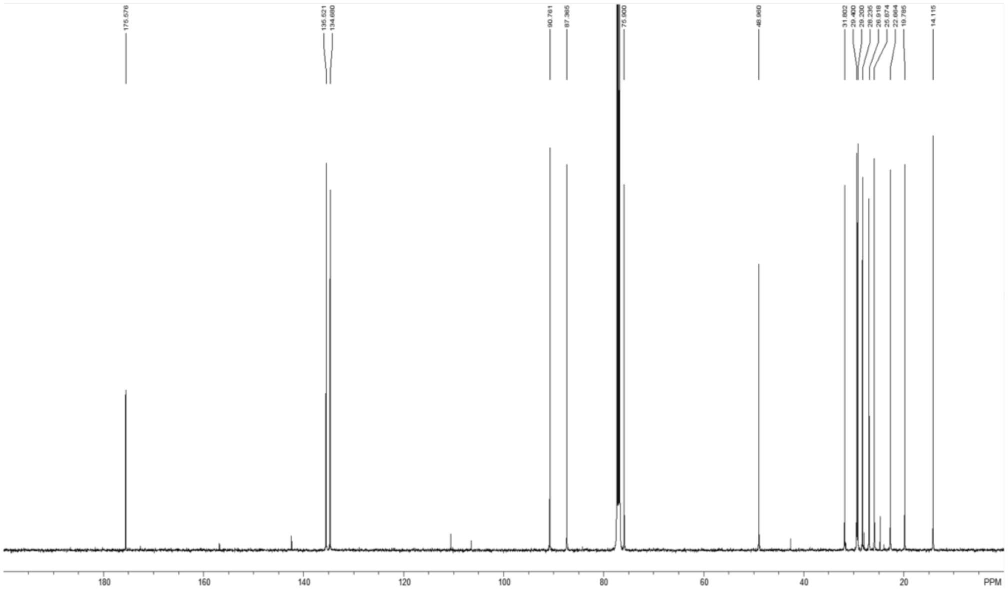

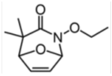

2.01c
^{1}H-NMR (CDCl$_3$, 500 MHz)

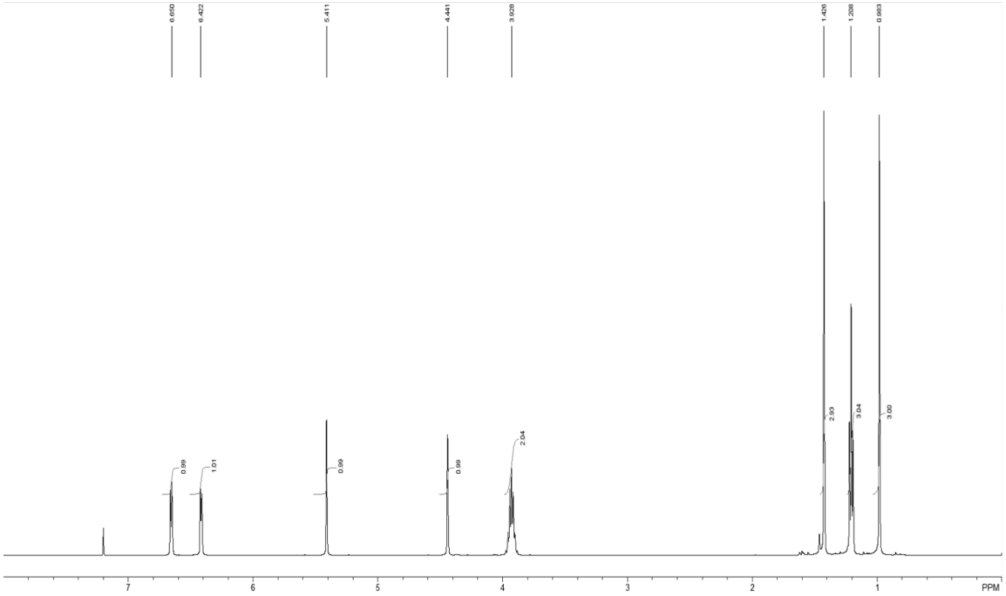

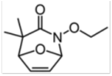

2.01c
^{13}C-NMR (CDCl$_3$, 125 MHz)

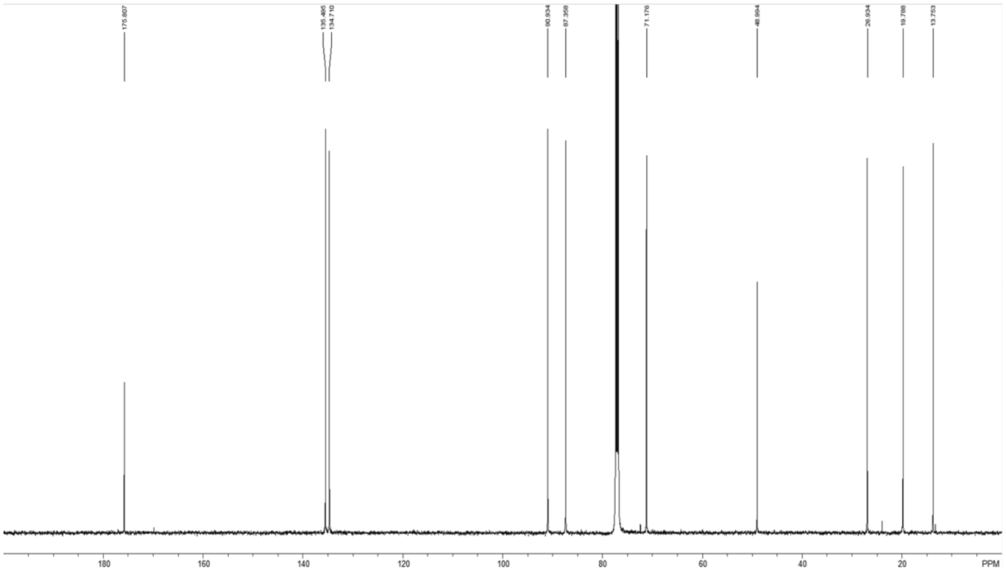

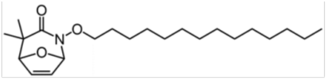

2.01d
^{1}H-NMR (CDCl$_3$, 500 MHz)

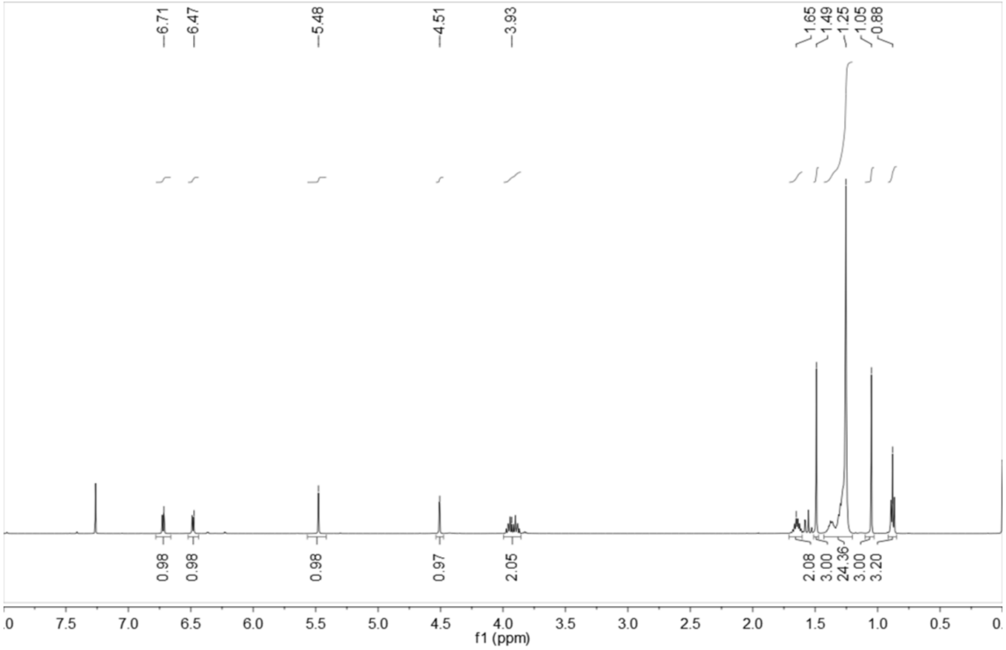

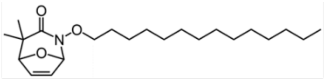

2.01d
^{13}C-NMR (CDCl$_3$, 125 MHz)

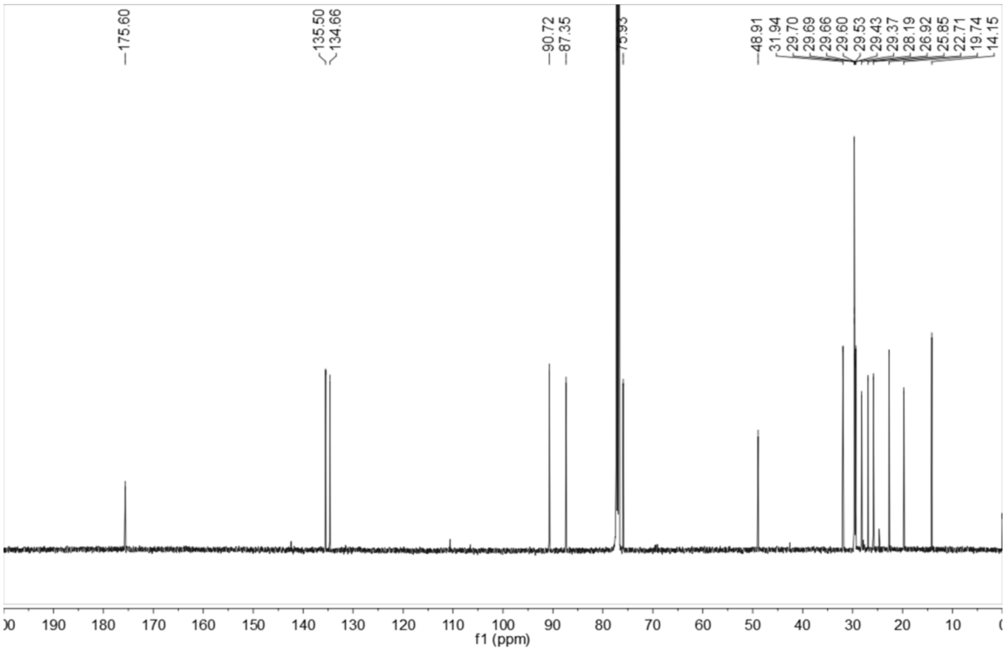

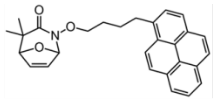

2.01e

^{1}H-NMR (CDCl$_3$, 300MHz)

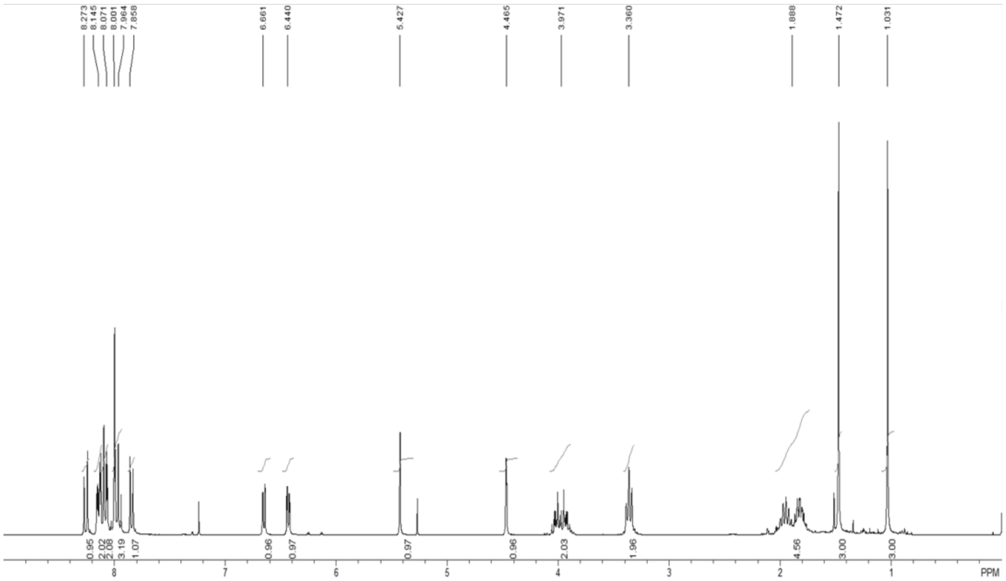

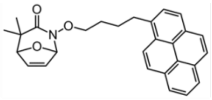

2.01e

^{13}C-NMR (CDCl$_3$, 75 MHz)

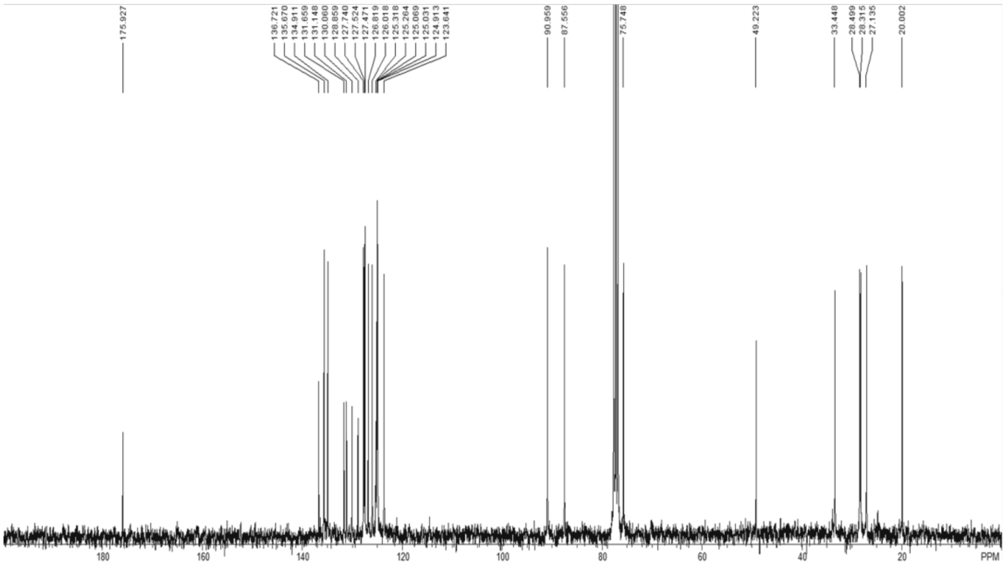

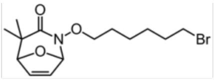

2.01f
^{1}H-NMR ($CDCl_3$, 300 MHz)

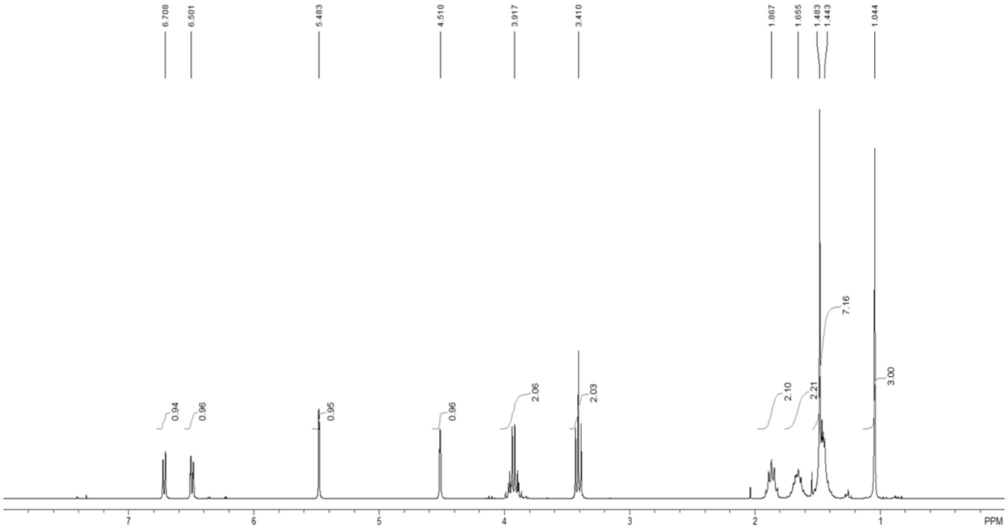

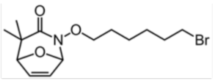

2.01f
^{13}C-NMR ($CDCl_3$, 75 MHz)

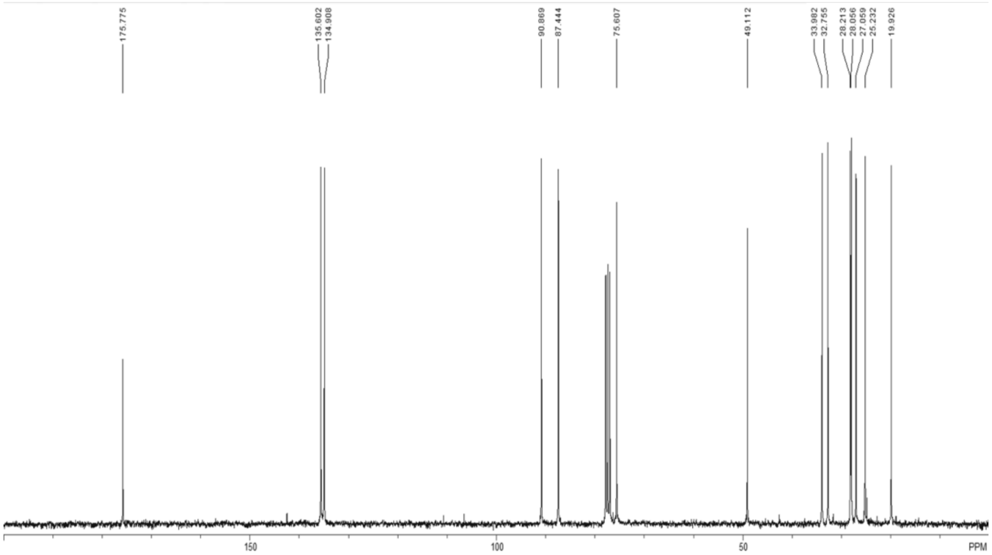

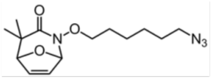

2.01g
^{1}H-NMR (CDCl$_3$, 300 MHz)

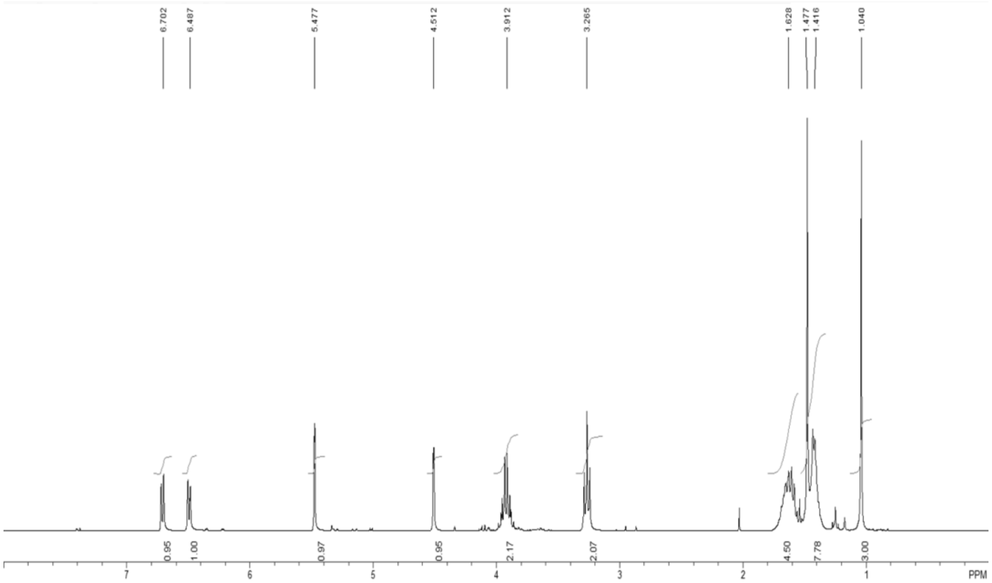

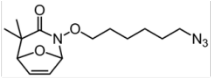

2.01g
^{13}C-NMR (CDCl$_3$, 75 MHz)

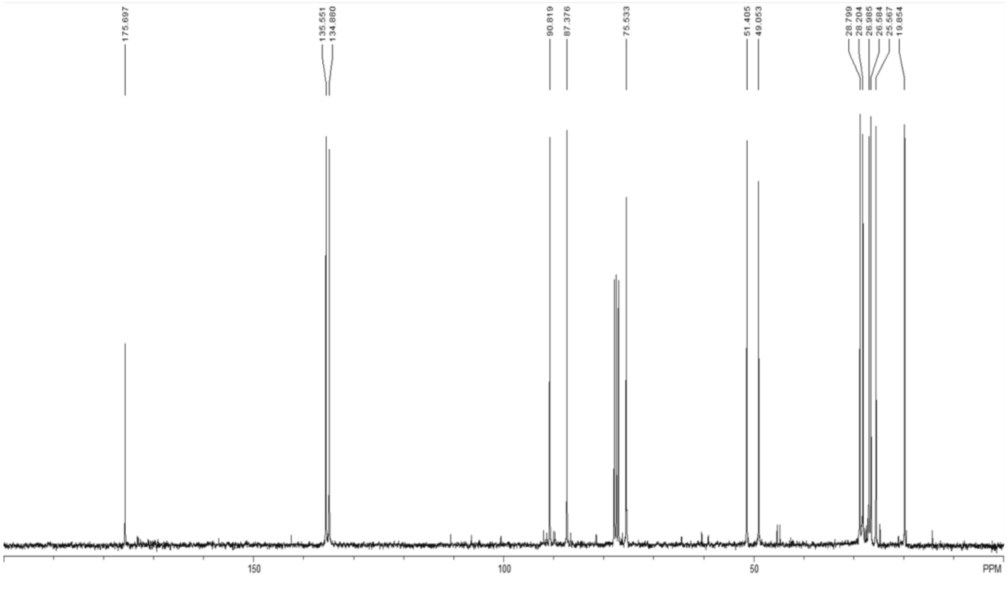

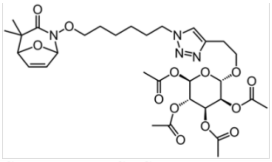

2.01h
^{1}H-NMR (CDCl$_3$, 300 MHz)

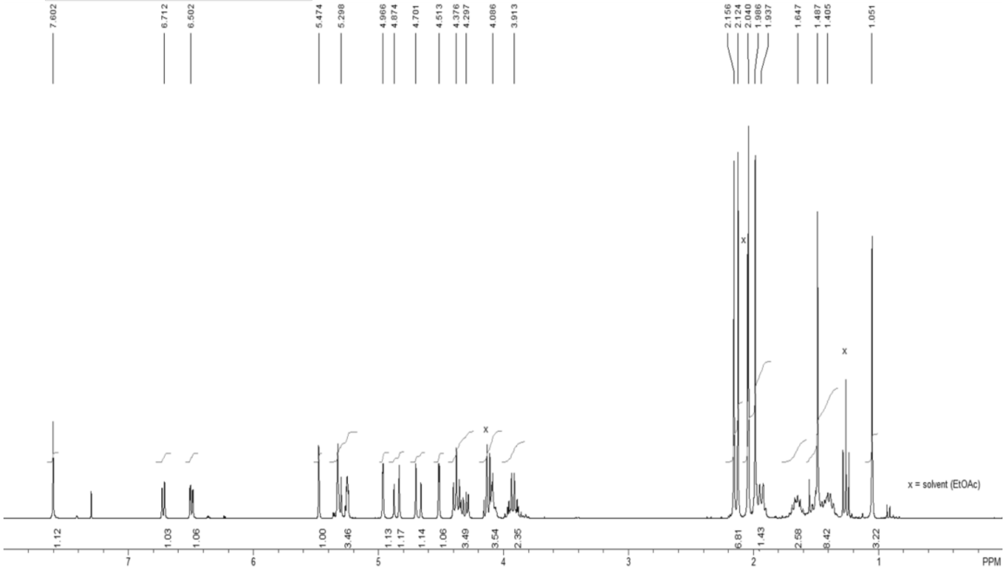

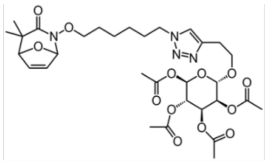

2.01h
^{13}C-NMR (CDCl$_3$, 75 MHz)

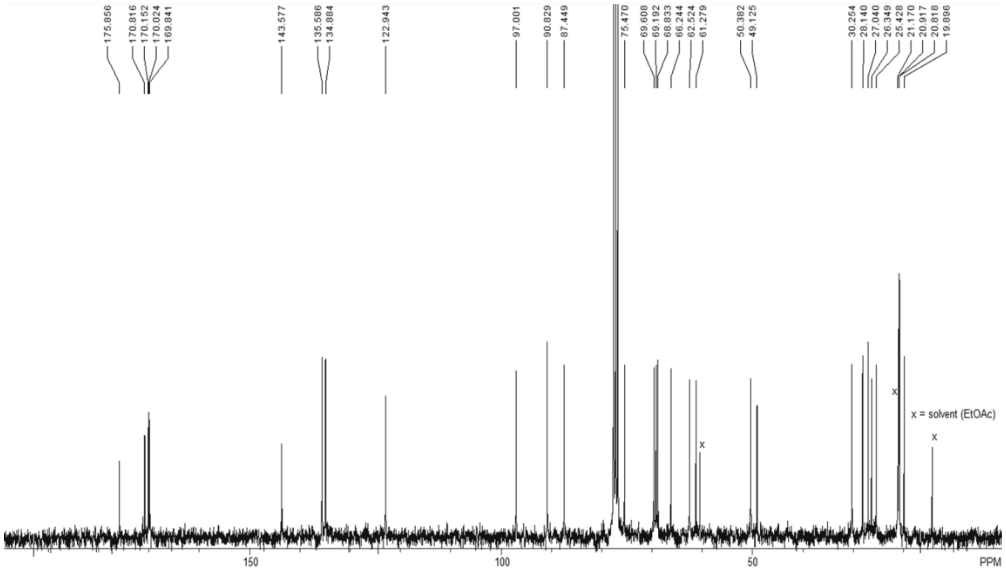

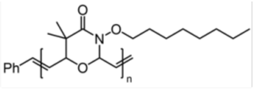

2.03a
^{1}H-NMR (CDCl$_3$, 500 MHz)

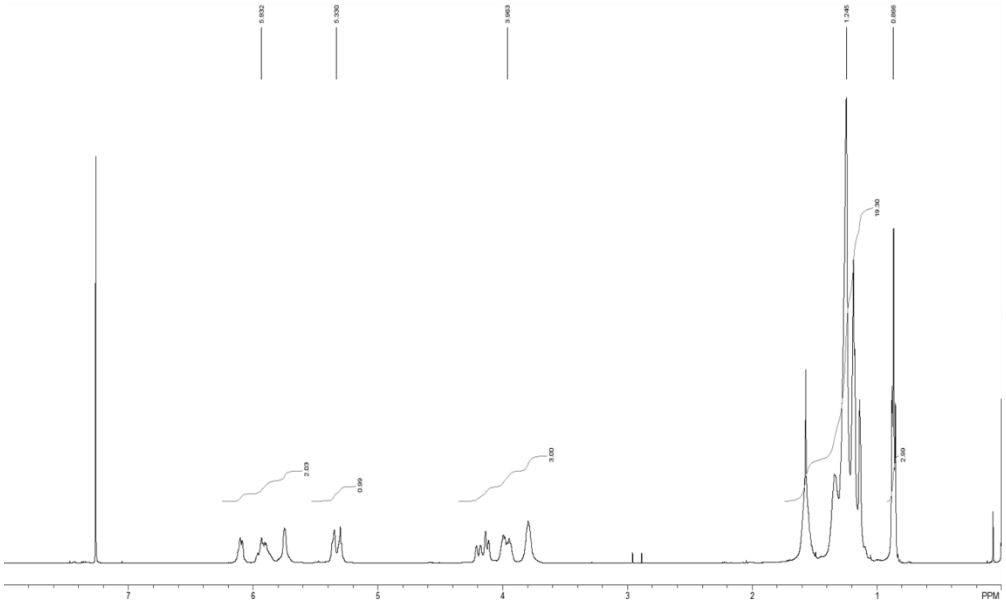

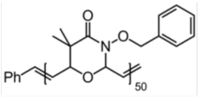

2.03b
^{1}H-NMR (CDCl$_3$, 500 MHz)

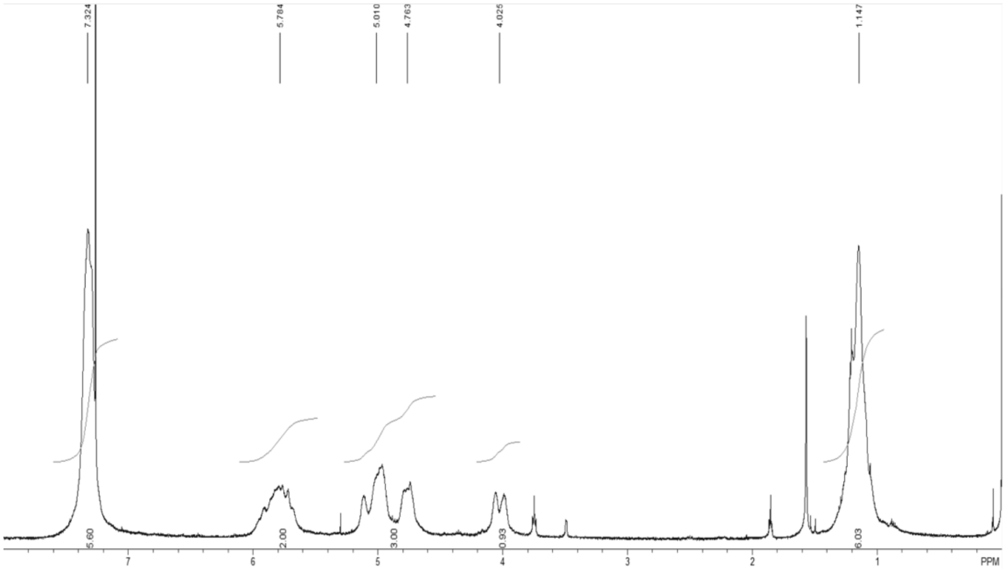

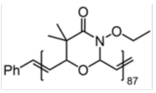

2.03c
^{1}H-NMR (CDCl$_3$, 500 MHz)

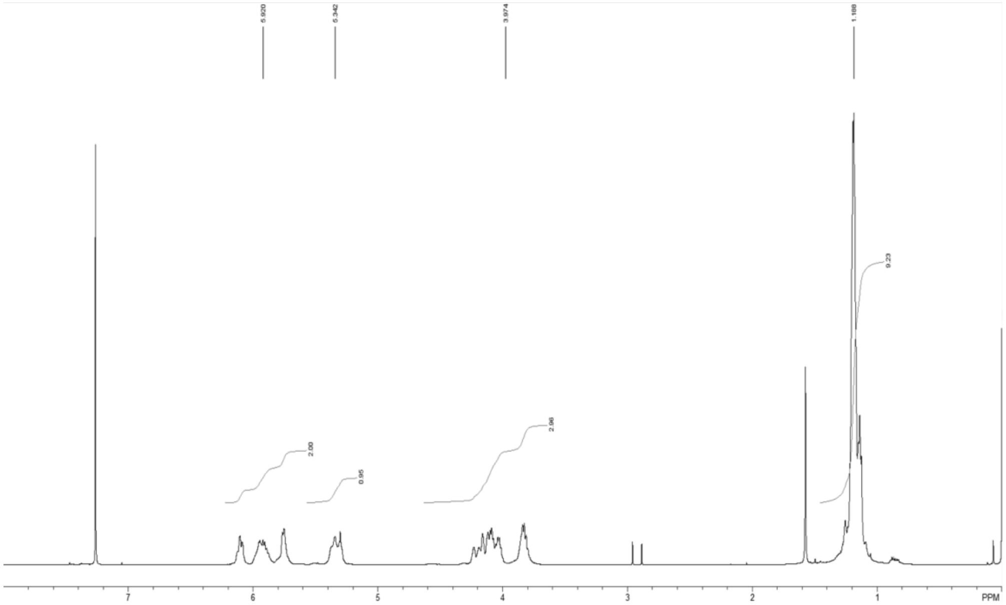

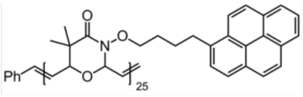

2.03e
^{1}H-NMR (CDCl$_3$, 500 MHz)

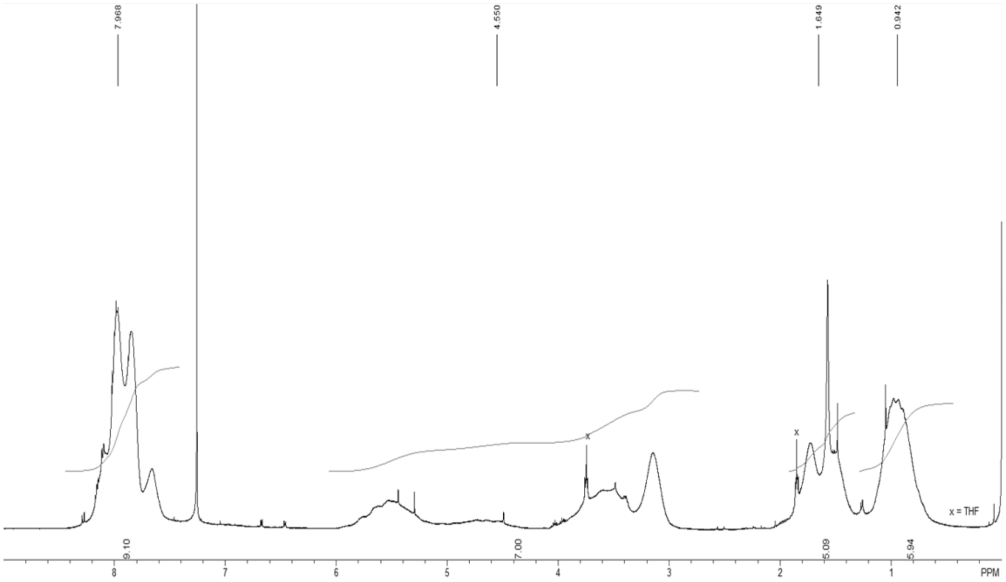

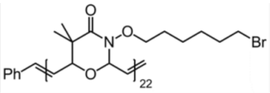
O
N
O
Br
Ph
O
22

2.03f
^{1}H-NMR (CDCl$_3$, 500 MHz)

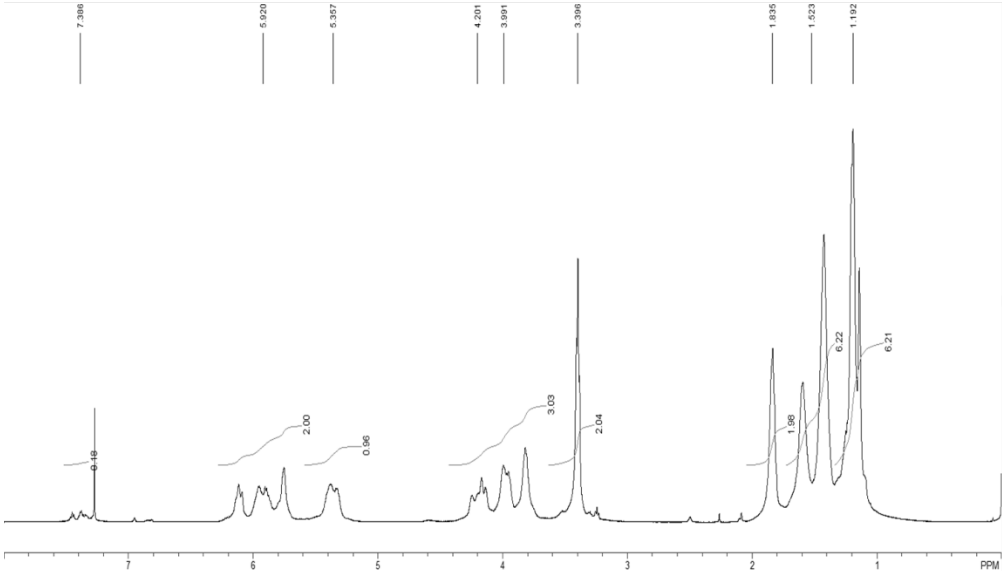

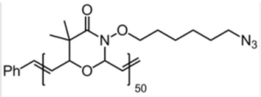
O
N
O
N3
Ph
O
50

2.03g
^{1}H-NMR (CDCl$_3$, 500 MHz)

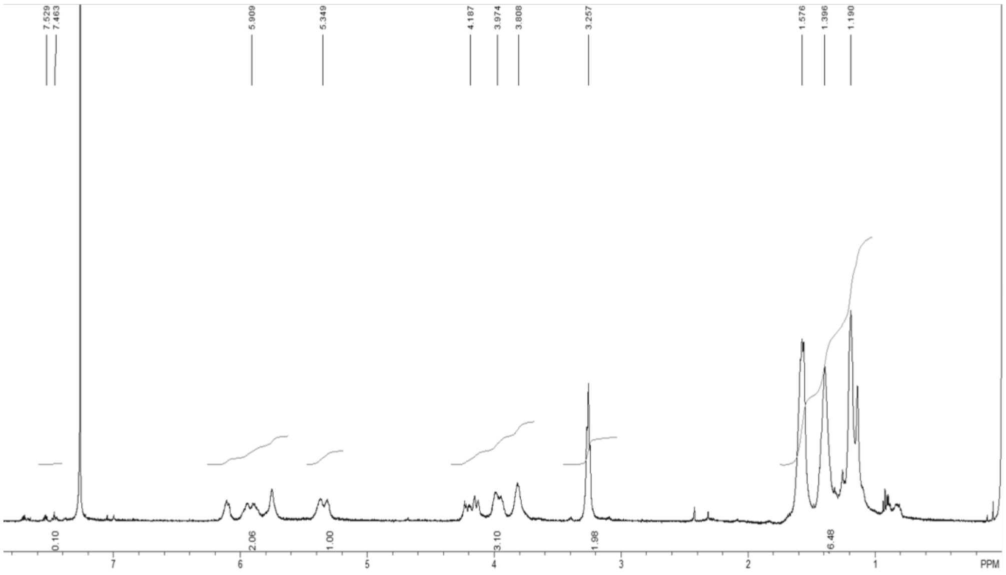

2.03h

^{1}H-NMR (CDCl$_3$, 500 MHz)

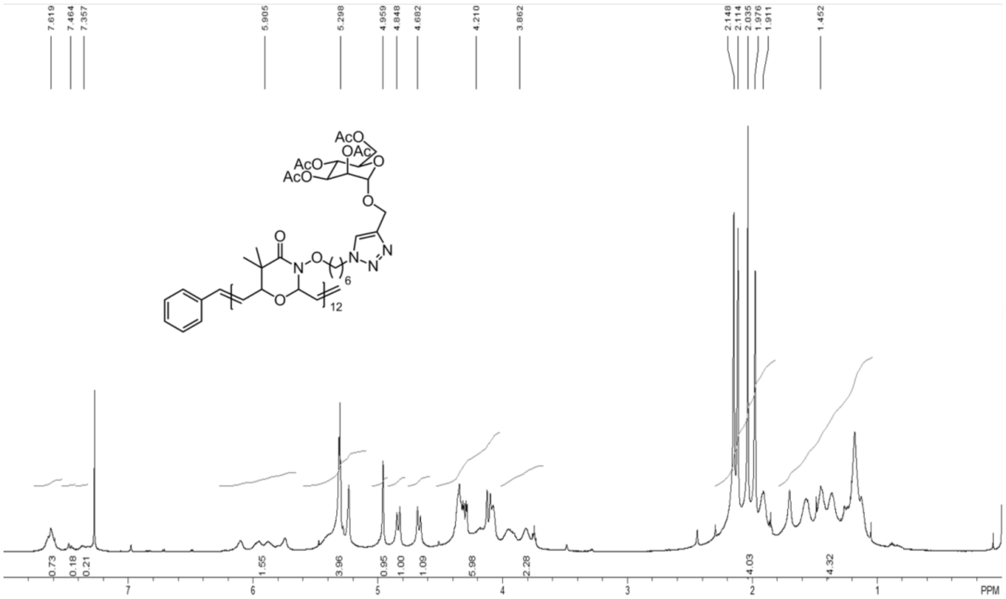

2.03i

^{1}H-NMR (DMSO-d$_6$, 500 MHz)

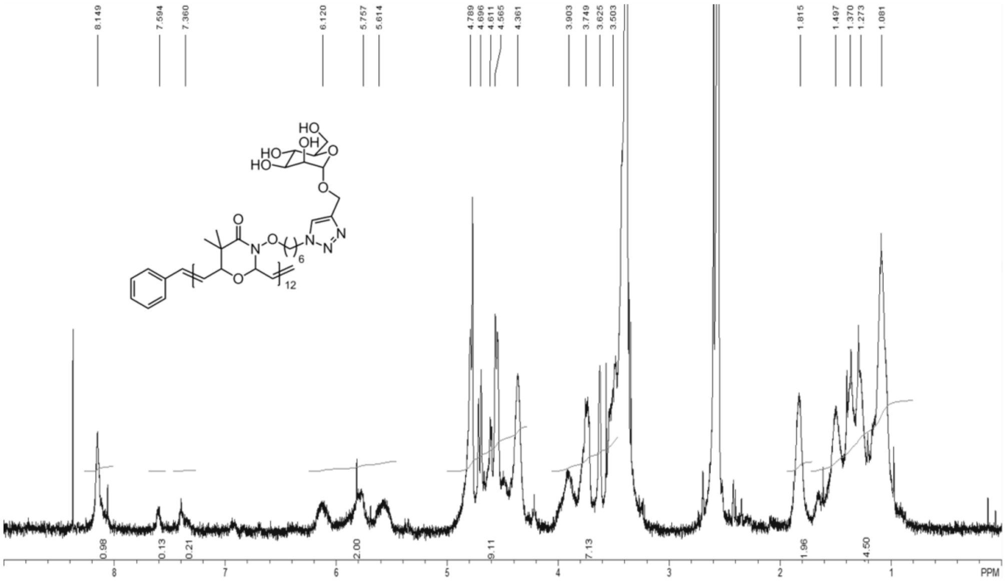

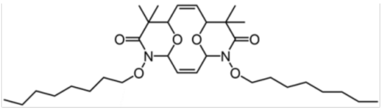

2.04

^{1}H-NMR ($CDCl_3$, 500 MHz)

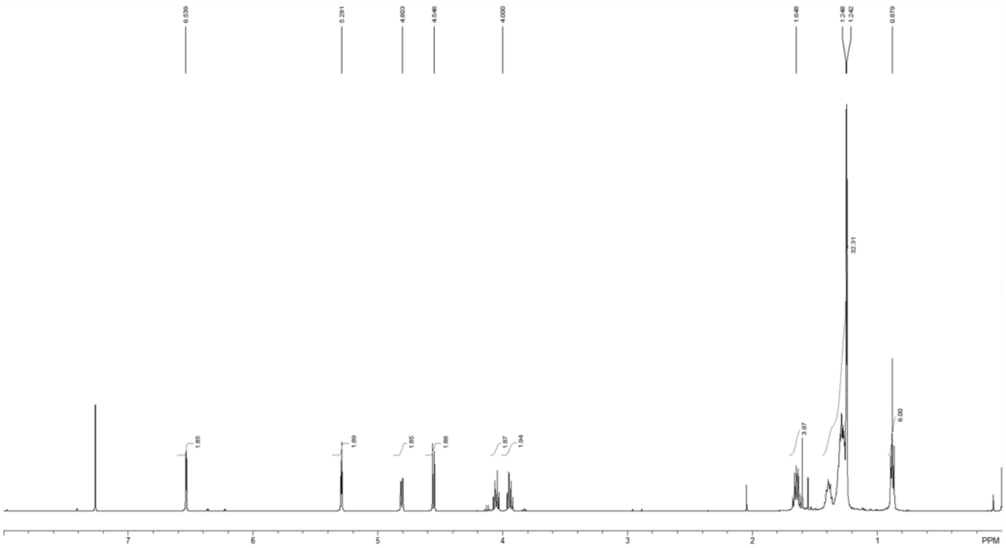

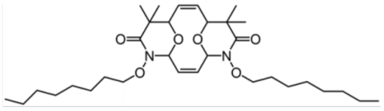

2.04

^{13}C-NMR ($CDCl_3$, 125 MHz)

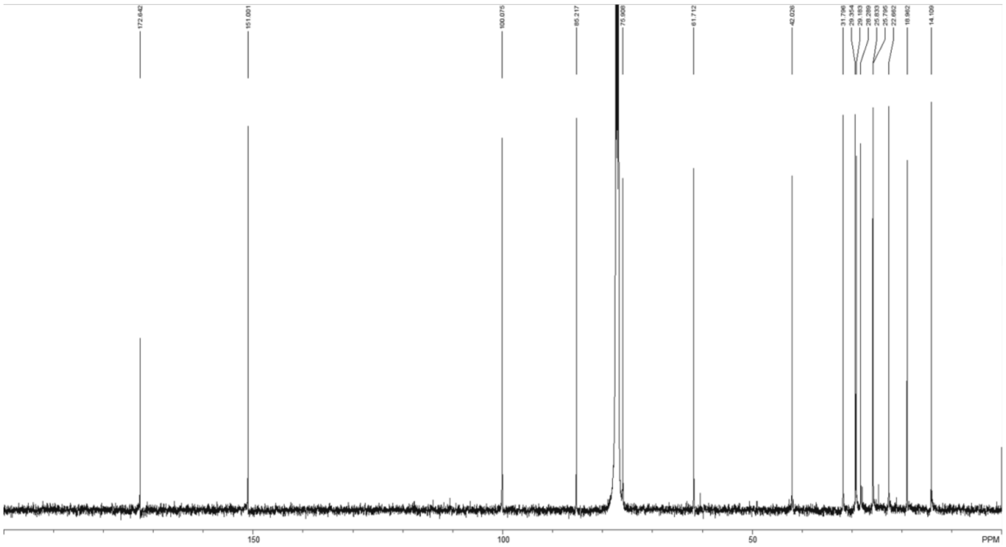

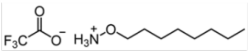

2.08a
^{1}H-NMR (CDCl$_3$, 500 MHz)

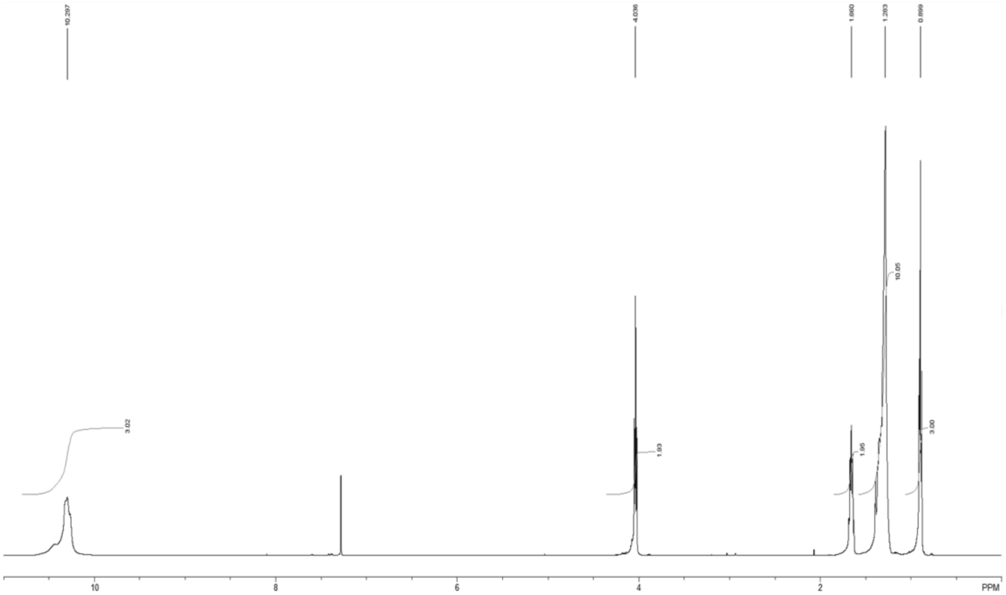

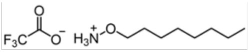

2.08a
^{13}C-NMR (CDCl$_3$, 125 MHz)

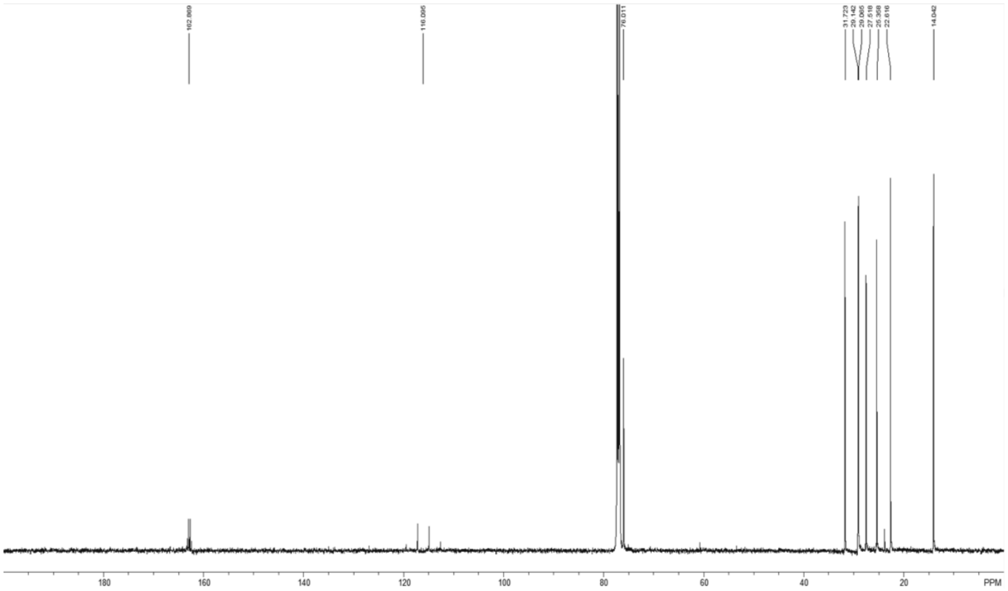

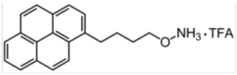

2.08e

^{1}H-NMR (CDCl$_3$, 300MHz)

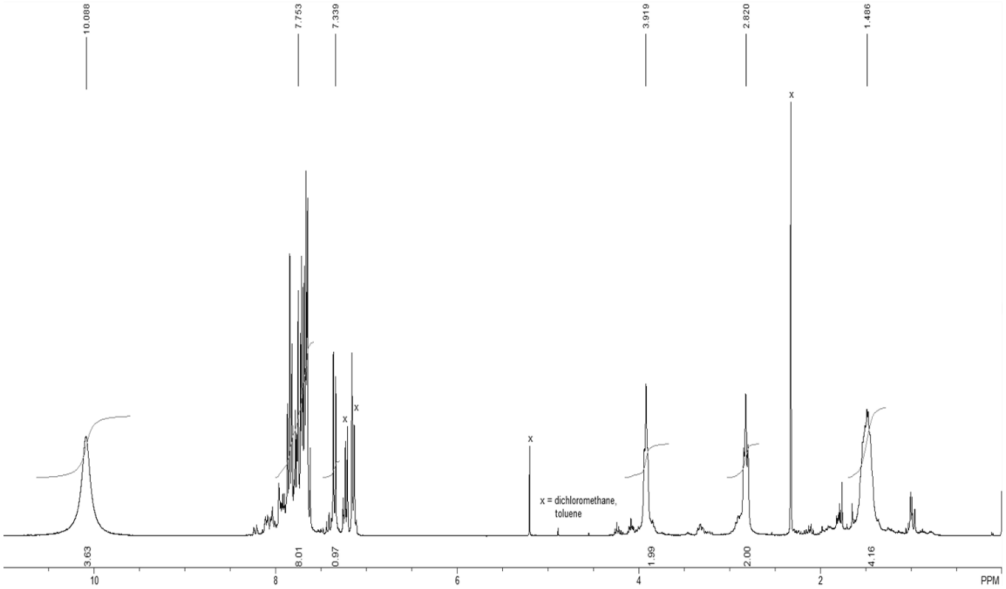

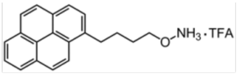

2.08e

^{13}C-NMR (CDCl$_3$, 75 MHz)

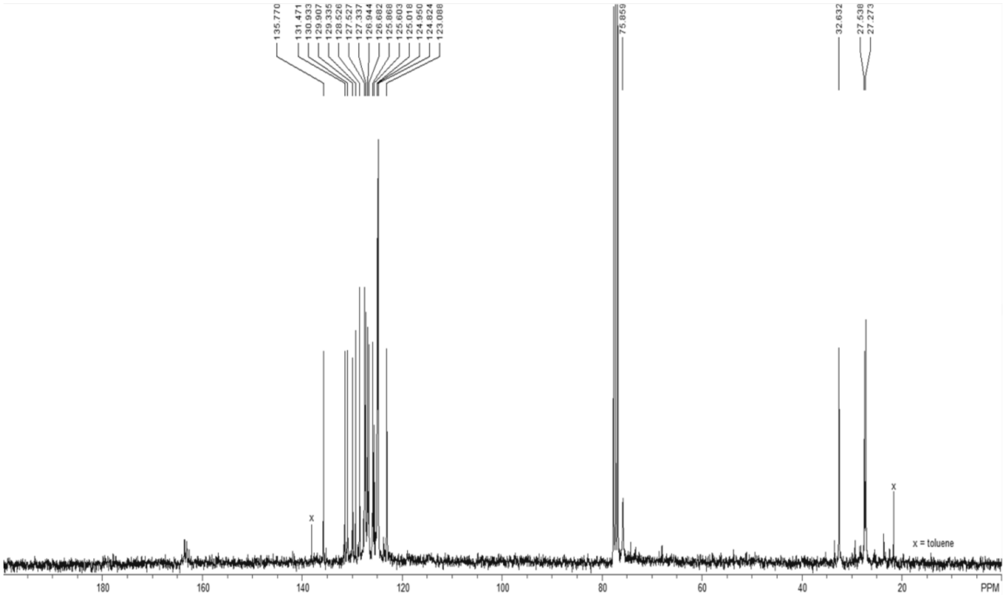

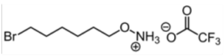

Br
O
NH3
O
CF3

2.08f
^{1}H-NMR (CDCl$_3$, 300 MHz)

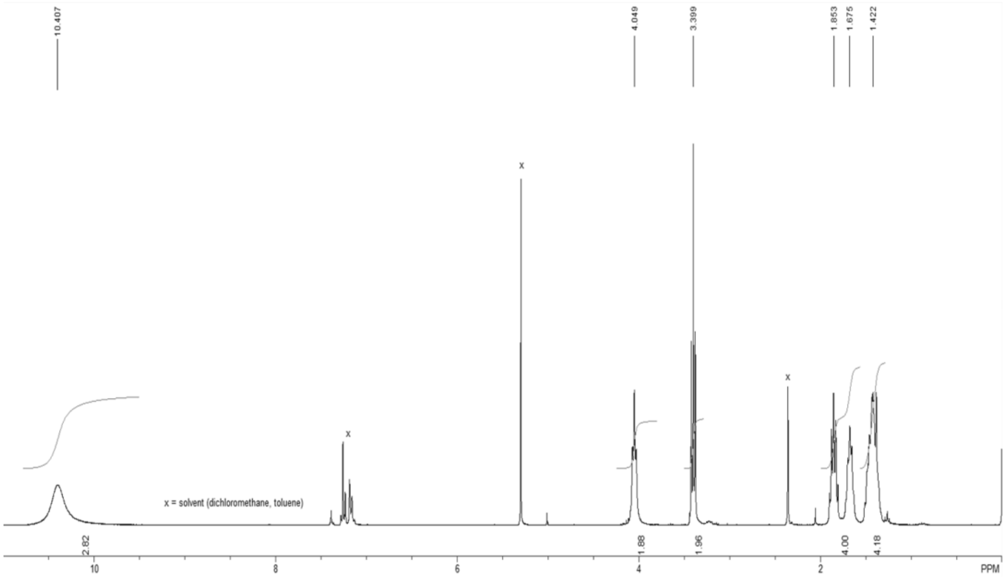

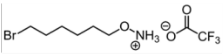

Br
O
NH3
O
CF3

2.08f
^{13}C-NMR (CDCl$_3$, 75 MHz)

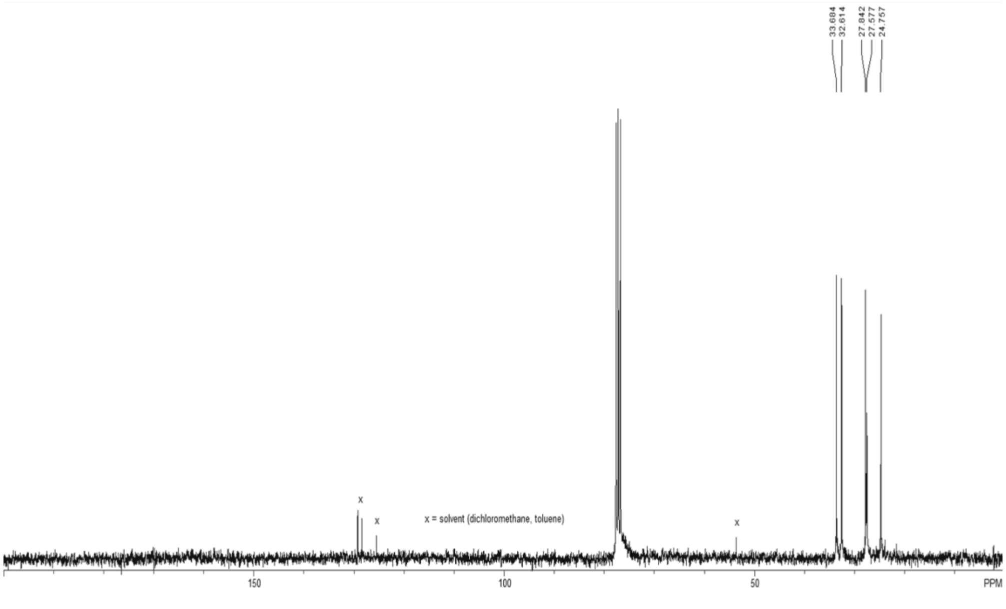

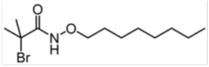

2.09a

^{1}H-NMR (CDCl$_3$, 400 MHz)

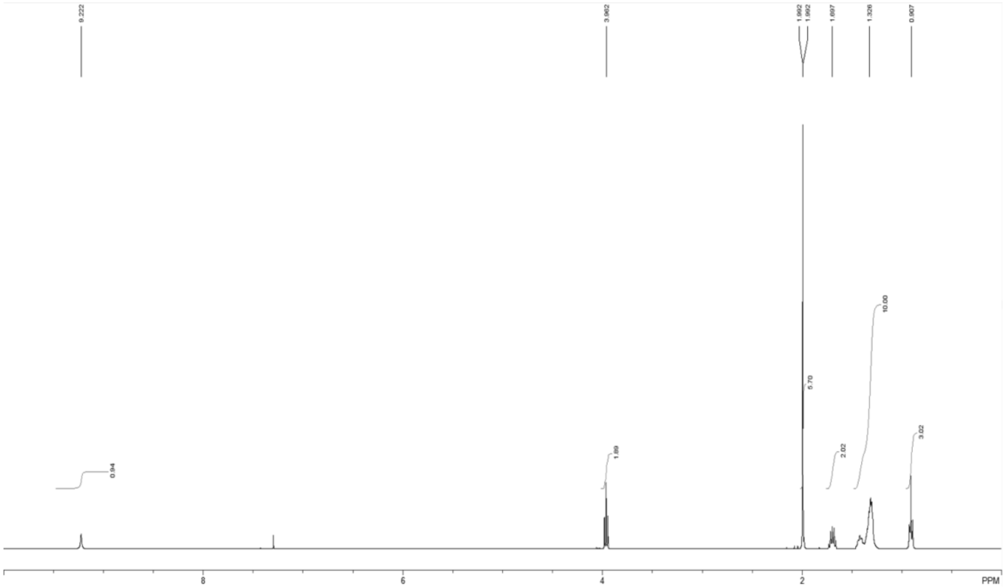

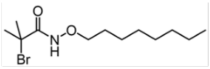

2.09a

^{13}C-NMR (CDCl$_3$, 100 MHz)

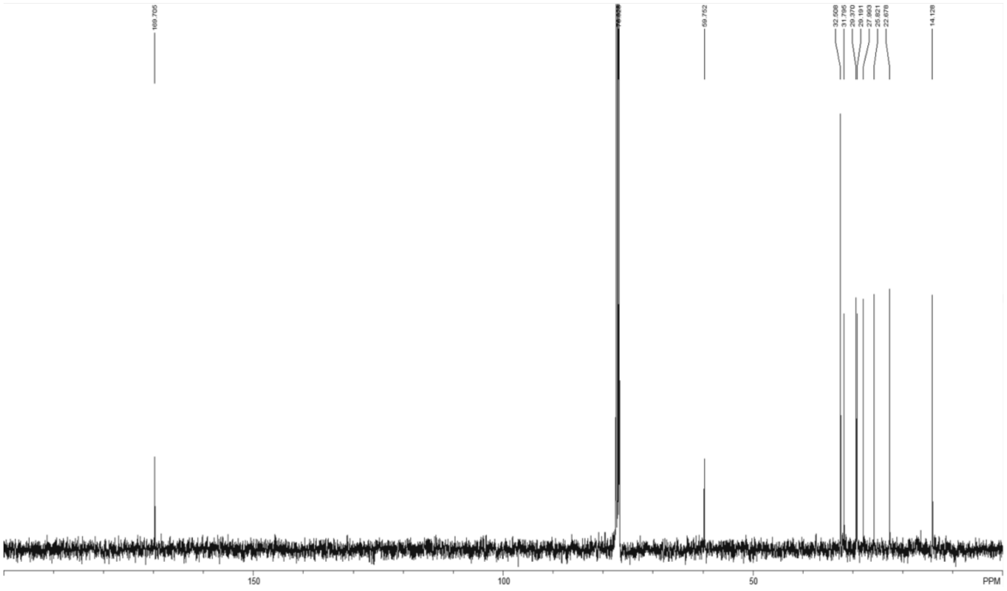

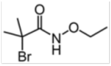

2.09c
^{1}H-NMR (CDCl$_3$, 500 MHz)

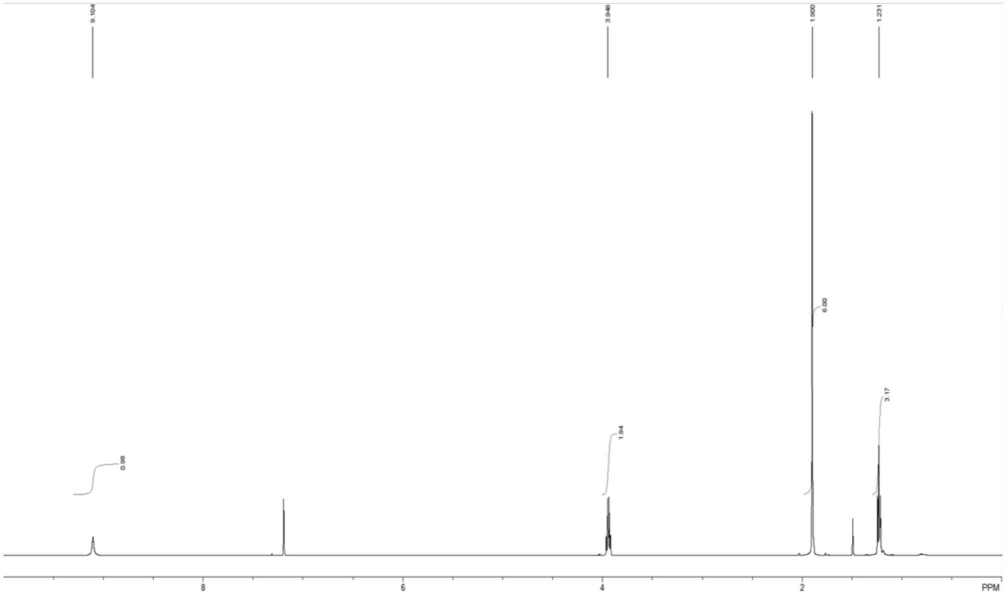

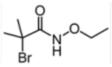

2.09c
^{13}C-NMR (CDCl$_3$, 125 MHz)

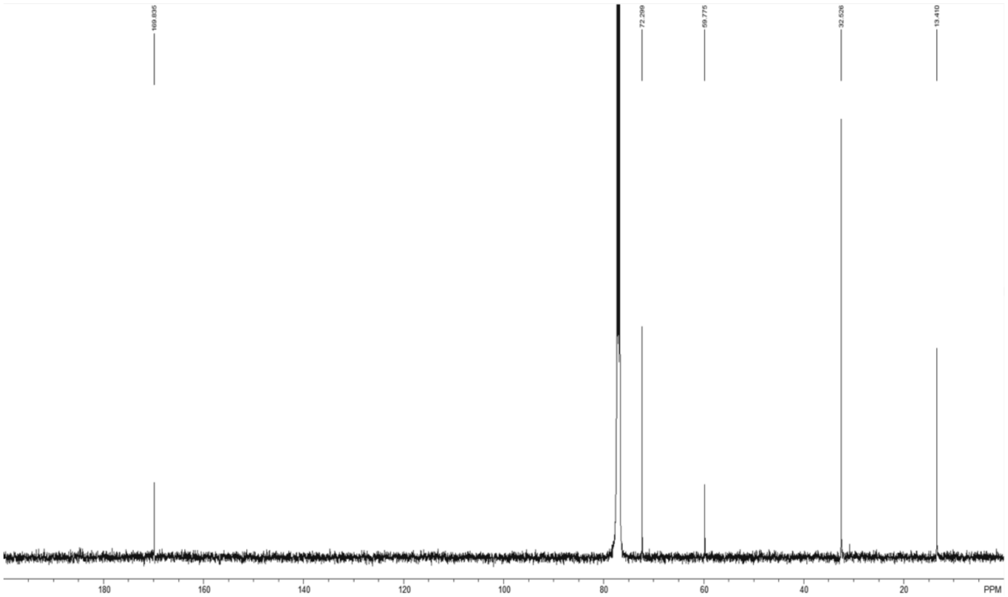

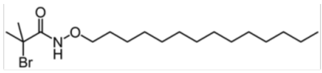

2.09d
^{1}H-NMR (CDCl$_3$, 500 MHz)

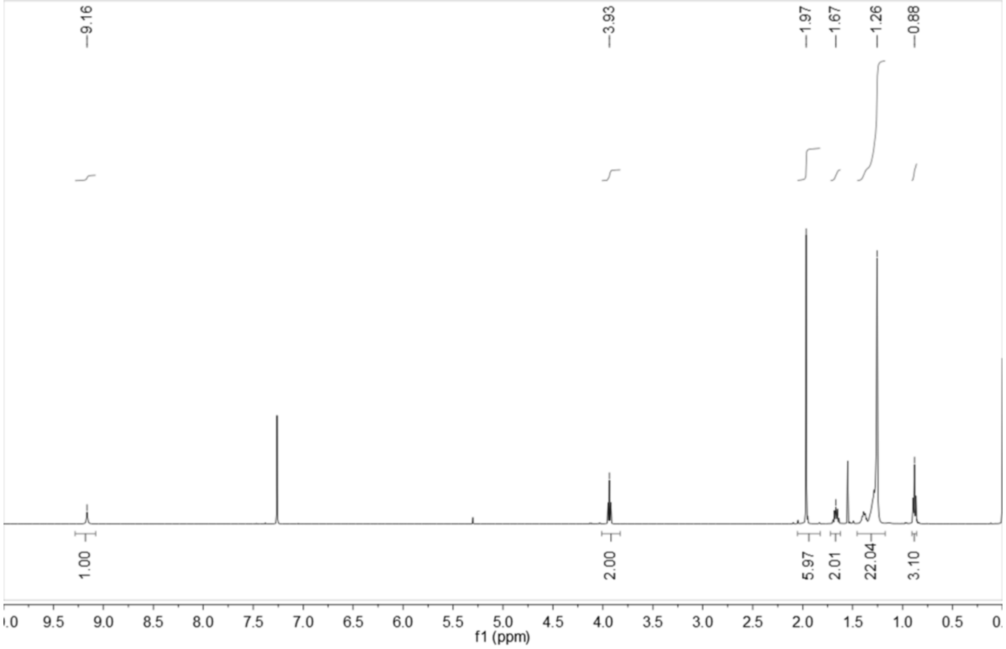

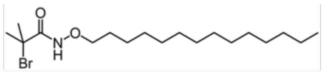

2.09d
^{13}C-NMR (CDCl$_3$, 125 MHz)

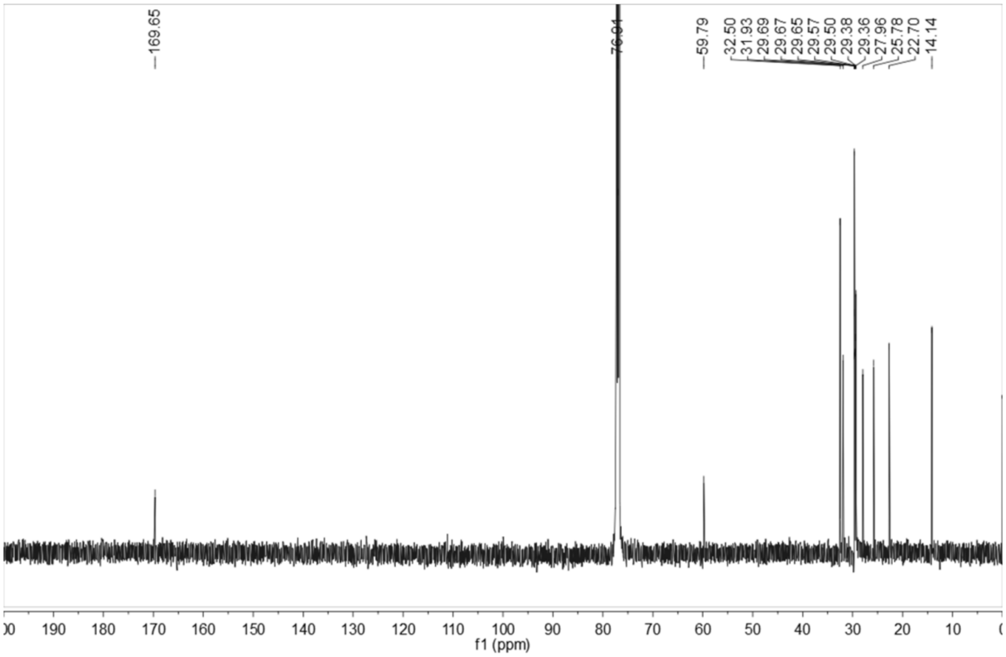

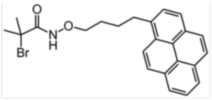

2.09e

^{1}H-NMR ($CDCl_3$, 300MHz)

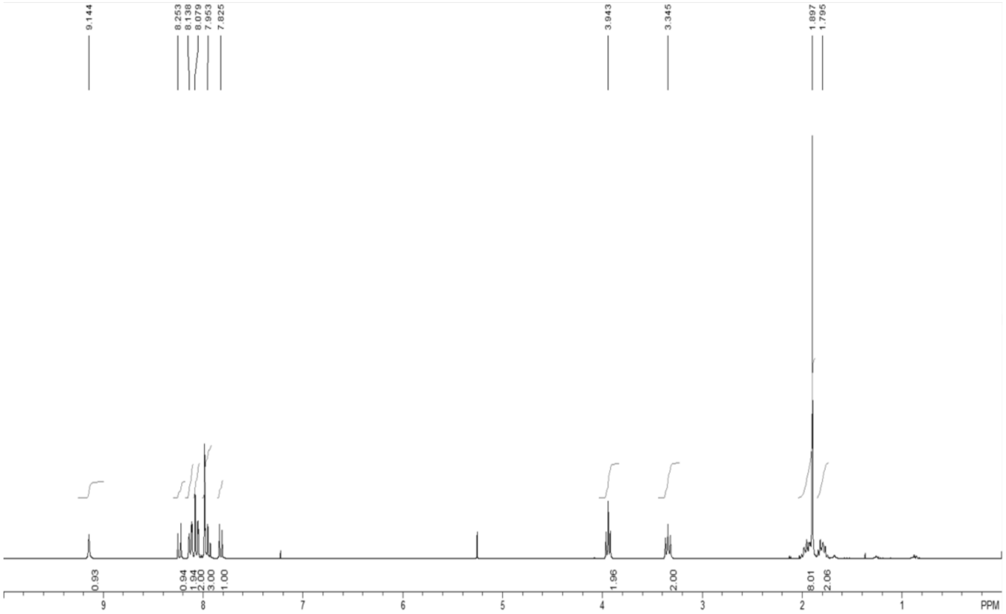

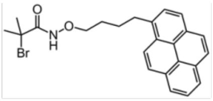

2.09e

^{13}C-NMR ($CDCl_3$, 75 MHz)

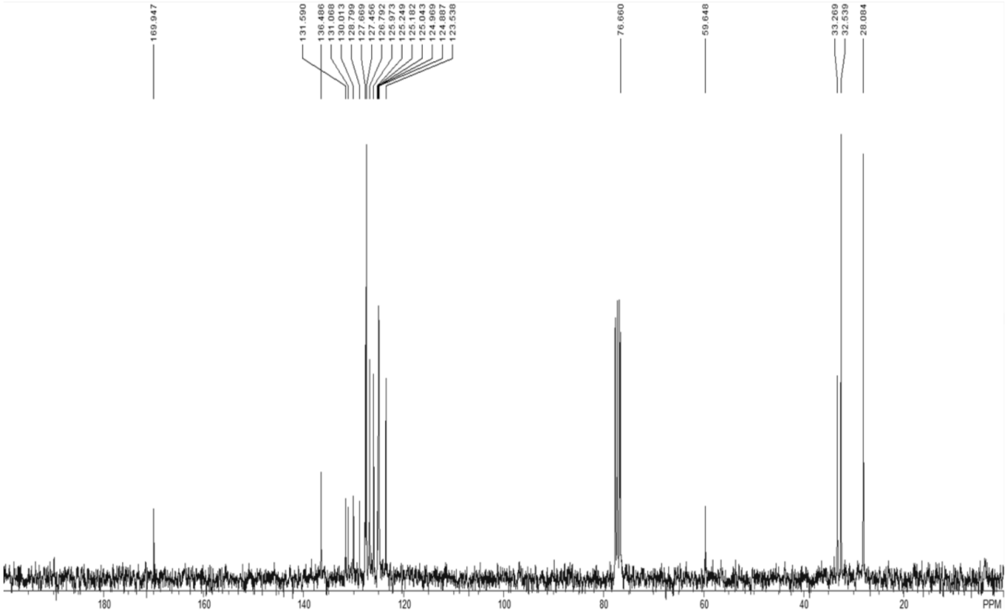

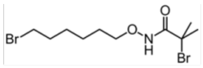

2.09f
^{1}H-NMR ($CDCl_3$, 300 MHz)

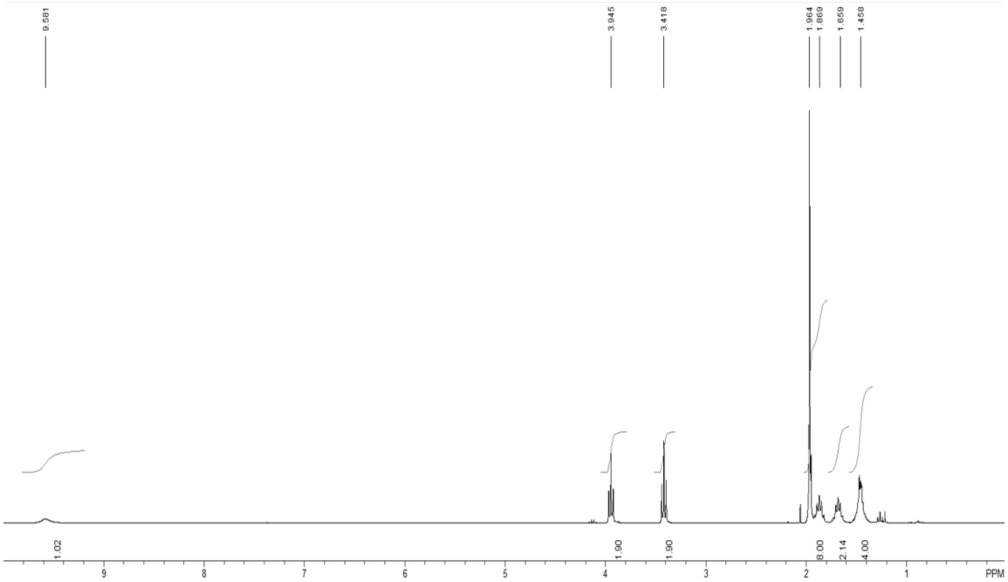

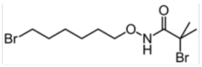

2.09f
^{13}C-NMR ($CDCl_3$, 75 MHz)

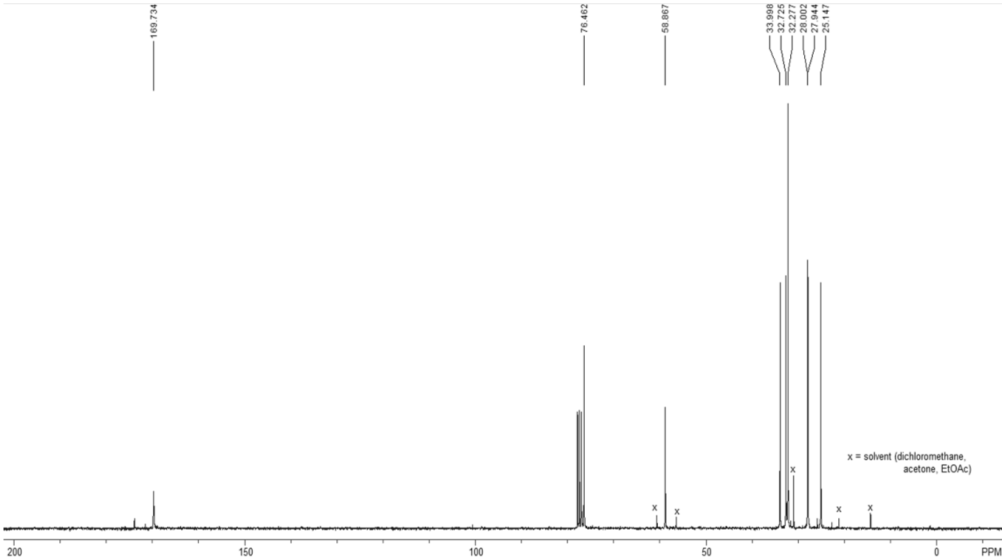

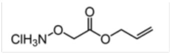

2.10
^{1}H-NMR (MeOH-d$_4$, 300 MHz)

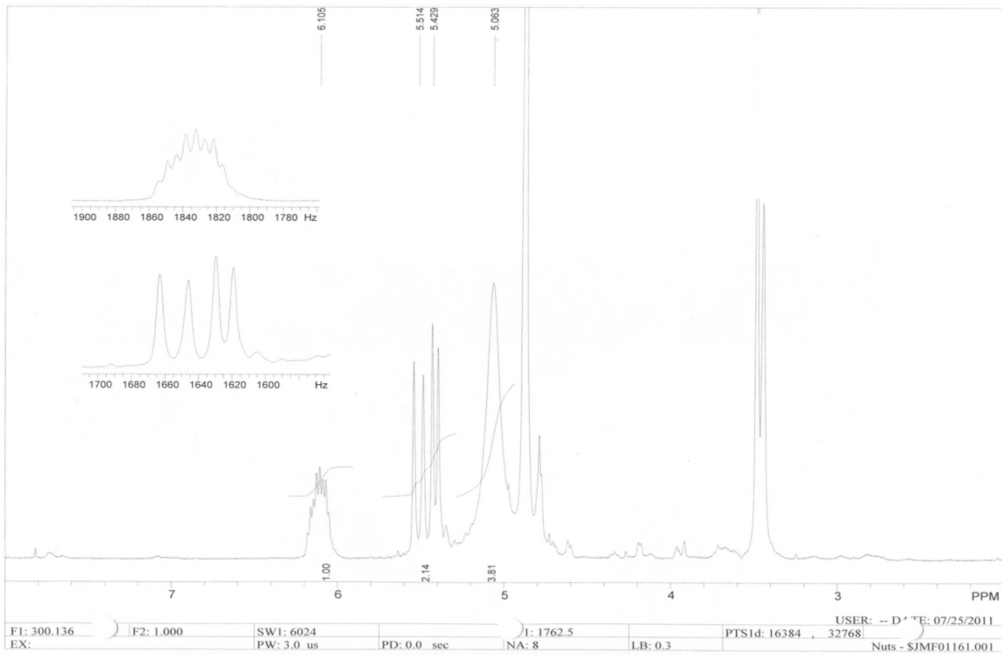

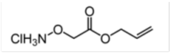

2.10
^{13}C-NMR (MeOH-d$_4$, 75 MHz)

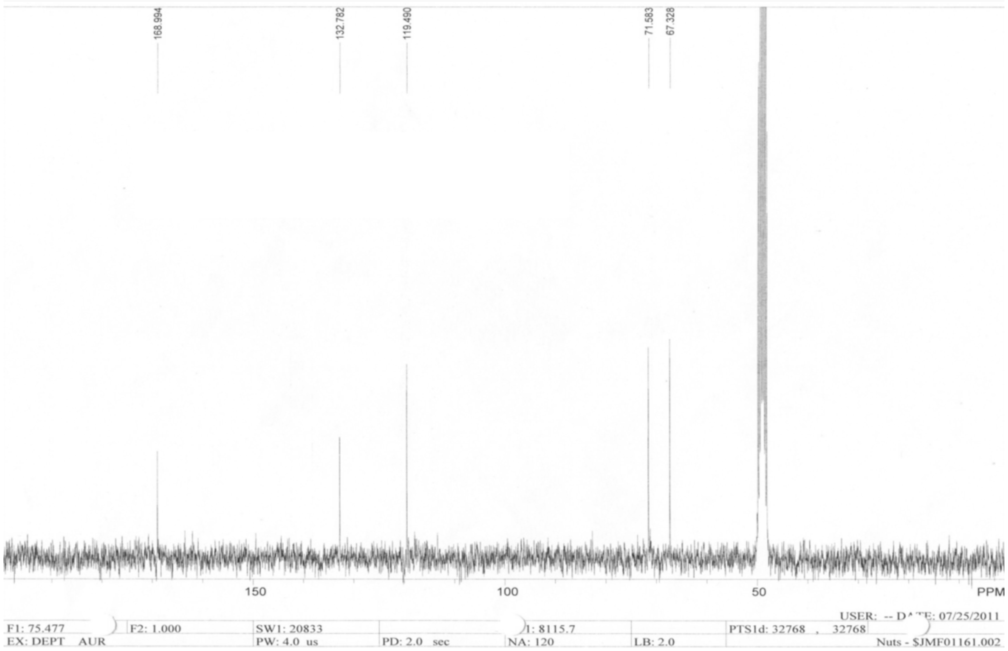

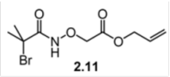

2.11

^{1}H-NMR (CDCl$_3$, 300 MHz)

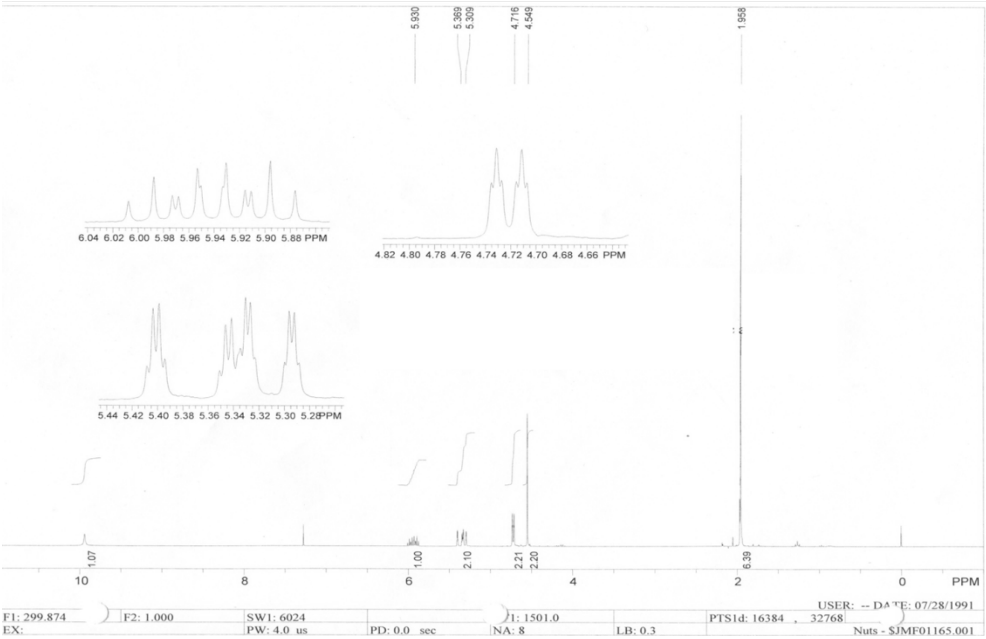

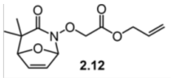

2.12

^{1}H-NMR (CDCl$_3$, 300 MHz)

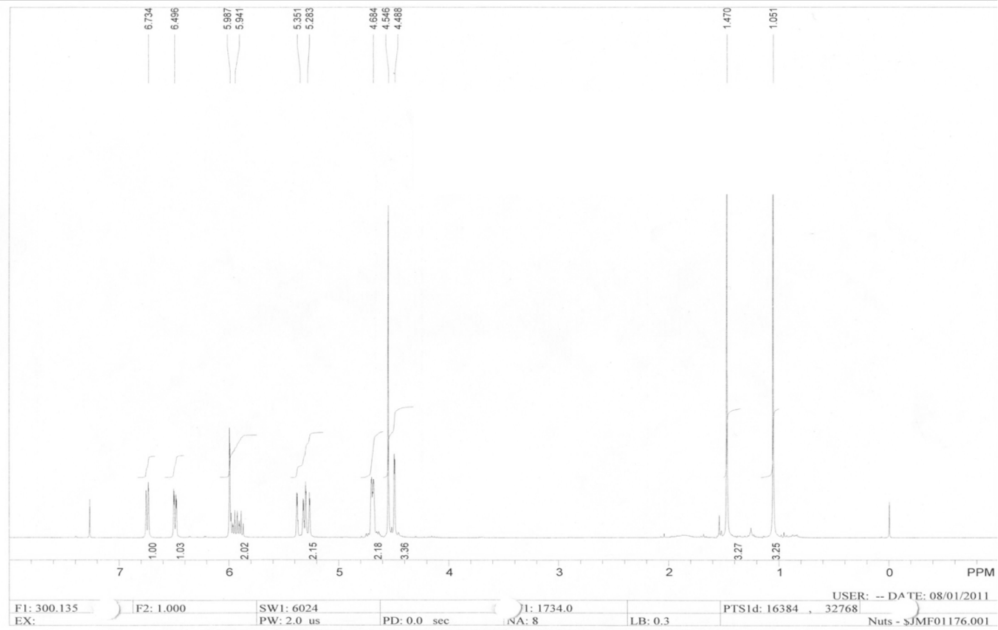

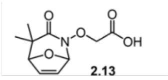

2.13

^{1}H-NMR (CDCl$_3$, 300 MHz)

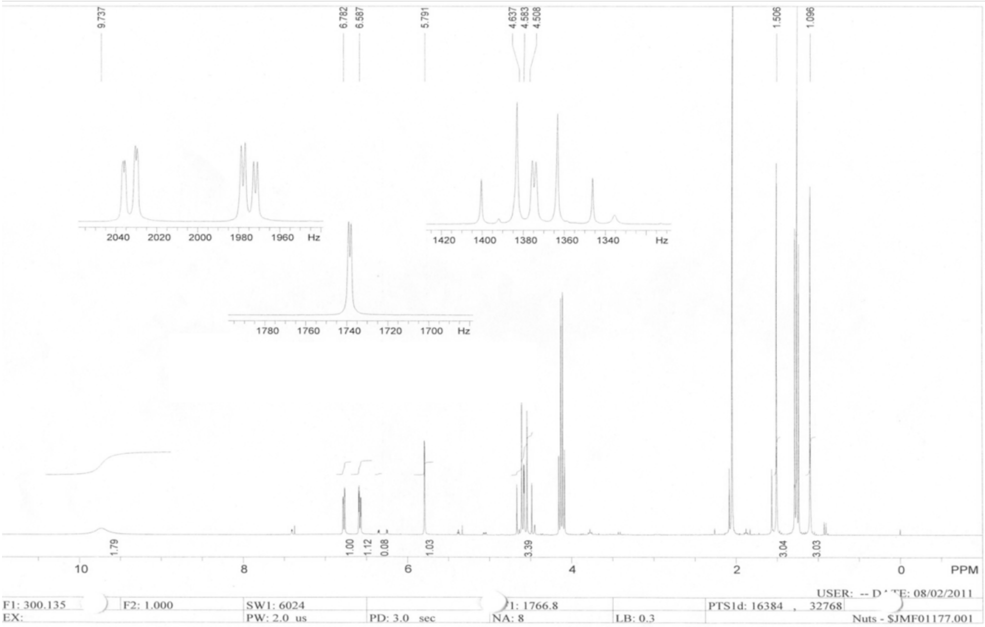

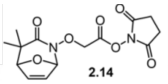

2.14

^{1}H-NMR (CDCl$_3$, 300 MHz)

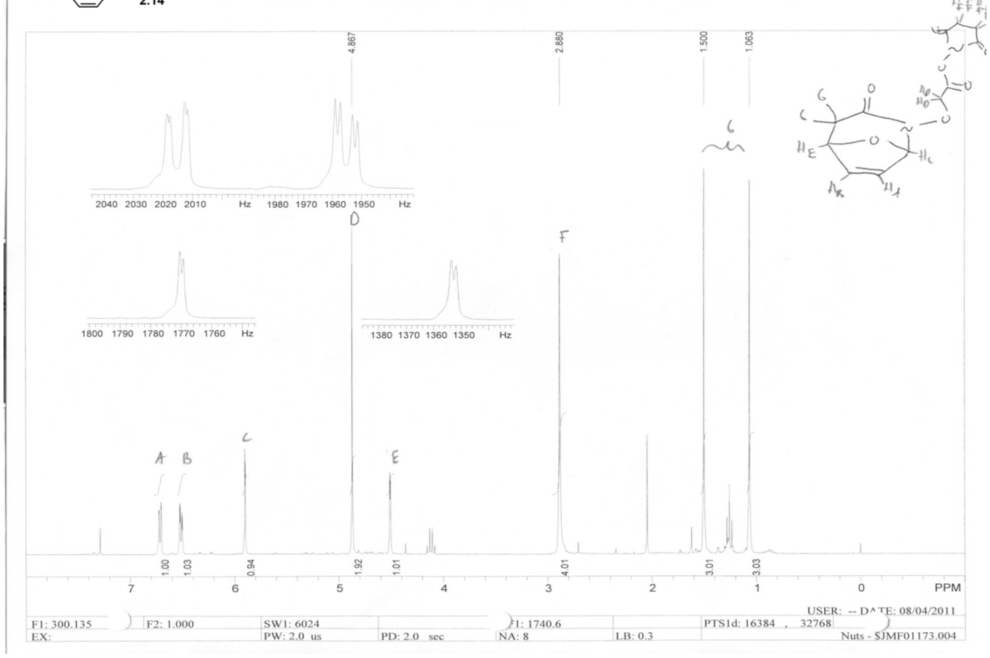

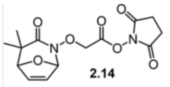

2.14

^{13}C-NMR (CDCl$_3$, 75 MHz)

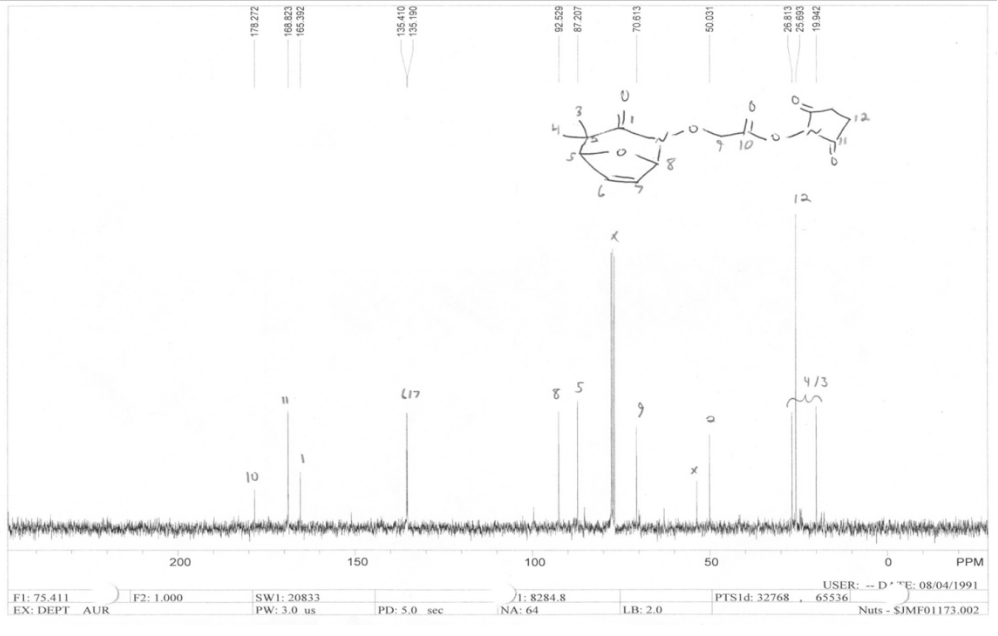

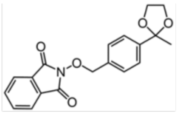

2.17

^{1}H-NMR (CDCl$_3$, 500 MHz)

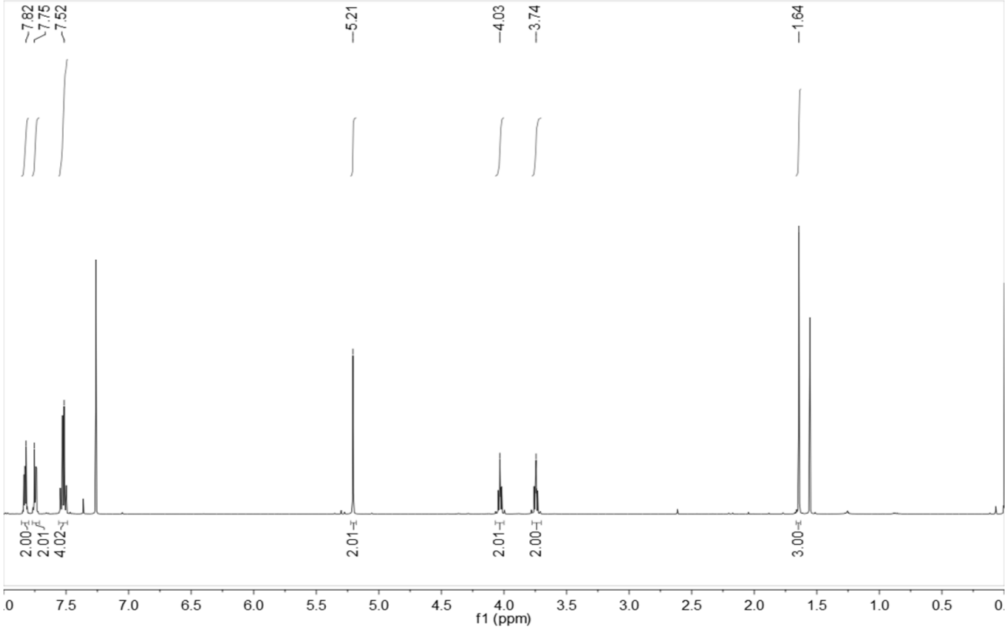

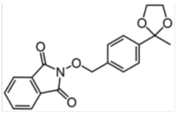

2.17

^{13}C-NMR (CDCl$_3$, 125 MHz)

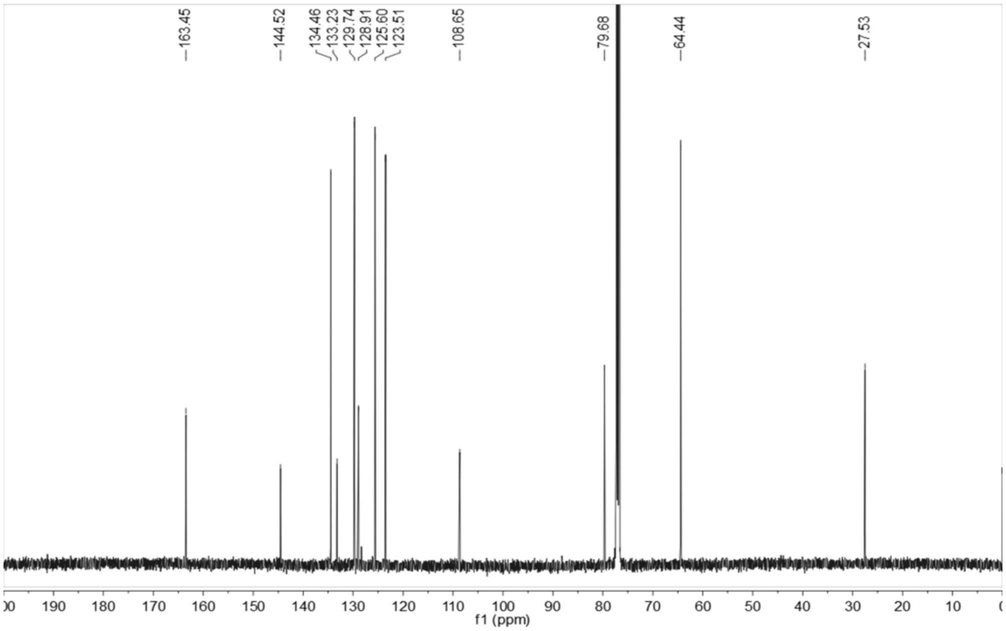

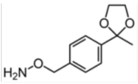

2.18
^{1}H-NMR ($CDCl_3$, 500 MHz)

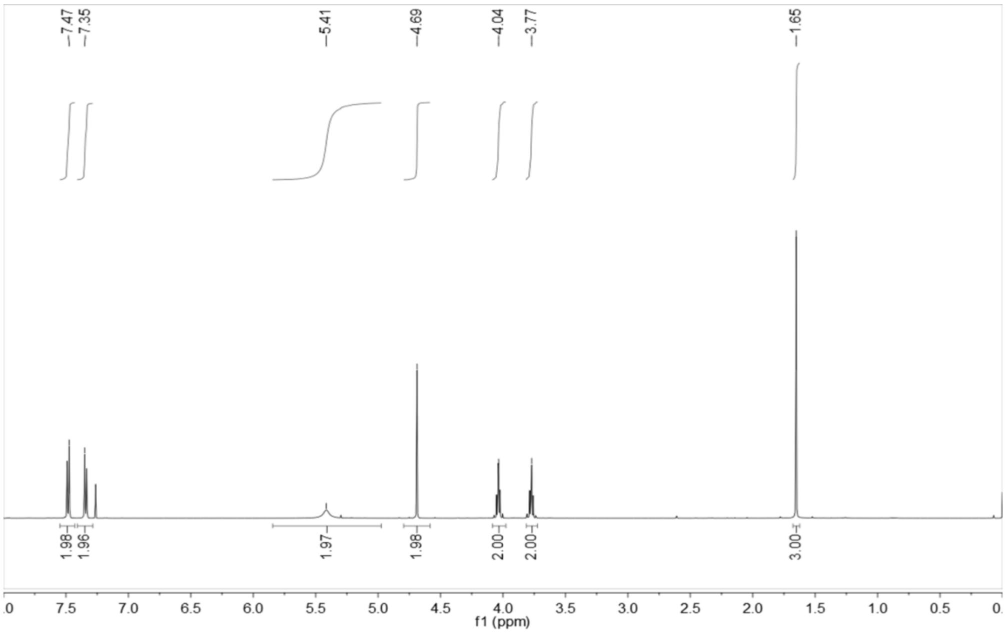

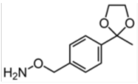

2.18
^{13}C-NMR ($CDCl_3$, 125 MHz)

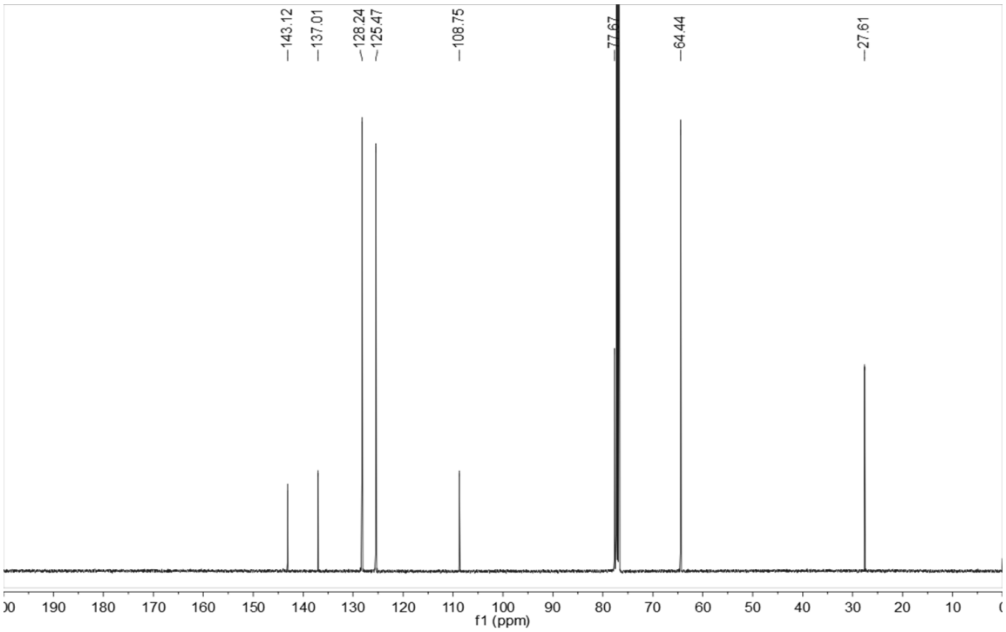

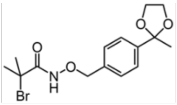

2.19
^{1}H-NMR (CDCl$_3$, 500 MHz)

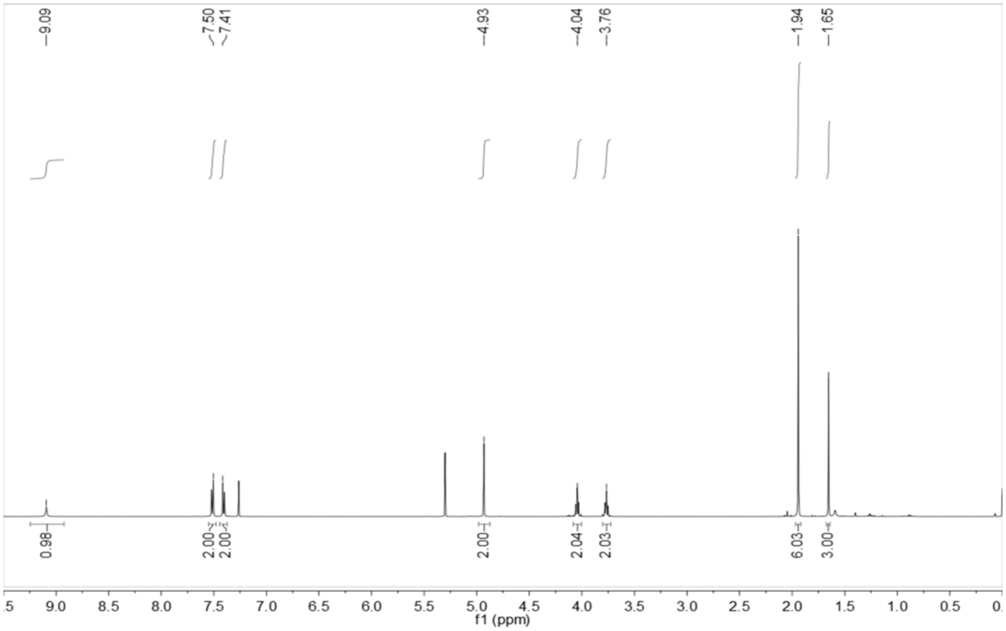

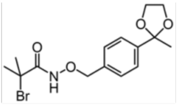

2.19
^{13}C-NMR (CDCl$_3$, 125 MHz)

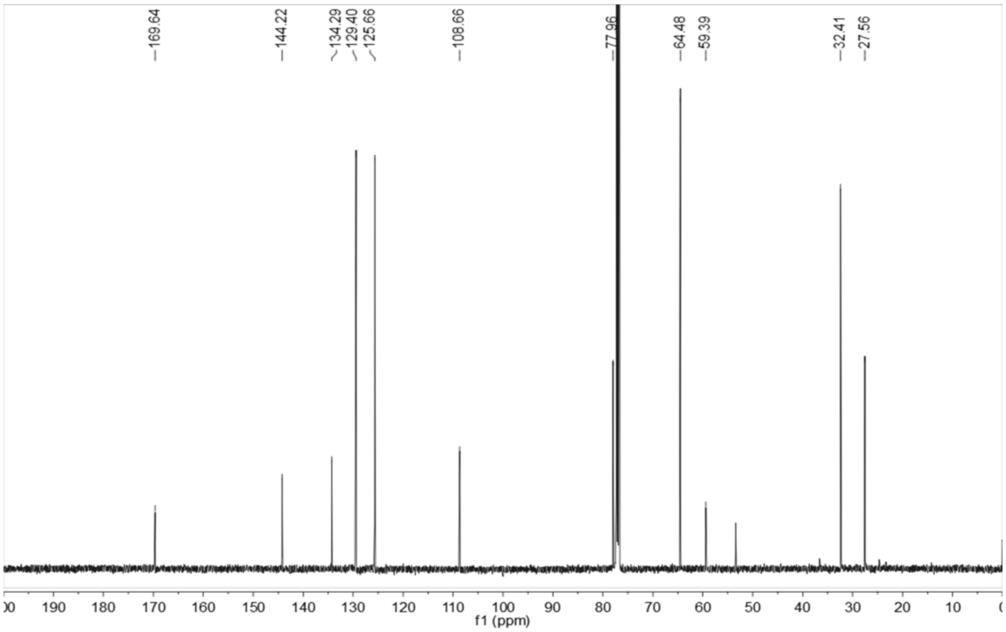

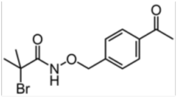

2.20
^{1}H-NMR (CDCl$_3$, 500 MHz)

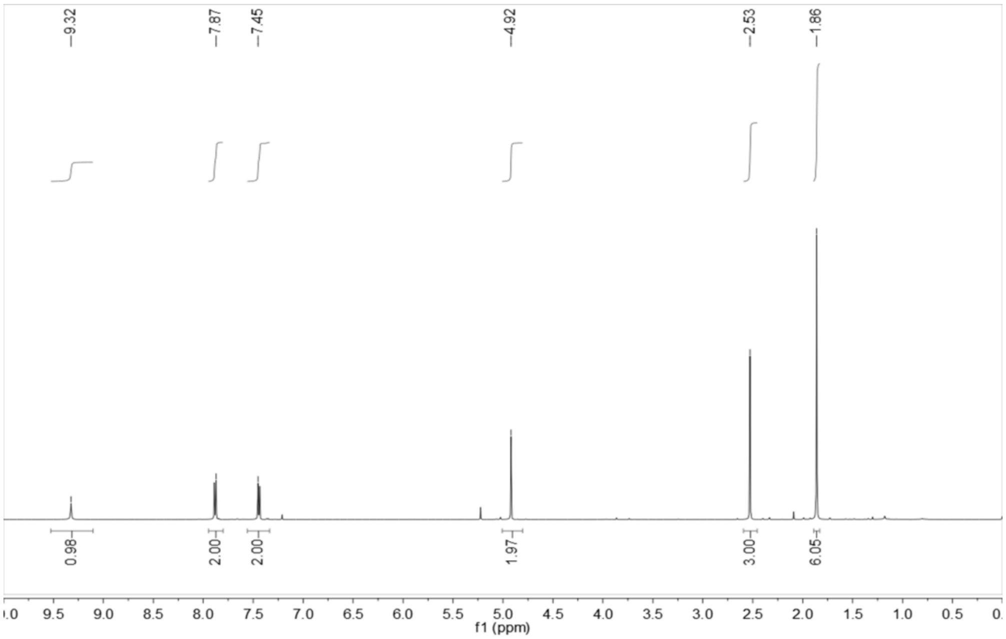

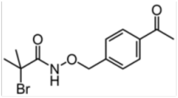

2.20
^{13}C-NMR (CDCl$_3$, 125 MHz)

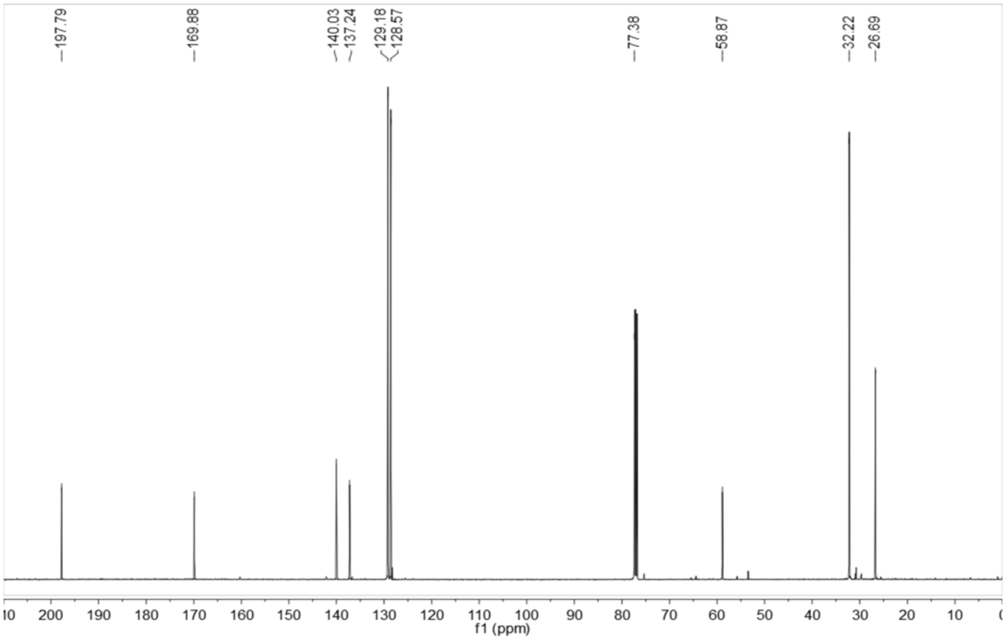

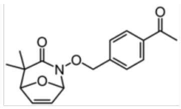

2.21
^{1}H-NMR ($CDCl_3$, 500 MHz)

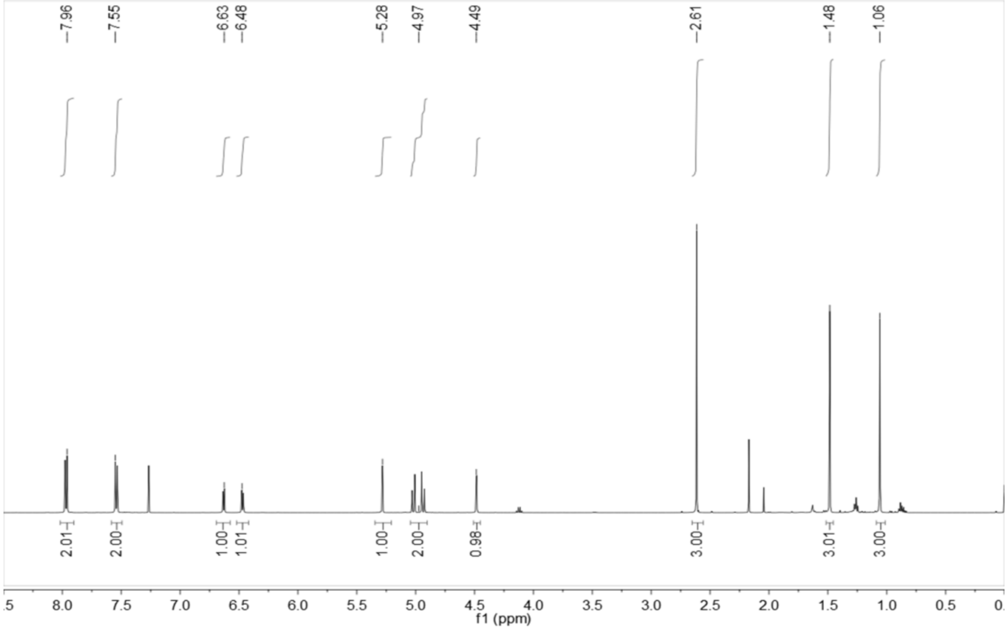

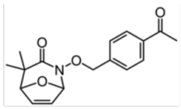

2.21
^{13}C-NMR ($CDCl_3$, 125 MHz)

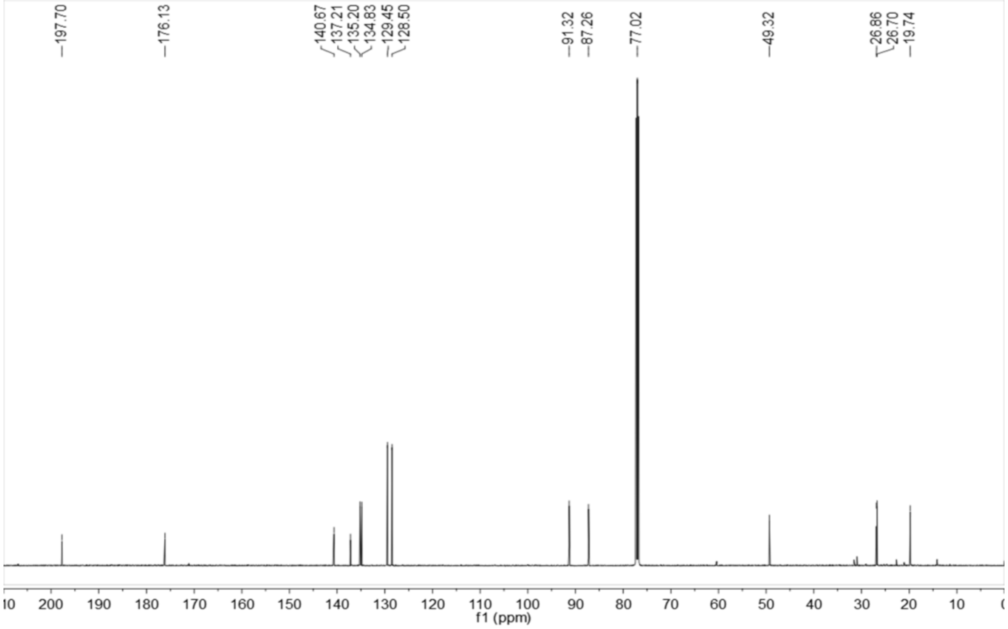

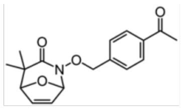

2.21
DEPT135 ($CDCl_3$, 125 MHz)

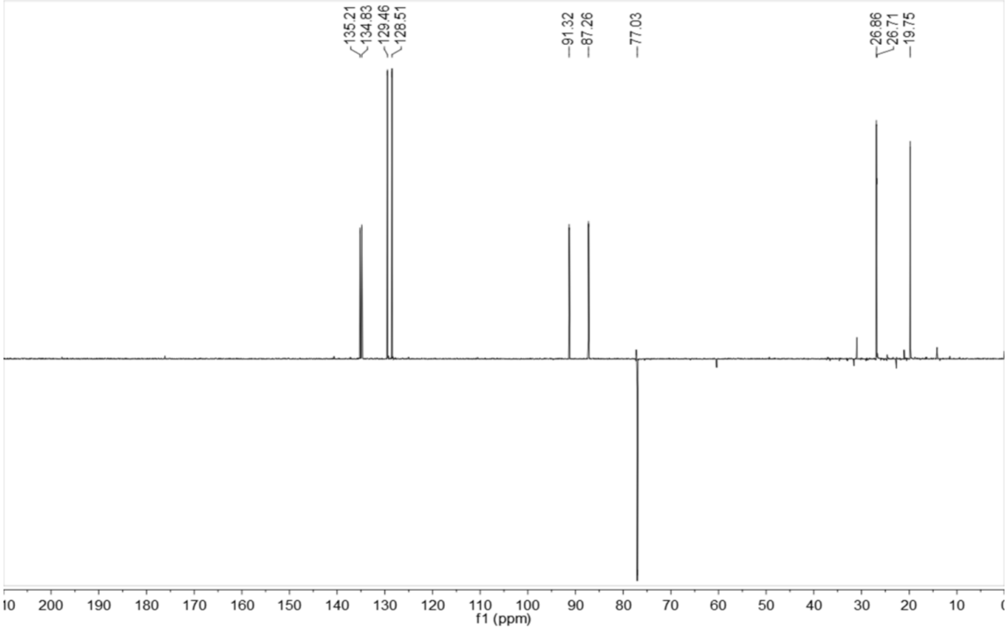

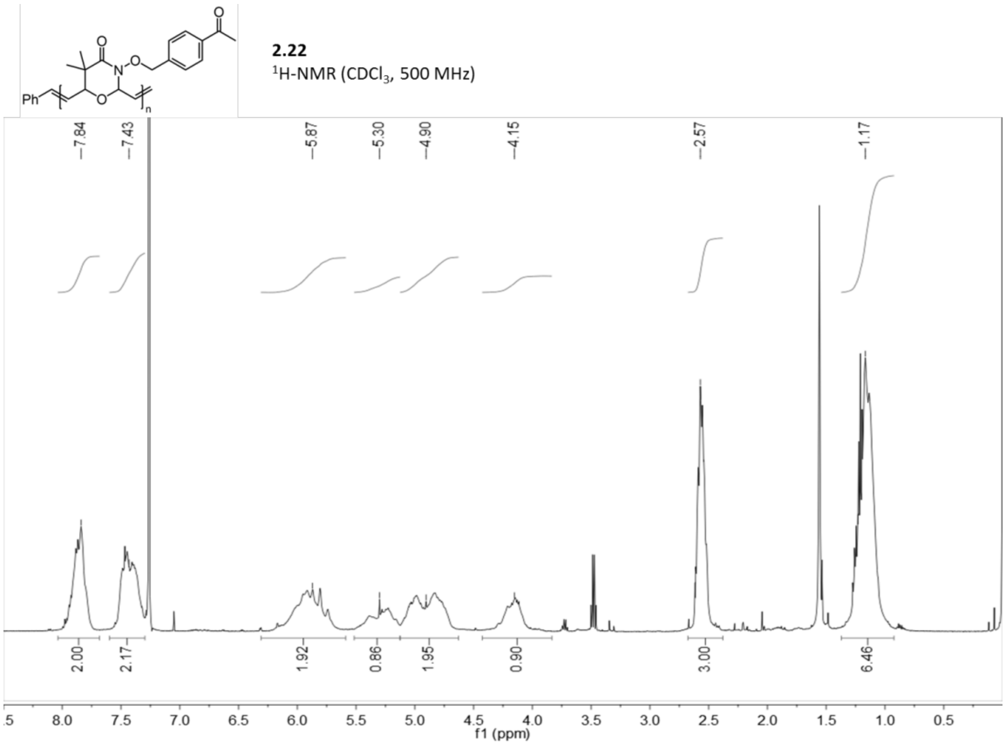

2.22

^{1}H-NMR ($CDCl_3$, 500 MHz)

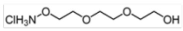
ClH3N
O
O
O
OH

2.23
^{1}H-NMR (MeOH-d_4, 500 MHz)

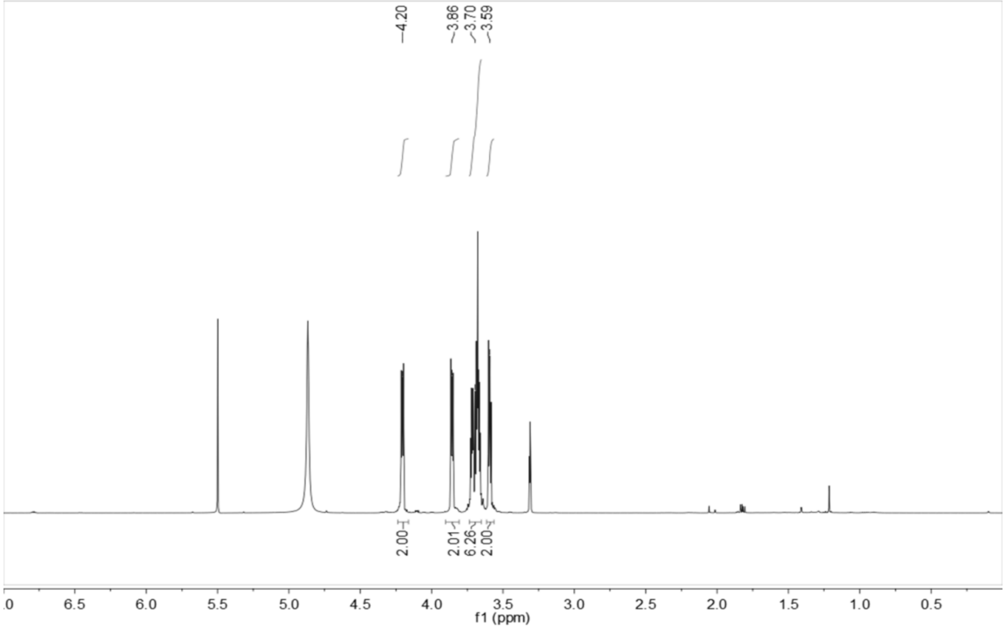

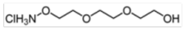
ClH3N
O
O
O
OH

2.23
^{13}C-NMR (CDCl$_3$, 125 MHz)

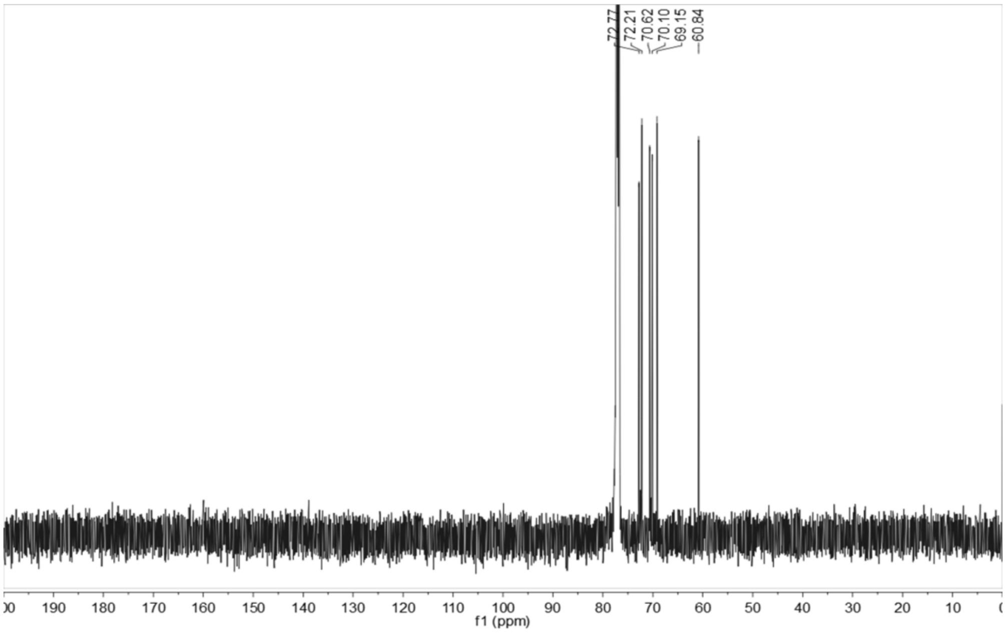

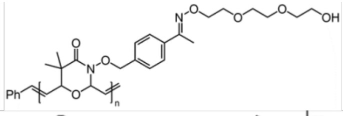

2.24
^{1}H-NMR (MeOH-d_4, 500 MHz)

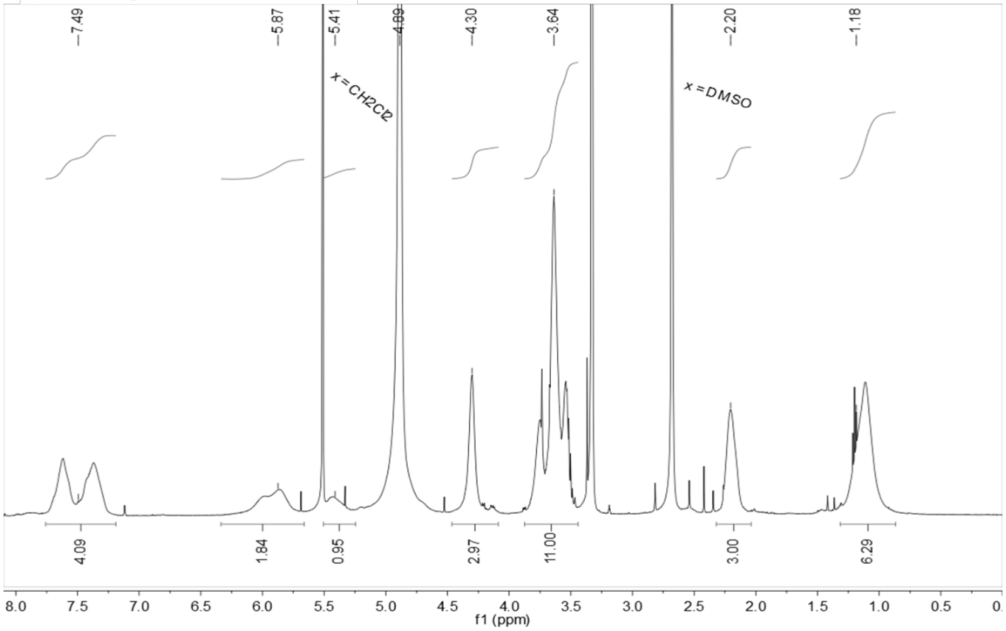

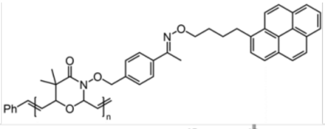

2.25
^{1}H-NMR (CDCl$_3$, 500 MHz)

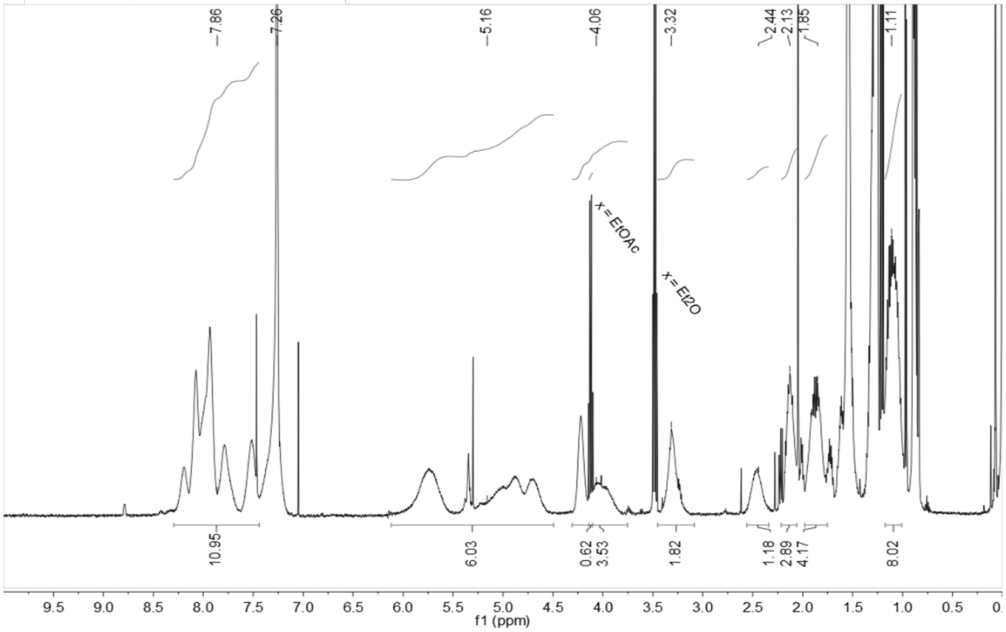

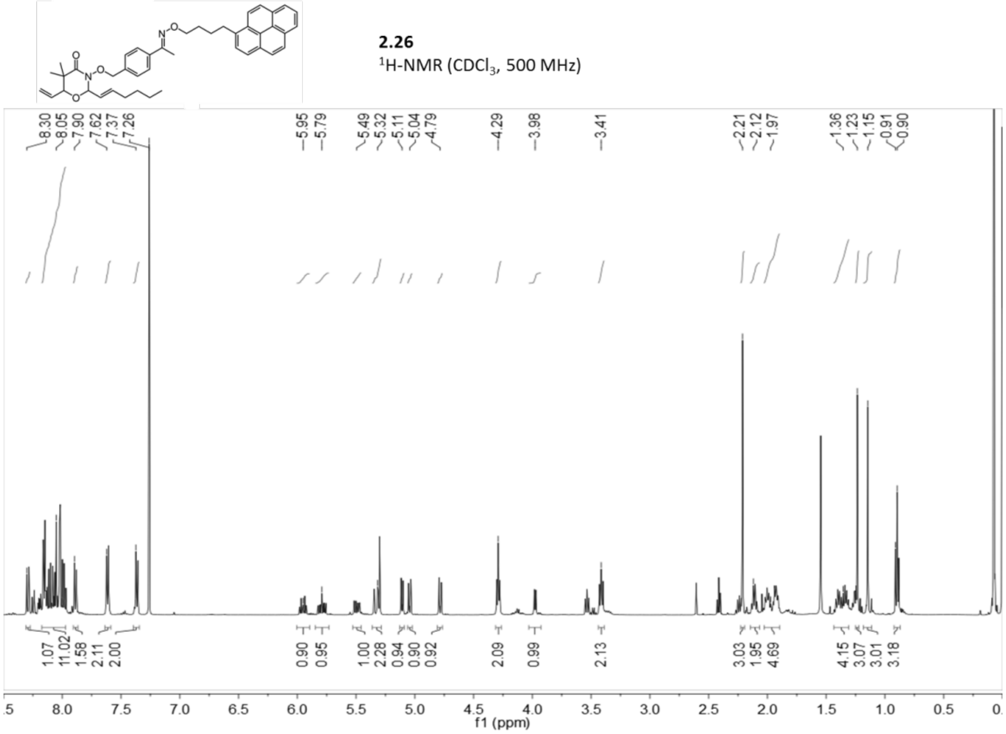

2.26

^{1}H-NMR (CDCl$_3$, 500 MHz)

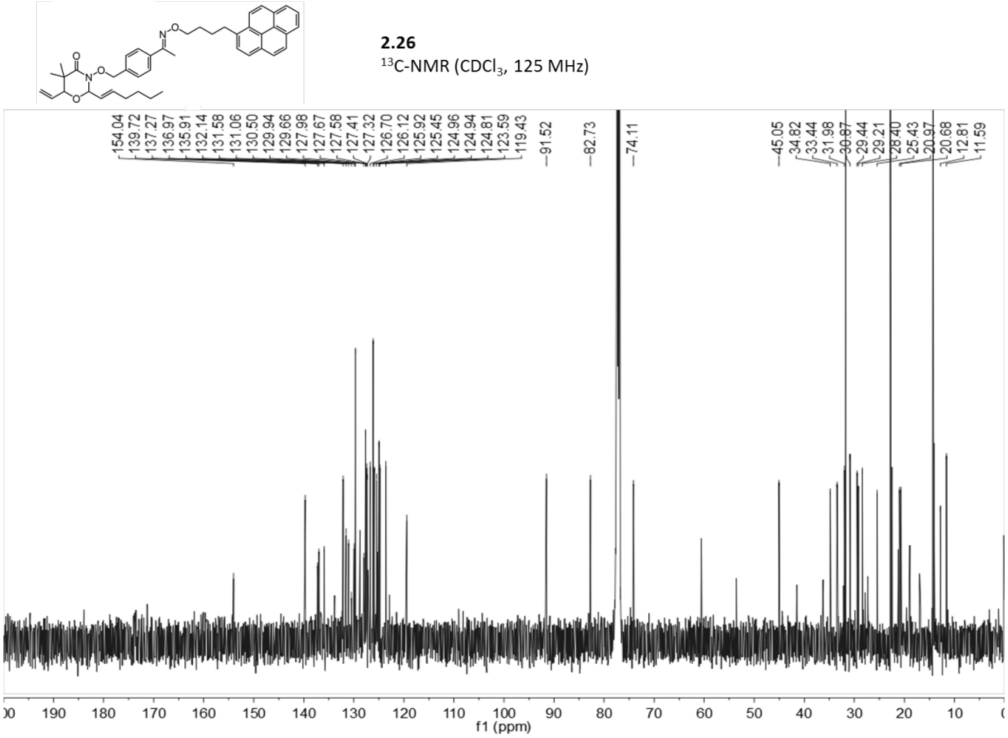

2.26

^{13}C-NMR (CDCl$_3$, 125 MHz)

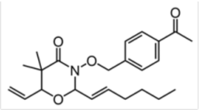

2.27
^{1}H-NMR ($CDCl_3$, 400 MHz)

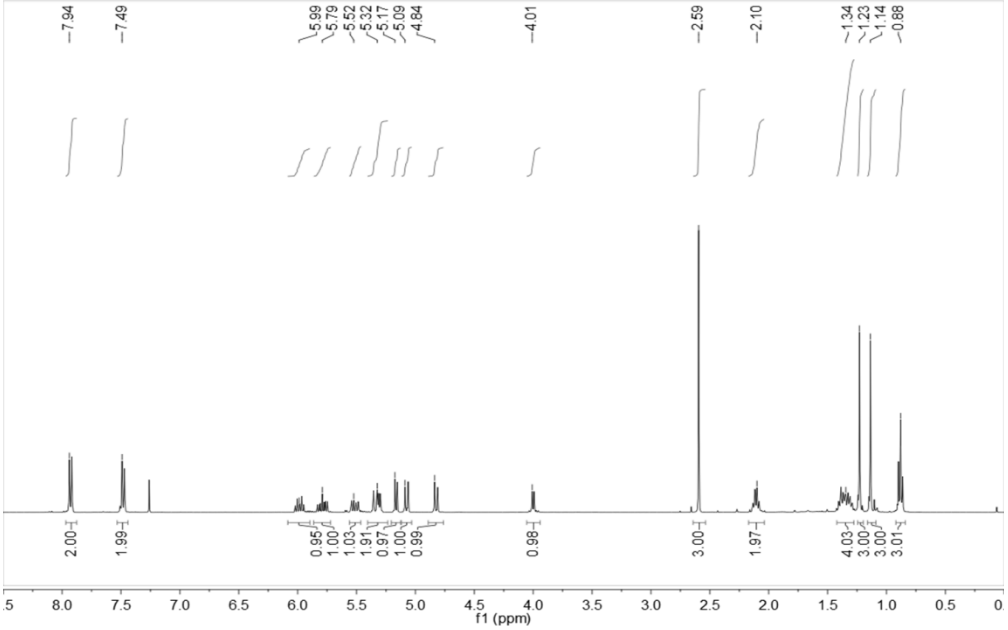

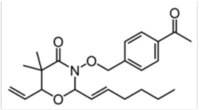

2.27
^{13}C-NMR ($CDCl_3$, 100 MHz)

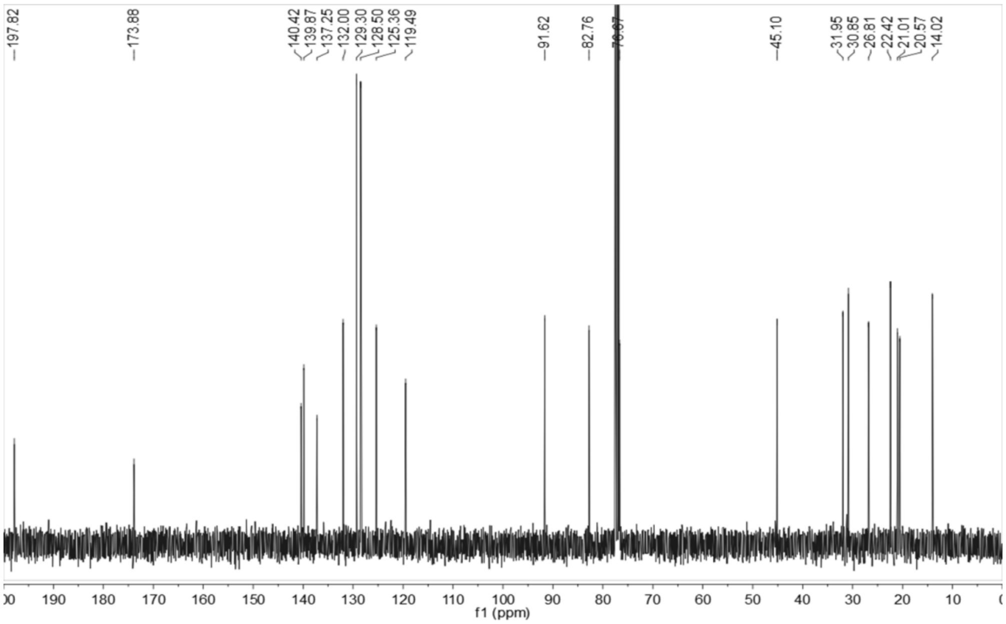

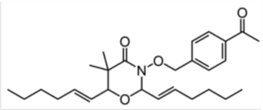

2.27’

^{1}H-NMR (CDCl$_3$, 400 MHz)

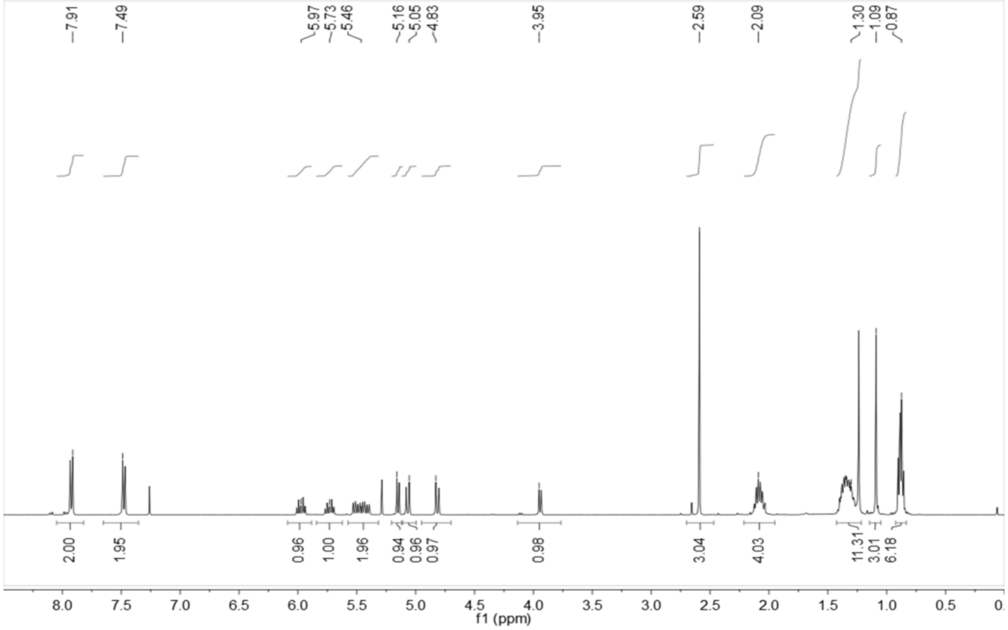

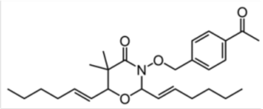

2.27’

^{1}H-NMR (CDCl$_3$, 400 MHz)

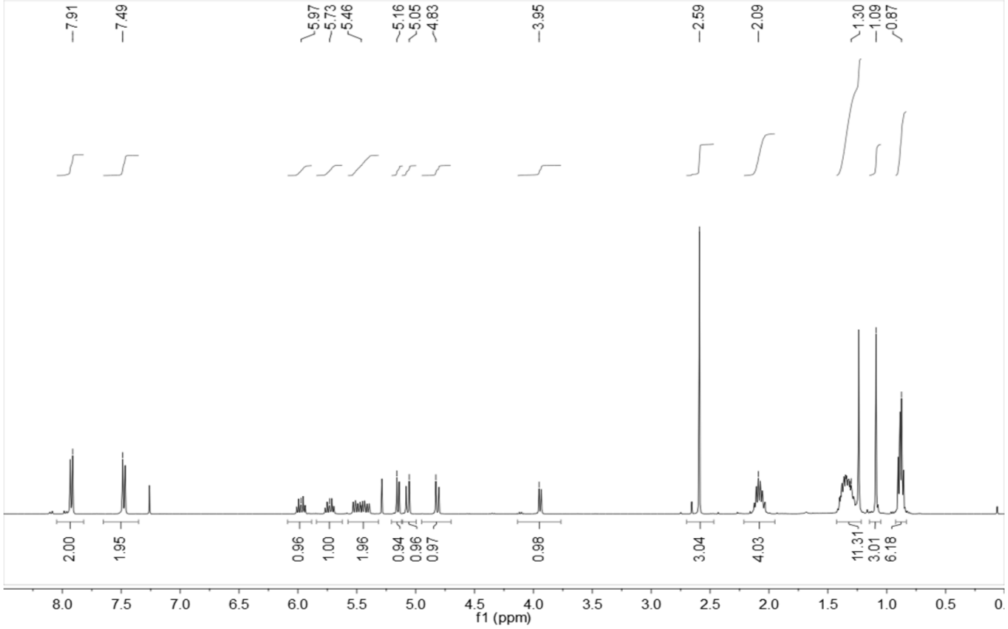

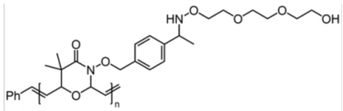
HN
O
O
O
OH
O
N
O
O
Ph
n

2.28
^{1}H-NMR ($CDCl_3$, 500 MHz)

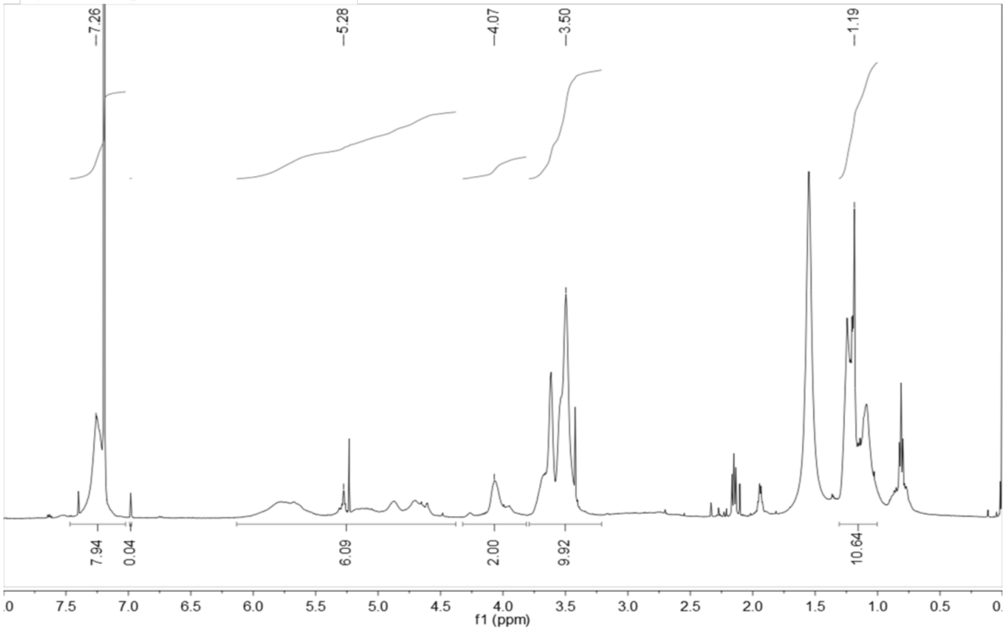

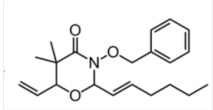

2.30
^{1}H-NMR ($CDCl_3$, 300 MHz)

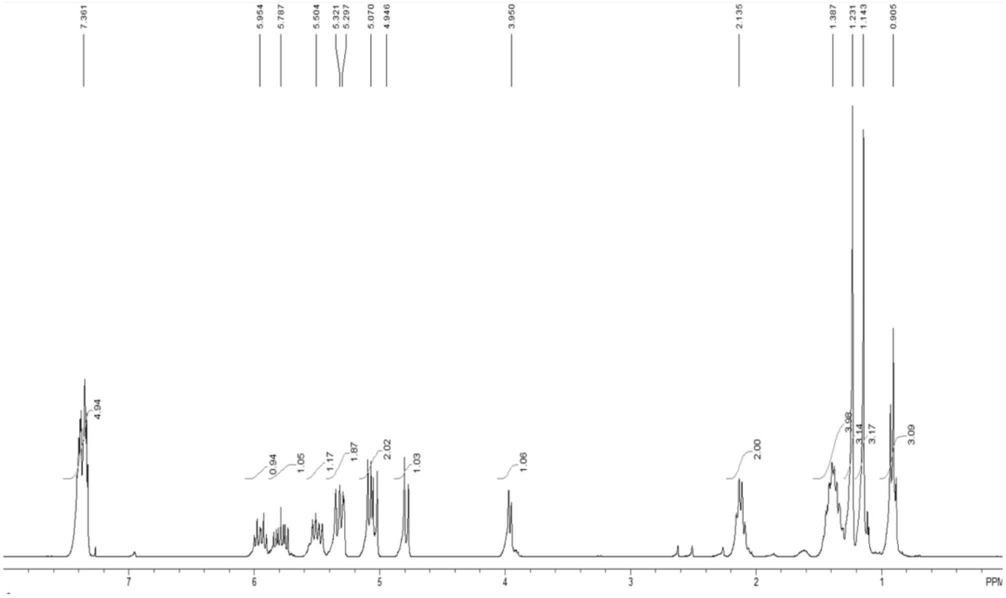

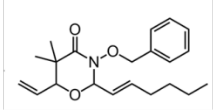

2.30
^{13}C-NMR ($CDCl_3$, 75 MHz)

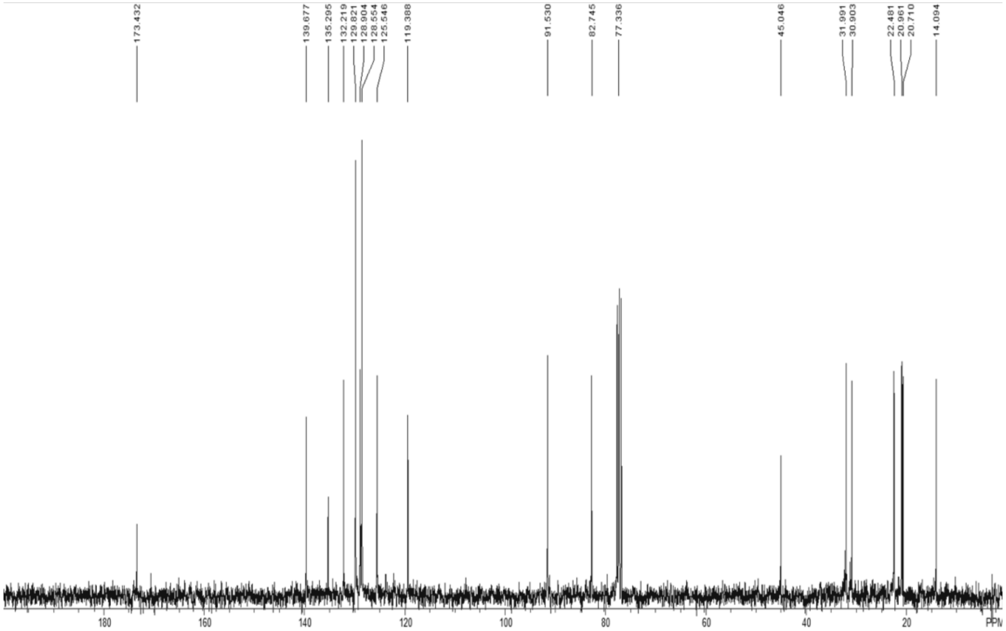

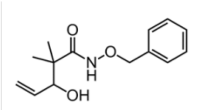

2.31
^{1}H-NMR (CDCl$_3$, 500 MHz)

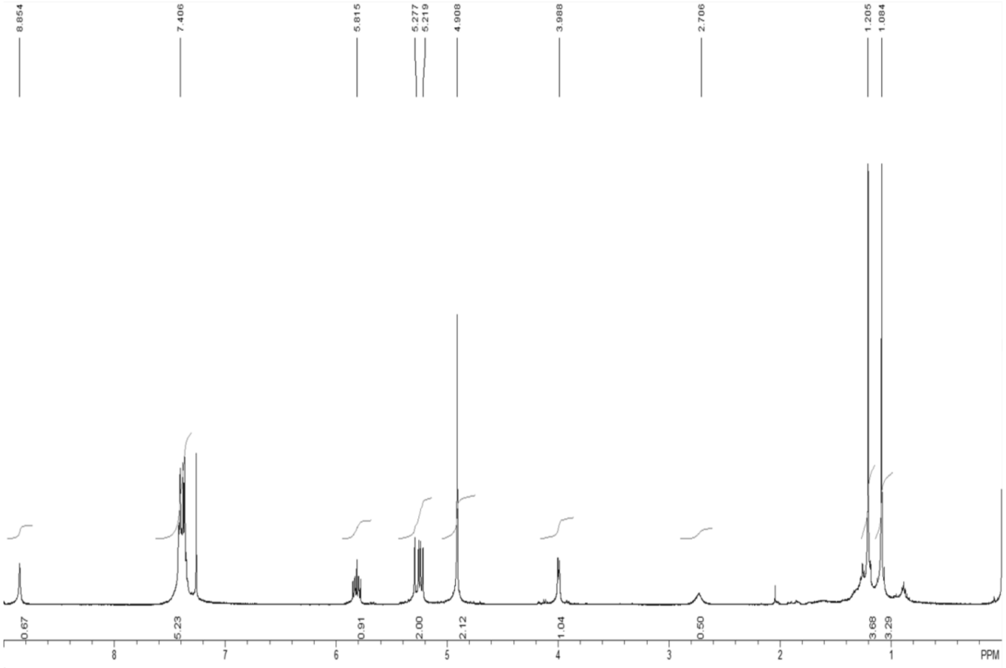

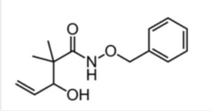

2.31
^{13}C-NMR (CDCl$_3$, 125 MHz)

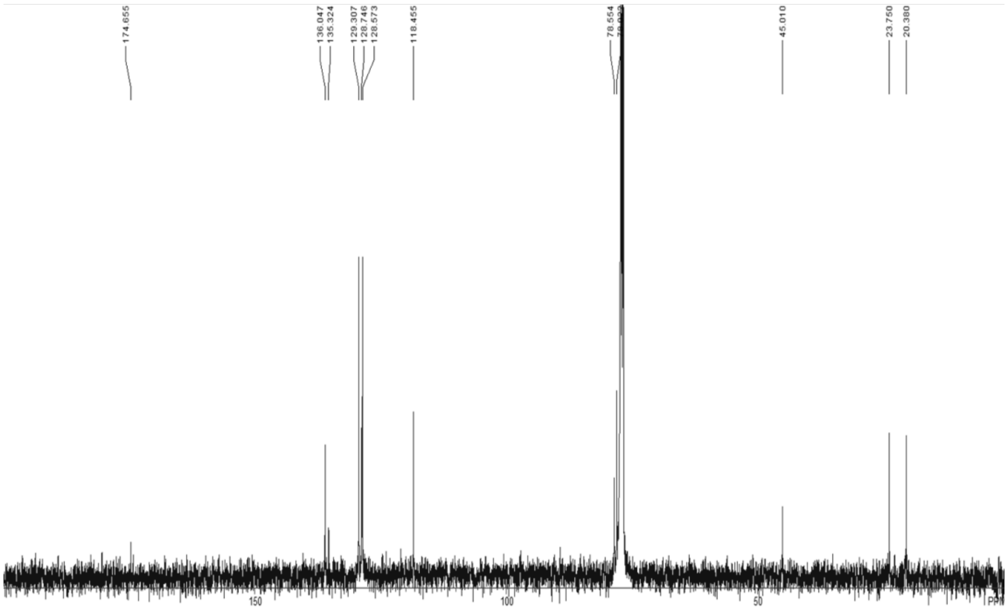

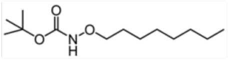

2.32a
^{1}H-NMR (CDCl$_3$, 500 MHz)

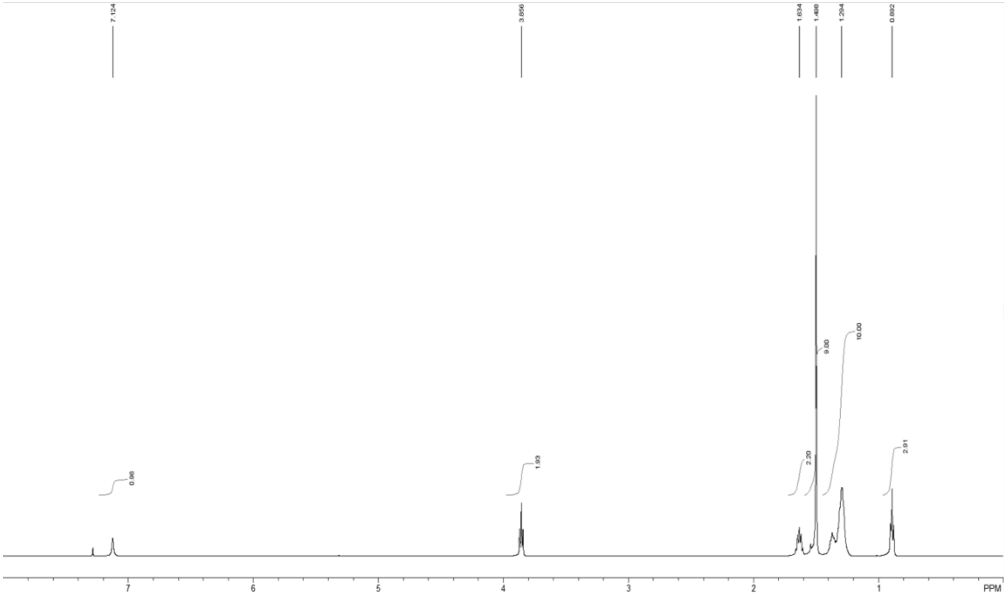

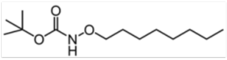

2.32a
^{13}C-NMR (CDCl$_3$, 125 MHz)

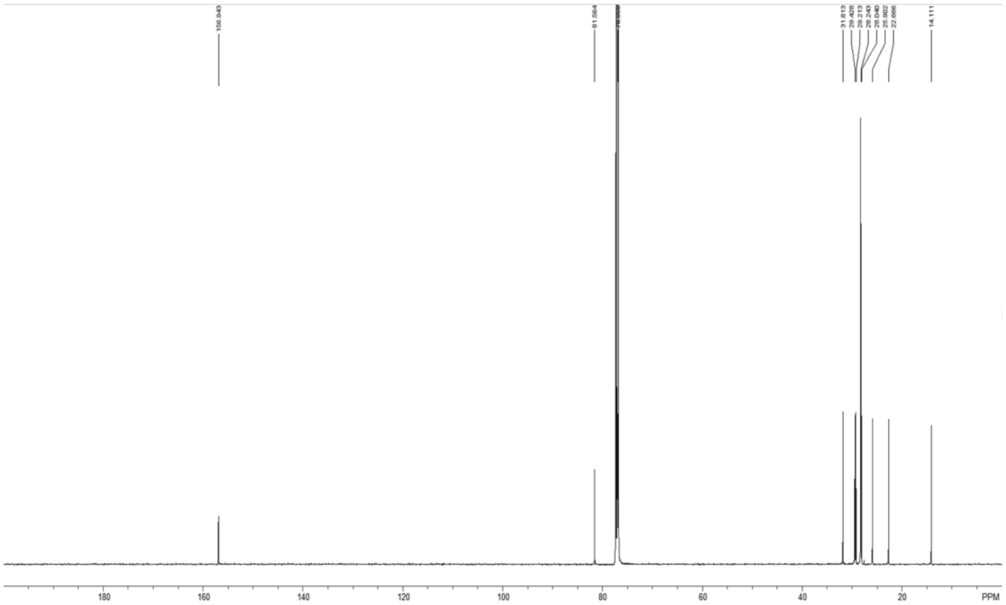

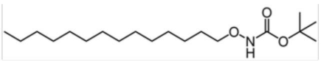

2.32d
^{1}H-NMR ($CDCl_3$, 500 MHz)

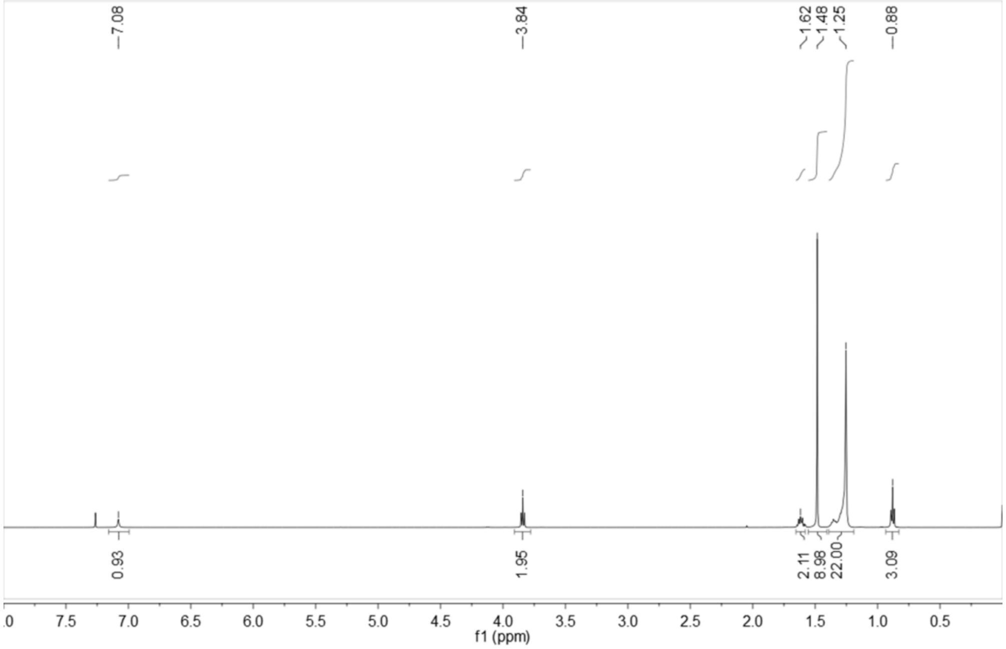

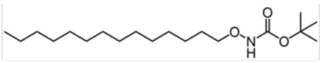

2.32d
^{13}C-NMR ($CDCl_3$, 125 MHz)

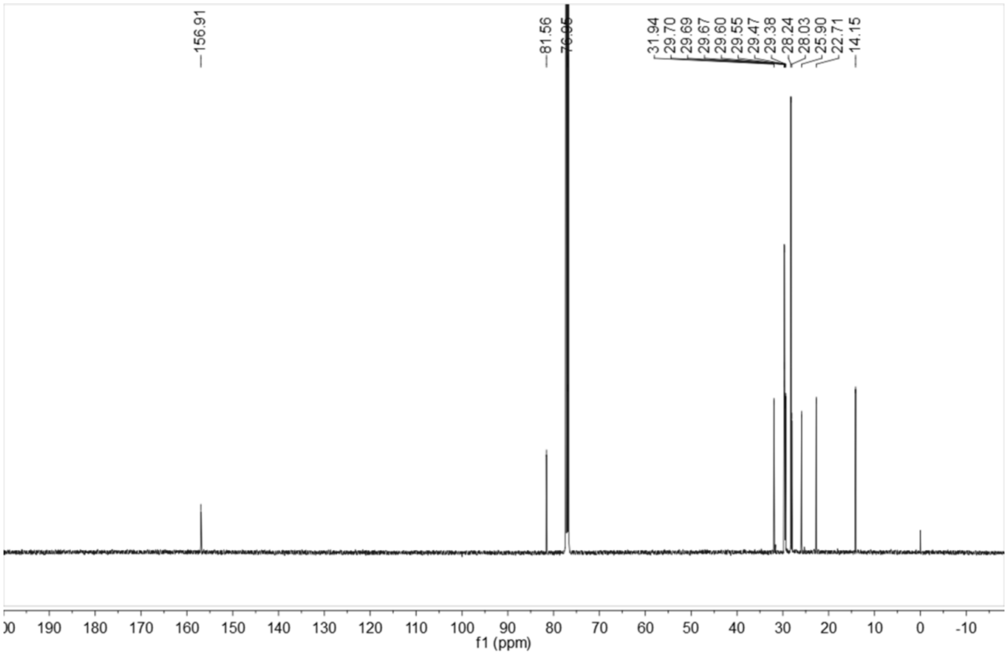

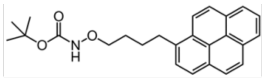

2.32e
^{1}H-NMR (CDCl$_3$, 300 MHz)

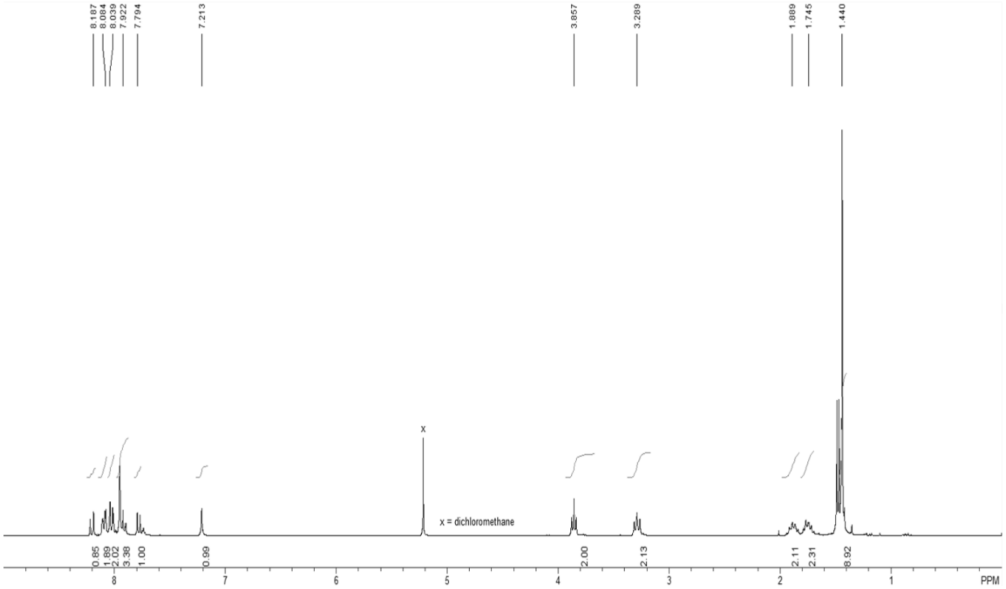

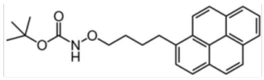

2.32e
^{13}C-NMR (CDCl$_3$, 75 MHz)

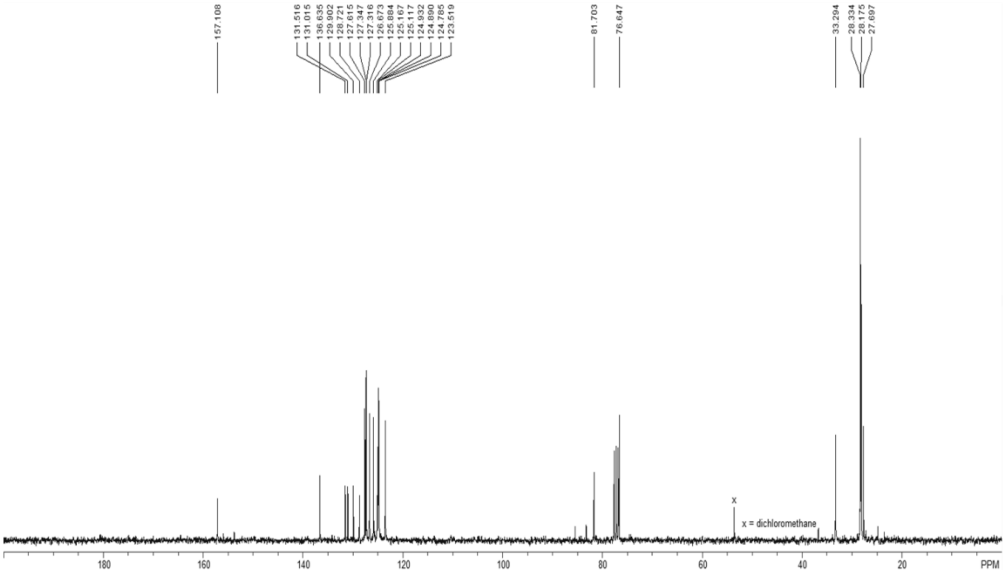

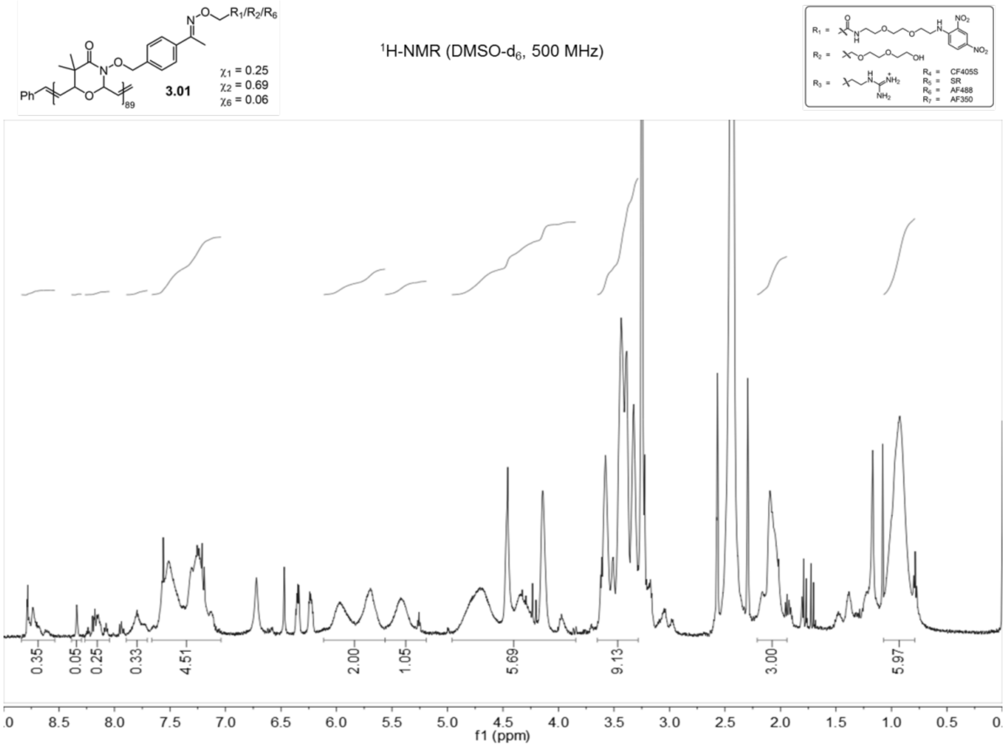
3.01
χ_1 = 0.25
χ_2 = 0.69
χ_6 = 0.06
Ph
89
R1/R2/R6
1H-NMR (DMSO-d6, 500 MHz)
R1 =
R2 =
R3 =
R4 = CF405S
R5 = SR
R6 = AF488
R7 = AF350
0.35
0.05
0.25
0.33
4.51
2.00
1.05
5.69
9.13
3.00
5.97
8.5
8.0
7.5
7.0
6.5
6.0
5.5
5.0
4.5
4.0
3.5
3.0
2.5
2.0
1.5
1.0
0.5
f1 (ppm)

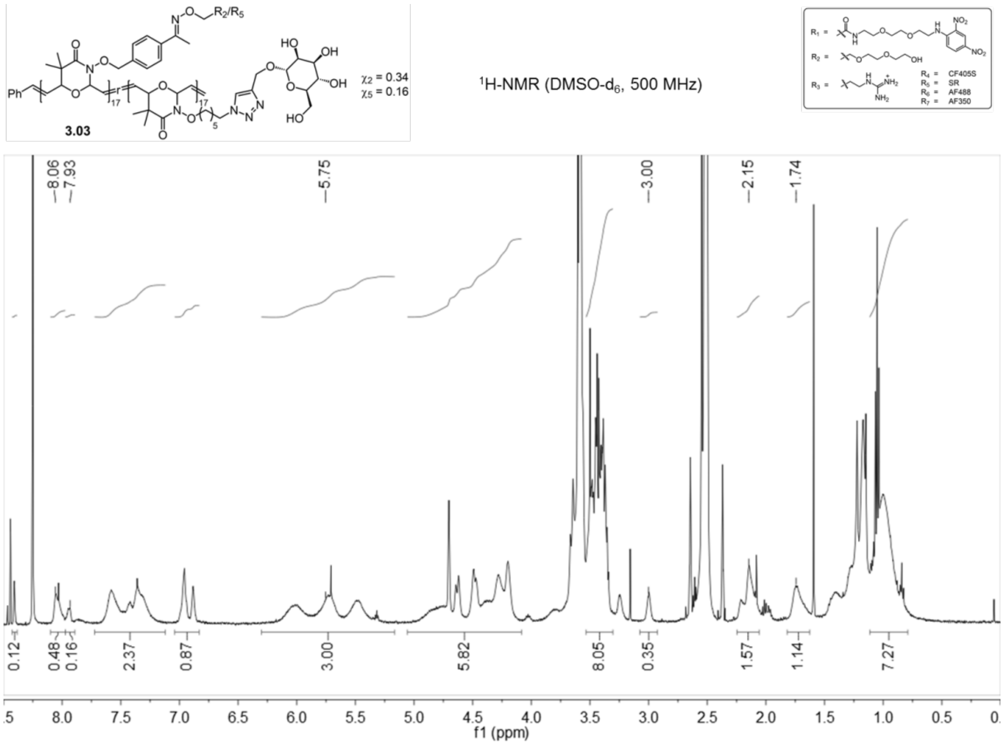
3.03
χ_2 = 0.34
χ_5 = 0.16
Ph
17
17
5
R2/R5
1H-NMR (DMSO-d6, 500 MHz)
R1 =
R2 =
R3 =
R4 = CF405S
R5 = SR
R6 = AF488
R7 = AF350
8.06
7.93
5.75
3.00
2.15
1.74
0.12
0.48
0.16
2.37
0.87
3.00
5.82
8.05
0.35
1.57
1.14
7.27
8.0
7.5
7.0
6.5
6.0
5.5
5.0
4.5
4.0
3.5
3.0
2.5
2.0
1.5
1.0
0.5
f1 (ppm)

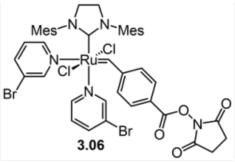
Mes
N
N
Mes
Cl
Ru
N
Cl
Br
N
Br
O
O
N
O
O

3.06

^{1}H-NMR (CDCl$_3$, 500 MHz)

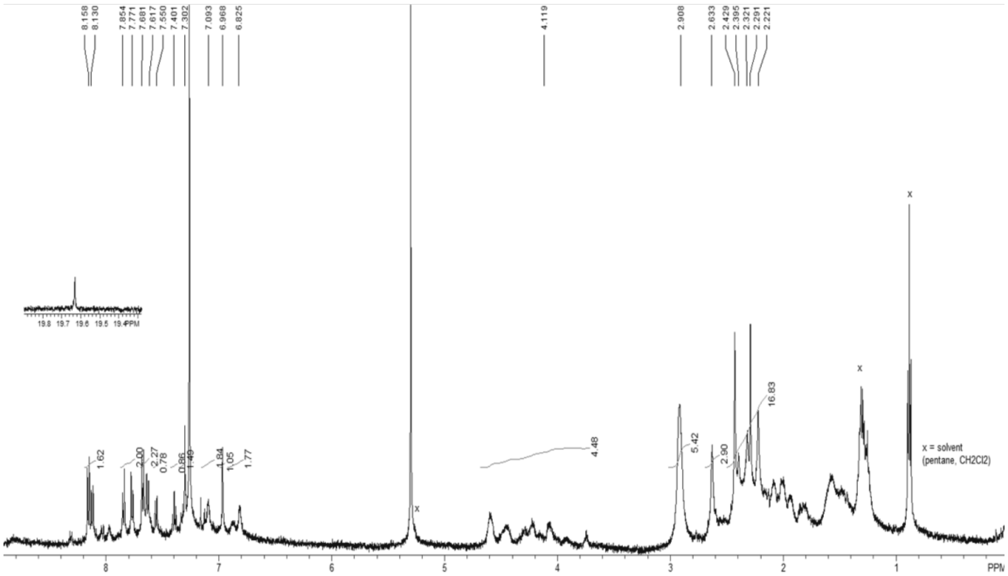

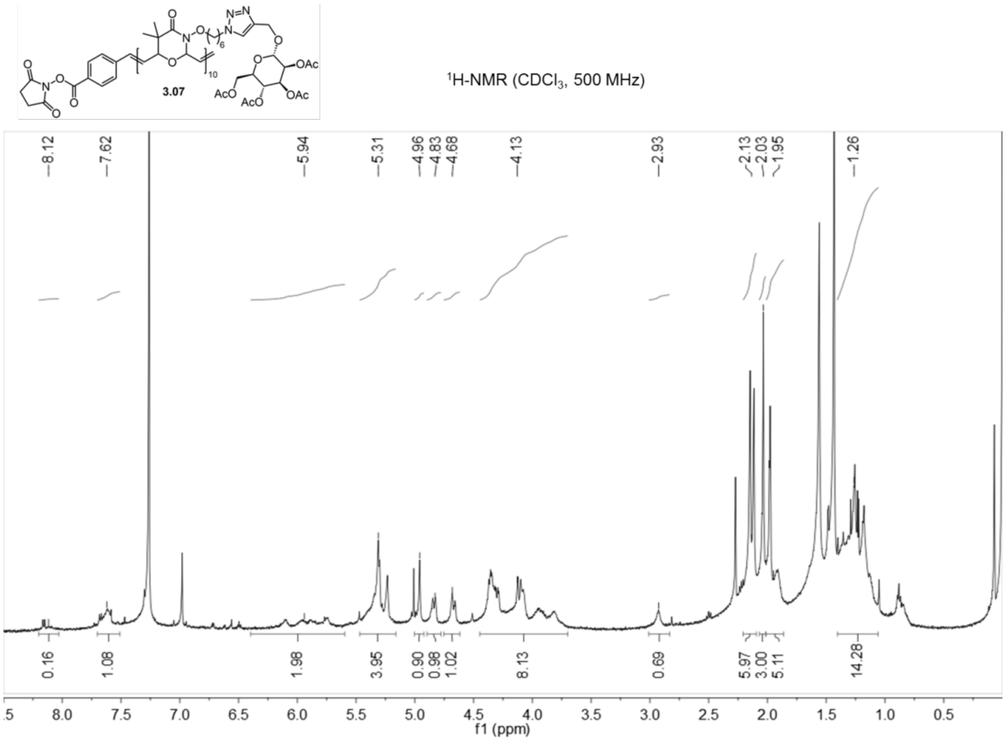

^{1}H-NMR ($CDCl_3$, 500 MHz)

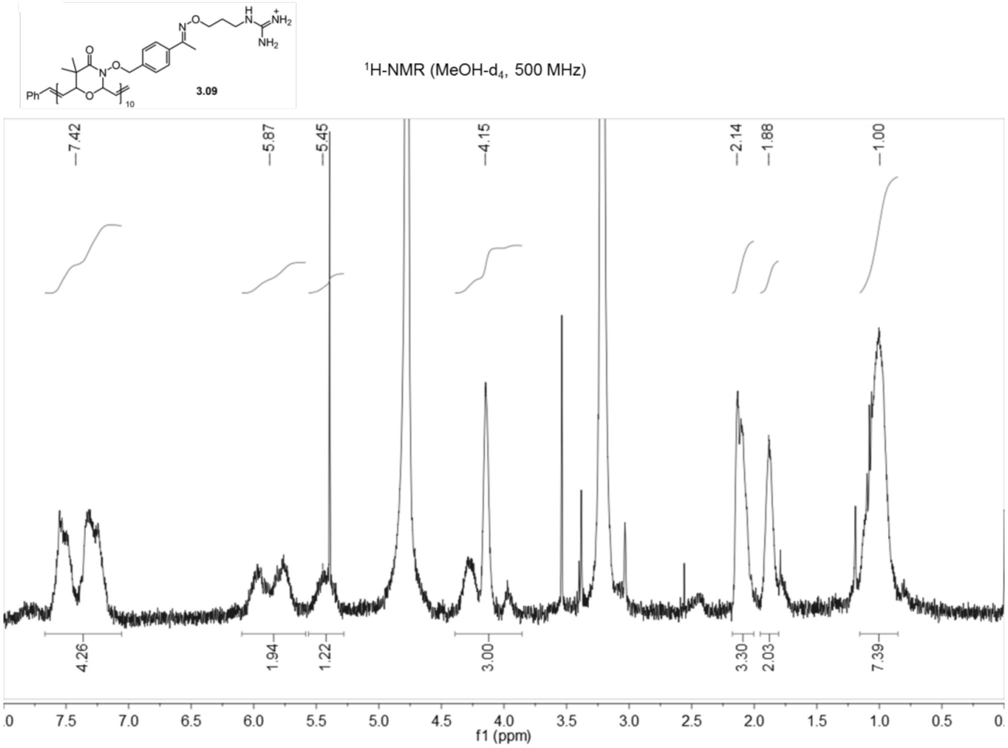

^{1}H-NMR (MeOH-d_4, 500 MHz)

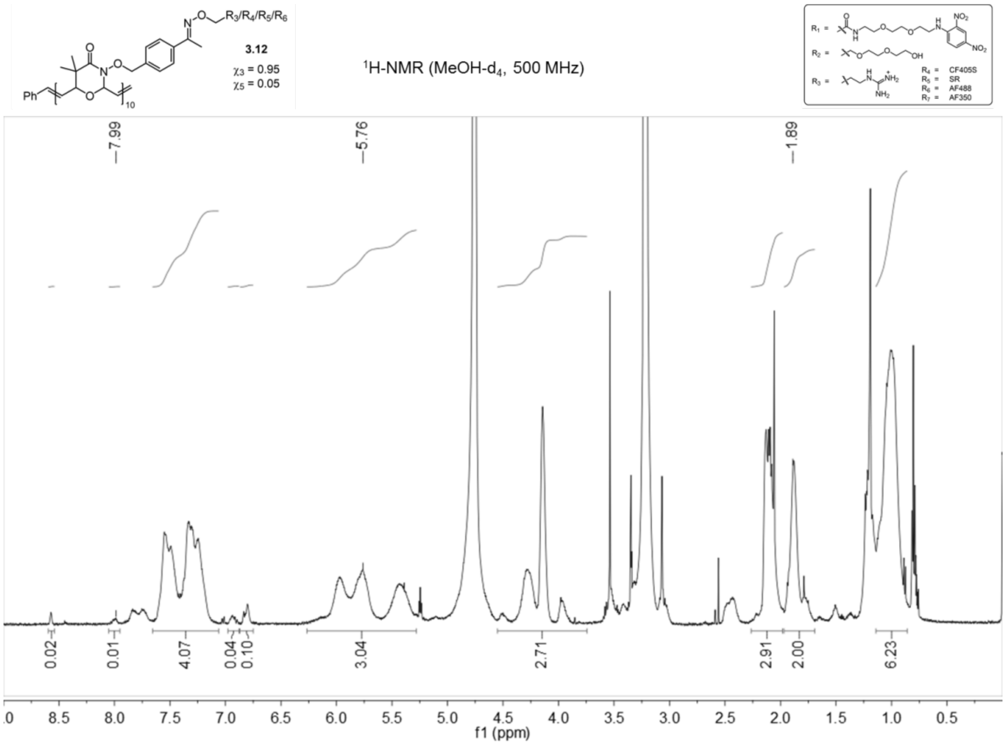
R3/R4/R5/R6
3.12
χ3 = 0.95
χ5 = 0.05
Ph
10
1H-NMR (MeOH-d4, 500 MHz)
R1 =
R2 =
R3 =
R4 = CF405S
R5 = SR
R6 = AF488
R7 = AF350
7.99
5.76
1.89
0.02
0.01
4.07
0.04
0.10
3.04
2.71
2.91
2.00
6.23
9.0
8.5
8.0
7.5
7.0
6.5
6.0
5.5
5.0
4.5
4.0
3.5
3.0
2.5
2.0
1.5
1.0
0.5
f1 (ppm)

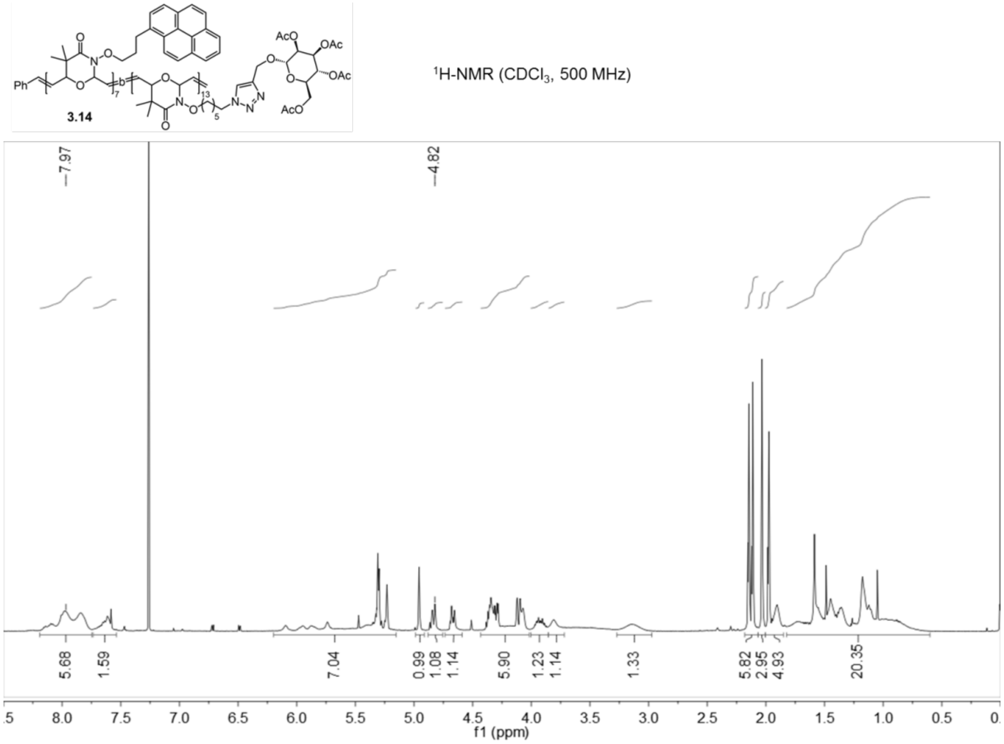
3.14
Ph
7
b
13
5
AcO
OAc
OAc
AcO
1H-NMR (CDCl3, 500 MHz)
7.97
4.82
5.68
1.59
7.04
0.99
1.08
1.14
5.90
1.23
1.14
1.33
5.82
2.95
4.93
20.35
8.5
8.0
7.5
7.0
6.5
6.0
5.5
5.0
4.5
4.0
3.5
3.0
2.5
2.0
1.5
1.0
0.5
0.0
f1 (ppm)

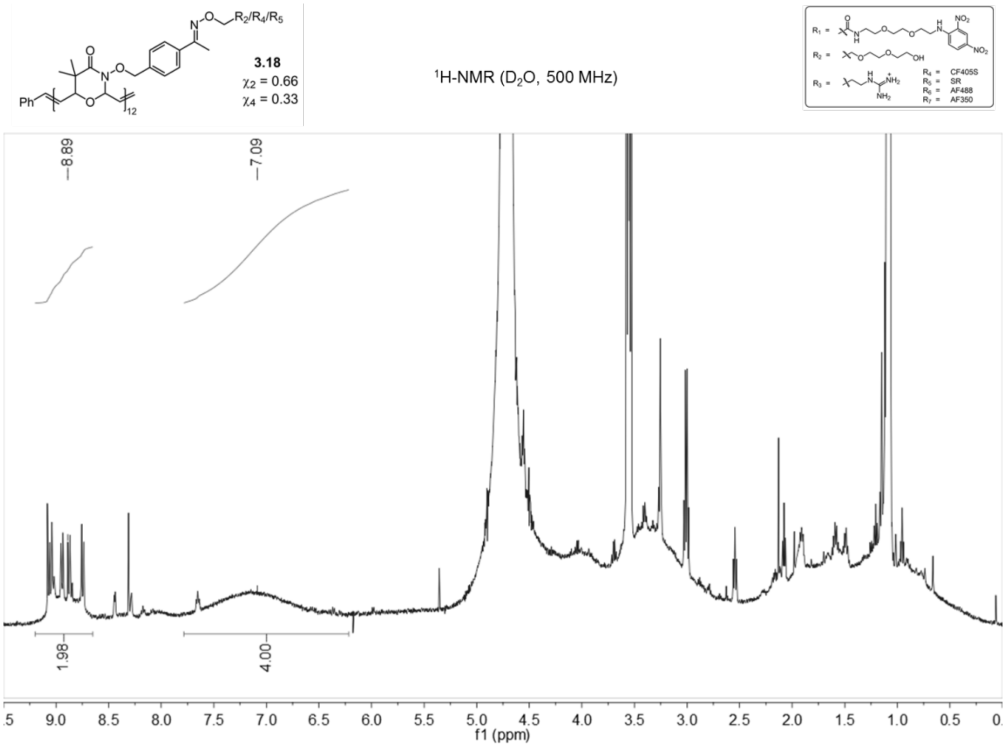
Ph
12
N
O
O
R₂/R₄/R₅
3.18
χ₂ = 0.66
χ₄ = 0.33
¹H-NMR (D₂O, 500 MHz)
R₁ =
R₂ =
R₃ =
NO₂
OH
NH₂
R₄ = CF405S
R₅ = SR
R₆ = AF488
R₇ = AF350
8.89
7.09
1.98
4.00
9.0
8.5
8.0
7.5
7.0
6.5
6.0
5.5
5.0
4.5
4.0
3.5
3.0
2.5
2.0
1.5
1.0
0.5
f1 (ppm)

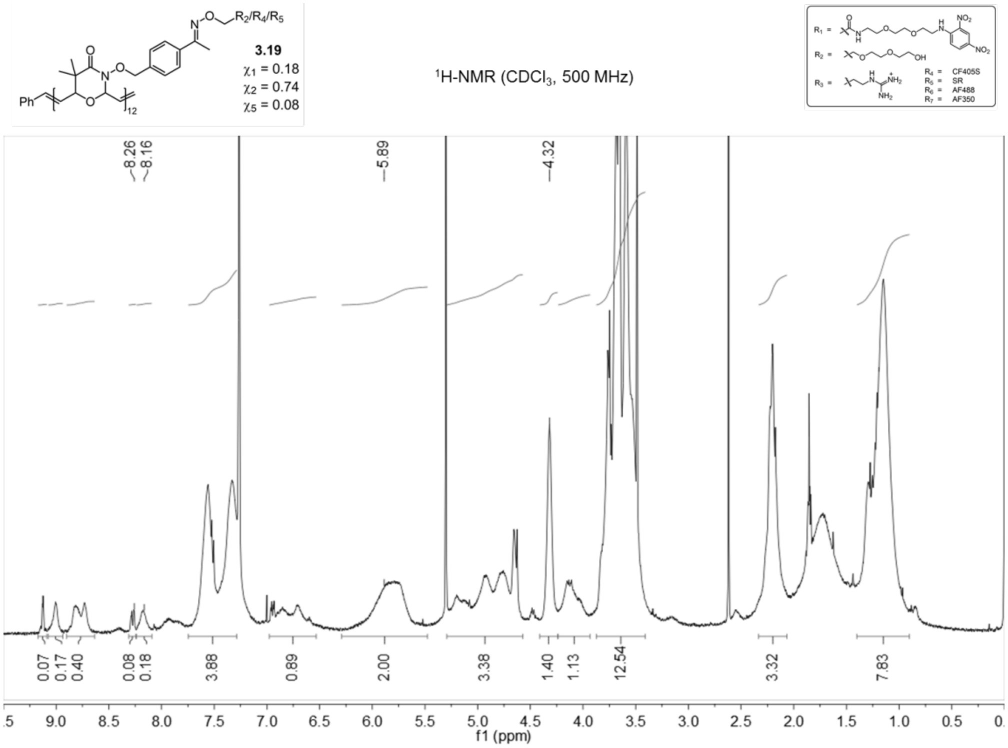
Ph
12
N
O
O
R₂/R₄/R₅
3.19
χ₁ = 0.18
χ₂ = 0.74
χ₅ = 0.08
¹H-NMR (CDCl₃, 500 MHz)
R₁ =
R₂ =
R₃ =
NO₂
OH
NH₂
R₄ = CF405S
R₅ = SR
R₆ = AF488
R₇ = AF350
8.26
8.16
5.89
4.32
0.07
0.17
0.40
0.08
0.18
3.88
0.89
2.00
3.38
1.40
1.13
12.54
3.32
7.83
9.0
8.5
8.0
7.5
7.0
6.5
6.0
5.5
5.0
4.5
4.0
3.5
3.0
2.5
2.0
1.5
1.0
0.5
f1 (ppm)

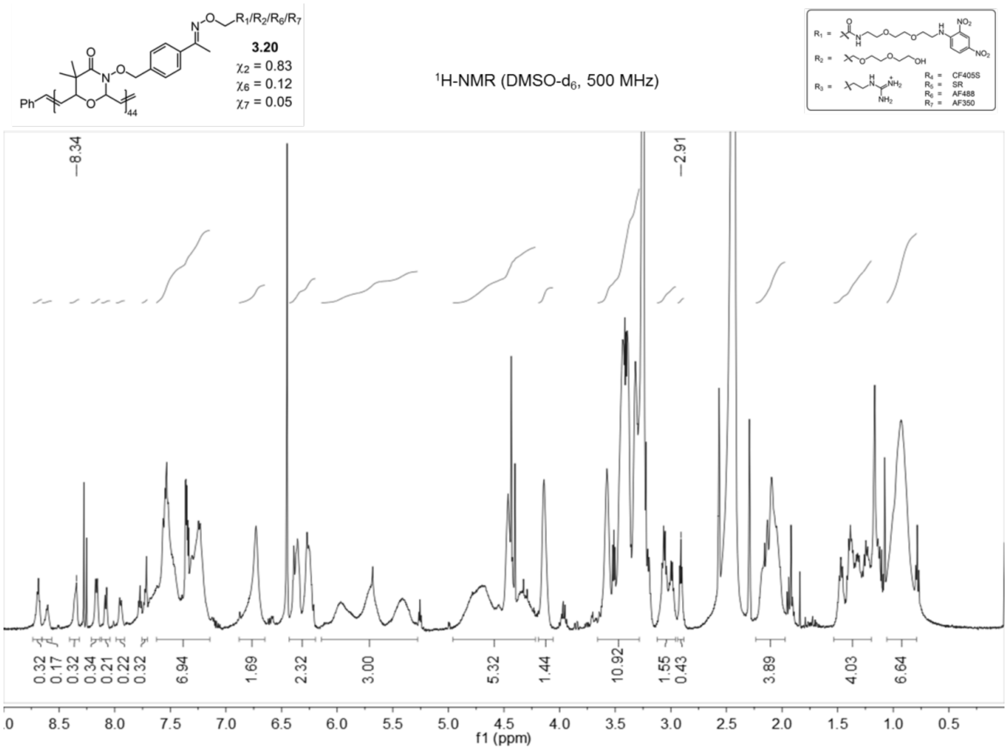
R1/R2/R6/R7
3.20
χ_2 = 0.83
χ_6 = 0.12
χ_7 = 0.05
Ph
44
^{1}H-NMR (DMSO-d$_6$, 500 MHz)
R1 =
R2 =
R3 =
R4 = CF405S
R5 = SR
R6 = AF488
R7 = AF350
8.34
2.91
0.32
0.17
0.32
0.34
0.21
0.22
0.32
6.94
1.69
2.32
3.00
5.32
1.44
10.92
1.55
0.43
3.89
4.03
6.64
f1 (ppm)
9.0 8.5 8.0 7.5 7.0 6.5 6.0 5.5 5.0 4.5 4.0 3.5 3.0 2.5 2.0 1.5 1.0 0.5

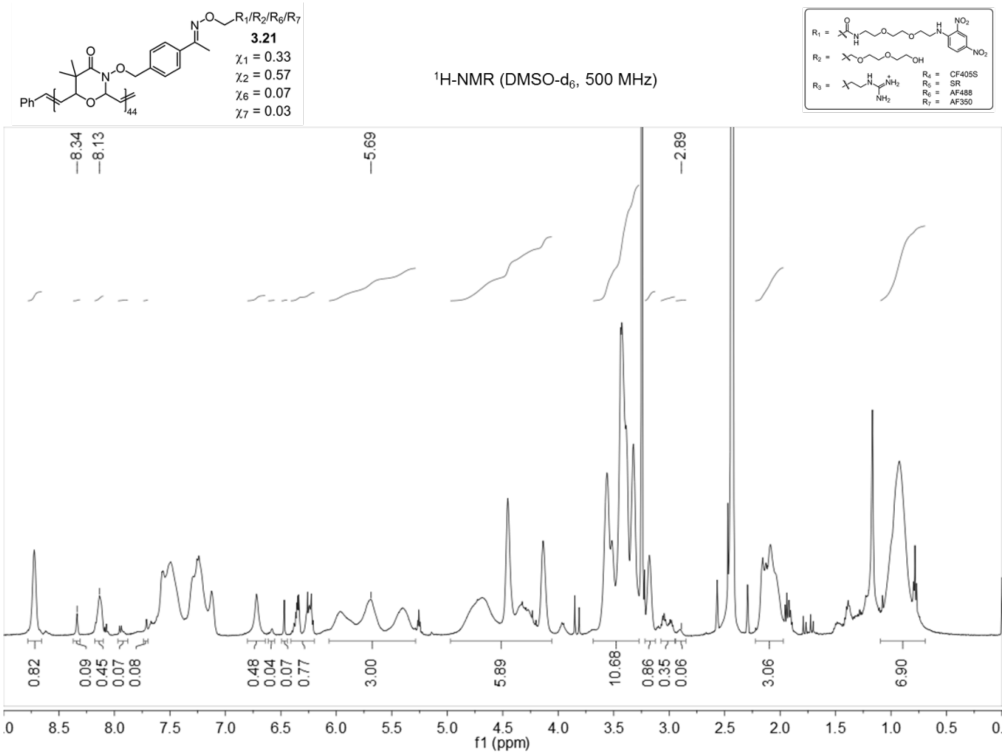
R1/R2/R6/R7
3.21
χ_1 = 0.33
χ_2 = 0.57
χ_6 = 0.07
χ_7 = 0.03
Ph
44
^{1}H-NMR (DMSO-d$_6$, 500 MHz)
R1 =
R2 =
R3 =
R4 = CF405S
R5 = SR
R6 = AF488
R7 = AF350
8.34
8.13
5.69
2.89
0.82
0.09
0.45
0.07
0.08
0.48
0.04
0.07
0.77
3.00
5.89
10.68
0.86
0.35
0.06
3.06
6.90
f1 (ppm)
9.0 8.5 8.0 7.5 7.0 6.5 6.0 5.5 5.0 4.5 4.0 3.5 3.0 2.5 2.0 1.5 1.0 0.5 0.0

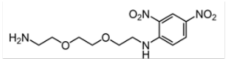
O$_2$N
NO$_2$
H$_2$N
O
O
N
H

3.25

^{1}H-NMR (CDCl$_3$, 400 MHz)

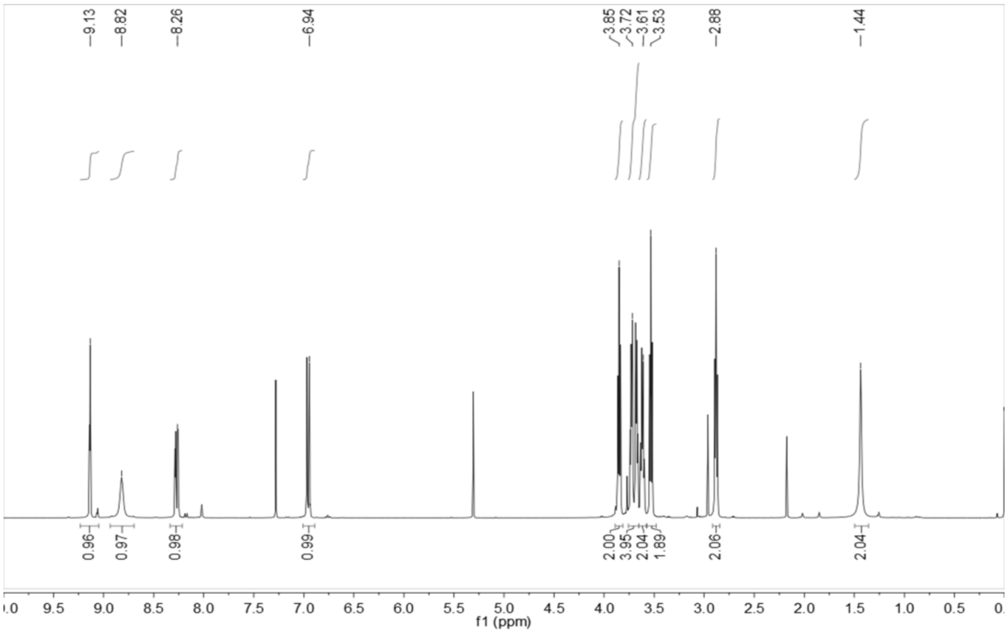

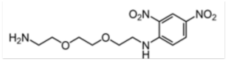
O$_2$N
NO$_2$
H$_2$N
O
O
N
H

3.25

^{13}C-NMR (CDCl$_3$, 100 MHz)

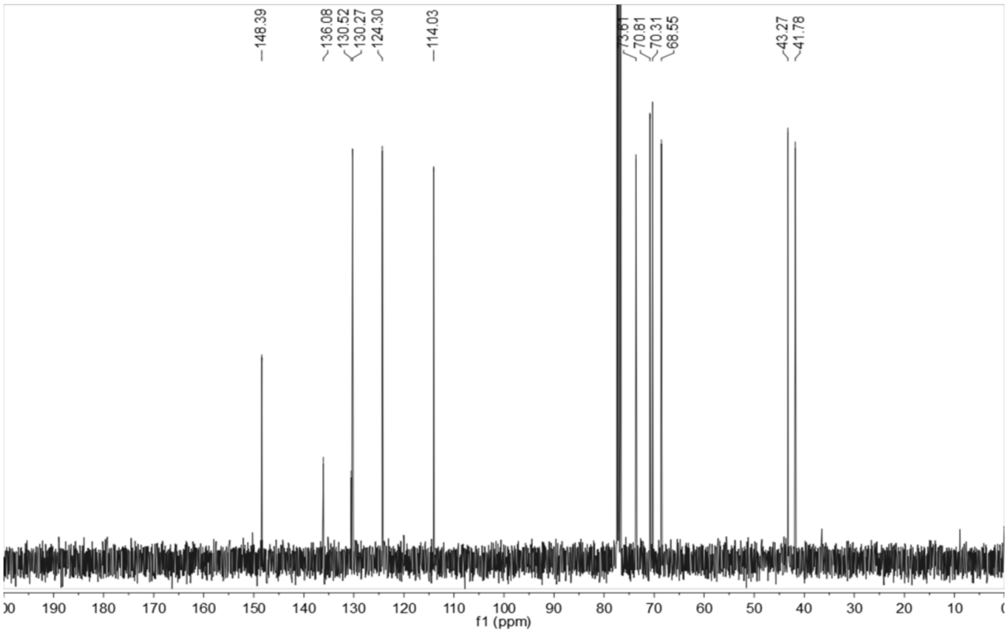

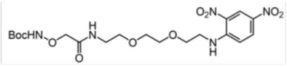
BocHN
O
H
N
O
O
O
O2N
NO2
N
H

3.26
^{1}H-NMR ($CDCl_3$, 400 MHz)

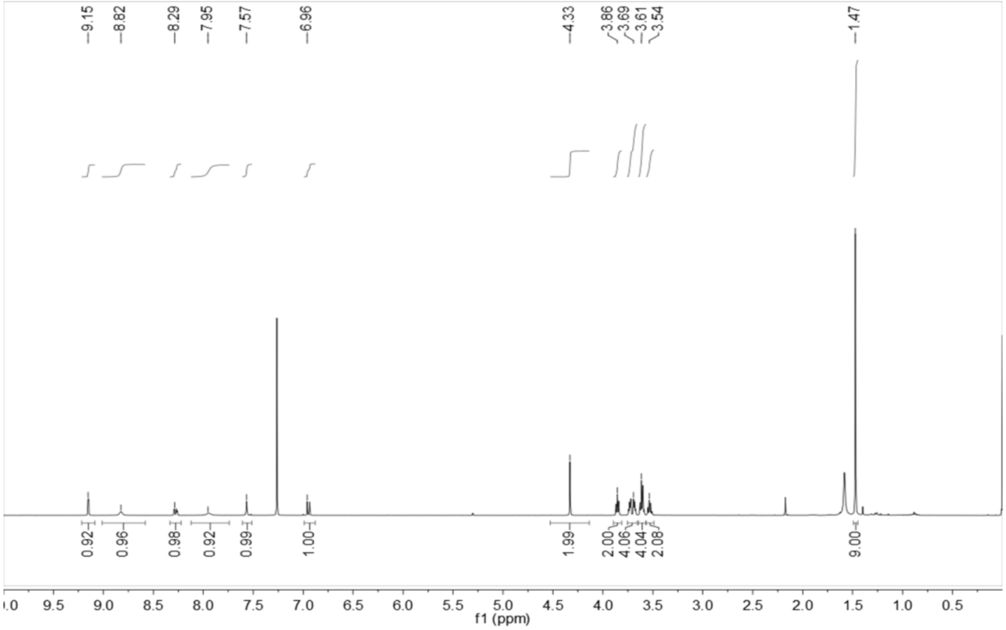

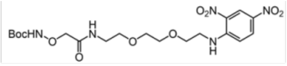
BocHN
O
H
N
O
O
O
O2N
NO2
N
H

3.26
^{13}C-NMR ($CDCl_3$, 100 MHz)

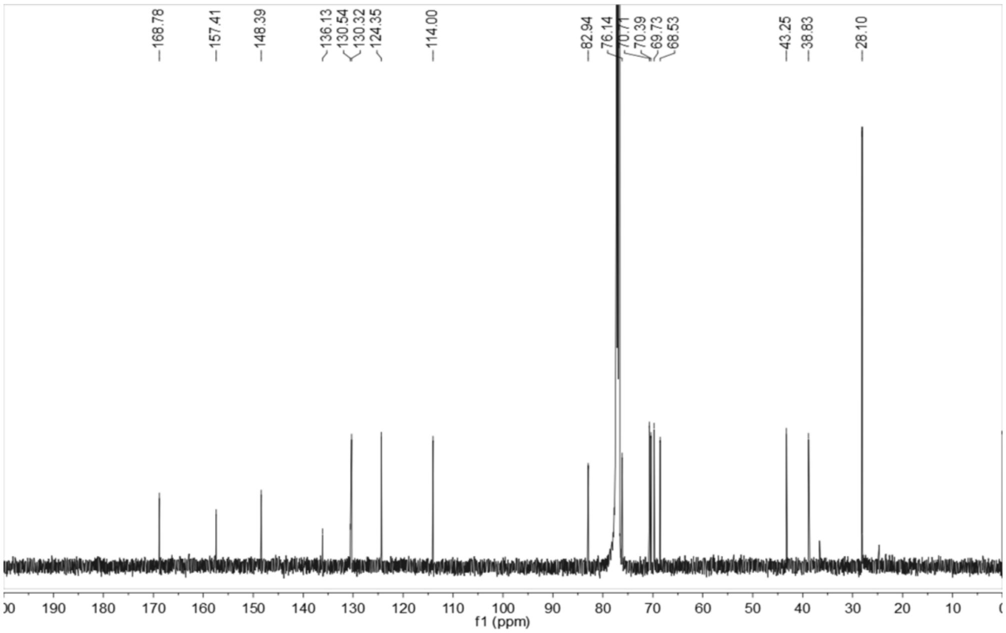

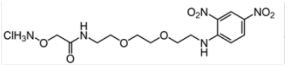

ClH3N
O
H
N
O
O
O
O2N
NO2
N
H

3.27
^{1}H-NMR (MeOH-d_4, 500 MHz)

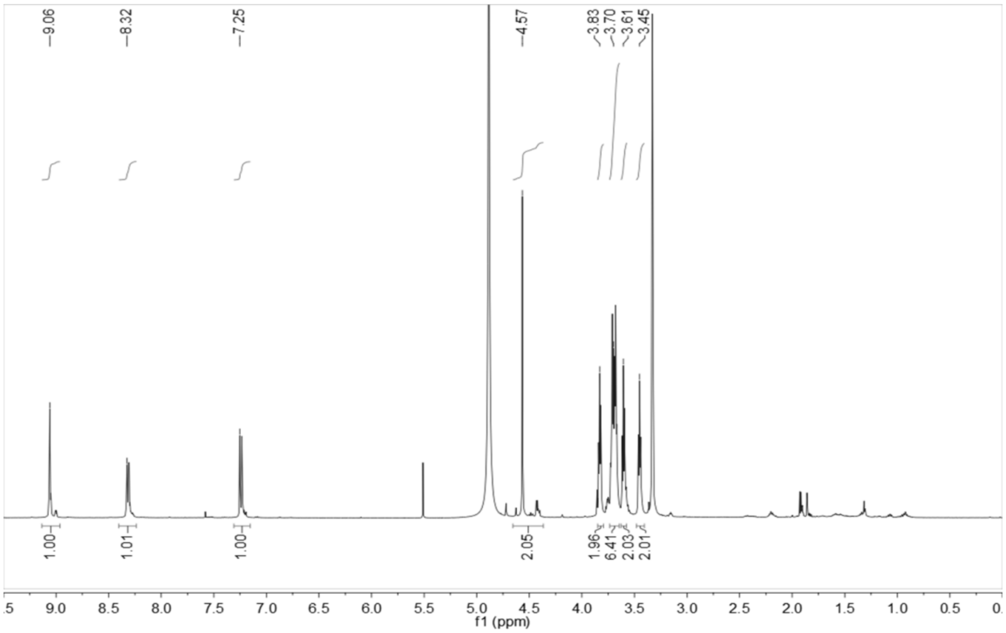

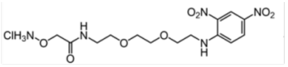

ClH3N
O
H
N
O
O
O
O2N
NO2
N
H

3.27
^{13}C-NMR (MeOH-d_4, 125 MHz)

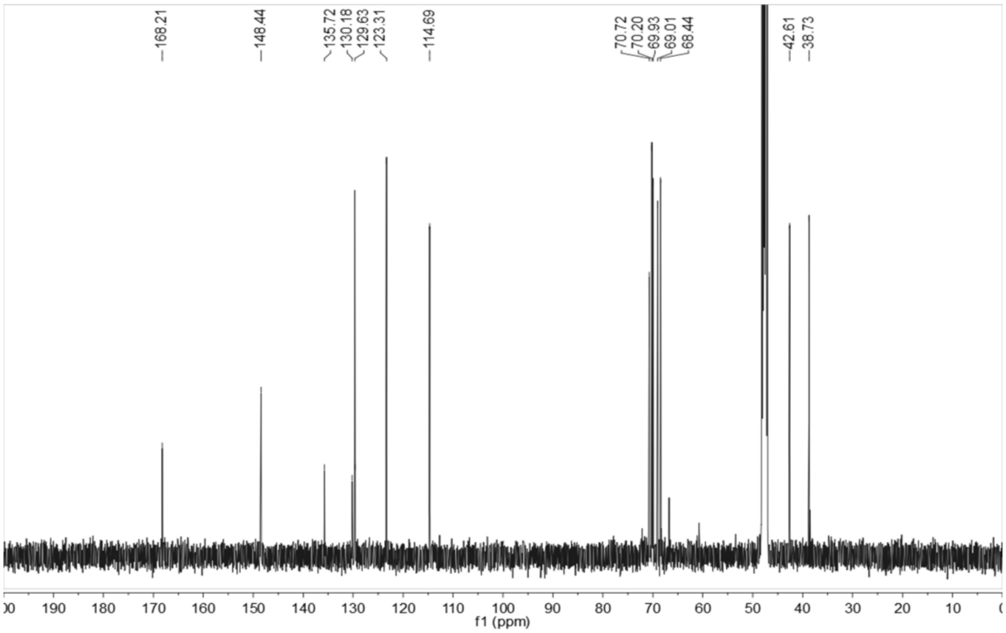

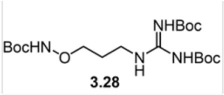
BocHN
O
N
H
NHBoc
NHBoc

3.28

¹H-NMR (CDCl$_3$, 500 MHz)

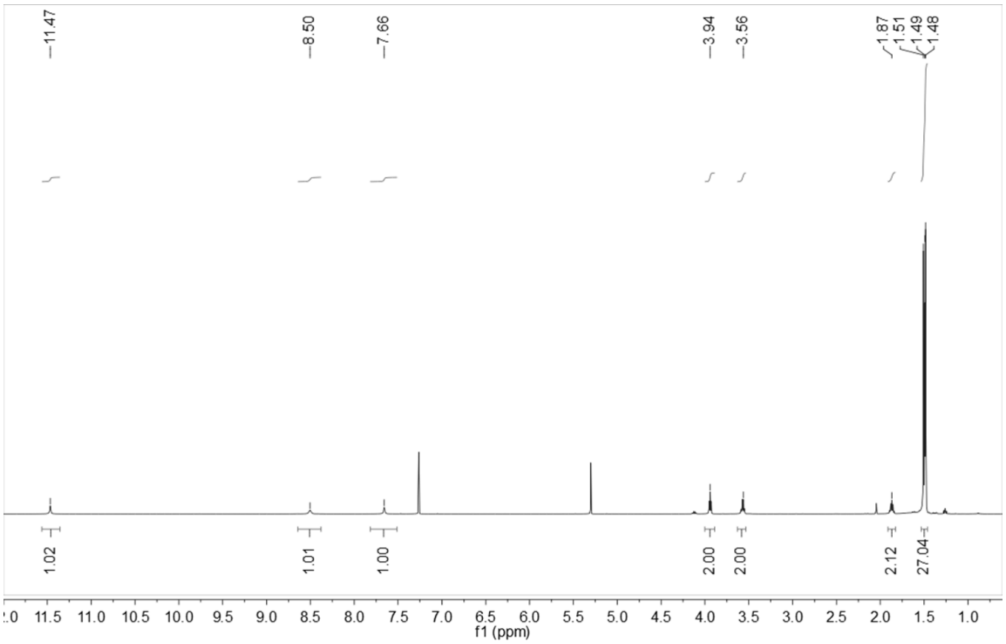

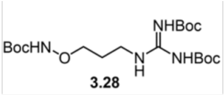
BocHN
O
N
H
NHBoc
NHBoc

3.28

¹³C-NMR (CDCl$_3$, 125 MHz)

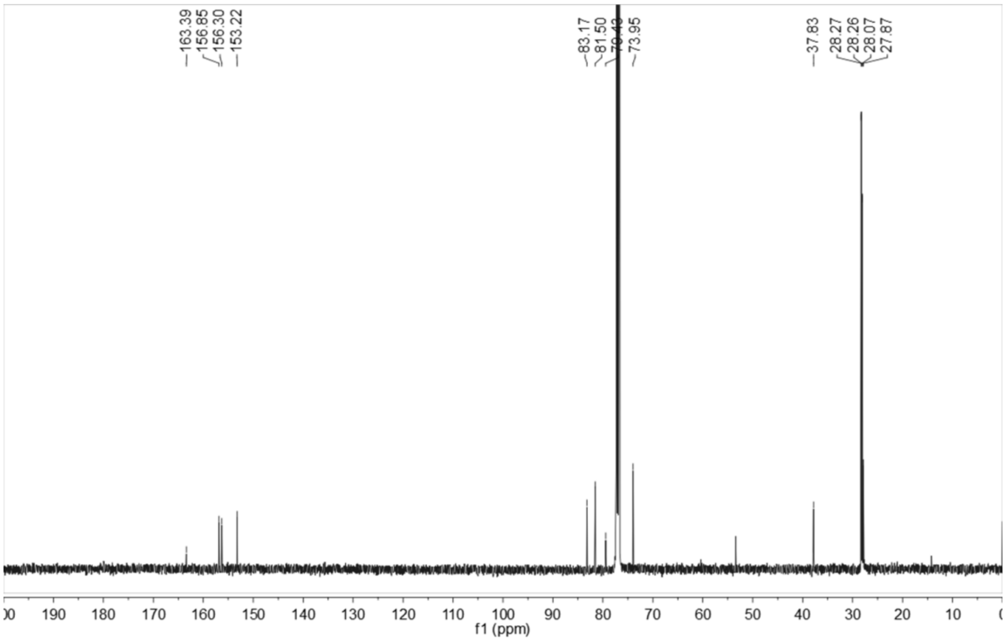

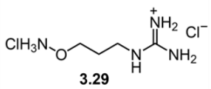

ClH$_3$N
O
N
H
NH$_2$
NH$_2$
+
Cl$^-$

3.29

^{1}H-NMR (MeOH-d$_4$, 500 MHz)

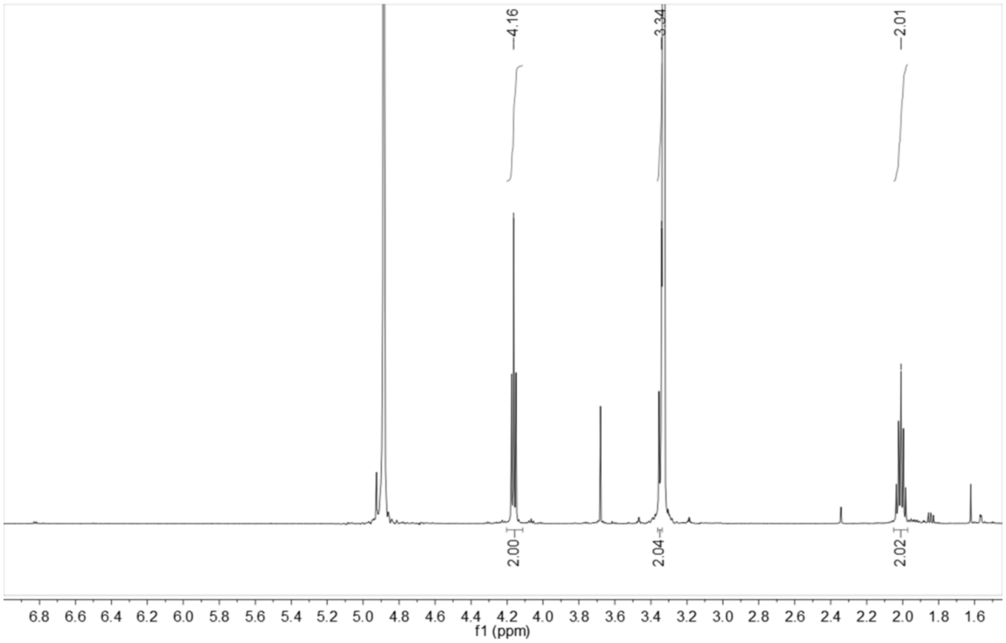

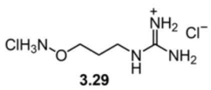

ClH$_3$N
O
N
H
NH$_2$
NH$_2$
+
Cl$^-$

3.29

^{13}C-NMR (MeOH-d$_4$, 125 MHz)

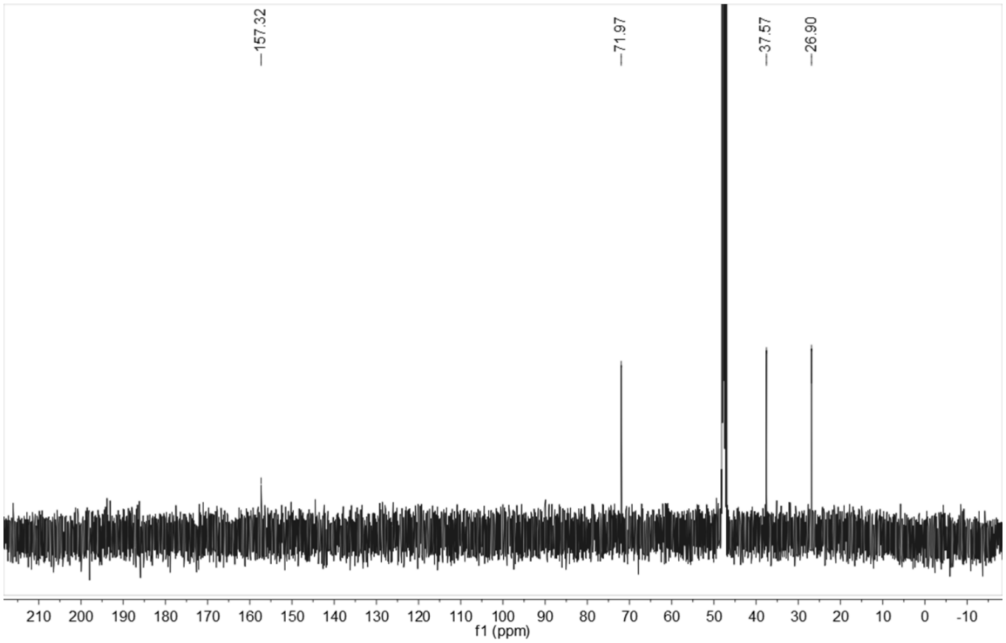

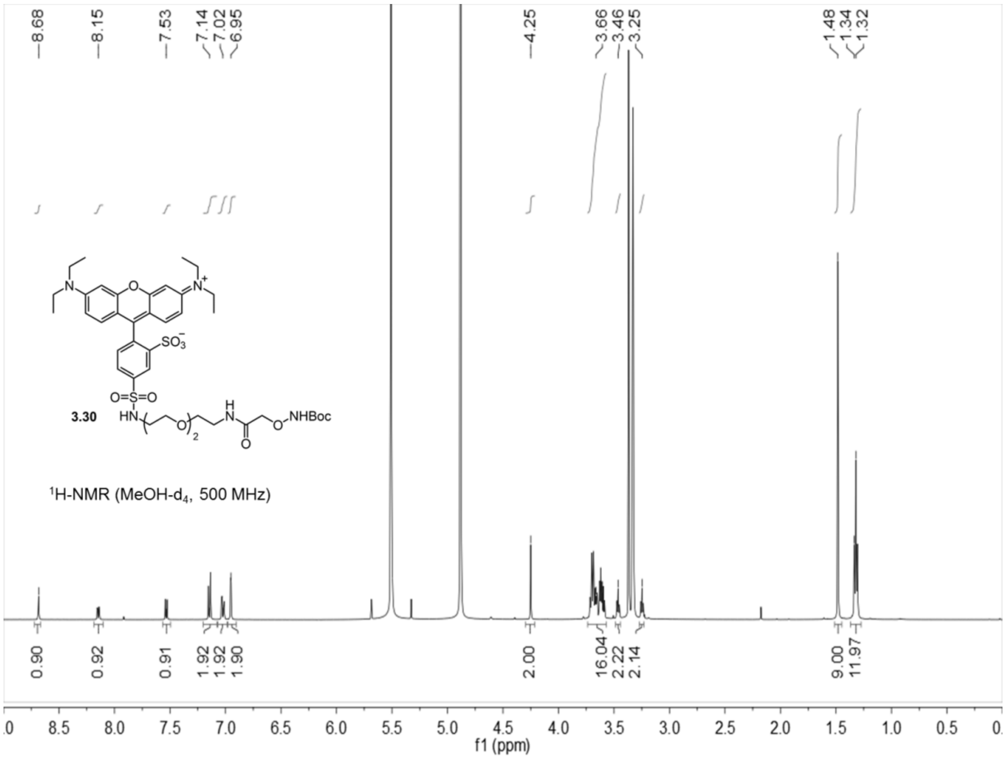
8.68
8.15
7.53
7.14
7.02
6.95
4.25
3.66
3.46
3.25
1.48
1.34
1.32
SO$_3^-$
O=S=O
HN
O
2
H
N
O
NHBoc
3.30
^{1}H-NMR (MeOH-d$_4$, 500 MHz)
0.90
0.92
0.91
1.92
1.92
1.90
2.00
16.04
2.22
2.14
9.00
11.97
8.5
8.0
7.5
7.0
6.5
6.0
5.5
5.0
4.5
4.0
3.5
3.0
2.5
2.0
1.5
1.0
0.5
f1 (ppm)

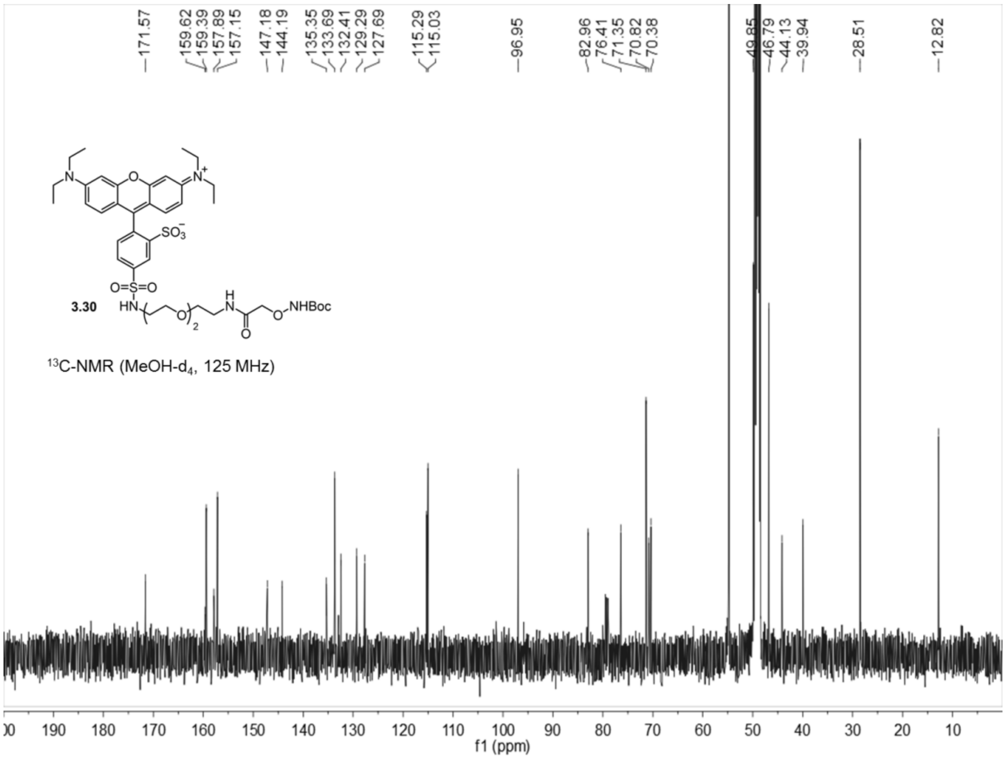
171.57
159.62
159.39
157.89
157.15
147.18
144.19
135.35
133.69
132.41
129.29
127.69
115.29
115.03
96.95
82.96
76.41
71.35
70.82
70.38
49.85
46.79
44.13
39.94
28.51
12.82
SO$_3^-$
O=S=O
HN
O
2
H
N
O
NHBoc
3.30
^{13}C-NMR (MeOH-d$_4$, 125 MHz)
190
180
170
160
150
140
130
120
110
100
90
80
70
60
50
40
30
20
10
f1 (ppm)

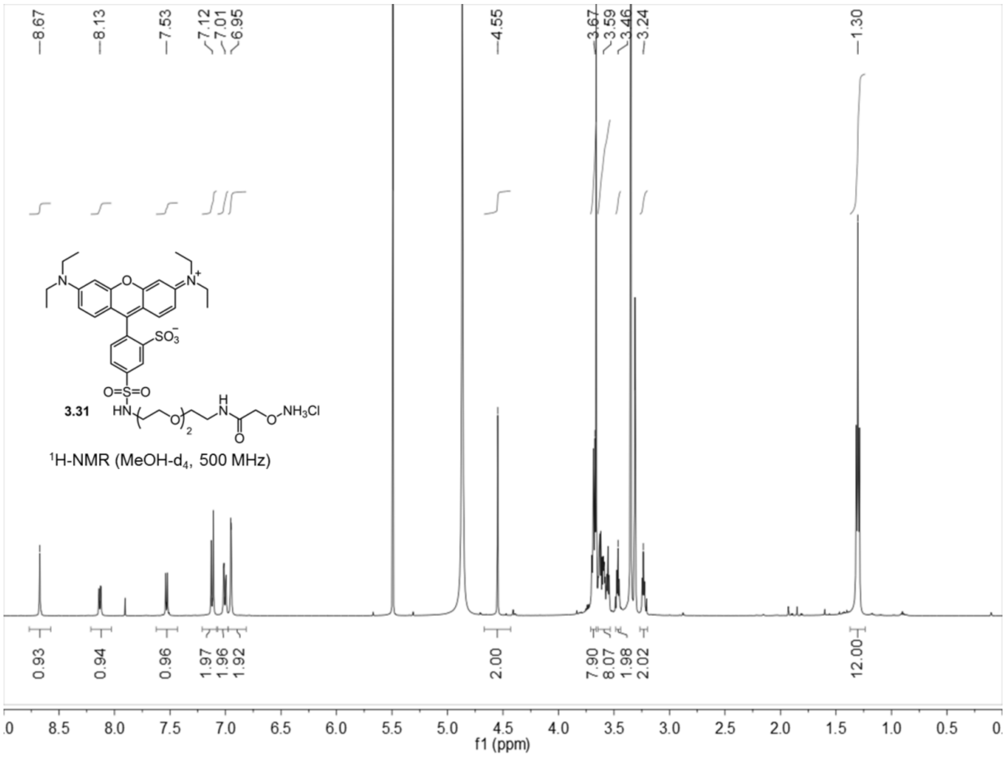
8.67
8.13
7.53
7.12
7.01
6.95
4.55
3.67
3.59
3.46
3.24
1.30
3.31
^{1}H-NMR (MeOH-d$_4$, 500 MHz)
0.93
0.94
0.96
1.97
1.96
1.92
2.00
7.90
8.07
1.98
2.02
12.00
8.5
8.0
7.5
7.0
6.5
6.0
5.5
5.0
4.5
4.0
3.5
3.0
2.5
2.0
1.5
1.0
0.5
f1 (ppm)

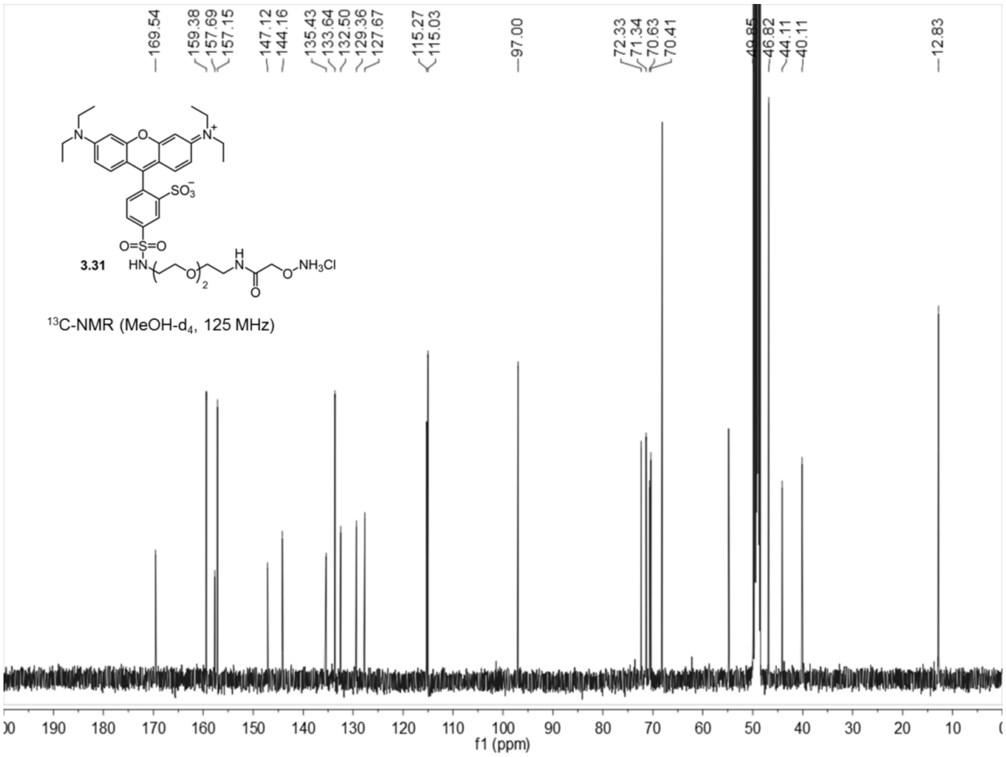
169.54
159.38
157.69
157.15
147.12
144.16
135.43
133.64
132.50
129.36
127.67
115.27
115.03
97.00
72.33
71.34
70.63
70.41
49.85
46.82
44.11
40.11
12.83
3.31
^{13}C-NMR (MeOH-d$_4$, 125 MHz)
190
180
170
160
150
140
130
120
110
100
90
80
70
60
50
40
30
20
10
f1 (ppm)

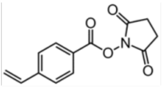

3.32
^{1}H-NMR (CDCl$_3$, 300 MHz)

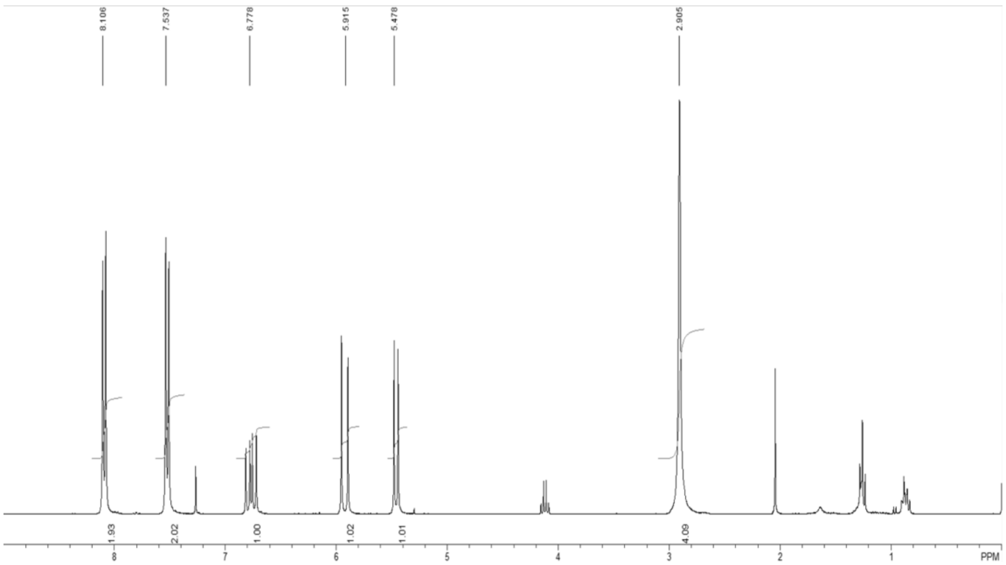

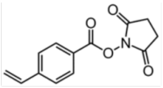

3.32
^{13}C-NMR (CDCl$_3$, 75 MHz)

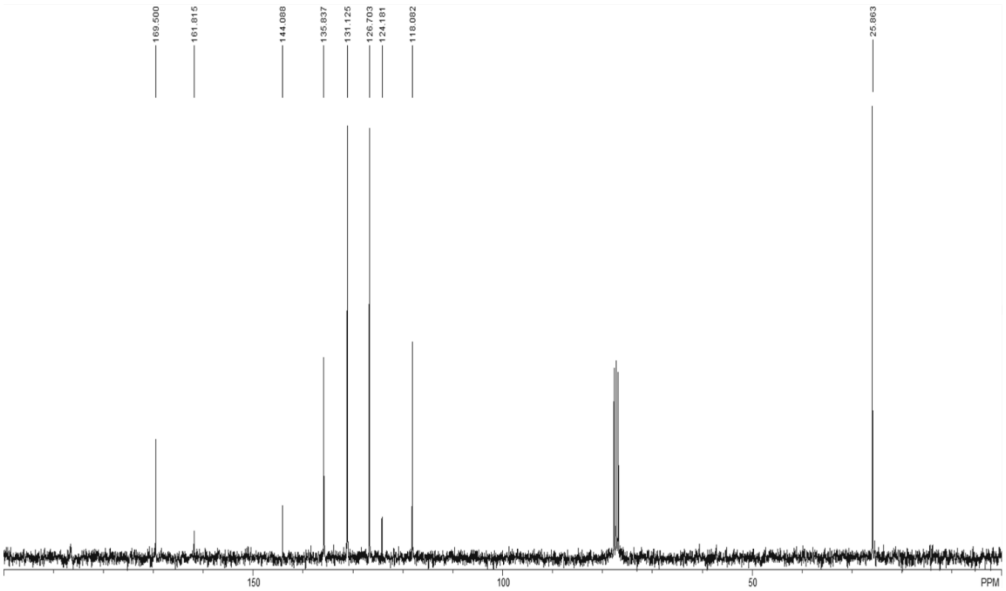

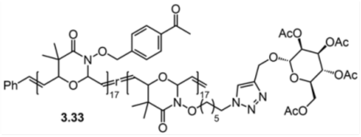
Ph
17
17
5
AcO
OAc
OAc
AcO

3.33

^{1}H-NMR (CDCl$_3$, 500 MHz)

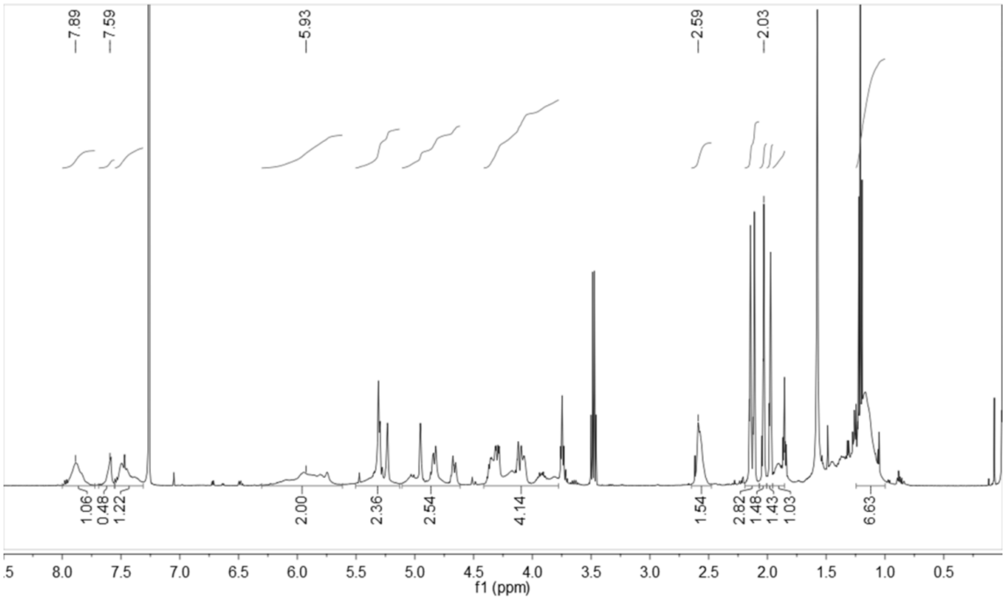

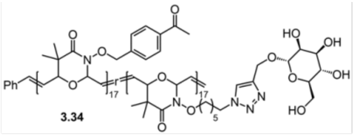
Ph
17
17
5
HO
OH
OH
HO

3.34

^{1}H-NMR (DMSO-d$_6$, 500 MHz)

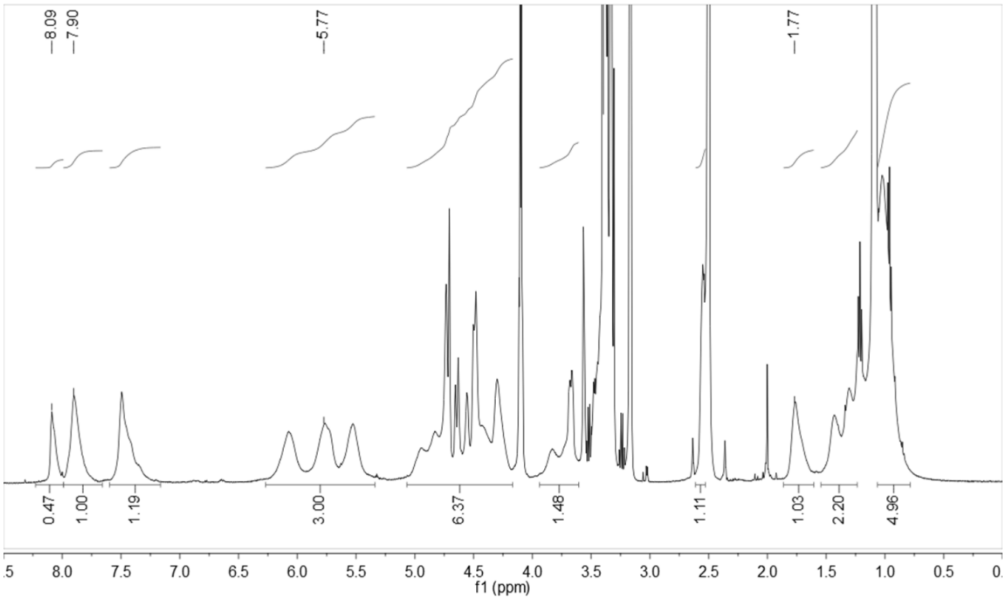

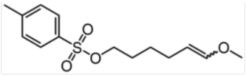

4.08
^{1}H-NMR (CDCl$_3$, 500 MHz)

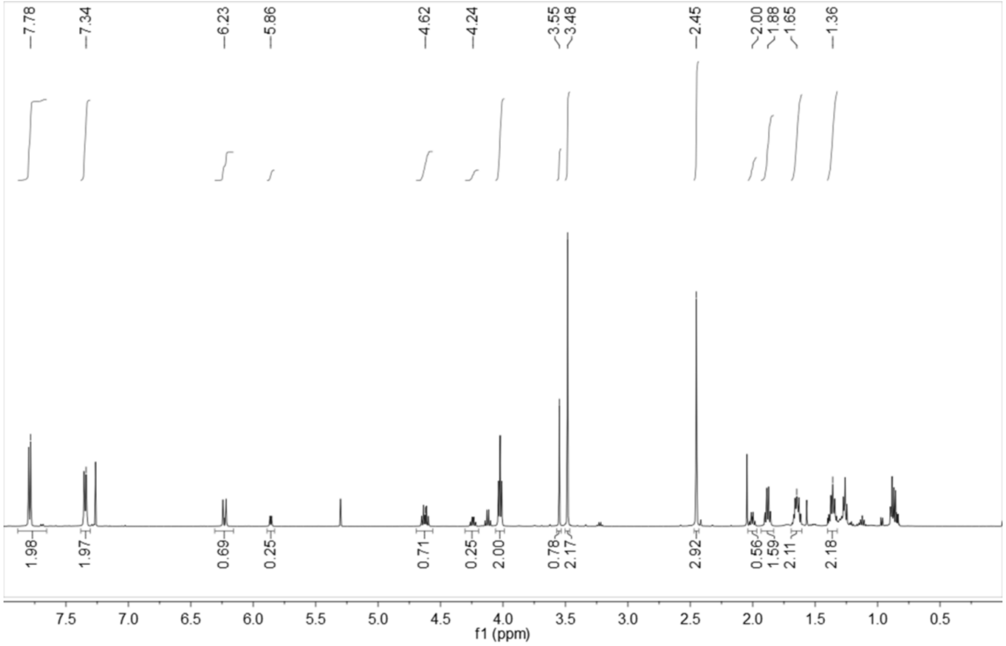

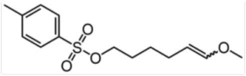

4.08
^{13}C-NMR (CDCl$_3$, 125 MHz)

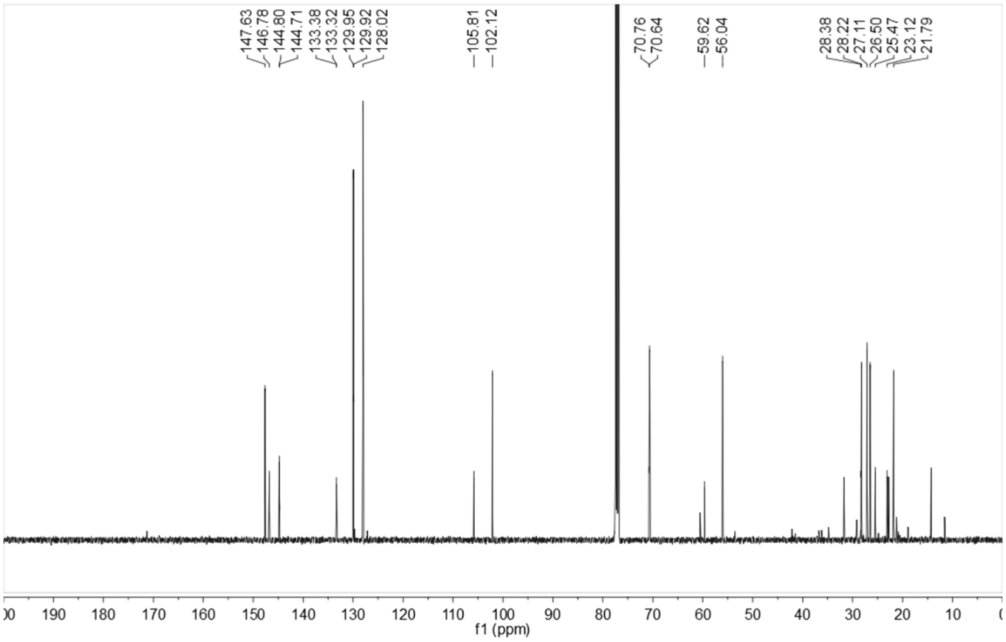

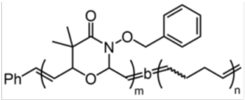

4.07
^{1}H-NMR (CDCl$_3$, 500 MHz)
Top: expansion of baseline, poly(**4.04**) peaks referenced
Bottom: full spectral height, pCOD peaks referenced

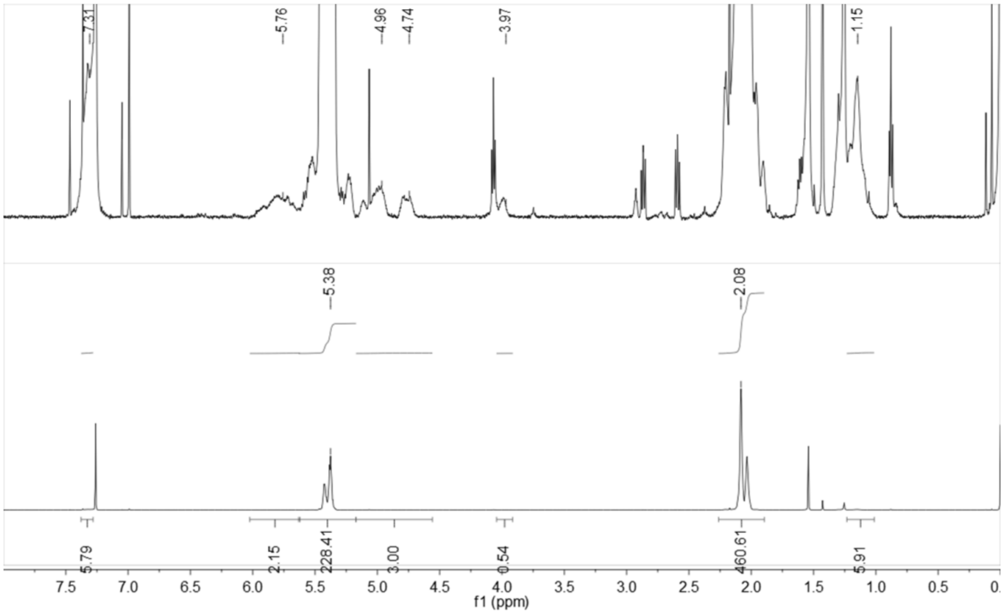

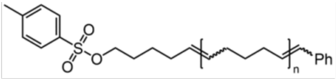

4.10
^{1}H-NMR (CDCl$_3$, 500 MHz)
[COD]$_0$:[**4.05**] = 460:1
Inset: Tosyl signals

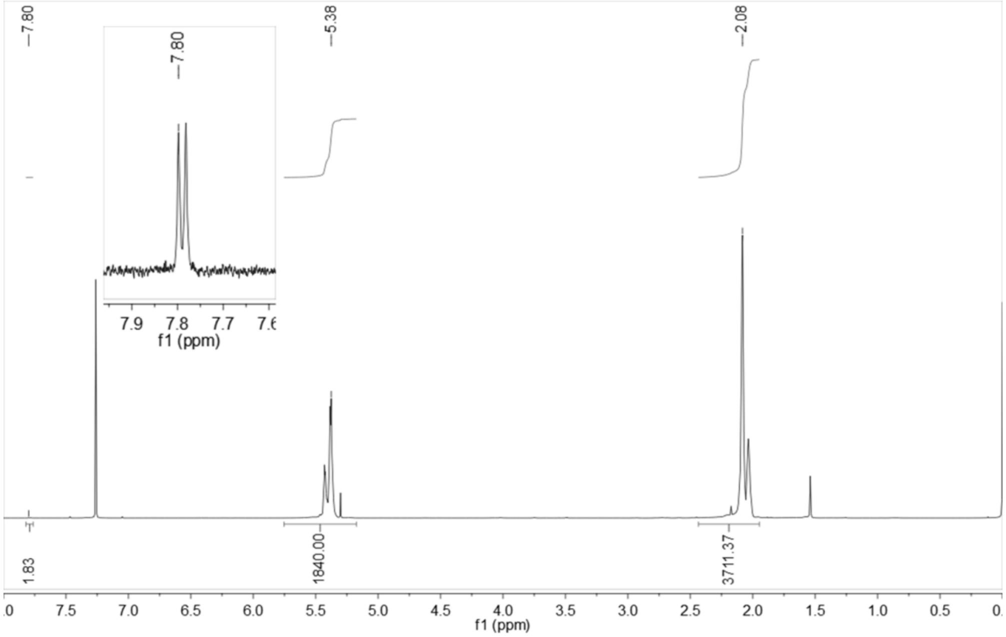

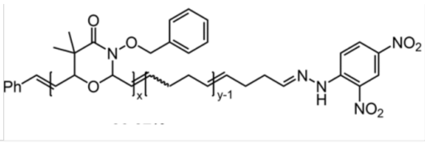
Ph
O
N
O
O
x
y-1
N
N
H
NO2
NO2

4.13
^{1}H-NMR (CDCl$_3$, 500 MHz)
$[\mathrm{COD}]_0$:[**4.05**] = 460:1
Inset: DNP signals

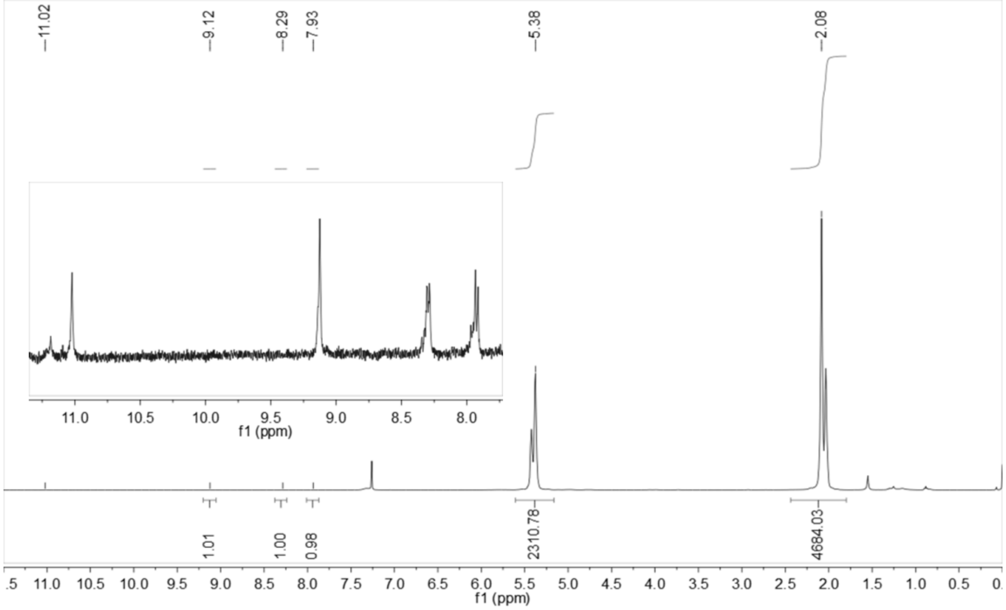

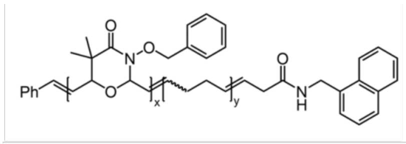
Ph
O
N
O
O
x
y
O
N
H

4.14
^{1}H-NMR (CDCl$_3$, 500 MHz)
$[\mathrm{COD}]_0$:[**4.05**] = 460:1

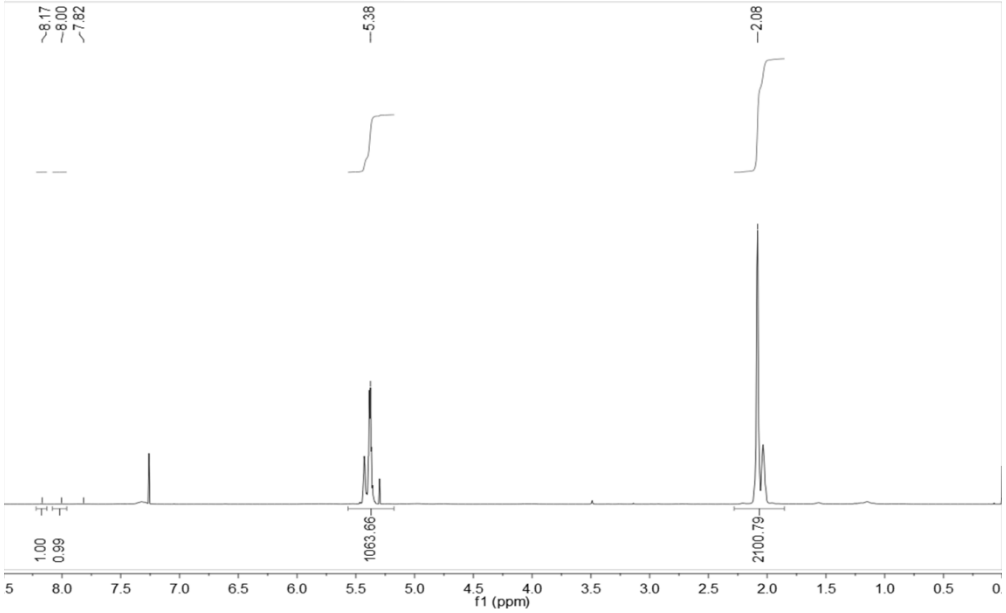

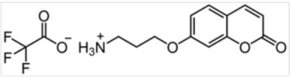
F
F
F
O
O⁻
H₃N⁺
O
O
O

4.17
^{1}H-NMR (MeOH-d_4, 500 MHz)

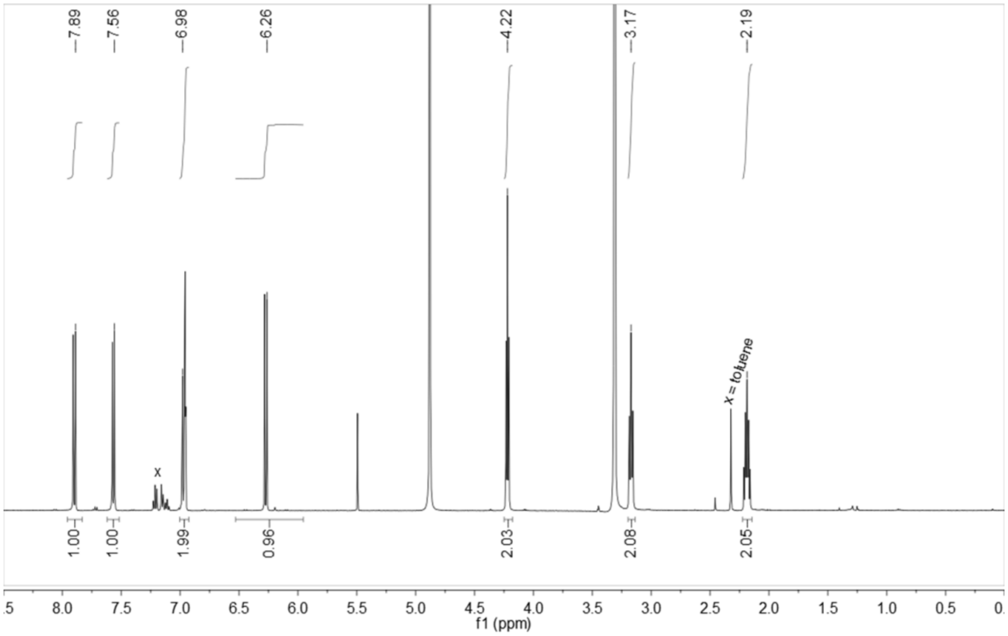

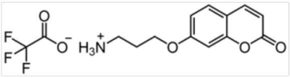
F
F
F
O
O⁻
H₃N⁺
O
O
O

4.17
^{13}C-NMR (MeOH-d_4, 125 MHz)

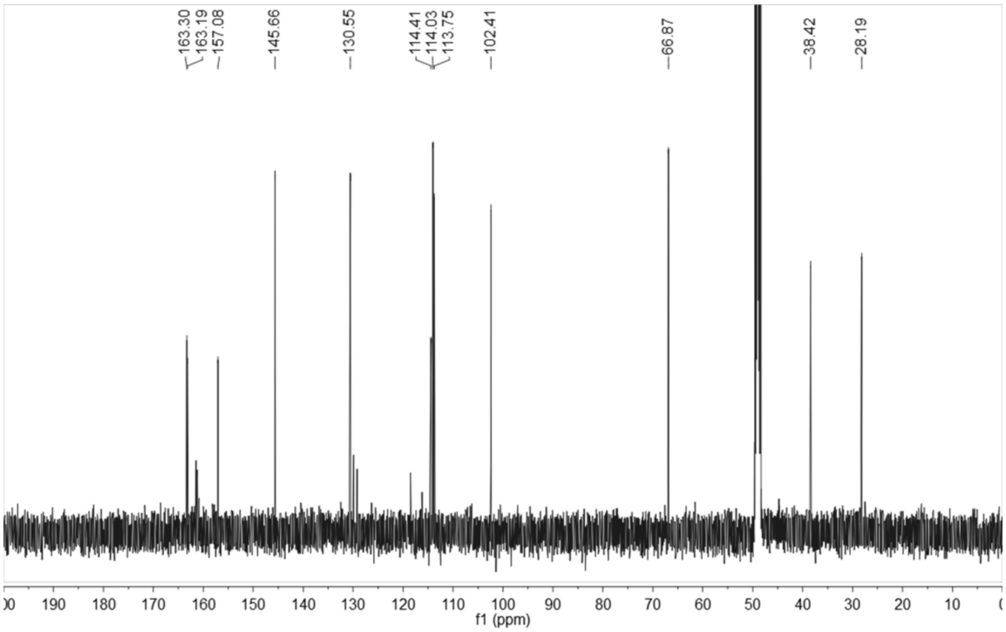

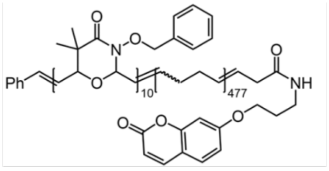
Ph
O
N
O
O
10
477
O
NH
O
O
O

4.18
^{1}H-NMR ($CDCl_3$, 500 MHz)
$[COD]_o$:[**4.05**] = 460:1
Inset: Coumarin signals

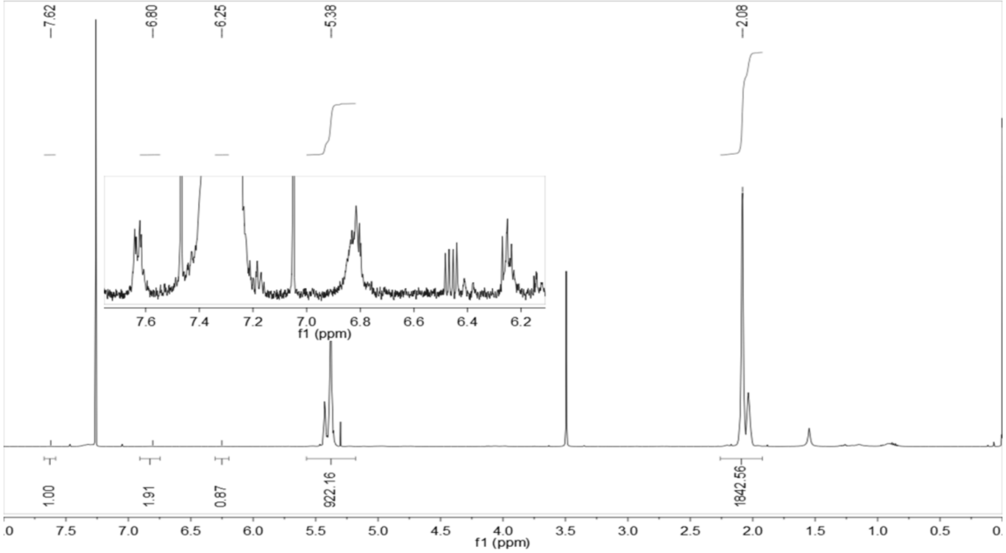

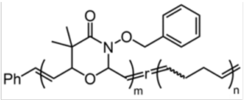

crude 4.20
^{1}H-NMR ($CDCl_3$, 500 MHz)
example $[\mathbf{4.04}]_o$:$[COD]_o$ = 150:50 → 84% conversion **4.04**

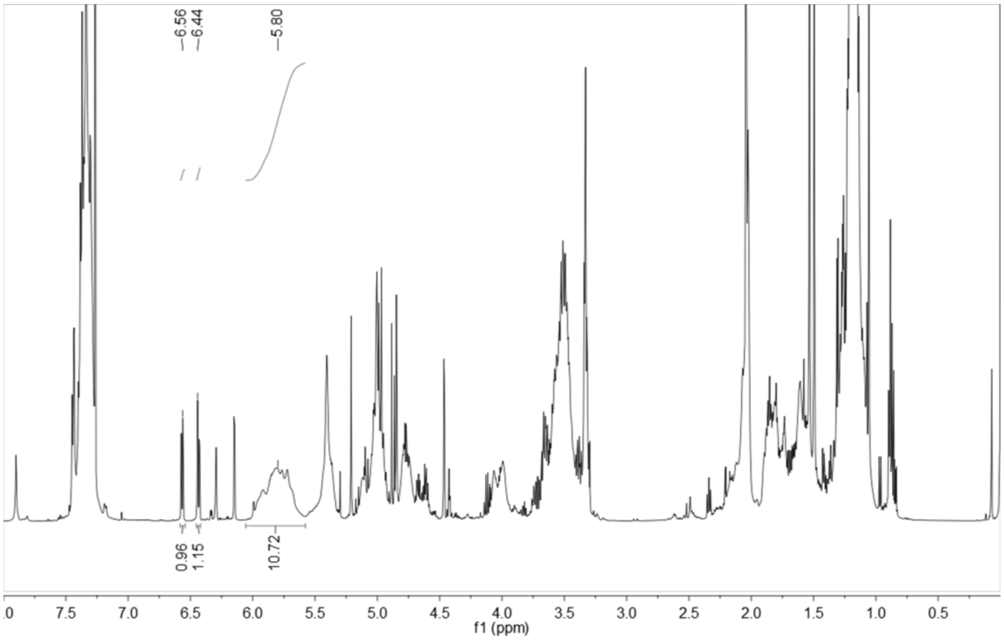

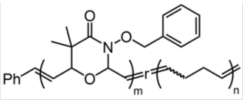

4.20 purified
^{1}H-NMR ($CDCl_3$, 500 MHz)
example $[\mathbf{4.04}]_o$:$[COD]_o$ = 150 : 50 → poly(**4.04**):pCOD = 3.6 : 1

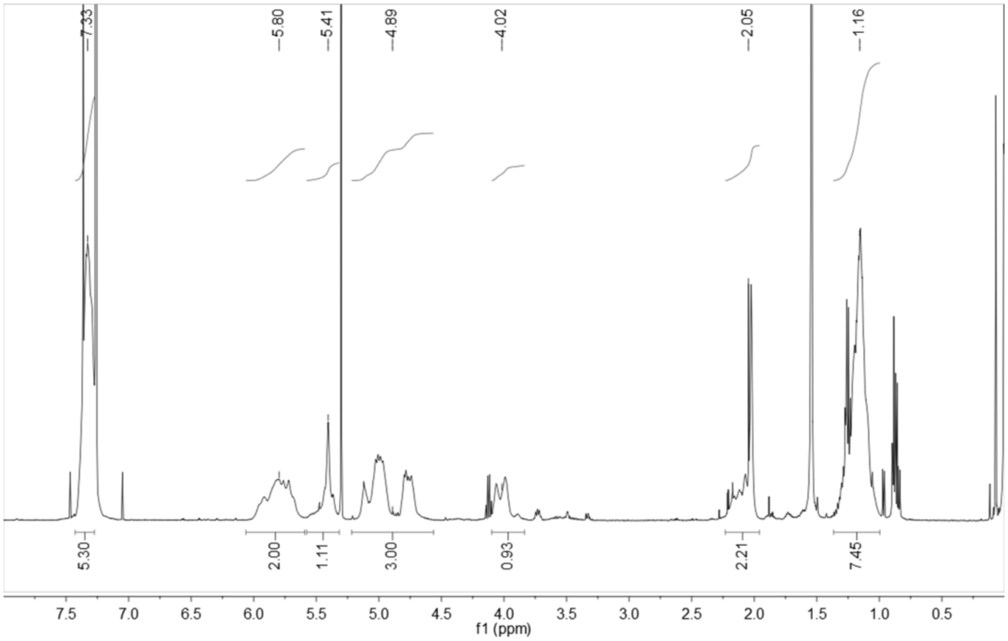

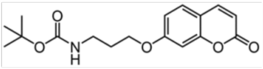

4.21
^{1}H-NMR (CDCl$_3$, 500 MHz)

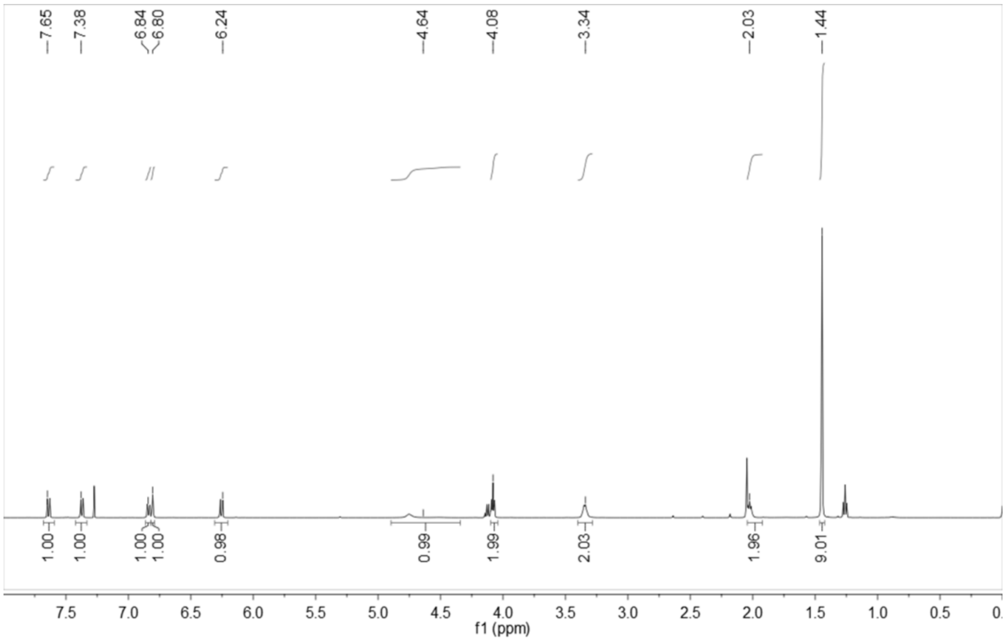

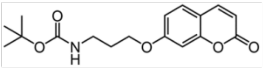

4.21
^{13}C-NMR (CDCl$_3$, 125 MHz)

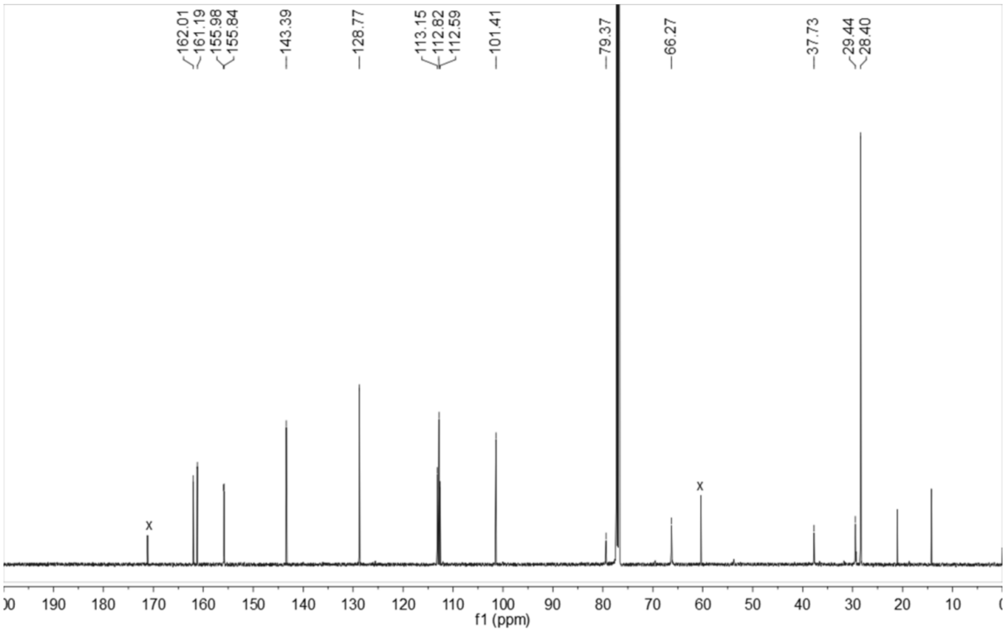

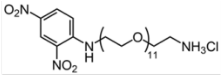
O2N
NO2
N
H
O
11
NH3Cl

A.01
^{1}H-NMR (MeOH-d$_4$, 500 MHz)

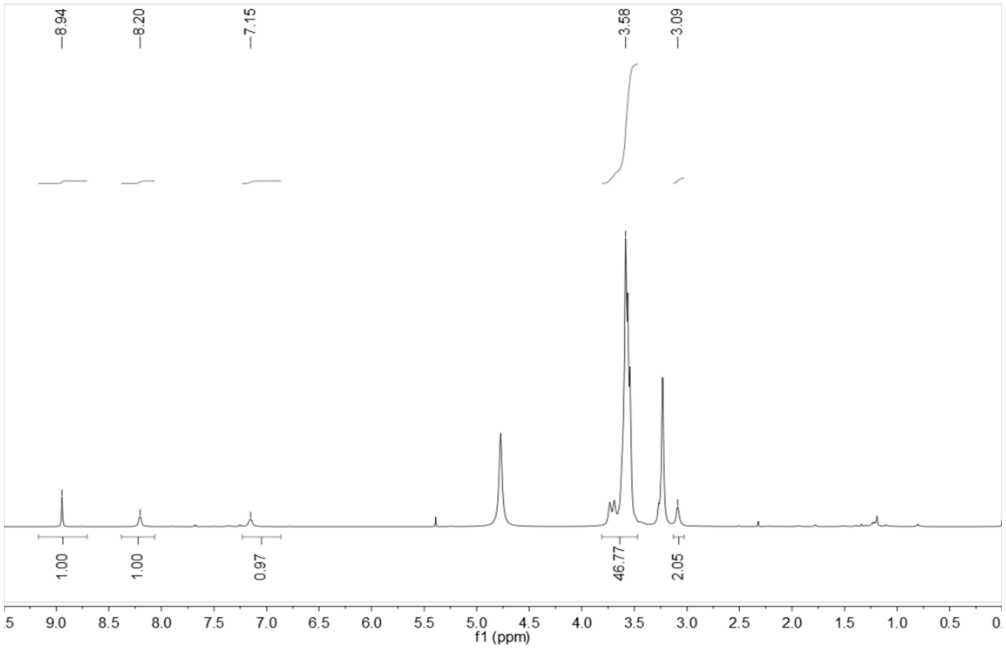

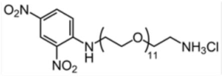
O2N
NO2
N
H
O
11
NH3Cl

A.01
^{13}H-NMR (MeOH-d$_4$, 125 MHz)

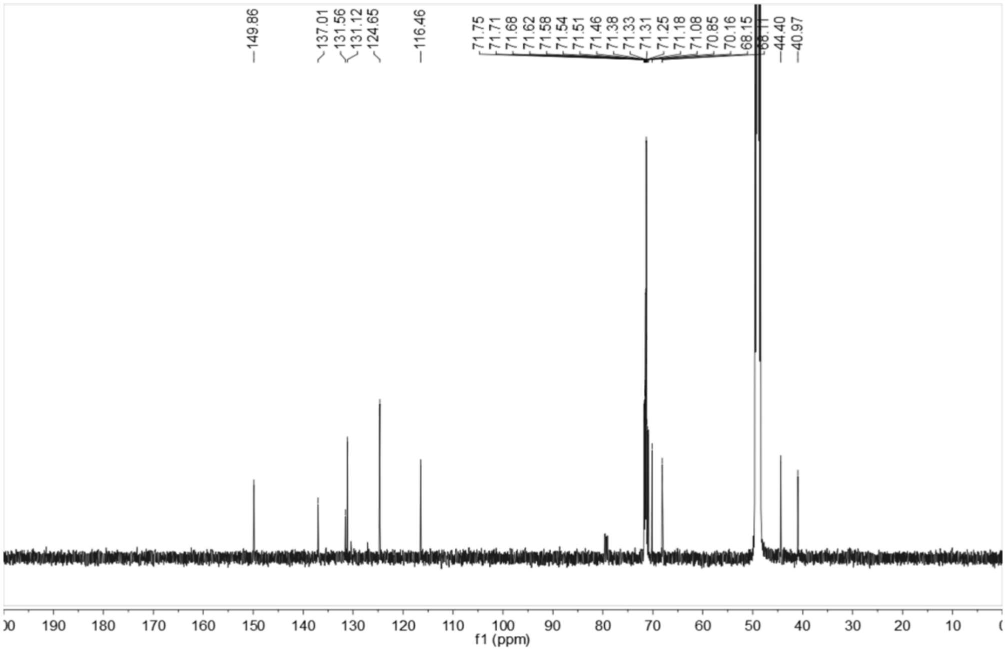

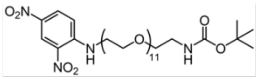
O$_2$N
N
H
O
11
N
H
O
O
NO$_2$

A.03
^{13}C-NMR (CDCl$_3$, 125 MHz)

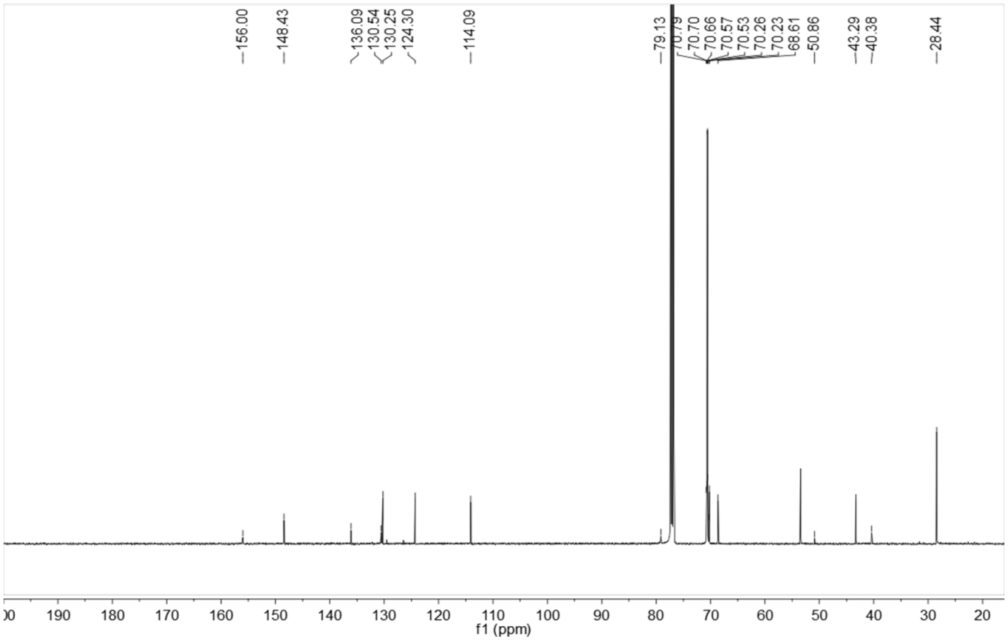

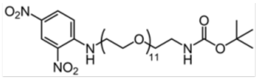
A.03
^{13}C-NMR (CDCl$_3$, 125 MHz)

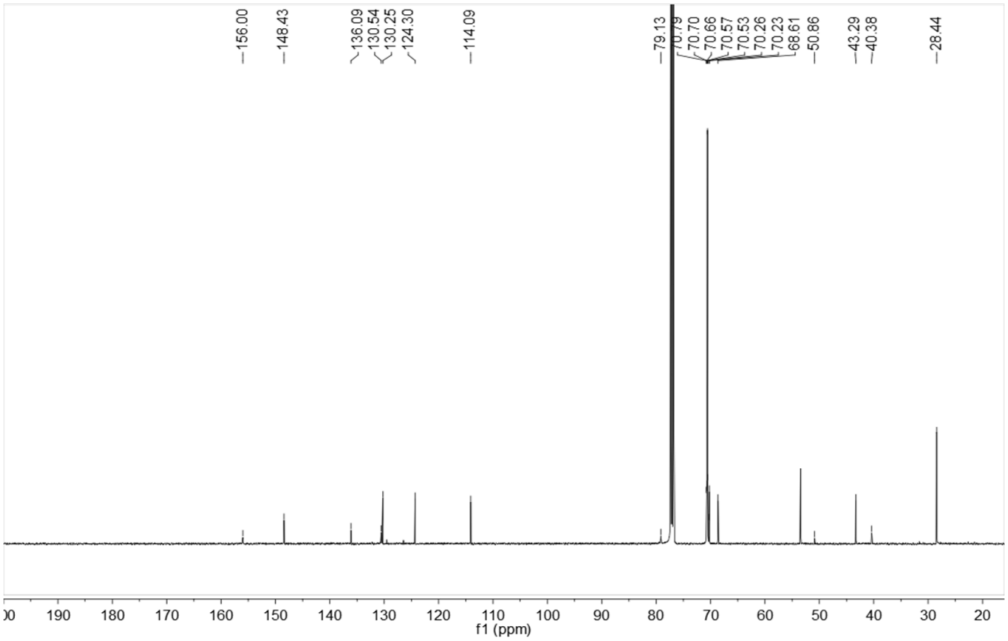

Compiled References

1. Duncan, R. The dawning era of polymer therapeutics. *Nat. Rev. Drug Discov.* **2003**, *2*, 347-360.

2. Mammen, M.; Chio, S.-K.; Whitesides, G. M. Polyvalent interactions in biological systems: implications for design and use of multivalent ligands and inhibitors. *Angew. Chem, Int. Ed.* **1998**, *37*, 2755-2794.

3. Kiessling, L. L.; Gestwicki, J. E.; Strong, L. E. Synthetic multivalent ligands as probes of signal transduction. *Angew. Chem. Int. Ed.* **2006**, *45*, 2348-2368.

4. Kiessling, L. L.; Splain, R. A. Chemical Approaches to Glycobiology. *Annu. Rev. Biochem.* **2010**, *79*, 619-653.

5. Kiessling, L. L.; Gestwicki, J. E.; Strong, L. E. Synthetic multivalent ligands in the exploration of cell-surface interactions. *Curr. Opin. Chem. Biol.* **2000**, *4*, 696-703.

6. Kiessling, L. L.; Grim, J. C. Glycopolymer probes of signal transduction. *Chemical Society Reviews* **2013**, *42*, 4476-4491.

7. Mortell, K. H.; Gingras, M.; Kiessling, L. L. Synthesis of Cell Agglutination Inhibitors by Ring–Opening Metathesis Polymerization. *J. Am. Chem. Soc.* **1994**, *116*, 10253-10254.

8. Schrock, R. R. Synthesis of stereoregular ROMP polymers using molybdenum and tungsten imido alkylidene initiators. *Dalton Trans.* **2011**, *40*, 7484-7495.

9. Schrock, R. R.; Hoveyda, A. H. Molybdenum and tungsten imido alkylidene complexes as efficient olefin-metathesis catalysts. *Angew. Chem. Int. Ed.* **2003**, *42*, 4592-4633.

10. Trnka, T. M.; Grubbs, R. H. The development of L2X2Ru = CHR olefin metathesis catalysts: An organometallic success story. *Acc. Chem. Res.* **2001**, *34*, 18-29.

11. Bielawski, C. W.; Grubbs, R. H. Living ring-opening metathesis polymerization. *Prog. Polym. Sci.* **2007**, *32*, 1-29.

12. Vougioukalakis, G. C.; Grubbs, R. H. Ruthenium-Based Heterocyclic Carbene-Coordinated Olefin Metathesis Catalysts. *Chem. Rev.* **2010**, *110*, 1746-1787.

13. Manning, D. D.; Hu, X.; Beck, P. J.; Kiessling, L. L. Synthesis of Sulfated Neoglycopolymers: Selective P-Selectin Inhibitors. *J. Am. Chem. Soc.* **1997**, *119*, 3161-3162.

14. Maynard, H. D.; Okada, S. Y.; Grubbs, R. H. Inhibition of cell adhesion to fibronectin by oligopeptide-substituted polynorbornenes. *J. Am. Chem. Soc.* **2001**, *123*, 1275-1279.

15. Lee, Y.; Sampson, N. S. Romping the cellular landscape: linear scaffolds for molecular recognition. *Curr. Opin. Struct. Biol.* **2006**, *16*, 544-550.

16. Binder, J. B.; Raines, R. T. Olefin metathesis for chemical biology. *Curr. Opin. Chem. Biol.* **2008**, *12*, 767-773.

17. Strong, L. E.; Kiessling, L. L. A General Synthetic Route to Defined, Biologically Active Multivalent Arrays. *J. Am. Chem. Soc.* **1999**, *121*, 6193-6196.

18. Buchmeiser, M. R. Homogeneous metathesis polymerization by well-defined group VI and group VIII transition-metal alkylidenes: Fundamentals and applications in the preparation of advanced materials. *Chem. Rev.* **2000**, *100*, 1565-1604.

19. Barrett, A. G. M.; Hopkins, B. T.; Kobberling, J. ROMPgel reagents in parallel synthesis. *Chem. Rev.* **2002**, *102*, 3301-3323.

20. Pontrello, J. K.; Allen, M. J.; Underbakke, E. S.; Kiessling, L. L. Solid-phase synthesis of polymers using the ring-opening metathesis polymerization. *J. Am. Chem. Soc.* **2005**, *127*, 14536-14537.

21. Yang, S. K.; Weck, M. Modular covalent multifunctionalization of copolymers. *Macromolecules* **2008**, *41*, 346-351.

22. Gauthier, M. A.; Gibson, M. I.; Klok, H. A. Synthesis of Functional Polymers by Post-Polymerization Modification. *Angew. Chem. Int. Ed.* **2009**, *48*, 48-58.

23. Kolonko, E. M.; Pontrello, J. K.; Mangold, S. L.; Kiessling, L. L. General Synthetic Route to Cell-Permeable Block Copolymers via ROMP. *J. Am. Chem. Soc.* **2009**, *131*, 7327-7333.

24. Allen, M. J.; Wangkanont, K.; Raines, R. T.; Kiessling, L. L. ROMP from ROMP: A New Approach to Graft Copolymer Synthesis. *Macromolecules* **2009**, *42*, 4023-4027.

25. Kanai, M.; Mortell, K. H.; Kiessling, L. L. Varying the Size of Multivalent Ligands: The Dependence of Concanavalin A Inhibition on Neoglycopolymer Length. *J. Am. Chem. Soc.* **1997**, *119*, 9931-9932.

26. Gestwicki, J. E.; Kiessling, L. L. Inter-receptor communication through arrays of bacterial chemoreceptors. *Nature* **2002**, *415*, 81-84.

27. Gestwicki, J. E.; Cairo, C. W.; Strong, L. E.; Oetjen, K. A.; Kiessling, L. L. Influencing receptor-ligand binding mechanisms with multivalent ligand architecture. *J. Am. Chem. Soc.* **2002**, *124*, 14922-14933.

28. Puffer, E. B.; Pontrello, J. K.; Hollenbeck, J. J.; Kink, J. A.; Kiessling, L. L. Activating B cell signaling with defined multivalent ligands. *ACS Chem. Biol.* **2007**, *2*, 252-262.

29. Rawat, M.; Gama, C. I.; Matson, J. B.; Hsieh-Wilson, L. C. Neuroactive Chondroitin Sulfate Glycomimetics. *J. Am. Chem. Soc.* **2008**, *130*, 2959-2961.

30. Courtney, A. H.; Puffer, E. B.; Pontrello, J. K.; Yang, Z. Q.; Kiessling, L. L. Sialylated multivalent antigens engage CD22 in trans and inhibit B cell activation. *Proc. Natl. Acad. Sci.* **2009**, *106*, 2500-2505.

31. Lee, Y.; Sampson, N. S. Polymeric ADAM Protein Mimics Interrogate Mammalian Sperm-Egg Binding. *Chembiochem* **2009**, *10*, 929-937.

32. Ivin, K. J.; Mol, J. C.: *Olefin metathesis and metathesis polymerization*; Academic Press: San Diego, 1997.

33. Schrock, R. R. Olefin metathesis by molybdenum imido alkylidene catalysts. *Tetrahedron* **1999**, *55*, 8141-8153.

34. Delaude, L.; Demonceau, A.; Noels, A. F. Highly Stereoselective Ruthenium-Catalyzed Ring-Opening Metathesis Polymerization of 2,3-Difunctionalized Norbornadienes and Their 7-Oxa Analogues. *Macromolecules* **1999**, *32*, 2091-2103.

35. Endo, K.; Grubbs, R. H. Chelated Ruthenium Catalysts for Z-Selective Olefin Metathesis. *J. Am. Chem. Soc.* **2011**, *133*, 8525-8527.

36. Keitz, B. K.; Endo, K.; Patel, P. R.; Herbert, M. B.; Grubbs, R. H. Improved Ruthenium Catalysts for Z-Selective Olefin Metathesis. *J. Am. Chem. Soc.* **2012**, *134*, 693-699.

37. Rosebrugh, L. E.; Marx, V. M.; Keitz, B. K.; Grubbs, R. H. Synthesis of Highly Cis, Syndiotactic Polymers via Ring-Opening Metathesis Polymerization Using Ruthenium Metathesis Catalysts. *J. Am. Chem. Soc.* **2013**, *135*, 10032-10035.

38. Lee, J. C.; Parker, K. A.; Sampson, N. S. Amino Acid-Bearing ROMP Polymers with a Stereoregular Backbone. *J. Am. Chem. Soc.* **2006**, *128*, 4578-4579.

39. Song, A.; Lee, J. C.; Parker, K. A.; Sampson, N. S. Scope of the Ring-Opening Metathesis Polymerization (ROMP) Reaction of 1-Substituted Cyclobutenes. *J. Am. Chem. Soc.* **2010**, *132*, 10513-10520.

40. Kobayashi, S.; Pitet, L. M.; Hillmyer, M. A. Regio- and Stereoselective Ring-Opening Metathesis Polymerization of 3-Substituted Cyclooctenes. *J. Am. Chem. Soc.* **2011**, *133*, 5794-5797.

41. Zhang, J.; Matta, M. E.; Hillmyer, M. A. Synthesis of Sequence-Specific Vinyl Copolymers by Regioselective ROMP of Multiply Substituted Cyclooctenes. *ACS Macro Lett.* **2012**, *1*, 1383-1387.

42. Zhang, J.; Matta, M. E.; Martinez, H.; Hillmyer, M. A. Precision Vinyl Acetate/Ethylene (VAE) Copolymers by ROMP of Acetoxy-Substituted Cyclic Alkenes. *Macromolecules* **2013**, *46*, 2535-2543.

43. Song, A.; Parker, K. A.; Sampson, N. S. Synthesis of Copolymers by Alternating ROMP (AROMP). *J. Am. Chem. Soc.* **2009**, *131*, 3444-3445.

44. Song, A.; Parker, K. A.; Sampson, N. S. Cyclic Alternating Ring-Opening Metathesis Polymerization (CAROMP). Rapid Access to Functionalized Cyclic Polymers. *Org. Lett.* **2010**, *12*, 3729-3731.

45. Vehlow, K.; Wang, D.; Buchmeiser, M. R.; Blechert, S. Alternating copolymerizations using a Grubbs-type initiator with an unsymmetrical, chiral N-heterocyclic carbene ligand. *Angew. Chem. Int. Ed.* **2008**, *47*, 2615-2618.

46. Kanai, M.; Mortell, K. H.; Kiessling, L. L. Varying the Size of Multivalent Ligands: The Dependence of Concanavalin A Binding on Neoglycopolymer Length. *J. Am. Chem. Soc.* **1997**, *119*, 9931-9932.

47. Song, A.-R.; Walker, S. G.; Parker, K. A.; Sampson, N. S. Antibacterial Studies of Cationic Polymers with Alternating, Random, and Uniform Backbones. *ACS Chem. Biol.* **2011**, *6*, 590-599.

48. Gordon, E. J.; Gestwicki, J. E.; Strong, L. E.; Kiessling, L. L. Synthesis of end-labeled multivalent ligands for exploring cell-surface-receptor-ligand interactions. *Chem. Biol.* **2000**, *7*, 9-16.

49. Hilf, S.; Kilbinger, A. F. M. Functional end groups for polymers prepared using ring-opening metathesis polymerization. *Nat. Chem.* **2009**, *1*, 537-546.

50. Leitgeb, A.; Wappel, J.; Slugovc, C. The ROMP toolbox upgraded. *Polymer* **2010**, *51*, 2927-2946.

51. Tasdelen, M. A.; Kahveci, M. U.; Yagci, Y. Telechelic polymers by living and controlled/living polymerization methods. *Prog. Polym. Sci.* **2011**, *36*, 455-567.

52. Nomura, K.; Abdellatif, M. M. Precise synthesis of polymers containing functional end groups by living ring-opening metathesis polymerization (ROMP): Efficient tools for synthesis of block/graft copolymers. *Polymer* **2010**, *51*, 1861-1881.

53. Nagarkar, A. A.; Crochet, A.; Fromm, K. M.; Kilbinger, A. F. M. Efficient Amine End-Functionalization of Living Ring-Opening Metathesis Polymers. *Macromolecules* **2012**, *45*, 4447-4453.

54. Matson, J. B.; Grubbs, R. H. Monotelechelic Poly(oxa)norbornenes by Ring-Opening Metathesis Polymerization Using Direct End-Capping and Cross-Metathesis. *Macromolecules* **2010**, *43*, 213-221.

55. Madkour, A. E.; Koch, A. H. R.; Lienkamp, K.; Tew, G. N. End-Functionalized ROMP Polymers for Biomedical Applications. *Macromolecules* **2010**, *43*, 4557-4561.

56. Mangold, S. L.; Carpenter, R. T.; Kiessling, L. L. Synthesis of fluorogenic polymers for visualizing cellular internalization. *Org. Lett.* **2008**, *10*, 2997-3000.

57. Fishman, J. M.; Kiessling, L. L. Synthesis of Functionalizable and Degradable Polymers by Ring-Opening Metathesis Polymerization. *Angew. Chem. Int. Ed.* **2013**, *52*, 5061-5064.

58. Schwab, P.; Grubbs, R. H.; Ziller, J. W. Synthesis and Applications of $RuCl_2$(=CHR')(PR_3)$_2$: The Influence of the Alkylidene Moiety on Metathesis Activity. *J. Am. Chem. Soc.* **1996**, *118*, 100-110.

59. Castle, T. C.; Hutchings, L. R.; Khosravi, E. Synthesis of block copolymers by changing living anionic polymerization into living ring opening metathesis polymerization. *Macromolecules* **2004**, *37*, 2035-2040.

60. Hilf, S.; Grubbs, R. H.; Kilbinger, A. F. M. Sacrificial synthesis of hydroxy-functionalized ROMP polymers: An efficiency study. *Macromolecules* **2008**, *41*, 6006-6011.

61. Hilf, S.; Kilbinger, A. F. M. Sacrificial Synthesis of Hydroxy-Telechelic Metathesis Polymers via Multiblock-Copolymers. *Macromolecules* **2009**, *42*, 1099-1106.

62. Lee, S.-G.; Brown, J. M.; Rogers, C. J.; Matson, J. B.; Krishnamurthy, C.; Rawat, M.; Hsieh-Wilson, L. C. End-functionalized glycopolymers as mimetics of chondroitin sulfate proteoglycans. *Chem. Sci.* **2010**, *1*, 322-325.

63. Mitchell, J. P.; Gibson, V. C.; Schrock, R. R. Chain-End Functionalization of Living Polymers Formed by the Ring-Opening Metathesis Polymerization of Norbornene *Macromolecules* **1991**, *24*, 1220-1221.

64. Nomura, K.; Schrock, R. R. Preparation of "Sugar Coated" Homopolymers and Multiblock ROMP Copolymers. *Macromolecules* **1996**, *29*, 540-545.

65. Louie, J.; Grubbs, R. H. Metathesis of electron-rich olefins: Structure and reactivity of electron-rich carbene complexes. *Organometallics* **2002**, *21*, 2153-2164.

66. Owen, R. M.; Gestwicki, J. E.; Young, T.; Kiessling, L. L. Synthesis and applications of end-labeled neoglycopolymers. *Org. Lett.* **2002**, *4*, 2293-2296.

67. Gestwicki, J. E.; Cairo, C. W.; Mann, D. A.; Owen, R. M.; Kiessling, L. L. Selective immobilization of multivalent ligands for surface plasmon resonance and fluorescence microscopy. *Anal. Biochem.* **2002**, *305*, 149-155.

68. Hilf, S.; Grubbs, R. H.; Kilbinger, A. F. M. End capping ring-opening olefin metathesis polymerization polymers with vinyl lactones. *J. Am. Chem. Soc.* **2008**, *130*, 11040-11048.

69. Mortell, K. H.; Gingras, M.; Kiessling, L. L. Synthesis of Cell Agglutination Inhibitors by Aqueous Ring-Opening Metathesis Polymerization. *J. Am. Chem. Soc.* **1994**, *116*, 12053-12054.

70. Fraser, C.; Grubbs, R. H. Synthesis of Glycopolymers of Controlled Molecular Weight by Ring Opening Metathesis Polymerization Using Well-Defined Ruthenium Carbene Catalysts. *Macromolecules* **1995**, *28*, 7248-7255.

71. Schwab, P.; France, M. B.; Ziller, J. W.; Grubbs, R. H. A series of well-defined metathesis catalysts - synthesis of [RuCl2(:CHR')(PR3)2] and their reactions. *Angew. Chem. Int. Ed.* **1995**, *34*, 2039-2041.

72. Schwab, P.; Grubbs, R. H.; Ziller, J. W. Synthesis and Applications of RuCl2(:CHR')(PR3)2: The Influence of the Alkylidene Moiety on Metathesis Activity. *J. Am. Chem. Soc.* **1996**, *118*, 100-110.

73. Ulman, M.; Grubbs, R. H. Ruthenium Carbene-Based Olefin Metathesis Initiators: Catalyst Decomposition and Longevity. *J. Org. Chem.* **1999**, *64*, 7202-7207.

74. Scholl, M.; Ding, S.; Lee, C. W.; Grubbs, R. H. Synthesis and Activity of a New Generation of Ruthenium-Based Olefin Metathesis Catalysts Coordinated with 1,3-Dimesityl-4,5-dihydroimidazol-2-ylidene Ligands. *Org. Lett.* **1999**, *1*, 953-956.

75. Bielawski, C. W.; Grubbs, R. H. Highly efficient ring-opening metathesis polymerization (ROMP) using new ruthenium catalysts containing N-heterocyclic carbene ligands. *Angew. Chem. Int. Ed.* **2000**, *39*, 2903-2906.

76. Mortell, K. H.; Weatherman, R. V.; Kiessling, L. L. Recognition Specificity of Neoglycopolymers Prepared by Ring-Opening Metathesis Polymerization. *J. Am. Chem. Soc.* **1996**, *118*, 2297-2298.

77. Manning, D. D.; Strong, L. E.; Hu, X.; Beck, P. J.; Kiessling, L. L. Neoglycopolymer Inhibitors of the Selectins. *Tetrahedron* **1997**, *53*, 11937-11952.

78. Biagini, S. C. G.; Gibson, V. C.; Giles, M. R.; Marshall, E. L.; North, M. Synthesis of penicillin derived polymers utilising ring-opening metathesis polymerisation methodology. *Chem. Comm.* **1997**, 1097-1098.

79. Gordon, E. J.; Sanders, W. J.; Kiessling, L. L. Synthetic Ligands Effect Cell Surface Strategies. *Nature* **1998**, *392*, 30-31.

80. Arimoto, H.; Nishimura, K.; Kinumi, T.; Hayakawa, I.; Uemura, D. Multivalent polymer of vancomycin: enhanced antibacterial activity against VRE. *Chem. Comm.* **1999**, 1361-1362.

81. Watson, K. J.; Anderson, D. R.; Nguyen, S. T. Toward polymeric anticancer drug cocktails from ring-opening metathesis polymerization. *Macromolecules* **2001**, *34*, 3507-3509.

82. Kolonko, E. M.; Kiessling, L. L. A polymeric domain that promotes cellular internalization. *J. Am. Chem. Soc.* **2008**, *130*, 5626-5627.

83. Lynn, D. M.; Mohr, B.; Grubbs, R. H.; Henling, L. M.; Day, M. W. Water-Soluble Ruthenium Alkylidenes: Synthesis, Characterization, and Application to Olefin Metathesis polymerization in Protic Solvents. *J. Am. Chem. Soc.* **2000**, *122*, 6601-6609.

84. Mohr, B.; Lynn, D. M.; Grubbs, R. H. Synthesis of Water-Soluble, Aliphatic Phosphines and Their Application to Well-Defined Ruthenium Olefin Metathesis Catalysts. *Organometallics* **1996**, *15*, 4317-4325.

85. Hong, S. H.; Grubbs, R. H. Highly active water-soluble olefin metathesis catalyst. *J. Am. Chem. Soc.* **2006**, *128*, 3508-3509.

86. Burtscher, D.; Grela, K. Aqueous Olefin Metathesis. *Angew. Chem. Int. Ed.* **2009**, *48*, 442-454.

87. Takashima, Y.; Uramatsu, K.; Jomori, D.; Harima, A.; Otsubo, M.; Yamaguchi, H.; Harada, A. Ring-Opening Metathesis Polymerization by a Ru Phosphine Derivative of Cyclodextrin in Water. *ACS Macro Lett.* **2013**, *2*, 384-387.

88. Love, J. A.; Morgan, J. P.; Trnka, T. M.; Grubbs, R. H. A practical and highly active ruthenium-based catalyst that effects the cross metathesis of acrylonitrile. *Angew. Chem. Int. Ed.* **2002**, *41*, 4035-4037.

89. Choi, T. L.; Grubbs, R. H. Controlled living ring-opening-metathesis polymerization by a fast-initiating ruthenium catalyst. *Angew. Chem. Int. Ed.* **2003**, *42*, 1743-1746.

90. Matson, J. B.; Grubbs, R. H. Synthesis of fluorine-18 functionalized nanoparticles for, use as in vivo molecular imaging agents. *J. Am. Chem. Soc* **2008**, *130*, 6731-6733.

91. Poree, D. E.; Giles, M. D.; Lawson, L. B.; He, J.; Grayson, S. M. Synthesis of Amphiphilic Star Block Copolymers and Their Evaluation as Transdermal Carriers. *Biomacromolecules* **2011**, *12*, 898-906.

92. Wang, Y.; Grayson, S. M. Approaches for the preparation of non-linear amphiphilic polymers and their applications to drug delivery. *Adv. Drug Delivery Rev.* **2012**, *64*, 852-865.

93. Hoskins, J. N.; Grayson, S. M. Cyclic polyesters: synthetic approaches and potential applications. *Polym. Chem.* **2011**, *2*, 289-299.

94. Laurent, B. A.; Grayson, S. M. Synthesis of Cyclic Dendronized Polymers via Divergent "Graft-from" and Convergent Click "Graft-to" Routes: Preparation of Modular Toroidal Macromolecules. *J. Am. Chem. Soc.* **2011**, *133*, 13421-13429.

95. Bielawski, C. W.; Benitez, D.; Grubbs, R. H. An "endless" route to cyclic polymers. *Science* **2002**, *297*, 2041-2044.

96. Boydston, A. J.; Xia, Y.; Kornfield, J. A.; Gorodetskaya, I. A.; Grubbs, R. H. Cyclic Ruthenium-Alkylidene Catalysts for Ring-Expansion Metathesis Polymerization. *J. Am. Chem. Soc.* **2008**, *130*, 12775-12782.

97. Zhang, K.; Lackey, M. A.; Cui, J.; Tew, G. N. Gels Based on Cyclic Polymers. *J. Am. Chem. Soc.* **2011**, *133*, 4140-4148.

98. Song, A. R.; Lee, J. C.; Parker, K. A.; Sampson, N. S. Scope of the Ring-Opening Metathesis Polymerization (ROMP) Reaction of 1-Substituted Cyclobutenes. *J. Am. Chem. Soc.* **2010**, *132*, 10513-10520.

99. Carlise, J. R.; Kriegel, R. M.; Rees, W. S., Jr.; Weck, M. Synthesis and Hydrolysis Behavior of Side-Chain Functionalized Norbornenes. *J. Org. Chem.* **2005**, *70*, 5550-5560.

100. Bertin, P. A.; Smith, D.; Nguyen, S. T. High-density doxorubicin-conjugated polymeric nanoparticles via ring-opening metathesis polymerization. *Chem. Comm.* **2005**, 3793-3795.

101. Pichavant, L.; Bourget, C.; Durrieu, M.-C.; Heroguez, V. Synthesis of pH-Sensitive Particles for Local Delivery of an Antibiotic via Dispersion ROMP. *Macromolecules* **2011**, *44*, 7879-7887.

102. Rao, N. V.; Mane, S.; Kishore, A.; Das, S. J.; Shunmugam, R. Norbornene Derived Doxorubicin Copolymers as Drug Carriers with pH Responsive Hydrazone Linker. *Biomacromolecules* **2012**, *13*, 221-230.

103. Johnson, J. A.; Lu, Y. Y.; Burts, A. O.; Lim, Y. H.; Finn, M. G.; Koberstein, J. T.; Turro, N. J.; Tirrell, D. A.; Grubbs, R. H. Core-Clickable PEG-Branch-Azide Bivalent-Bottle-Brush Polymers by ROMP: Grafting-Through and Clicking-To. *J. Am. Chem. Soc.* **2011**, *133*, 559-566.

104. Johnson, J. A.; Lu, Y. Y.; Burts, A. O.; Xia, Y.; Durrell, A. C.; Tirrell, D. A.; Grubbs, R. H. Drug-Loaded, Bivalent-Bottle-Brush Polymers by Graft-through ROMP. *Macromolecules* **2010**, *43*, 10326-10335.

105. Jeffrey, C. S.; Barnes, K. L.; Eickhoff, J. A.; Carson, C. R. Generation and Reactivity of Aza-Oxyallyl Cationic Intermediates: Aza-[4+3] Cycloaddition Reactions for Heterocycle Synthesis. *J. Am. Chem. Soc.* **2011**, *133*, 7688-7691.

106. Baessler, K. A.; Lee, Y.; Roberts, K. S.; Facompre, N.; Sampson, N. S. Multivalent fertilin beta oligopeptides: The dependence of fertilization inhibition on length and density. *Chem. Biol.* **2006**, *13*, 251-259.

107. Roberts, K. S.; Sampson, N. S. Increased polymer length of oligopeptide-substituted polynorbornenes with LiCl. *J. Org. Chem.* **2003**, *68*, 2020-2023.

108. Baessler, K. A.; Lee, Y.; Sampson, N. S. β1 Integrin Is an Adhesion Protein for Sperm Binding to Eggs. *ACS Chem. Biol.* **2009**, *4*.

109. Jung, H.; Carberry, T. P.; Weck, M. Synthesis of First- and Second-Generation Poly(amide)-Dendronized Polymers via Ring-Opening Metathesis Polymerization. *Macromolecules* **2011**, *44*, 9075-9083.

110. Gestwicki, J. E.; Strong, L. E.; Cairo, C. W.; Boehm, F. J.; Kiessling, L. L. Cell aggregation by scaffolded receptor clusters. *Chem. Biol.* **2002**, *9*, 163-169.

111. Griffith, B. R.; Allen, B. L.; Rapraeger, A. C.; Kiessling, L. L. A polymer scaffold for protein oligomerization. *J. Am. Chem. Soc.* **2004**, *126*, 1608-1609.

112. Schaefer, M.; Hanik, N.; Kilbinger, A. F. M. ROMP Copolymers for Orthogonal Click Functionalizations. *Macromolecules* **2012**, *45*, 6807-6818.

113. Kolb, H. C.; Finn, M. G.; Sharpless, K. B. Click chemistry: Diverse chemical function from a few good reactions. *Angew. Chem. Int. Ed.* **2001**, *40*, 2004-2021.

114. Binder, W. H.; Kluger, C. Combining ring-opening metathesis polymerization (ROMP) with Sharpless-type "click" reactions: An easy method for the preparation of side chain functionalized poly(oxynorbornenes). *Macromolecules* **2004**, *37*, 9321-9330.

115. Mansfeld, U.; Pietsch, C.; Hoogenboom, R.; Becer, C. R.; Schubert, U. S. Clickable initiators, monomers and polymers in controlled radical polymerizations - a prospective combination in polymer science. *Polym. Chem.* **2010**, *1*, 1560-1598.

116. Boren, B. C.; Narayan, S.; Rasmussen, L. K.; Zhang, L.; Zhao, H.; Lin, Z.; Jia, G.; Fokin, V. V. Ruthenium-Catalyzed Azide−Alkyne Cycloaddition: Scope and Mechanism. *J. Am. Chem.l Soc.* **2008**, *130*, 8923-8930.

117. Xia, Y.; Verduzco, R.; Grubbs, R. H.; Kornfield, J. A. Well-Defined Liquid Crystal Gels from Telechelic Polymers. *J. Am. Chem. Soc.* **2008**, *130*, 1735-1740.

118. Binder, W. H.; Kluger, C.; Josipovic, M.; Straif, C. J.; Friedbacher, G. Directing Supramolecular Nanoparticle Binding onto Polymer Films: Film Formation and Influence of Receptor Density on Binding Densities. *Macromolecules* **2006**, *39*, 8092-8101.

119. Kluger, C.; Binder, W. H. Functionalized poly(oxanorbornene)-block-copolymers: preparation via ROMP/click-methodology. *J. Polym. Sci., Part A: Polym. Chem.* **2006**, *45*, 485-499.

120. Yang, S. K.; Weck, M. Modular Covalent Multifunctionalization of Copolymers. *Macromolecules* **2007**, *41*, 346-351.

121. Colak, S.; Tew, G. N. Amphiphilic Polybetaines: The Effect of Side-Chain Hydrophobicity on Protein Adsorption. *Biomacromolecules* **2012**, *13*, 1233-1239.

122. Bertin, P. A.; Watson, K. J.; Nguyen, S. T. Indomethacin-containing nanoparticles derived from amphiphilic polynorbornene: a model ROMP-based drug encapsulation system. *Macromolecules* **2004**, *37*, 8364-8372.

123. Eren, T.; Tew, G. N. Phosphonic acid-based amphiphilic diblock copolymers derived from ROMP. *J. Polym. Sci., Part A: Polym. Chem.* **2009**, *47*, 3949-3956.

124. Colak, S.; Tew, G. N. Dual-Functional ROMP-Based Betaines: Effect of Hydrophilicity and Backbone Structure on Nonfouling Properties. *Langmuir* **2012**, *28*, 666-675.

125. Som, A.; Tezgel, A. O.; Gabriel, G. J.; Tew, G. N. Self-Activation in De Novo Designed Mimics of Cell-Penetrating Peptides. *Angew. Chem. Int. Ed.* **2011**, *50*, 6147-6150.

126. Lienkamp, K.; Madkour, A. E.; Kumar, K.-N.; Nuesslein, K.; Tew, G. N. Antimicrobial Polymers Prepared by Ring-Opening Metathesis Polymerization: Manipulating Antimicrobial Properties by Organic Counterion and Charge Density Variation. *Chem. Eur. J.* **2009**, *15*, 11715-11722.

127. Dettmer, C. M.; Gray, M. K.; Torkelson, J. M.; Nguyen, S. T. Synthesis and Functionalization of ROMP-Based Gradient Copolymers of 5-Substituted Norbornenes. *Macromolecules* **2004**, *37*, 5504-5512.

128. Ambade, A. V.; Yang, S. K.; Weck, M. Supramolecular ABC triblock copolymers. *Angew. Chem. Int. Ed.* **2009**, *48*, 2894-2898.

129. Nair, K. P.; Breedveld, V.; Weck, M. Modulating mechanical properties of self-assembled polymer networks by multi-functional complementary hydrogen bonding. *Soft Matter* **2011**, *7*, 553-559.

130. Gibbs, J. M.; Park, S.-J.; Anderson, D. R.; Watson, K. J.; Mirkin, C. A.; Nguyen, S. T. Polymer−DNA Hybrids as Electrochemical Probes for the Detection of DNA. *J. Am. Chem. Soc.* **2005**, *127*, 1170-1178.

131. Allen, M. J.; Raines, R. T.; Kiessling, L. L. Contrast agents for magnetic resonance imaging synthesized with ring-opening metathesis polymerization. *J. Am. Chem. Soc.* **2006**, *128*, 6534-6535.

132. Miki, K.; Kimura, A.; Oride, K.; Kuramochi, Y.; Matsuoka, H.; Harada, H.; Hiraoka, M.; Ohe, K. High-Contrast Fluorescence Imaging of Tumors In Vivo Using Nanoparticles of Amphiphilic Brush-Like Copolymers Produced by ROMP. *Angew. Chem. Int. Ed.* **2011**, *50*, 6567-6570.

133. Miki, K.; Oride, K.; Kimura, A.; Kuramochi, Y.; Matsuoka, H.; Harada, H.; Hiraoka, M.; Ohe, K. Influence of Side Chain Length on Fluorescence Intensity of ROMP-Based Polymeric Nanoparticles and Their Tumor Specificity in In-Vivo Tumor Imaging. *Small* **2011**, *7*, 3536-3547.

134. Sankaran, N. B.; Rys, A. Z.; Nassif, R.; Nayak, M. K.; Metera, K.; Chen, B.; Bazzi, H. S.; Sleiman, H. F. Ring-Opening Metathesis Polymers for Biodetection and Signal Amplification: Synthesis and Self-Assembly. *Macromolecules* **2010**, *43*, 5530-5537.

135. Metera, K. L.; Hanni, K. D.; Zhou, G.; Nayak, M. K.; Bazzi, H. S.; Juncker, D.; Sleiman, H. F. Luminescent Iridium(III)-Containing Block Copolymers: Self-Assembly into Biotin-Labeled Micelles for Biodetection Assays. *ACS Macro Lett.* **2012**, *1*, 954-959.

136. Miller, P. W.; Long, N. J.; Vilar, R.; Gee, A. D. Synthesis of ^{11}C, ^{18}F, ^{15}O, and ^{13}N radiolabels for positron emission tomography. *Angew. Chem. Int. Ed.* **2008**, *47*, 8998-9033.

137. Ametamey, S. M.; Honer, M.; Schubiger, P. A. Molecular Imaging with PET. *Chem. Rev.* **2008**, *108*, 1501-1516.

138. Maeda, H.; Wu, J.; Sawa, T.; Matsumura, Y.; Hori, K. Tumor vascular permeability and the EPR effect in macromolecular therapeutics: a review. *J. Control. Release* **2000**, *65*, 271-284.

139. Merbach, A. E.; Toth, E. *The Chemistry of Contrast Agents in Medical Magnetic Resonance Imaging*; John Wiley & Sons Ltd., 2001.

140. Tweedle, M. F.; Kumar, K. Magnetic resonance imaging (MRI) contrast agents. *Top. Biol. Inorg. Chem.* **1999**, *2*, 1-43.

141. Reichert, D. E.; Lewis, J.; Anderson, C. J. Metal complexes as diagnostic tools. *Coord. Chem. Rev.* **1999**, *184*, 3-66.

142. Caravan, P.; Ellison, J. J.; McMurry, T. J.; Lauffer, R. B. Gadolinium(III) Chelates as MRI Contrast Agents: Structure, Dynamics, and Applications. *Chem. Rev.* **1999**, *99*, 2293-2352.

143. Uzgiris, E. E.; Cline, H.; Moasser, B.; Grimmond, B.; Amaratunga, M.; Smith, J. F.; Goddard, G. Conformation and Structure of Polymeric Contrast Agents for Medical Imaging. *Biomacromolecules* **2004**, *5,* 54-61.

144. Aime, S.; Botta, M.; Terreno, E. Gd(III)-based contrast agents for MRI. *Adv. Inorg. Chem.* **2005**, *57*, 173-237.

145. Raymond, K. N.; Pierre, V. C. Next Generation, High Relaxivity Gadolinium MRI Agents. *Bioconjugate Chem.* **2005**, *16*, 3-8.

146. Bertozzi, C. R.; Kiessling, L. L. Chemical glycobiology. *Science* **2001**, *291*, 2357-2364.

147. Kiessling, L. L.; Strong, L. E.; Gestwicki, J. E. Principles for Multivalent Ligand Design. *Annu. Rep. Med. Chem.* **2000**, *35*, 321-330.

148. Cairo, C. W.; Gestwicki, J. E.; Kanai, M.; Kiessling, L. L. Control of Multivalent Interactions by Binding Epitope Density. *J. Am. Chem. Soc.* **2002**, *124*, 1615-1619.

149. Weatherman, R. V.; Kiessling, L. L. Fluorescence Anisotropy Assays Reveal Affinity and Specificity of *C*- and *O*-Glycosides for Concanavalin A. *J. Org. Chem.* **1996**, *61*, 534-538.

150. Gama, C. I.; Tully, S. E.; Sotogaku, N.; Clark, P. M.; Rawat, M.; Vaidehi, N.; Goddard, W. A., III; Nishi, A.; Hsieh-Wilson, L. C. Sulfation patterns of glycosaminoglycans encode molecular recognition and activity. *Nat. Chem. Biol.* **2006**, *2*, 467-473.

151. Tully, S. E.; Rawat, M.; Hsieh-Wilson, L. C. Discovery of a TNF-α Antagonist Using Chondroitin Sulfate Microarrays. *J. Am. Chem. Soc.* **2006**, *128*, 7740-7741.

152. Sotogaku, N.; Tully, S. E.; Gama, C. I.; Higashi, H.; Tanaka, M.; Hsieh-Wilson, L. C.; Nishi, A. Activation of phospholipase C pathways by a synthetic chondroitin sulfate-E

tetrasaccharide promotes neurite outgrowth of dopaminergic neurons. *J. Neurochem.* **2007**, *103*, 749-760.

153. Shipp, E. L.; Hsieh-Wilson, L. C. Profiling the sulfation specificities of glycosaminoglycan interactions with growth factors and chemotactic proteins using microarrays. *Chem. Biol.***2007**, *14*, 195-208.

154. Zhu, X.; Bansal, N. P.; Evans, J. P. Identification of key functional amino acids of the mouse fertilin β (ADAM2) disintegrin loop for cell-cell adhesion during fertilization. *J. Biol. Chem.* **2000**, *275*, 7677-7683.

155. Bigler, D.; Takahashi, Y.; Chen, M. S.; Almeida, E. A. C.; Osbourne, L.; White, J. M. Sequence-specific interaction between the disintegrin domain of mouse ADAM 2 (fertilin β) and murine eggs. Role of the α6 integrin subunit. *J. Biol. Chem.* **2000**, *275*, 11576-11584.

156. Baessler, K. A.; Lee, Y.; Roberts, K. S.; Facompre, N.; Sampson, N. S. Multivalent Fertilinβ Oligopeptides: The Dependence of Fertilization Inhibition on Length and Density. *Chem. Biol.* **2006**, *13*, 251-259.

157. Cochran, A. G. Antagonists of protein-protein interactions. *Chem. Biol.* **2000**, *7*, R85-R94.

158. Griffiths, E. K.; Krawczyk, C.; Kong, Y. Y.; Raab, M.; Hyduk, S. J.; Bouchard, D.; Chan, V. S.; Kozieradzki, I.; Oliveira-Dos-Santos, A. J.; Wakeham, A.; Ohashi, P. S.; Cybulsky, M. I.; Rudd, C. E.; Penninger, J. M. Positive regulation of T cell activation and integrin adhesion by the adapter Fyb/Slap. *Science* **2001**, *293*, 2260-2263.

159. Maheshwari, G.; Brown, G.; Lauffenburger, D. A.; Wells, A.; Griffith, L. G. Cell adhesion and motility depend on nanoscale RGD clustering. *J. Cell Sci.* **2000**, *113*, 1677-1686.

160. Viola, A.; Schroeder, S.; Sakakibara, Y.; Lanzavecchia, A. T lymphocyte costimulation mediated by reorganization of membrane microdomains. *Science* **1999**, *283*, 680-682.

161. Gordon, E. J.; Sanders, W. J.; Kiessling, L. L. Synthetic ligands point to cell surface strategies. *Nature* **1998**, *392*, 30-31.

162. Goodnow, C. C. Balancing immunity and tolerance: deleting and tuning lymphocyte repertoires. *Proc. Natl. Acad. Sci.* **1996**, *93*, 2264-2271.

163. Healy, J. I.; Goodnow, C. C. Positive versus negative signaling by lymphocyte antigen receptors. *Annu. Rev. Immunol.* **1998**, *16*, 645-670.

164. Courtney, A. H.; Puffer, E. B.; Pontrello, J. K.; Yang, Z.-Q.; Kiessling, L. L. Sialylated multivalent antigens engage CD22 in trans and inhibit B cell activation. *Proc. Natl. Acad. Sci.* **2009**, *106*, 2500-2505.

165. Gestwicki, J. E.; Strong, L. E.; Borchardt, S. L.; Cairo, C. W.; Schnoes, A. M.; Kiessling, L. L. Designed potent multivalent chemoattractants for Escherichia coli. *Bioorg. Med. Chem.* **2001**, *9*, 2387-2393.

166. Lamanna, A. C.; Gestwicki, J. E.; Strong, L. E.; Borchardt, S. L.; Owen, R. M.; Kiessling, L. L. Conserved amplification of chemotactic responses through chemoreceptor interactions. *J. Bacteriol.* **2002**, *184*, 4981-4987.

167. Vives, E.; Brodin, P.; Lebleu, B. A truncated HIV-1 Tat protein basic domain rapidly translocates through the plasma membrane and accumulates in the cell nucleus. *J. Biol. Chem.* **1997**, *272*, 16010-16017.

168. Lewin, M.; Carlesso, N.; Tung, C.-H.; Tang, X.-W.; Cory, D.; Scadden, D. T.; Weissleder, R. Tat peptide-derivatized magnetic nanoparticles allow in vivo tracking and recovery of progenitor cells. *Nat. Biotechnol.* **2000**, *18*, 410-414.

169. Torchilin, V. P.; Rammohan, R.; Weissig, V.; Levchenko, T. S. TAT peptide on the surface of liposomes affords their efficient intracellular delivery even at low temperature and in the presence of metabolic inhibitors. *Proc. Natl. Acad. Sci.* **2001**, *98*, 8786-8791.

170. Snyder, E. L.; Dowdy, S. F. Cell Penetrating Peptides in Drug Delivery. *Pharm. Res.* **2004**, *21*, 389-393.

171. Futaki, S. Oligoarginine vectors for intracellular delivery: design and cellular-uptake mechanisms. *Biopolymers* **2006**, *84*, 241-249.

172. Tyagi, M.; Rusnati, M.; Presta, M.; Giacca, M. Internalization of HIV-1 Tat requires cell surface heparan sulfate proteoglycans. *J. Biol. Chem.* **2001**, *276*, 3254-3261.

173. Schmidt, N. W.; Lis, M.; Zhao, K.; Lai, G. H.; Alexandrova, A. N.; Tew, G. N.; Wong, G. C. L. Molecular Basis for Nanoscopic Membrane Curvature Generation from Quantum Mechanical Models and Synthetic Transporter Sequences. *J. Am. Chem. Soc.* **2012**, *134*, 19207-19216.

174. Stoddart, A.; Jackson, A. P.; Brodsky, F. M. Plasticity of B cell receptor internalization upon conditional depletion of clathrin. *Mol. Biol. Cell* **2005**, *16*, 2339-2348.

175. Hou, P.; Araujo, E.; Zhao, T.; Zhang, M.; Massenburg, D.; Veselits, M.; Doyle, C.; Dinner, A. R.; Clark, M. R. B cell antigen receptor signaling and internalization are mutually exclusive events. *PLoS Biol.* **2006**, *4*, 1147-1158.

176. Chandran, S. S.; Dickson, K. A.; Raines, R. T. Latent fluorophore based on the trimethyl lock. *J. Am. Chem. Soc.* **2005**, *127*, 1652-1653.

177. Lavis, L. D.; Chao, T.-Y.; Raines, R. T. Latent blue and red fluorophores based on the trimethyl lock. *ChemBioChem* **2006**, *7*, 1151-1154.

178. Amsberry, K. L.; Gerstenberger, A. E.; Borchardt, R. T. Amine prodrugs which utilize hydroxy amide lactonization. II. A potential esterase-sensitive amide prodrug. *Pharm. Res.* **1991**, *8*, 455-461.

179. Kataoka, K.; Harada, A.; Nagasaki, Y. Block copolymer micelles for drug delivery: design, characterization and biological significance. *Adv. Drug Delivery Rev.* **2001**, *47*, 113-131.

180. Murthy, N.; Xu, M.; Schuck, S.; Kunisawa, J.; Shastri, N.; Frechet, J. M. J. A macromolecular delivery vehicle for protein-based vaccines: Acid-degradable protein-loaded microgels. *Proc. Natl. Acad. Sci.* **2003**, *100*, 4995-5000.

181. Boas, U.; Heegaard, P. M. H. Dendrimers in drug research. *Chem. Soc. Rev.* **2004**, *33*, 43-63.

182. Lee, C. C.; MacKay, J. A.; Frechet, J. M. J.; Szoka, F. C. Designing dendrimers for biological applications. *Nat. Biotechnol.* **2005**, *23*, 1517-1526.

183. Kiick, K. L. Polymer therapeutics. *Science* **2007**, *317*, 1182-1183.

184. O'Keefe, T. L.; Williams, G. T.; Davies, S. L.; Neuberger, M. S. Hyperresponsive B cells in CD22-deficient mice. *Science* **1996**, *274*, 798-801.

185. Nitschke, L. The role of CD22 and other inhibitory co-receptors in B-cell activation. *Curr. Opin. Immunol.* **2005**, *17*, 290-297.

186. Razi, N.; Varki, A. Masking and unmasking of the sialic acid-binding lectin activity of CD22 (Siglec-2) on B lymphocytes. *Proc. Natl. Acad. Sci.* **1998**, *95*, 7469-7474.

187. Collins, B. E.; Blixt, O.; DeSieno, A. R.; Bovin, N.; Marth, J. D.; Paulson, J. C. Masking of CD22 by cis ligands does not prevent redistribution of CD22 to sites of cell contact. *Proc. Natl. Acad. Sci.* **2004**, *101*, 6104-6109.

188. Grubbs, R.H. *Handbook of Metathesis*. Wiley VCH: Weinheim. 2003.

189. Ivin, K. J.; Mol, I. C., *Olefin Metathesis and Metathesis Polymerization, Second Edition*; Academic Press, 1996.

190. Slugovc, C. The ring opening metathesis polymerisation toolbox. *Macromol. Rapid Commun.* **2004**, *25*, 1283-1297.

191. Gilliom, L. R.; Grubbs, R. H. Titanacyclobutanes derived from strained, cyclic olefins: the living polymerization of norbornene. *J. Am. Chem. Soc.* **1986**, *108*, 733-742.

192. Wallace, K. C.; Schrock, R. R. Ring-opening polymerization of norbornene by a tantalum catalyst: a living polymerization. *Macromolecules* **1987**, *20*, 448-450.

193. Schrock, R. R.; Krouse, S. A.; Knoll, K.; Feldman, J.; Murdzek, J. S.; Yang, D. C. Controlled ring-opening metathesis polymerization by molybdenum and tungsten alkylidene complexes. *J. Mol. Catal.* **1988**, *46*, 243-253.

194. Nguyen, S. T.; Johnson, L. K.; Grubbs, R. H.; Ziller, J. W. Ring-opening metathesis polymerization (ROMP) of norbornene by a Group VIII carbene complex in protic media. *J. Am. Chem. Soc.* **1992**, *114*, 3974-3975.

195. Borrok, M. J.; Kolonko, E. M.; Kiessling, L. L. Chemical Probes of Bacterial Signal Transduction Reveal That Repellents Stabilize and Attractants Destabilize the Chemoreceptor Array. *ACS Chem. Biol.* **2008**, *3*, 101-109.

196. Smith, D.; Pentzer, E. B.; Nguyen, S. T. Bioactive and Therapeutic ROMP Polymers. *Polym. Rev.* **2007**, *47*, 419-459.

197. Lienkamp, K.; Madkour, A. E.; Musante, A.; Nelson, C. F.; Nusslein, K.; Tew, G. N. Antimicrobial Polymers Prepared by ROMP with Unprecedented Selectivity: A Molecular Construction Kit Approach. *J. Am. Chem. Soc.* **2008**, *130*, 9836-9843.

198. Robertson, N. J.; Kostalik, H. A. I. V.; Clark, T. J.; Mutolo, P. F.; Abruna, H. D.; Coates, G. W. Tunable High Performance Cross-Linked Alkaline Anion Exchange Membranes for Fuel Cell Applications. *J. Am. Chem. Soc.* **2010**, *132*, 3400-3404.

199. Johnson, J. A.; Lu, Y.-Y.; Burts, A. O.; Lim, Y.-H.; Finn, M. G.; Koberstein, J. T.; Turro, N. J.; Tirrell, D. A.; Grubbs, R. H. Core-Clickable PEG-Branch-Azide Bivalent-Bottle-Brush Polymers by ROMP: Grafting-Through and Clicking-To. *J. Am. Chem. Soc.* **2011**, *133*, 559-566.

200. Fraser, C.; Hillmyer, M. A.; Gutierrez, E.; Grubbs, R. H. Degradable Cyclooctadiene/Acetal Copolymers: Versatile Precursors to 1,4-Hydroxytelechelic Polybutadiene and Hydroxytelechelic Polyethylene. *Macromolecules* **1995**, *28*, 7256-7261.

201. Hilf, S.; Kilbinger, A. F. M. Thiol-functionalized ROMP polymers via Sacrificial Synthesis. *Macromolecules* **2009**, *42*, 4127-4133.

202. Walker, R.; Conrad, R. M.; Grubbs, R. H. The Living ROMP of *trans*-Cyclooctene. *Macromolecules* **2009**, *42*, 599-605.

203. Boger, D. L.; Coleman, R. S. Diels-Alder reactions of heterocyclic azadienes: total synthesis of PDE I, PDE II, and PDE I dimer methyl ester. *J. Am. Chem. Soc.* **1987**, *109*, 2717-2727.

204. Afarinkia, K.; Vinader, V.; Nelson, T. D.; Posner, G. H. Diels-Alder cycloadditions of 2-pyrones and 2-pyridones. *Tetrahedron* **1992**, *48*, 9111-9171.

205. Bandlish, B. K.; Brown, J. N.; Timberlake, J. W.; Trefonas, L. M. Synthesis and structure of a trimer of 4,5-dihydropyridazine. *J. Org. Chem.* **1973**, *38*, 1102-1105.

206. Howell, J.; Goddard, J. D.; Tam, W. A relative approach for determining ring strain energies of heterobicyclic alkenes. *Tetrahedron* **2009**, *65*, 4562-4568.

207. Wright, D. L.; Usher, L. C.; Estrella-Jimenez, M. Unusual Influence of Substituents on Ring-Opening Metathesis Reactions. *Org. Lett.* **2001**, *3*, 4275-4277.

208. Mihovilovic, M. D.; Groetzl, B.; Kandioller, W.; Snajdrova, R.; Muskotal, A.; Bianchi, D. A.; Stanetty, P. Facile synthesis and ring-opening cross metathesis of carbo- and heterocyclic bicyclo[3.2.1]oct-6-en-3-ones using gaseous olefinic reaction partners. *Adv. Synth. Catal.* **2006**, *348*, 463-470.

209. Buchowicz, W.; Holerca, M. N.; Percec, V. Self-Inhibition of Propagating Carbenes in ROMP of 7-Oxa-bicyclo[2.2.1]hept-2-ene-5,6-dicarboxylic Acid Dendritic Diesters Initiated with Ru(:CHPh)Cl2(PCy3)(1,3-dimesityl-4,5-dihydroimidazol-2-ylidene). *Macromolecules* **2001**, *34*, 3842-3848.

210. Haigh, D. M.; Kenwright, A. M.; Khosravi, E. Nature of the Propagating Species in Ring-Opening Metathesis Polymerizations of Oxygen-Containing Monomers Using Well-Defined Ruthenium Initiators. *Macromolecules* **2005**, *38*, 7571-7579.

211. Gawin, R.; Makal, A.; Wozniak, K.; Mauduit, M.; Grela, K. A dormant ruthenium catalyst bearing a chelating carboxylate ligand: in situ activation and application in metathesis reactions. *Angew. Chem. Int. Ed.* **2007**, *46*, 7206-7209.

212. Gstrein, X.; Burtscher, D.; Szadkowska, A.; Barbasiewicz, M.; Stelzer, F.; Grela, K.; Slugovc, C. Ruthenium quinoline and quinoxaline complexes: Thermally triggered initiators for ring opening metathesis polymerization. *J. Polym. Sci. Part A: Polym. Chem.* **2007**, *45*, 3494-3500.

213. Ben-Asuly, A.; Tzur, E.; Diesendruck, C. E.; Sigalov, M.; Goldberg, I.; Lemcoff, N. G. A thermally switchable latent ruthenium olefin metathesis catalyst. *Organometallics* **2008**, *27*, 811-813.

214. Kang, E.-H.; Lee, I. S.; Choi, T.-L. Ultrafast Cyclopolymerization for Polyene Synthesis: Living Polymerization to Dendronized Polymers. *J. Am. Chem. Soc.* **2011**, *133*, 11904-11907.

215. Vedrenne, E.; Dupont, H.; Oualef, S.; Elkaïm, L.; Grimaud, L. Dramatic Effect of Boron-Based Lewis Acids in Cross-Metathesis Reactions. *Synlett* **2005**, *2005*, 670-672.

216. Steinbach, T.; Alexandrino, E. M.; Wahlen, C.; Landfester, K.; Wurm, F. R. Poly(phosphonate)s via Olefin Metathesis: Adjusting Hydrophobicity and Morphology. *Macromolecules* **2014**, *47*, 4884-4893.

217. Sutthasupa, S.; Shiotsuki, M.; Sanda, F. Recent advances in ring-opening metathesis polymerization, and application to synthesis of functional materials. *Polym. J.* **2010**, *42*, 905-915.

218. Kratz, K.; Xie, W.; Lee, A.; Freeman, B. D.; Emrick, T. Phosphorylcholine-Substituted ROMP Polyolefin Coatings Provide Fouling Resistance to Membrane Materials. *Macromol. Mater. Eng.* **2011**, *296*, 1142-1148.

219. Feast, W. J. Application of ROMP in the synthesis of functional polymers: Electro-active polymeric materials. *NATO Sci. Ser., II* **2002**, *56*, 177-183.

220. Gibbs, J. M.; Park, S.-J.; Anderson, D. R.; Watson, K. J.; Mirkin, C. A.; Nguyen, S. T. Polymer-DNA Hybrids as Electrochemical Probes for the Detection of DNA. *J. Am. Chem. Soc.* **2005**, *127*, 1170-1178.

221. Gorodetskaya, I. A.; Gorodetsky, A. A.; Vinogradova, E. V.; Grubbs, R. H. Functionalized Hyperbranched Polymers via Olefin Metathesis. *Macromolecules* **2009**, *42*, 2895-2898.

222. Winnik, F. M. Photophysics of preassociated pyrenes in aqueous polymer solutions and in other organized media. *Chem. Rev.* **1993**, *93*, 587-614.

223. Tornoe, C. W.; Christensen, C.; Meldal, M. Peptidotriazoles on Solid Phase: [1,2,3]-Triazoles by Regiospecific Copper(I)-Catalyzed 1,3-Dipolar Cycloadditions of Terminal Alkynes to Azides. *J. Org. Chem.* **2002**, *67*, 3057-3064.

224. Iha, R. K.; Wooley, K. L.; Nystrom, A. M.; Burke, D. J.; Kade, M. J.; Hawker, C. J. Applications of Orthogonal "Click" Chemistries in the Synthesis of Functional Soft Materials. *Chem. Rev.* **2009**, *109*, 5620-5686.

225. Boren, B. C.; Narayan, S.; Rasmussen, L. K.; Zhang, L.; Zhao, H.; Lin, Z.; Jia, G.; Fokin, V. V. Ruthenium-Catalyzed Azide-Alkyne Cycloaddition: Scope and Mechanism. *J. Am. Chem. Soc.* **2008**, *130*, 8923-8930.

226. Gauthier, M. A.; Gibson, M. I.; Klok, H.-A. Synthesis of functional polymers by post-polymerization modification. *Angew. Chem. Int. Ed.* **2009**, *48*, 48-58.

227. Romulus, J.; Henssler, J. T.; Weck, M. Postpolymerization Modification of Block Copolymers. *Macromolecules* **2014**, *47*, 5437-5449.

228. Patterson, D. M.; Nazarova, L. A.; Prescher, J. A. Finding the Right (Bioorthogonal) Chemistry. *ACS Chem. Biol.* **2014**, *9*, 592-605.

229. Courtney, A. H.; Bennett, N. R.; Zwick, D. B.; Hudon, J.; Kiessling, L. L. Synthetic Antigens Reveal Dynamics of BCR Endocytosis during Inhibitory Signaling. *ACS Chem. Biol.* **2014**, *9*, 202-210.

230. Snider, B. B.; Hui, R. A. H. F.; Kulkarni, Y. S. Intramolecular [2+2] cycloadditions of ketenes. *J. Am. Chem. Soc.* **1985**, *107*, 2194-2196.

231. Wang, L.; Zhang, Z.; Brock, A.; Schultz, P. G. Addition of the keto functional group to the genetic code of Escherichia coli. *Proc. Natl. Acad. Sci.* **2003**, *100*, 56-61.

232. Gauthier, M. A.; Klok, H.-A. Peptide/protein-polymer conjugates: synthetic strategies and design concepts. *Chem. Commun.* **2008**, 2591-2611.

233. Lu, H.; Wang, D.; Kazane, S.; Javahishvili, T.; Tian, F.; Song, F.; Sellers, A.; Barnett, B.; Schultz, P. G. Site-Specific Antibody-Polymer Conjugates for siRNA Delivery. *J. Am. Chem. Soc.* **2013**, *135*, 13885-13891.

234. Terent'ev, A. O.; Krylov, I. B.; Sharipov, M. Y.; Kazanskaya, Z. M.; Nikishin, G. I. Generation and cross-coupling of benzyl and phthalimide-N-oxyl radicals in a cerium(IV) ammonium nitrate/N-hydroxyphthalimide/ArCH2R system. *Tetrahedron* **2012**, *68*, 10263-10271.

235. Sun, J.; Dong, Y.; Cao, L.; Wang, X.; Wang, S.; Hu, Y. Highly efficient chemoselective deprotection of *O,O*-acetals and *O,O*-ketals catalyzed by molecular iodine in acetone. *J. Org. Chem.* **2004**, *69*, 8932-8934.

236. Beak, P.; Basha, A.; Kokko, B.; Loo, D. The geometry of displacements at nonstereogenic atoms: the formal displacement of alkoxide from alkoxyamines by organolithium reagents. *J. Am. Chem. Soc.* **1986**, *108*, 6016-6023.

237. Kalia, J.; Raines, R. T. Hydrolytic Stability of Hydrazones and Oximes. *Angew. Chem. Int. Ed.* **2008**, *47*, 7523-7526.

238. Nicolaou, K. C.; Hummel, C. W.; Nakada, M.; Shibayama, K.; Pitsinos, E. N.; Saimoto, H.; Mizuno, Y.; Baldenius, K. U.; Smith, A. L. Total synthesis of calicheamicin .gamma.1I. 3. The final stages. *J. Am. Chem. Soc.* **1993**, *115*, 7625-7635.

239. Da Silva, E.; Prandi, J.; Beau, J.-M. Synthesis of the esperamicin A1 trisaccharide. *J. Chem. Soc., Chem. Comm.* **1994**, 2127-2128.

240. Cardillo, G.; Hashem, M. A.; Tomasini, C. Functionalisation of unsaturated amides: synthesis of chiral α- or β-hydroxy acids. *J. Chem. Soc., Perkin Trans.1* **1990**, 1487-1488.

241. Bandini, E.; Martelli, G.; Spunta, G.; Bongini, A.; Panunzio, M. Synthesis of Perhydrooxazinones from 2-Aza-3-Trimethylsilyloxy-1,3-Butadiene. A General Route to 3,3-Disubstituted-β-Hydroxy Acids. *Synlett* **1999**, 1735-1738.

242. Shoichet, M. S. Polymer Scaffolds for Biomaterials Applications. *Macromolecules* **2010**, *43*, 581-591.

243. Liechty, W. B.; Kryscio, D. R.; Slaughter, B. V.; Peppas, N. A. Polymers for drug delivery systems. *Annu. Rev. Chem. Biomol. Eng.* **2010**, *1*, 149-173.

244. Cicchi, S.; Fabbrizzi, P.; Ghini, G.; Brandi, A.; Foggi, P.; Marcelli, A.; Righini, R.; Botta, C. Pyrene-Excimers-Based Antenna Systems. *Chem. Euro. J.* **2009**, *15*, 754-764.

245. Gilmore, J. M.; Scheck, R. A.; Esser-Kahn, A. P.; Joshi, N. S.; Francis, M. B. *N*-terminal protein modification through a biomimetic transamination reaction. *Angew. Chem. Int. Ed.* **2006**, *45*, 5307-5311.

246. Jones, D. S.; Hammaker, J. R.; Tedder, M. E. A convenient synthesis of *N*-(tert-butyloxycarbonyl)aminooxy ethers. *Tet. Lett.* **2000**, *41*, 1531-1533.

247. Gujadhur, R.; Venkataraman, D.; Kintigh, J. T. Formation of aryl-nitrogen bonds using a soluble copper(I) catalyst. *Tet. Lett.* **2001**, *42*, 4791-4793.

248. Langer, R.; Folkman, J. Polymers for the sustained release of proteins and other macromolecules. *Nature* **1976**, *263*, 797-800.

249. Rhine, W. D.; Hsieh, D. S. T.; Langer, R. Polymers for sustained macromolecule release: procedures to fabricate reproducible systems and control release kinetics. *J. Pharm. Sci.* **1980**, *69*, 265-270.

250. Rhine, W. D.; Sukhatme, V.; Hsieh, D. S. T.; Langer, R.: In *Controlled Release of Bioactive Materials* Academic Press: New York, New York, 1980; 177-188.

251. Hsieh, D. S. T.; Langer, R.; Folkman, J. Magnetic modulation of release of macromolecules from polymers. *Proc. Natl. Acad. Sci.* **1981**, *78*, 1863-1867.

252. Greco, F.; Vicent, M. J. Polymer-drug conjugates: current status and future trends. *Front. Biosci.* **2008**, *13*, 2744-2756.

253. Farokhzad, O. C.; Langer, R. Impact of Nanotechnology on Drug Delivery. *ACS Nano* **2009**, *3*, 16-20.

254. Kopecek, J. Polymer-drug conjugates: Origins, progress to date and future directions. *Adv. Drug Delivery Rev.* **2013**, *65*, 49-59.

255. Ringsdorf, H. Structure and properties of pharmacologically active polymers. *J. Polym. Sci., Polym. Symp.* **1975**, *51*, 135-153.

256. Duncan, R.; Kopecek, J. Soluble synthetic polymers as potential drug carriers. *Adv. Polym. Sci.* **1984**, *57*, 51-101.

257. Matsumura, Y.; Maeda, H. A new concept for macromolecular therapeutics in cancerchemotherapy: mechanism of tumortropic accumulation of proteins and the antitumor agent Smancs. *Cancer Res* **1986**, *46*, 6387-6392.

258. Wang, D.; Goldring, S. R. The Bone, the Joints and the Balm of Gilead. *Mol. Pharm.* **2011**, *8*, 991-993.

259. Yuan, F.; Quan, L.-d.; Cui, L.; Goldring, S. R.; Wang, D. Development of macromolecular prodrug for rheumatoid arthritis. *Adv. Drug Delivery Rev.* **2012**, *64*, 1205-1219.

260. Fox, M. E.; Szoka, F. C.; Fréchet, J. M. J. Soluble Polymer Carriers for the Treatment of Cancer: The Importance of Molecular Architecture. *Acc. Chem. Res.* **2009**, *42*, 1141-1151.

261. Nasongkla, N.; Chen, B.; Macaraeg, N.; Fox, M. E.; Fréchet, J. M. J.; Szoka, F. C. Dependence of Pharmacokinetics and Biodistribution on Polymer Architecture: Effect of Cyclic Versus Linear Polymers. *J. Am. Chem. Soc.* **2009**, *131*, 3842-3843.

262. Mauri, C.; Bosma, A. Immune Regulatory Function of B Cells. *Annu. Rev. Immunol.* **2012**, *30*, 221-241.

263. Goldsby, R. A.; Kindt, T. J.; Osborne, B. A.: *Immunology*; 4th ed.; W.H. Freeman and Co.: New York, New York, 2000.

264. Liu, F.-T.; Bohn, J. W.; Ferry, E. L.; Yamamoto, H.; Molinaro, C. A.; Sherman, L. A.; Klinman, N. R.; Katz, D. H. Monoclonal dinitrophenyl-specific murine IgE antibody: preparation, isolation, and characterization. *J. Immunol.* **1980**, *124*, 2728-2737.

265. Peacock, J. S.; Barisas, B. G. Antigen-specific mouse lymphocyte stimulation by DNP-conjugated T-independent antigens studied by photobleaching recovery. *J. Supramol. Struct. Cell. Biochem.* **1981**, *17*, 37-49.

266. Sato, K.; Ochi, A. Inhibition of B-cell receptor-antigen complex internalization by FcγRIIB1 signals. *Immunol. Lett.* **1998**, *61*, 135-143.

267. Siemasko, K.; Clark, M. R. The control and facilitation of MHC class II antigen processing by the BCR. *Curr. Opin. Immunol.* **2001**, *13*, 32-36.

268. Bryant, P.; Ploegh, H. Class II MHC peptide loading by the professionals. *Curr. Opin. Immunol.* **2004**, *16*, 96-102.

269. Steinman, R. M.; Cohn, Z. A. Identification of a novel cell type in peripheral lymphoid organs of mice. II. Functional properties in vitro. *J. Exp. Med.* **1974**, *139*, 380-397.

270. Banchereau, J.; Steinman, R. M. Dendritic cells and the control of immunity. *Nature* **1998**, *392*, 245-252.

271. Steinman, R. M. Dendritic cells: understanding immunogenicity. *Eur. J. Immunol.* **2007**, *37*, S53-S60.

272. Gordon, S. Pattern recognition receptors: doubling up for the innate immune response. *Cell* **2002**, *111*, 927-930.

273. Akira, S.; Hemmi, H. Recognition of pathogen-associated molecular patterns by TLR family. *Immunol. Lett.* **2003**, *85*, 85-95.

274. Figdor, C. G.; Van Kooyk, Y.; Adema, G. J. C-type lectin receptors on dendritic cells and Langerhans cells. *Nat. Rev. Immunol.* **2002**, *2*, 77-84.

275. Geijtenbeek, T. B. H.; Engering, A.; van Kooyk, Y. DC-SIGN, a C-type lectin on dendritic cells that unveils many aspects of dendritic cell biology. *J. Leukocyte Biol.* **2002**, *71*, 921-931.

276. Svajger, U.; Anderluh, M.; Jeras, M.; Obermajer, N. C-type lectin DC-SIGN: An adhesion, signalling and antigen-uptake molecule that guides dendritic cells in immunity. *Cell. Signalling* **2010**, *22*, 1397-1405.

277. Geijtenbeek, T. B. H.; Krooshoop, D. J. E. B.; Bleijs, D. A.; Van Vliet, S. J.; Van Duijnhoven, G. C. F.; Grabovsky, V.; Alon, R.; Figdor, C. G.; Van Kooyk, Y. DC-SIGN-ICAM-2 interaction mediates dendritic cell trafficking. *Nat. Immunol.* **2000**, *1*, 353-357.

278. Geijtenbeek, T. B. H.; Torensma, R.; Van Vliet, S. J.; Van Duijnhoven, G. C. F.; Adema, G. J.; Van Kooyk, Y.; Figdor, C. G. Identification of DC-SIGN, a novel dendritic cell-specific ICAM-3 receptor that supports primary immune responses. *Cell* **2000**, *100*, 575-585.

279. Engering, A.; Geijtenbeek, T. B. H.; Van Vliet, S. J.; Wijers, M.; Van Liempt, E.; Demaurex, N.; Lanzavecchia, A.; Fransen, J.; Figdor, C. G.; Piguet, V.; Van Kooyk, Y. The dendritic cell-specific adhesion receptor DC-SIGN internalizes antigen for presentation to T cells. *J. Immunol.* **2002**, *168*, 2118-2126.

280. Garcia-Vallejo, J. J.; van Kooyk, Y. The physiological role of DC-SIGN: A tale of mice and men. *Trends Immunol.* **2013**, *34*, 482-486.

281. Prost, L. R.; Grim, J. C.; Tonelli, M.; Kiessling, L. L. Noncarbohydrate Glycomimetics and Glycoprotein Surrogates as DC-SIGN Antagonists and Agonists. *ACS Chem. Biol.* **2012**, *7*, 1603-1608.

282. Grim, J. C. Chemical Probes of Dendritic Cell C-Type Lectin Receptors. University of Wisconsin - Madison, 2014.

283. Wu, L.; Martin, T. D.; Carrington, M.; KewalRamani, V. N. Raji B cells, misidentified as THP-1 cells, stimulate DC-SIGN-mediated HIV transmission. *Virology* **2004**, *318*, 17-23.

284. Bielawski, C. W.; Louie, J.; Grubbs, R. H. Tandem Catalysis: Three Mechanistically Distinct Reactions from a Single Ruthenium Complex. *J. Am. Chem. Soc.* **2000**, *122*, 12872-12873.

285. Burtscher, D.; Saf, R.; Slugovc, C. Fluorescence-labeled olefin metathesis polymerization initiators. *J. Polym. Sci., Part A: Polym. Chem.* **2006**, *44*, 6136-6145.

286. Goun, E. A.; Pillow, T. H.; Jones, L. R.; Rothbard, J. B.; Wender, P. A. Molecular transporters: synthesis of oligoguanidinium transporters and their application to drug delivery and real-time imaging. *ChemBioChem* **2006**, *7*, 1497-1515.

287. Fuchs, S. M.; Raines, R. T. Pathway for Polyarginine Entry into Mammalian Cells. *Biochemistry* **2004**, *43*, 2438-2444.

288. Poon, G. M. K.; Gariepy, J. Cell-surface proteoglycans as molecular portals for cationic peptide and polymer entry into cells. *Biochem. Soc. Trans.* **2007**, *35*, 788-793.

289. Langer, R.; Tirrell, D. A. Designing materials for biology and medicine. *Nature* **2004**, *428*, 487-492.

290. Nair, L. S.; Laurencin, C. T. Biodegradable polymers as biomaterials. *Prog. Polym. Sci.* **2007**, *32*, 762-798.

291. Tschan, M. J. L.; Brule, E.; Haquette, P.; Thomas, C. M. Synthesis of biodegradable polymers from renewable resources. *Polym. Chem.* **2012**, *3*, 836-851.

292. Song, J. H.; Murphy, R. J.; Narayan, R.; Davies, G. B. H. Biodegradable and compostable alternatives to conventional plastics. *Philos. Trans. R. Soc., B* **2009**, *364*, 2127-2139.

293. Tokiwa, Y.; Calabia, B. P.; Ugwu, C. U.; Aiba, S. Biodegradability of plastics. *Int. J. Mol. Sci.* **2009**, *10*, 3722-3742.

294. Tamada, J. A.; Langer, R. Erosion kinetics of hydrolytically degradable polymers. *Proc. Natl. Acad. Sci.* **1993**, *90*, 552-556.

295. Cummings, R. T.; Salowe, S. P.; Cunningham, B. R.; Wiltsie, J.; Park, Y. W.; Sonatore, L. M.; Wisniewski, D.; Douglas, C. M.; Hermes, J. D.; Scolnick, E. M. A peptide-based fluorescence resonance energy transfer assay for Bacillus anthracis lethal factor protease. *Proc. Nat. Acad. Sci.* **2002**, *99*, 6603-6606.

296. Nagai, T.; Miyawaki, A. A high-throughput method for development of FRET-based indicators for proteolysis. *Biochem. Biophys. Res. Commun.* **2004**, *319*, 72-77.

297. Suzuki, M.; Ito, Y.; Sakata, I.; Sakai, T.; Husimi, Y.; Douglas, K. T. Caspase-3 sensitive signaling in vivo in apoptotic HeLa cells by chemically engineered intramolecular fluorescence resonance energy transfer mutants of green fluorescent protein. *Biochem. Biophys. Res. Commun.* **2005**, *330*, 454-460.

298. Sunbul, M.; Jaschke, A. Contact-mediated quenching for RNA imaging in bacteria with a fluorophore-binding aptamer. *Angew. Chem. Int. Ed.* **2013**, *52*, 13401-13404.

299. Johansson, M. K.; Fidder, H.; Dick, D.; Cook, R. M. Intramolecular Dimers: A New Strategy to Fluorescence Quenching in Dual-Labeled Oligonucleotide Probes. *J. Am. Chem. Soc.* **2002**, *124*, 6950-6956.

300. Jeffrey, C. S.; Anumandla, D.; Carson, C. R. 1,4-Diamination of Cyclic Dienes via a [4+3] Cycloaddition of Diaza-allyl Cationic Intermediates. *Org. Lett.* **2012**, *14*, 5764-5767.

301. Lohse, A. G.; Hsung, R. P. [4+3] Cycloaddition Reactions of Nitrogen-Stabilized Oxyallyl Cations. *Chem. Euro. J.* **2011**, *17*, 3812-3822.

302. de Graaf, A. J.; Mastrobattista, E.; Vermonden, T.; van Nostrum, C. F.; Rijkers, D. T. S.; Liskamp, R. M. J.; Hennink, W. E. Thermosensitive Peptide-Hybrid ABC Block Copolymers Obtained by ATRP: Synthesis, Self-Assembly, and Enzymatic Degradation. *Macromolecules* **2012**, *45*, 842-851.

303. Watanabe, M.; Wegmann, D. R.; Ochi, A.; Hozumi, N. Antigen presentation by a B-cell line transfected with cloned immunoglobulin heavy- and light-chain genes specific for a defined hapten. *Proc. Natl. Acad. Sci.* **1986**, *83*, 5247-5251.

304. Mulder, K. F. Sustainable Consumption and Production of Plastics? *Technological Forecasting and Social Change* **1998**, *58*, 105-124.

305. Stevens, M. P.: *Polymer chemistry: an introduction*; Oxford University Press: New York, 1999.

306. Elias, H.-G.: *An introduction to plastics*; Wiley-VCH: Weinheim, 2003.

307. Okada, M. Chemical syntheses of biodegradable polymers. *Prog. Polym. Sci.* **2001**, *27*, 87-133.

308. Thomas, C. M.; Lutz, J.-F. Precision synthesis of biodegradable polymers. *Angew. Chem. Int. Ed.* **2011**, *50*, 9244-9246.

309. Jing, F.; Smith, M. R., III; Baker, G. L. Cyclohexyl-substituted polyglycolides with high glass transition temperatures. *Macromolecules* **2007**, *40*, 9304-9312.

310. Fiore, G. L.; Jing, F.; Young, V. G., Jr.; Cramer, C. J.; Hillmyer, M. A. High Tg aliphatic polyesters by the polymerization of spirolactide derivatives. *Polym. Chem.* **2010**, *1*, 870-877.

311. Liu, Y.; Turner, S. R. Synthesis and properties of cyclic diester based aliphatic copolyesters. *J. Polym. Sci. Part A: Polym. Chem.* **2010**, *48*, 2162-2169.

312. Wu, L.; Mincheva, R.; Xu, Y.; Raquez, J.-M.; Dubois, P. High Molecular Weight Poly(butylene succinate-co-butylene furandicarboxylate) Copolyesters: From Catalyzed Polycondensation Reaction to Thermomechanical Properties. *Biomacromolecules* **2012**, *13*, 2973-2981.

313. Burke, D. J.; Kawauchi, T.; Kade, M. J.; Leibfarth, F. A.; McDearmon, B.; Wolffs, M.; Kierstead, P. H.; Moon, B.; Hawker, C. J. Ketene-Based Route to rigid Cyclobutanediol Monomers for the Replacement of BPA in High Performance Polyesters. *ACS Macro Lett.* **2012**, *1*, 1228-1232.

314. Shin, J.; Lee, Y.; Tolman, W. B.; Hillmyer, M. A. Thermoplastic Elastomers Derived from Menthide and Tulipalin A. *Biomacromolecules* **2012**, *13*, 3833-3840.

315. Lavilla, C.; Alla, A.; Martinez, d. I. A.; Munoz-Guerra, S. High Tg Bio-Based Aliphatic Polyesters from Bicyclic d-Mannitol. *Biomacromolecules* **2013**, *14*, 781-793.

316. Fox, T. G.; Flory, P. J. The glass temperature and related properties of polystyrene. Influence of molecular weight. *J. Polym. Sci.* **1954**, *14*, 315-319.

317. Santangelo, P. G.; Roland, C. M. Molecular Weight Dependence of Fragility in Polystyrene. *Macromolecules* **1998**, *31*, 4581-4585.

318. Lavoie, A. R.; Ho, M. H.; Waymouth, R. M. Alternating stereospecific copolymerization of cyclopentene and ethylene with constrained geometry catalysts. *Chem. Comm.* **2003**, 864-865.

319. Yoshida, Y.; Mohri, J.; Ishii, S.; Mitani, M.; Saito, J.; Matsui, S.; Makio, H.; Nakano, T.; Tanaka, H.; Onda, M.; Yamamoto, Y.; Mizuno, A.; Fujita, T. Living copolymerization of ethylene with norbornene catalyzed by bis(pyrrolide-imine) titanium complexes with MAO. *J. Am. Chem. Soc.* **2004**, *126*, 12023-12032.

320. Na, S. J.; Wu, C. J.; Yoo, J.; Kim, B. E.; Lee, B. Y. Copolymerization of 5,6-Dihydrodicyclopentadiene and Ethylene. *Macromolecules* **2008**, *41*, 4055-4057.

321. Yu, S. T.; Na, S. J.; Lim, T. S.; Lee, B. Y. Preparation of a Bulky Cycloolefin/Ethylene Copolymer and Its Tensile Properties. *Macromolecules* **2009**, *43*, 725-730.

322. Hong, M.; Cui, L.; Liu, S.; Li, Y. Synthesis of Novel Cyclic Olefin Copolymer (COC) with High Performance via Effective Copolymerization of Ethylene with Bulky Cyclic Olefin. *Macromolecules* **2012**, *45*, 5397-5402.

323. Grulke, E. A.; Immergut, E. H.; Brandrup, J.: *Polymer handbook*; Wiley: New York.

324. Mäder, D.; Bruch, M.; Maier, R.-D.; Stricker, F.; Mülhaupt, R. Glass Transition Temperature Depression of Elastomers Blended with Poly(propene)s of Different Stereoregularities. *Macromolecules* **1999**, *32*, 1252-1259.

325. Bates, F. S.; Fredrickson, G. H. Block copolymers-designer soft materials. *Phys. Today* **1999**, *52*, 32-38.

326. Bates, F. S.; Hillmyer, M. A.; Lodge, T. P.; Bates, C. M.; Delaney, K. T.; Fredrickson, G. H. Multiblock Polymers: Panacea or Pandora's Box? *Science* **2012**, *336*, 434-440.

327. Wang, Y.; Hillmyer, M. A. Polyethylene-poly(L-lactide) diblock copolymers: Synthesis and compatibilization of poly(L-lactide)/polyethylene blends. *J. Polym. Sci. Part A: Polym. Chem.* **2001**, *39*, 2755-2766.

328. Hiemenz, P. C.; Lodge, T. P.: *Polymer Chemistry*; 2nd ed.; Taylor & Francis Group, 2007.

329. Chang, E. P. Viscoelastic properties of pressure-sensitive adhesives. *J. Adhes.* **1997**, *60*, 233-248.

330) Creton, C. Materials Science of Pressure-Sensitive Adhesives. In *Processing of Polymers* 1997; Ed. Meijer, H.G.H., Wiley-VCH: Weinheim, 707-741.

331. Riegler, S.; Slugovc, C.; Trimmel, G.; Stelzer, F. Block copolymers via ROMP - awakening the sleeping beauty. *Macromol. Symp.* **2004**, *217*, 231-246.

332. Elacqua, E.; Lye, D. S.; Weck, M. Engineering Orthogonality in Supramolecular Polymers: From Simple Scaffolds to Complex Materials. *Acc. Chem. Res.* **2014**, *47*, 2405-2416.

333. Martinez, H.; Ren, N.; Matta, M. E.; Hillmyer, M. A. Ring-opening metathesis polymerization of 8-membered cyclic olefins. *Polym. Chem.* **2014**, *5*, 3507-3532.

334. Tuba, R.; Al-Hashimi, M.; Bazzi, H. S.; Grubbs, R. H. One-Pot Synthesis of Poly(vinyl alcohol) (PVA) Copolymers via Ruthenium Catalyzed Equilibrium Ring-Opening Metathesis Polymerization of Hydroxyl Functionalized Cyclopentene. *Macromolecules* **2014**, *47*, 8190-8195.

335. Cohn, D.; Hotovely Salomon, A. Designing biodegradable multiblock PCL/PLA thermoplastic elastomers. *Biomaterials* **2005**, *26*, 2297-2305.

336. Lipik, V. T.; Kong, J. F.; Chattopadhyay, S.; Widjaja, L. K.; Liow, S. S.; Venkatraman, S. S.; Abadie, M. J. M. Thermoplastic biodegradable elastomers based on ε-caprolactone and L-lactide block co-polymers: A new synthetic approach. *Acta. Biomater.* **2010**, *6*, 4261-4270.

337. Hillmyer, M. A.; Tolman, W. B. Aliphatic Polyester Block Polymers: Renewable, Degradable, and Sustainable. *Acc. Chem. Res.* **2014**, *47*, 2390-2396.

338. Bielawski, C. W.; Grubbs, R. H. Increasing the Initiation Efficiency of Ruthenium-Based Ring-Opening Metathesis Initiators: Effect of Excess Phosphine. *Macromolecules* **2001**, *34*, 8838-8840.

339. Hammond, G. S.; Stout, C. A.; Lamola, A. A. Mechanisms of photochemical reactions in solution. XXV. The photodimerization of coumarin. *J. Am. Chem. Soc.* **1964**, *86*, 3103-3106.

340. Wolff, T.; Goerner, H. Photodimerization of coumarin revisited: Effects of solvent polarity on the triplet reactivity and product pattern. *Phys. Chem. Chem. Phys.* **2004**, *6*, 368-376.

341. Ciamician, G.; Silber, P. Chemical light action. V. *Ber. Dtsch. Chem. Ges.* **1902**, *35*, 4128-4131.

342. Chen, Y.; Geh, J. L. Copolymers derived from 7-acryloyloxy-4-methylcoumarin and acrylates: 1. Copolymerizability and photocrosslinking behaviors. *Polymer* **1996**, *37*, 4473-4480.

343. Trenor, S. R.; Long, T. E.; Love, B. J. Photoreversible chain extension of poly(ethylene glycol). *Macromol. Chem. Phys.* **2004**, *205*, 715-723.

344. Trenor, S. R.; Shultz, A. R.; Love, B. J.; Long, T. E. Coumarins in Polymers: From Light Harvesting to Photo-Cross-Linkable Tissue Scaffolds. *Chem. Rev.* **2004**, *104*, 3059-3077.

345. Liu, M. O.; Lin, H.-F.; Yang, M.-C.; Lai, M.-J.; Chang, C.-C.; Shiao, P.-L.; Chen, I.-M.; Chen, J.-Y. Thermal, dynamic mechanical and rheological properties of metallocene-catalyzed

cycloolefin copolymers (mCOCs) with high glass transition temperature. *Mater. Lett.* **2007**, *61*, 457-462.

346. Yamazaki, M. Industrialization and application development of cyclo-olefin polymer. *J. Mol. Catal. A: Chem.* **2004**, *213*, 81-87.

347. Mol, J. C. Industrial applications of olefin metathesis. *J. Mol. Catal. A: Chem.* **2004**, *213*, 39-45.

348. Fujita, M.; Coates, G. W. Synthesis and Characterization of Alternating and Multiblock Copolymers from Ethylene and Cyclopentene. *Macromolecules* **2002**, *35*, 9640-9647.

349. Liu, S.; Yao, Z.; Cao, K.; Li, B.; Zhu, S. Preparation of polar ethylene-norbornene copolymers by metallocene terpolymerization with triisobutylaluminum-protected but-3-en-1-ol. *Macromol. Rapid Commun.* **2009**, *30*, 548-553.

350. Segalman, R. A. Patterning with block copolymer thin films. *Mater. Sci. Eng., R* **2005**, *R48*, 191-226.

351. Cheng, J. Y.; Ross, C. A.; Smith, H. I.; Thomas, E. L. Templated self-assembly of block copolymers: top-down helps bottom-up. *Adv. Mater.* **2006**, *18*, 2505-2521.

352. Bang, J.; Jeong, U.; Ryu, D. Y.; Russell, T. P.; Hawker, C. J. Block Copolymer Nanolithography: Translation of Molecular Level Control to Nanoscale Patterns. *Adv. Mater.* **2009**, *21*, 4769-4792.

353. Kim, H.-C.; Park, S.-M.; Hinsberg, W. D. Block Copolymer Based Nanostructures: Materials, Processes, and Applications to Electronics. *Chem. Rev.* **2010**, *110*, 146-177.

354. Tang, C.; Sivanandan, K.; Stahl, B. C.; Fredrickson, G. H.; Kramer, E. J.; Hawker, C. J. Multiple Nanoscale Templates by Orthogonal Degradation of a Supramolecular Block Copolymer Lithographic System. *ACS Nano* **2010**, *4*, 285-291.

355. Satoh, K.; Poelma, J. E.; Campos, L. M.; Stahl, B.; Hawker, C. J. A facile synthesis of clickable and acid-cleavable PEO for acid-degradable block copolymers. *Polym. Chem.* **2012**, *3*, 1890-1898.

356. Naesman, J. A. H.; Pensar, K. G. An improved one-pot preparation of 2-furanones. *Synthesis* **1985**, 786-788.

357. Ji, S.; Hoye, T. R.; Macosko, C. W. Controlled Synthesis of High Molecular Weight Telechelic Polybutadienes by Ring-Opening Metathesis Polymerization. *Macromolecules* **2004**, *37*, 5485-5489.

358. Klareskog, L.; Amara, K.; Malmstroem, V. Adaptive immunity in rheumatoid arthritis: anticitrulline and other antibodies in the pathogenesis of rheumatoid arthritis. *Curr. Opin. Rheumatol.* **2014**, *26*, 72-79.

359. Koenders, M. I.; van den Berg, W. B. Novel therapeutic targets in rheumatoid arthritis. *Trends Pharmacol. Sci.* **2015**, *36*, 189-195.

360. Chen, J.; Pompano, R. R.; Santiago, F. W.; Maillat, L.; Sciammas, R.; Sun, T.; Han, H.; Topham, D. J.; Chong, A. S.; Collier, J. H. The use of self-adjuvanting nanofiber vaccines to elicit high-affinity B cell responses to peptide antigens without inflammation. *Biomaterials* **2013**, *34*, 8776-8785.

361. Mora-Solano, C.; Collier, J. H. Engaging adaptive immunity with biomaterials. *J. Mat. Chem. B* **2014**, *2*, 2409-2421.

362. Pompano, R. R.; Chen, J.; Verbus, E. A.; Han, H.; Fridman, A.; McNeely, T.; Collier, J. H.; Chong, A. S. Titrating T-Cell Epitopes within Self-Assembled Vaccines Optimizes CD4+ Helper T Cell and Antibody Outputs. *Adv. Healthcare Mat.* **2014**, *3*, 1898-1908.

363. Keller, S.; Wilson, J. T.; Patilea, G. I.; Kern, H. B.; Convertine, A. J.; Stayton, P. S. Neutral polymer micelle carriers with pH-responsive, endosome-releasing activity modulate antigen trafficking to enhance CD8+ T cell responses. *J. Control. Rel.* **2014**, *191*, 24-33.

364. Ivanovska, I. L.; De Pablo, P. J.; Ibarra, B.; Sgalari, G.; MacKintosh, F. C.; Carrascosa, J. L.; Schmidt, C. F.; Wuite, G. J. L. Bacteriophage capsids: Tough nanoshells with complex elastic properties. *Proc. Natl. Acad. Sci.* **2004**, *101*, 7600-7605.

365. Kuznetsova, T. G.; Starodubtseva, M. N.; Yegorenkov, N. I.; Chizhik, S. A.; Zhdanov, R. I. Atomic force microscopy probing of cell elasticity. *Micron* **2007**, *38*, 824-833.

366. Roos, W. H.; Bruinsma, R.; Wuite, G. J. L. Physical virology. *Nat. Phys.* **2010**, *6*, 733-743.

367. Tuson, H. H.; Auer, G. K.; Renner, L. D.; Hasebe, M.; Tropini, C.; Salick, M.; Crone, W. C.; Gopinathan, A.; Huang, K. C.; Weibel, D. B. Measuring the stiffness of bacterial cells from growth rates in hydrogels of tunable elasticity. *Mol. Microbiol.* **2012**, *84*, 874-891.

368. Huebsch, N.; Arany, P. R.; Mao, A. S.; Shvartsman, D.; Ali, O. A.; Bencherif, S. A.; Rivera-Feliciano, J.; Mooney, D. J. Harnessing traction-mediated manipulation of the cell/matrix interface to control stem-cell fate. *Nat. Mater.* **2010**, *9*, 518-526.

369. Engler, A. J.; Sen, S.; Sweeney, H. L.; Discher, D. E. Matrix elasticity directs stem cell lineage specification. *Cell* **2006**, *126*, 677-689.

370. Guvendiren, M.; Burdick, J. A. Stiffening hydrogels to probe short- and long-term cellular responses to dynamic mechanics. *Nat. Commun.* **2012**, *3*, 792.

371. Musah, S.; Morin, S. A.; Wrighton, P. J.; Zwick, D. B.; Jin, S.; Kiessling, L. L. Glycosaminoglycan-Binding Hydrogels Enable Mechanical Control of Human Pluripotent Stem Cell Self-Renewal. *ACS Nano* **2012**, *6*, 10168-10177.

372. Musah, S.; Wrighton, P. J.; Zaltsman, Y.; Zhong, X.; Zorn, S.; Parlato, M. B.; Hsiao, C.; Palecek, S. P.; Chang, Q.; Murphy, W. L.; Kiessling, L. L. Substratum-induced differentiation of human pluripotent stem cells reveals the coactivator YAP is a potent regulator of neuronal specification. *Proc. Natl. Acad. Sci.* **2014**, *111*, 13805-13810.

373. Beningo, K. A.; Wang, Y.-L. Fc-receptor-mediated phagocytosis is regulated by mechanical properties of the target. *J. Cell Sci.* **2002**, *115*, 849-856.

374. Banquy, X.; Suarez, F.; Argaw, A.; Rabanel, J.-M.; Grutter, P.; Bouchard, J.-F.; Hildgen, P.; Giasson, S. Effect of mechanical properties of hydrogel nanoparticles on macrophage cell uptake. *Soft Matter* **2009**, *5*, 3984-3991.

375. Wan, Z.; Zhang, S.; Fan, Y.; Liu, K.; Du, F.; Davey, A. M.; Zhang, H.; Han, W.; Xiong, C.; Liu, W. B Cell Activation Is Regulated by the Stiffness Properties of the Substrate Presenting the Antigens. *J. Immunol.* **2013**, *190*, 4661-4675.

376. Natkanski, E.; Lee, W.-Y.; Mistry, B.; Casal, A.; Molloy, J. E.; Tolar, P. B Cells Use Mechanical Energy to Discriminate Antigen Affinities. *Science* **2013**, *340*, 1587-1590.

377. Judokusumo, E.; Tabdanov, E.; Kumari, S.; Dustin, M. L.; Kam, L. C. Mechanosensing in T Lymphocyte Activation. *Biophys. J.* **2012**, *102*, L5-L7.

378. O'Connor, R. S.; Hao, X.; Shen, K.; Bashour, K.; Akimova, T.; Hancock, W. W.; Kam, L. C.; Milone, M. C. Substrate Rigidity Regulates Human T Cell Activation and Proliferation. *J. Immunol.* **2012**, *189*, 1330-1339.

379. Hoare, T.; Pelton, R. Engineering Glucose Swelling Responses in Poly(*N*-isopropylacrylamide)-Based Microgels. *Macromolecules* **2007**, *40*, 670-678.

380. Hoare, T.; Pelton, R. Titrametric Characterization of pH-Induced Phase Transitions in Functionalized Microgels. *Langmuir* **2006**, *22*, 7342-7350.

381. Dische, Z. Detection and colorimetric determination of heptoses. *J. Biol. Chem.* **1953**, *204*, 983-997.

382. Osborn, M. J. The gram-negative cell wall I. Evidence for the role of 2-keto-3-deoxyoctonate in the lipopolysaccharide of Salmonella typhimurium. *Proc. Natl. Acad. Sci.* **1963**, *50*, 499-506.

383. Haskins, W. T.; Anacker, R. L.; Bickel, W. D.; Milner, K. C.; Ribi, E. Determination of heptose in endotoxins. *J. Bacteriol.* **1966**, *92*, 284.

384. Wright, B. G.; Rebers, P. A. Procedure for determining heptose and hexose in lipopolysaccharides. Modification of the cysteine-sulfuric acid method. *Anal. Biochem.* **1972**, *49*, 307-319.

385. Domke, J.; Radmacher, M. Measuring the Elastic Properties of Thin Polymer Films with the Atomic Force Microscope. *Langmuir* **1998**, *14*, 3320-3325.

386. Wang, L. H.; Rothberg, K. G.; Anderson, R. G. W. Mis-assembly of clathrin lattices on endosomes reveals a regulatory switch for coated pit formation. *J. Cell Biol.* **1993**, *123*, 1107-1118.

387. Lamaze, C.; Schmid, S. L. The emergence of clathrin-independent pinocytic pathways. *Curr. Opin. Cell Biol.* **1995**, *7*, 573-580.

388. Butt, H.-J.; Jaschke, M. Calculation of thermal noise in atomic force microscopy. *Nanotechnology* **1995**, *6*, 1.